QUANTUM MECHANICAL STUDY OF DIFFERENT TYPES OF NUCLEIC ACID SENSORS

THESIS SUBMITTED FOR THE AWARD OF THE DEGREE OF

Doctor of Philosophy

in

Applied Physics

By

Asheesh Kumar

Enrolment No. :- 594/11

Under the Supervision of

Prof. Devesh Kumar

Department of Applied Physics
School for Physical Sciences
Babasaheb Bhimrao Ambedkar University, Lucknow,
U.P., (India) – 226025
March, 2019

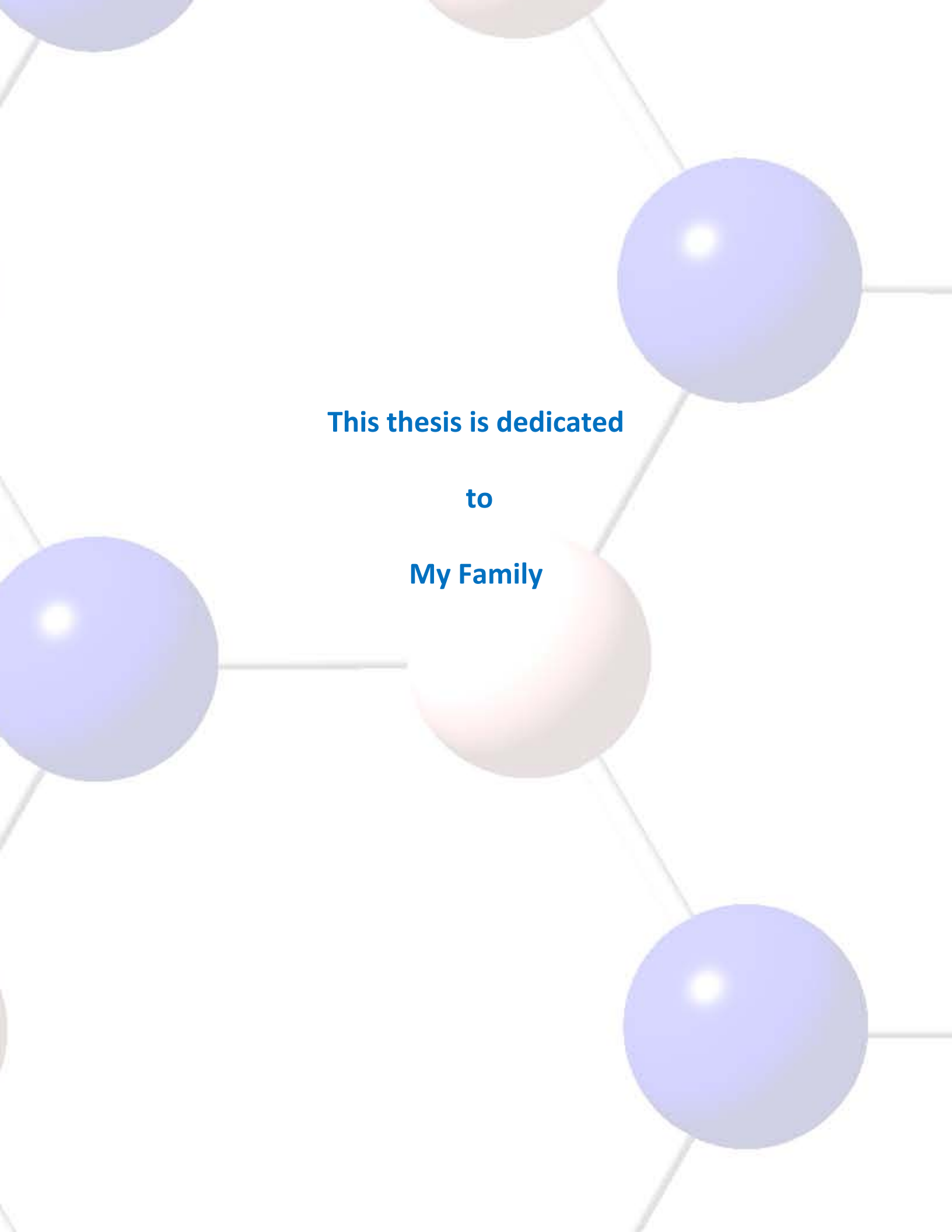

This thesis is dedicated

to

My Family

DECLARATION

I declare that the thesis titled **"Quantum Mechanical Study of Different Types of Nucleic Acid Sensors"** has been prepared by me under the supervision of Prof. Devesh Kumar, Department of Applied Physics, School for Physical Sciences, Babasaheb Bhimrao Ambedkar University, Lucknow. No part of this thesis has formed the basis for the award of any degree, diploma or fellowship previously. Further, I declare that the material embodied in the present work is based on original research work and the indebtedness to others has been duly acknowledged at relevant places. This is also declared that the thesis is essentially free from all kinds of plagiarism.

(Asheesh Kumar)
Department of Applied Physics
School for Physical Sciences
Babasaheb Bhimrao Ambedkar University
Vidya Vihar, Raebareli Road
Lucknow, (U.P.), India- 226025

Date: 12th March 2019
Place: Lucknow

CERTIFICATE

This is to certify that the thesis titled **"Quantum Mechanical Study of Different Types of Nucleic Acid Sensors"** submitted by **Mr. Asheesh Kumar** is an original research work and has not been previously submitted in part or full for the award of any other degree or diploma to this or any other university or institutions.

The thesis submitted to the Babasaheb Bhimrao Ambedkar University Lucknow satisfies all the requirements as stipulated in the *Doctor of Philosophy (Ph.D.) regulations -1999 as amended in 2010* and it is fit for submission and evaluation for the award of Doctor of Philosophy of the University.

Date: 12th March 2019

Supervisor

Head of Department

ACKNOWLEDGEMENT

It is hard to believe that a wonderful journey of writing my thesis is coming to an end, but I would like to take this opportunity to thank people who have had immense contribution to my life. To them I would like to convey my heartfelt gratitude and sincere appreciation.

It is a great honour and privilege for me to record my deep sense of gratitude and sincere thanks to my supervisor Prof. Devesh Kumar, Head of the Department, for his persistent encouragement, perpetual motivation, everlasting patience, constructive criticism and valuable technical inputs in research that have benefitted me to an extent which is beyond expression. I really admire his ability to handle the problems in a superb and calm way and especially the ability to balance research interests and personal pursuits. I also thank his family, Mrs. Sangeeta Rai, Ms. Jayneeta Rai, and Mr. Jayaditya Rai for their hospitality. I consider myself fortunate to be associated with my guide who gave a decisive turn and a significant boost to my career. Thank you sir, from the bottom of my heart for being there whenever I needed you.

I feel delighted in expressing my gratitude to the faculty of our department for their continuous encouragement and moral support of Prof. B.C. Yadav, Dr. Ramesh Chandra, Dr. Anil Kumar Yadav, Dr. Devendra Singh and Dr. K. B. Thapa and for their blessings.

I heartily acknowledge the help and motivation provided by the office staff of the department who was always ready to support me at every stage of my research work.

A Special thanks to the entire MPDS team with a special mention and high regards to Prof. G. N. Sastry, whose stimulating suggestions and encouragement helped me to complete my research work. I am also highly grateful to Ms. Leena Chatterjee.

Further, I would like to thank the facilities of the Central Library and the Computer Center, Babasaheb Bhimrao Ambedkar University, Lucknow.

The financial support of the UGC, New Delhi is gratefully acknowledged.

I feel delighted in expressing my gratitude to the present lab members Mr. Narinder Kumar, Ms. Nidhi Awasthi, Ms. Rolly Yadav, Ms. Anamika Shukla and Ms. Shivani Chaudhary who were always ready to help me even during the odd hours. I wish them good luck for their future. I also thank the past lab members for their ever willing cooperation: Dr. Suresh Kumar, Dr. Jitendra Kumar, Dr. Pranav Upadhyay, Dr. Deep Kumar and Dr. Dharmveer Singh. I am also thankful to Dr. Ruchi, Mr. Surya and Mr. Rajkamal.

At final note, I would like to thank the most inspirational, influential and the most loving persons of my life, my family, specially my mother Mrs. Namita Kumari, my father Mr. Ajay Kumar and sisters Ms. Shalini Kumari, Ms. Simran Kumari, my elder brother Dr. Ritesh Kumar and my dear nephew Priyanshu where the most basic source of my life energy resides and who are the real moral boosters. Their unconditional love and support always consistently provided me the strength to pursue my goals. I owe them everything for all their sacrifices in making me what I am today.

Asheesh Kumar

(Asheesh Kumar)

ABSTRACT

The nucleic acid primarily consists of phosphoric acid, sugar and a mixture of organic bases (purines and pyrimidine). The two main classes of nucleic acids are deoxyribonucleic acid (DNA) and ribonucleic acid (RNA). DNA is the main blueprint for life and constitutes the genetic material in all living organisms and most viruses. RNA is the genetic material of certain viruses, but it is also found in all living cells, where it plays an important role in certain processes such as protein synthesis.

Among the various advanced functionalized materials, carbon nanostructures (CNSs) are one of the most promising classes. These materials have emerged as a choice of materials in biotechnological and biomedical applications such as drug delivery systems and DNA sequencing agents as well as in material science.

It is very important and interesting to study the noncovalent functionalization of carbonaceous materials. Such noncovalent interactions between the CNSs and biomolecular systems provide the prototypical example of nano-bio interface. The major noncovalent interactions involving CNSs are primarily π–π, CH-π, cation–π and anion–π interactions. Quantifying such interactions and identifying various factors which influence such interactions are questions of outstanding fundamental interest.

The inimitable properties of the carbonaceous materials make them appropriate for various potential applications in areas ranging from electronics to medicine. Therefore, it has become important to quantify such interactions and also to discover the factors that affect the noncovalent interactions.

PREFACE

Exploring the nature of interaction at nano-bio interface is crucial in understanding various applications of carbon materials such as DNA sequencing (personalized medicines), diagnosis of lethal diseases (bio-sensors) and cancer therapy (drug delivery systems). As the nanoparticle enters the body, proteins interact with them and form a complex termed as protein-corona which signifies the biological identity of the particle. The biodistribution of the nanoparticle and the further biological responses of the body depend on this protein-corona. Hence, it is important to study the interaction of peptides with carbon materials to understand the mechanism of carbon based drug delivery system. Developing chemical and bio-sensors based on carbon materials has become an area of prime interest since the physical and electronic properties of these materials are vulnerable to external environment. Among the various existing noncovalent interactions π−π stacking and cation−π interactions play an important role in carbon nano chemistry.

Chapter 1 presents a literature survey of work done so far on biological molecules with a special emphasis on the nucleic acid sensors and carbon nanostructures along with the computational quantum mechanical techniques prevalent in the area.

Chapter 2 discusses mathematical details of quantum mechanical methods. It also gives a glimpse of the theoretical methods helpful in study of bio-molecules, metal ions, small molecules and carbon nanostructures complexes.

Chapter 3 provides a comparison between the interaction of nucleic bases with graphene and boron nitride graphene. This chapter sheds light on the connection between the theoretical and experimental studies.

Chapter 4 is focussed on the interaction of modified nucleic bases (MMNBs) with the graphene and doped graphene models. In this chapter, the interaction energies were corrected for the basis set superposition error. The trend of the interaction energy is studied in detail along with the AIM analysis.

Chapter 5 describes one of the first attempt to explore the interaction of mono cations (alkali metal ions) with the single walled carbon nanotube. This chapter provides a detailed insight on the variation of important parameters like interaction energy, Homo-Lumo gap, and associated Mulliken charge analysis with different position of metal ion in single walled carbon nanotube.

Chapter 6 summarizes the general conclusion drawn from the thesis and also the future prospects from the thesis are discussed.

LIST OF ABBREVIATIONS

1.	A	Adenine
2.	AA	Ascorbic Acid
3.	AlG	Aluminium Doped Graphene
4.	BCP	Bond Critical Point
5.	BE	Binding Energy
6.	BG	Boron Doped Graphene
7.	BNG	Boron Nitride Graphene
8.	BNNTs	Boron Nitride Nanotubes
9.	BSSE	Basis Set Superposition Error
10.	BS1	Basis Set 1
11.	BS2	Basis Set 2
12.	BS3	Basis Set 3
13.	C	Cytosine
14.	CAF	Caffeine
15.	CCP	Cage Critical Point
16.	CNS	Carbon nanostructure
17.	CNT	Carbon Nanotube
18.	0D	Zero-Dimensional
19.	1D	One-Dimensional
20.	2D	Two-Dimensional
21.	DA	Dopamine
22.	FD	Fermi Dirac
23.	DFT	Density Functional Theory
24.	DNA	Deoxyribonucleic Acid
25.	dsDNA	Double Stranded Deoxyribonucleic Acid

26.	FETs	Field Effect Transistors
27.	FF	Force Field
28.	G	Guanine
29.	GaG	Gallium Doped Graphene
30.	GeG	Germanium Doped Graphene
31.	GGA	Generalised Gradient Approximation
32.	GNR	Graphene Nano Ribbon
33.	GQD	Graphene Quantum Dot
34.	GR	Graphene
35.	GTO	Gaussian Type Orbiatl
36.	HF	Hartree-Fock
37.	HOMO	Highest Occupied Molecular Orbital
38.	HX	Hypoxantine
39.	ICs	Initial Configurations
40.	IE	Interaction Energy
41.	LCAO	Linera Combination of Atomic Orbitals
42.	LDA	Local Density Approximation
43.	LUMO	Lowest Unoccupied Molecular Orbital
44.	MD	Molecular Dynamics
45.	MESP	Molecular Electrostatic Potential
46.	MM	Molecular Mechanics
47.	MNBs	Modified Nucleic Bases
48.	MO	Molecular Orbital
49.	MWCNT	Multi Walled Carbon nanotube
50.	NBs	Nucleic Bases

51.	NCP	Nuclear Critical Point
52.	NG	Nitrogen Doped Graphene
53.	NiG	Nickel Doped Graphene
54.	NP	Nano Particle
55.	PD	Parallel Displaced
56.	PSA	Prostate Specific Antigen
57.	QTAIM	Quantum Theory of Atoms in Molecules
58.	QM	Quantum Mechanics
59.	RCP	Ring Critical Point
60.	RGO	Reduced Graphene Oxide
61.	RNA	Ribonucleic Acid
62.	SCF	Self Consistent Field
63.	SERS	Surface Enhanced Raman Scattering
64.	SG	Silicon Doped Graphene
65.	SG	Sulphur Doped Graphene
66.	ssDNA	Single Stranded Deoxyribonucleic Acid
67.	STO	Slater Type Orbital
68.	SWCNT	Single Walled Carbon Nanotube
69.	T	Thymine
70.	TF	Thomas Fermi
71.	U	Uracil
72.	UA	Uric Acid
73.	UV	Ultra violet
74.	vW	van der Waals
75.	X	Xanthine

LIST OF TABLES

LIST OF FIGURES

TABLE OF CONTENTS

Chapter 1

Introduction

CHAPTER 1

INTRODUCTION

1.1 Nucleic Acid

Nucleic acids are biomolecules which are essential for all known forms of life. Nucleic acids were named for their initial discovery within the nucleus, and for the presence of phosphate groups (related to phosphoric acid). Nucleic acids (DNA and RNA) perform a variety of crucial functions in organisms. DNA stores and transfers genetic information, it serves as the template for the synthesis of new DNA and RNAs, while RNAs carry out protein synthesis. Nucleic acids contain only a few different components, but they have great structural diversity. This diversity results from the many possible combinations of those few components due to the large sizes of DNA and RNA.

1.1.1 Structures of Nucleic Acid

There are two classes of nucleic acids i.e. DNA (Deoxyribonucleic acid) and RNA (Ribonucleic acid). Although they have significantly different structures, one can describe both DNA and RNA as polynucleotide (polymers of nucleotides).

1.1.2 Nucleotides and Nucleosides

Each nucleotide sub-unit of a nucleic acid contains a phosphate group, a sugar component, and a heterocyclic ring system (heterocyclic base). The portion of nucleotide containing just the sugar and heterocyclic base is called a nucleoside. Heterocyclic base contains either a pyrimidine or a purine ring. Pyrimidine is an aromatic organic compound with two nitrogens at C1 and C3 position of a six membered ring.

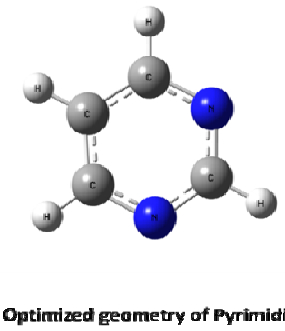

Figure 1.1: Structure of pyrimidine.

Pyrimidines in DNA and RNA: Cytosine (C) and Uracil (U) in RNA, Cytosine (C) and Thymine (T) in DNA.

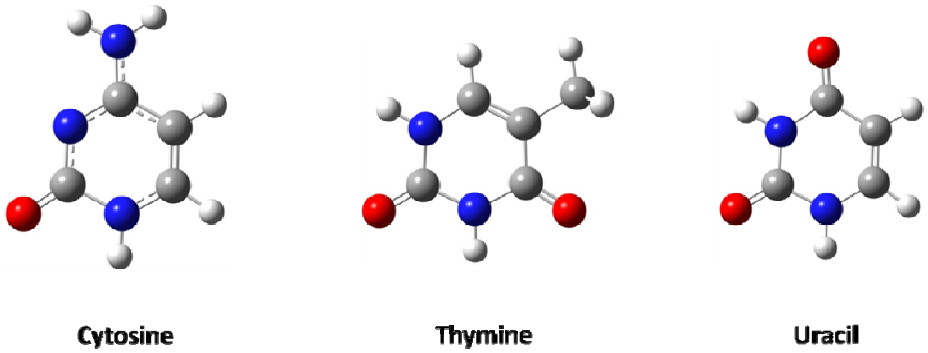

Figure 1.2: Optimized structures of pyrimidines.

Some of the important properties of pyrimidine and purines are:

- Pyrimidine conformations are planar, purines are somewhat puckered (small wrinkles or folds).
- Since, pyrimidines and purines are aromatic, they can absorb ultraviolet (UV) light.
- DNA and RNA concentration in a sample can be found by measuring UV absorbance.

Purine is an aromatic organic compound that consists of a pyrimidine ring and an imadazole ring ($C_3H_4N_2$).

Purines in DNA and RNA: Adenine (A) and Guanine (G) in DNA and RNA both.

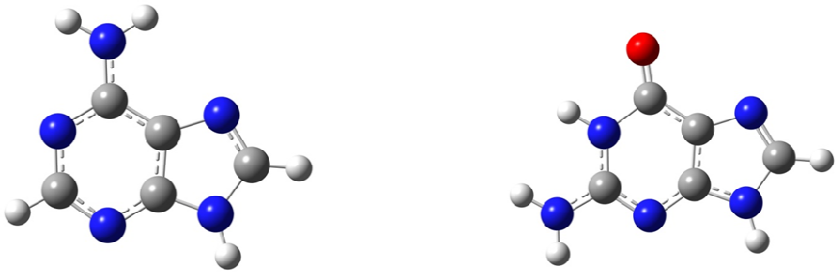

Figure 1.3: Optimized Structures of purines.

1.2 Carbon

Carbon was named after the Latin word carbo, which means “charcoal” in the year 1789 by A. L. Lavoisier. It exists in nature in myriad forms, both as natural and synthetic allotropic forms. The properties of all the allotropic forms are entirely different from each other. In the periodic table, carbon belongs to the group IV and this element prevails in all the organic life on earth. Among all the chemical components this element is present in approximately 95% in matter, thereby speaking about its importance.[1] Beside the other element present in the periodic table, the carbon atom possesses the ability to bind with a number of different atoms thereby resulting in the formation of a large variety of compounds.[2] It consists of 6 protons, 6 electrons, and x neutrons, where x may be 6, 7 or 8, thereby resulting in different isotopes like ^{12}C, (most commonly found isotope in nature), ^{13}C and ^{14}C (radioactive isotope). The ground state atomic configuration of C is

$1s^2 2s^2 2p^2$. While dealing with the elemental form, the 2 electrons are seen to fill the inner atomic orbitals. The electronic arrangement is shown below:

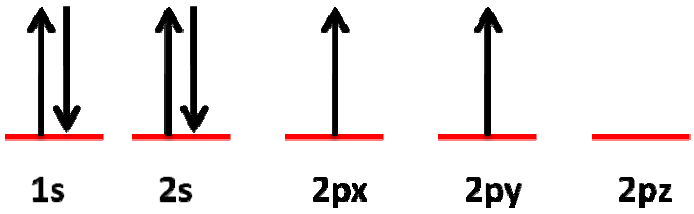

Figure 1.4: Schematic representation of the electrons in different orbitals for carbon.

Based on the different hybridizations of atomic orbital, the carbon allotrope may be further classified as: diamond has sp^3 hybridization, graphitic having sp^2 hybridization and in case of amorphous carbon, it exhibits both types of hybridizations (i.e. sp^2 and sp^3).

1.2.1 Allotropes of carbon

Although carbon had been known since many centuries but the main breakthrough in the field of carbon science is noteworthy after the discovery of fullerenes, carbon nanotubes (CNTs), and graphene.

The youngest allotrope of carbon, graphene, has a planar arrangement of carbon atoms that are packed in a two-dimensional hexagonal lattice fashion.[3] Andre Geim and Konstantin Novoselov were jointly awarded with the Nobel prize in 2010 for graphene.[4] Its extended honeycomb network is the basic building unit of other important carbon allotropes such as 3D graphite, that is formed by the stacking of several layers of graphene, 1D nanotube, formed by rolling the graphene and the 0D fullerene that may be obtained by wrapping of graphene.[5]

Fullerenes are the allotropes that comprise of carbon atoms only. The most stable and prominent allotrope of fullerene is C60.[6,7] It consists of a spherical shape with sixty

structurally equivalent sp^2-hybridized carbon atoms that resemble a football. In 1996, Robert F. Curl Jr., Harold W. Kroto and Richard E. Smalley were jointly awarded the Nobel prize of chemistry for the discovery of fullerenes.[8] The buckybowls are bowl shaped hydrocarbons termed as the cap structures of CNTs. It forms a family of curved aromatic compounds with fullerenes and CNTs.[9,10] Due to their chemical and physical properties, buckybowls have drawn tremendous amount of attention of the researchers.[11,12] With the aid of computations, some studies help to understand some novel properties of buckybowls.[13-16]

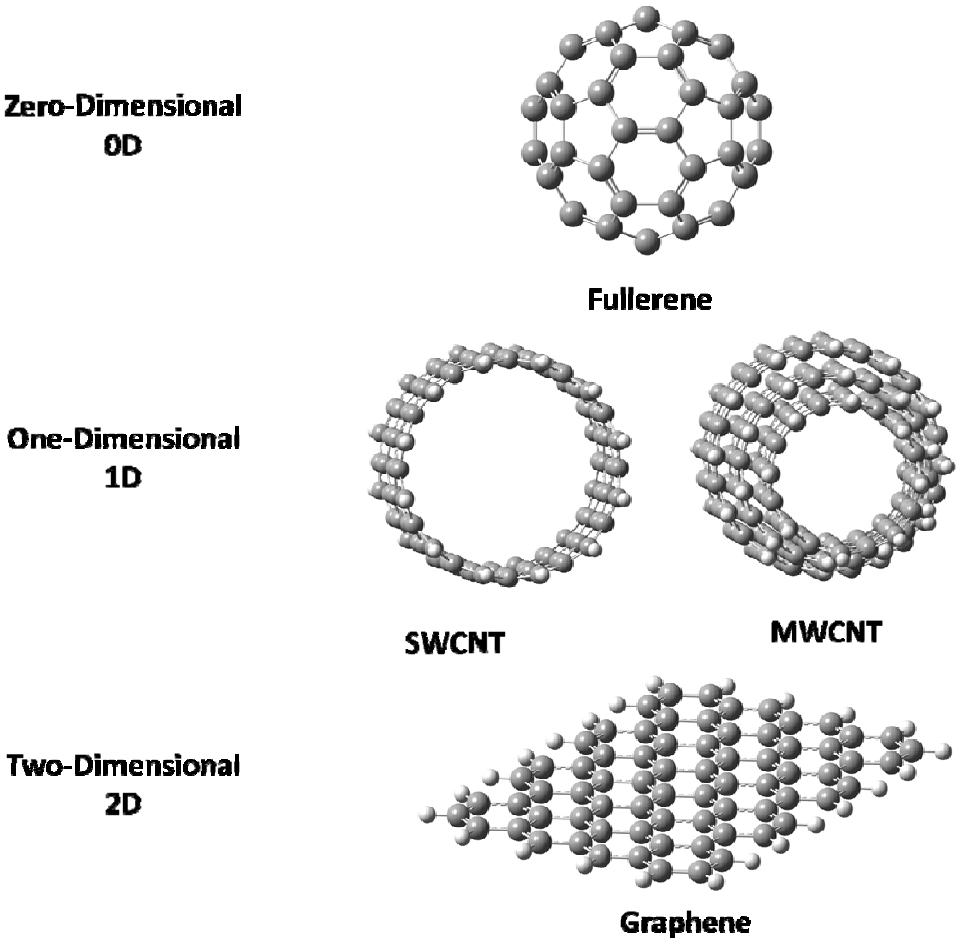

Figure1.5: Structures of carbon allotropes.

1.2.2 Graphene: Historical Background

Andrew Giem and co workers at the University of Manchester discovered the graphene using the scotch tape method.[17,18] This discovery of graphene led to a revolution, thereafter, it was considered as a next generation material. The electrons in graphene follow a linear dispersion relation and act like massless relativistic particles.[19] This led to a number of very distinct (idiosyncratic) properties like quantum hall effect[20-23], ambipolar electric field effect[17,24], good optical transparency[25-27] etc.

Due to its unmatched high carrier mobilities (200 000 cm^2/Vs),[28] high thermal and electrical conductivity,[29-31] graphene-based electronic devices can revolutionalize the electronic industry. In the field of telecommunication and defence technology, the unparalled properties of graphene like strong non-linear optical conductance and emitters paved the way for the fabrication of good terahertz detectors.[32-34] Thus, in the present scenario, it is the graphene that has bridged the gap between the different branches of science like engineering, chemistry, physics, and materials science.[35-37]

1.2.3 Graphene

Graphene is a mono-atom-thick planar sheet of carbon atoms with sp^2 hybridization exquisitely organized in a honeycomb lattice. Graphite is said to be formed by a stack of a large number of sheets of graphene having 3.35 Å interplanar spacing; approximately 3 million layers of stacked graphene sheets can be observed in 1-mm thick graphite flake. This is the thinnest material that can be imagined in the universe. Though it is the lightest known (density of 0.77 mg/m^2) material yet it is the strongest material measured, with strength nearly 100-300 times higher in comparison to steel. On account of its astounding

structural and physicochemical properties[38-42], this exhilarating novel material quickly instigated mammoth interest in many disciplines like energy storage and conversion, [46,47] field emission display,[48,49] high-frequency electronics, nanoelectronics[43-45] and transparent conductors.[50]

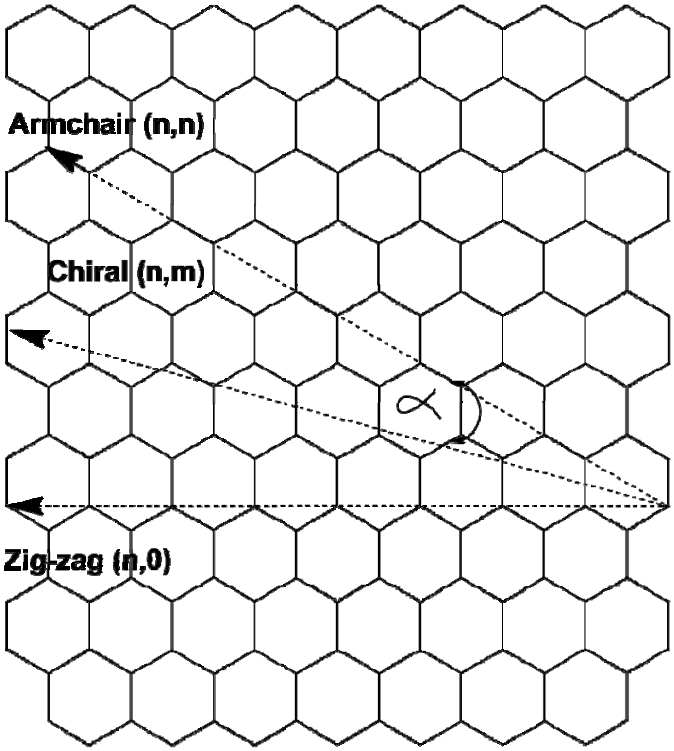

Figure 1.6: The honeycomb structure of graphene. The chiral angle (α) determines the type of nanotube.

1.2.4 Effect of Doping in Graphene

Significant implementation of graphene is in the field of electronic devices that demands graphene to perform diverse electronic functions. So, tuning the electronic properties of graphene is quite essential. Hence, doping by different procedures like hetero-atom substitution, edge functionalizations, chemical absorption, and defects were found to be efficacious in order to tune the electronic properties. With the doping of N- or B-atoms,

the single walled carbon nanotube (SWCNT) may behave as n-type or p-type respectively. Doping can also transmute the electrical properties of graphene.[51]

Martins et al. [52] investigated the transport and electronic properties of the boron doped graphene. Employing the ab-initio methodology, they exemplified the presence of boron atom at the GNR edges which may be the cause of metal to semiconductor transition. Not only this, they also recommended that with suitable doping, the electronic current can also be fine tuned. Gunlycke et al. [53] outlined that by using the density functional theory (DFT) calculations, the graphene, precisely the zig-zag nanoribbons which were terminated by various atoms had an important influence on the electronic structures of these graphene at a short distance away from the fermi-level. The zig-zag nanoribbons passivated with the hydrogen atoms or different groups leads to the spin polarization in equilibrium, while the nanoribbons passivated with oxygen or imine groups were found to be unpolarized thereby providing a non-identical low bias transport characteristics. Sodi et al. [54] investigated the atomic substitution and they performed the edge functionalizations in graphene nanoribbons. The oxygen substitution in the zig-zag nanoribbons displayed the semi metal transition extremely well. It is explored in the investigation that double-edge functionalization is responsible for the reduction in semiconductor gap. The transition from semiconductor to metal can be observed with the N, B and pyridine-like bulk substitution in graphene.

Since the last decade, different zero dimensional (0D) and one-dimensional (1D) nanomaterials are the key stimulus for the novel and desirable sensor development.[55-58] These include quantum dots,[59,60] carbon nanotube,[67-70] nanoparticles,[61,62] nanowires[63-66] and a lot more.

1.3 Biosensors

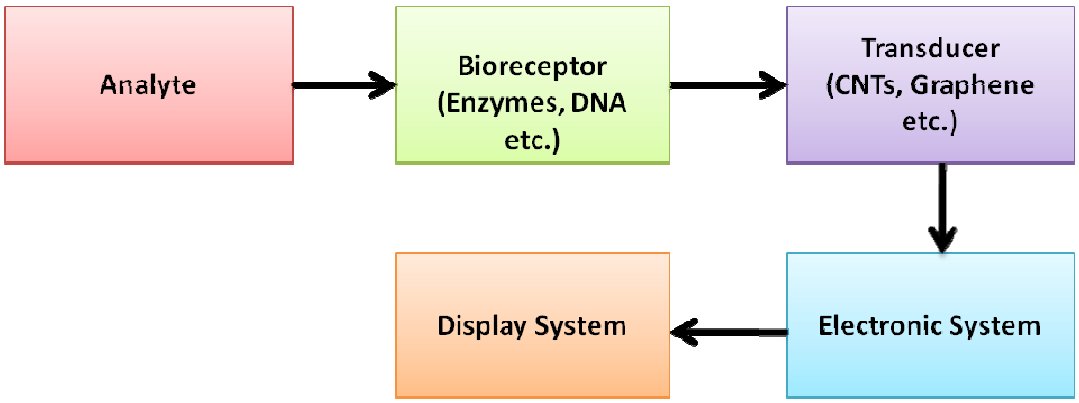

Figure 1.7: Block diagram of a biosensor

Analyte: It is a substance of our interest that needs detection. For example, glucose is an 'analyte' in a biosensor to detect glucose level in a sample.

Bioreceptor: It is a molecule that particularly identifies the analyte and is termed as a bioreceptor. A bioreceptor may be an enzyme, aptamer, antibody or deoxyribonucleic acid (DNA). The process involved in the generation of signal (in the form of heat, light, change in pH, charge or mass change, etc.) upon interacting with the analyte is termed bio-recognition.

Transducer: The transducer is the main part of a biosensor and converts one form of energy into another. In a biosensor, the role of transducer is to convert the bio-recognition event into a measurable signal. Different carbon nanostructures such as carbon nanotubes and graphene, can be used as a transducer.

Electronics System: This is the part of a biosensor that processes the transduced signal and generates it for display. This system is comprised of complex electronic circuits that execute signal conditioning such as amplification and conversion of signals from analogue into digital form.

Display System: The display consists of a user interpretation system such as the liquid crystal display of a computer or a direct printer that generates numbers or curves understandable by the user. This part often consists of a combination of hardware and software that generates results of the biosensor in a user-friendly manner. The output signal on the display can be numeric, graphic, tabular or an image, depending on the requirements of the end user.

Sensors have changed and instilled a great deal of interest in many fields that may range from detection of gas molecules to the biological entities which may be detected in real-time using the chemical signals. Generally, a sensor consists of a transducer and an active sensing element. A sensor may produce electrical, thermal, optical or magnetic signal. The sensing element detects the analyte and is primarily responsible for it, however it is the transducer which converts the chemical or biological event into a suitable signal that may be employed with or without amplification to acertain the analyte.

In 1956, first biosensor was developed by Leland C. Clark Jr. #He is known as the 'father of biosensors'. The biosensor usually contains biological sensing material like proteins (e.g., enzymes, cell receptors, antibodies), oligo- or polynucleotides, microorganisms, or even whole biological tissues.[71,72]

Generally there are two main parts of biosensors that are common: a transducer and a receptor. A receptor is bioactive molecule while transducer is responsible to convert the chemical information from the recognition event into a measurable signal. The receptor is excluded in diverse biosensors because the direct interaction of the analyte with the transducer takes place and produce measurable changes in its properties. Therefore, graphene and its co-members may be used as the transducing platform in

biosensing.[73,74] In the case of in-vitro biosensing, the sample solution (such as blood serum, urine, milk products etc.) is dropped at the top of the biosensor, and the output signal recoded provides useful information on the composition of the solution. However, in vivo biosensing pertains to the dynamic systems to estimate the spatial distribution of the concentration of an analyte in a living organism.

1.3.1 Detection of Nucleic Acid

For the detection of single stranded DNAs (ssDNA), and double stranded DNAs (dsDNA), its subunits like nucleobases, nucleotides; graphene has been used for sensitive and selective electrochemical detection. Such predictions with the aid of DNA sensors paved a new way for the DNA sequencing and DNA analysis. The four nucleobases (Adenine, Cytosine, Guanine, Thymine and Uracil) have distinct oxidation potentials. Huang et al. with the help of reduced graphene oxide and functionalizing it with –COOH groups electrochemically detected Guanine and Adenine.[75] The high sensitivity in this case is acquired due to the outstanding properties of reduced graphene oxide (rGO), electrostatic attraction between the positively charged nucleic bases and negatively charged –COOH groups. The π-π interaction is equally important and plays the central role. Guanosine was successfully detected using the rGO-chitosan electrode.[76]

Hypoxanthine is a purine derivative. A sensor to detect hypoxanthine was constructed using rGO.[77]

1.3.2 Detection of other biomolecules

The deficiency of dopamine may leads to Parkinson's disease. Dopamine (DA) is an important neurotransmitter, deficiency of which underlies Parkinson's disease. DA detection is challenged by its low physiological concentration (0.01 mM–1 mM) and interference from much more abundant ascorbic acid (AA) and uric acid (UA). A chitosan–rGO composite electrode for DA detection was demonstrated by Wang et al.[78] Cholesterol, one of the main part of cell membranes[79] leads to some very serious health issues like cerebral thrombosis, heart diseases, and atherosclerosis. The rGO sheet, used to develop the very sensitive amperometric sensor to detect cholesterol was successfully developed.[80]

1.4 Carbon nanotubes

1.4.1 Introduction

The carbon nanotubes were discovered by the Japan electron microscopist, Sumo Iijima,[81] in the year 1991 which may be obtained by rolling the graphene sheet. He came up with such a beautiful discovery while he was studying the material deposited on the cathode during the arc-evaporation synthesis of fullerenes. The CNTs are closed cylindrical shape that may be obtained by rolling the graphene sheet. They were known to exist with a diameter varying between 1 to 3nm.[82] Depending upon the curvature and chirality, these CNTs have different electronic, physical and chemical properties. The nanotubes are generally classified into different categories based upon the chirality such as armchair nanotube (n,n), zig-zag nanotube (n,0) and chiral nanotube (n,m). They are also classified depending upon the number of walls associated with nanotubes like single

walled carbon nanotube (SWCNT), double walled carbon nanotube (DWCNT), multi walled carbon nanotube (MWCNT).

1.4.2 Properties of Carbon nanotubes

It is well known that carbon atoms in CNTs have a hexagonal lattice pattern where each carbon atom is covalently bonded to the three neighbouring carbon atoms via sp^2 hybridization. Hence the 4^{th} valence electron which is free in each of these units, gets delocalized over all the atoms and thereby it contributes to the electrical nature of the CNTs. CNTs behave as metals or semi-metals based on the chirality. They exhibit high surface area, high aspect ratio, and noteworthy high mechanical strength. The CNTs can be utilized in transistors, switching applications and in other advanced electronics.[83] It can also be used as an emitter. The CNTs, as an emitter can work at a lower threshold voltage and this makes it superior among other materials. Not only the electronic and mechanical properties but also the thermal properties are quite interesting of these carbon nanotubes. Though their size is quite small, the quantum effects are remarkable and specific heat at low temperature and thermal conductivity validate the presence of the one-dimensional quantization of phonon band structure of CNTs. The nanotubes have some very outstanding properties e.g. the tensile strength of CNTs is 100 times more than that of steel. Also, the electrical and thermal conductivities are close to copper.[84,85] CNTs are considered as one of the strongest material in nature. The literature suggests that CNTs are extremely strong materials, particularly in the axial direction.[86] Sinnot et al. performed the theoretical work to study the mechanical properties of CNTs[87], and reported that Young's modulus of SWNTs could be comparable with that of a diamond.

The CNTs can be efficiently used as electrochemical biosensors due to their outstanding properties like electron transfer, electrical and electrochemical properties. In the field of biosensing, owing to some remarkable properties like small size, large surface area, high conductivity, chemical stability, sensitivity and fast electron transfer rate make them ideal for the use in this field. Recently, Shobha et al.[88] explored that the early stage detection of the prostate cancer is feasible via the functionalizations of the DNA strands that detect the prostate specific antigen (PSA) which is found in the blood samples.

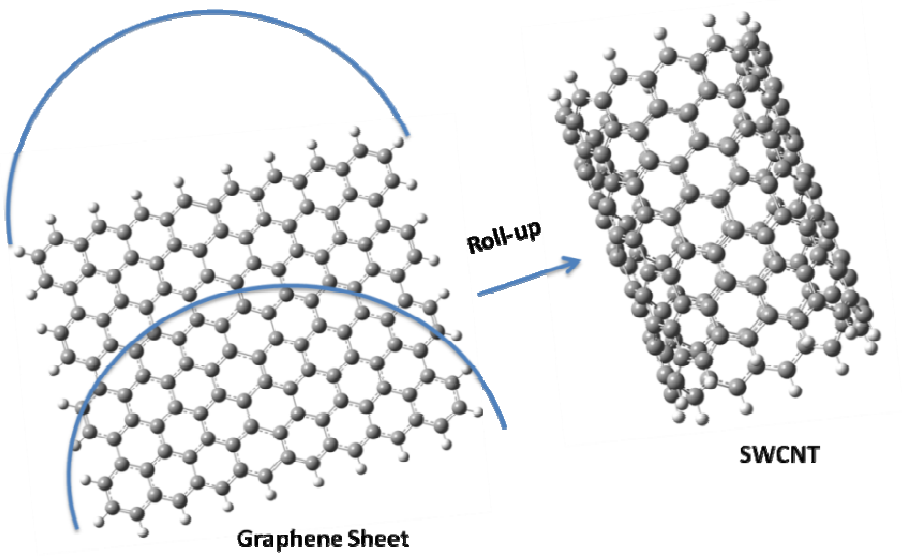

Figure 1.8: Carbon nanotubes are obtained by wrapping a graphene sheet.

The diameter of the tube can be expressed as:

$$d_t = a(n^2 + nm + m^2)^{\frac{1}{2}} \qquad (1.1)$$

where, a is the C-C bond distance, n and m are the chiral indices.

1.5 Non-covalent Interactions

The covalent bond is said to be formed between the two proximate atoms as a result of electron sharing between them. The idea of covalent bonding was traced many years earlier where different authors furnished a deeper intuition to the covalent bonds.[89-93] One of the prospective implementation of non-covalent interaction in the field of biology is the field of drug delivery system. Therefore, indispensably, these interactions (i.e. bimolecular) with carbon nanostructures (CNSs) via non-covalent interaction are accountable. Since in the CNSs, the aromatic rings of carbon are usually found therefore, the interactions like cation-π, CH-π and π-π are commonly found in comparison to hydrogen bonding. Generally the chemists are interested to notice the breaking and formation of bonds.

For their distinguished work in supramolecular chemistry, in 1987, Jean-Marie Lehn and Charles J. Pedersen, were jointly awarded the prestigious Nobel prize in chemistry, which mainly involves noncovalent type of interactions.[94] Since then, this interaction has been studied extensively. It was the landmark in the study of noncovalent interactions. The saga of the non-covalent interaction dates back in 1870, when Van der Waals articulated the dissimilitude noticed among the real gas and ideal gas state function which are responsible for the attracting forces between gas molecules.[95] These forces of attraction are because of the non-bonded interactions which were termed as Van der Waals interaction. F. London in the year 1930, after the discovery of quantum mechanics, took major steps in expounding these inter-molecular forces.[96] Later, on counting other non-bonded interactions, like cation-π, π-π and hydrogen bonding, etc. these interactions were termed as non-covalent interactions. The non-covalent interactions are said to be

transpired from the interactions between induced dipoles or permanent like (a) permanent dipole and induced dipole, (b) permanent dipole and permanent dipole, (c) instantaneous dipole and induced dipole. The overall interactions energy of the non-covalent interaction is said to be the union of different energy integrants like electrostatic, dispersion components, charge transfer, exchange-repulsion and induction. The individual strength of these non-covalent interaction might be minuscule but then contribution to study the inclusive stability becomes note worthy.[97,98] Therefore it can be said that these non-covalent interactions result in the emergence of supramolecular assembly, while the covalent interactions results to form a classical molecule. In the case of CNSs, the cation-π, π-π interactions and XH-π interactions are the common non-covalent interaction.

The noncovalent interaction can be mainly classified into two categories: (a) interaction between ion and a neutral molecule and (b) interaction between the two neutral molecules. For the crystal packing and molecular recognition, the interactions like cation-π, π-π interactions and XH-π interactions play a key role. Apart from the above mentioned interactions, the anion neutral and cation neutral molecule non-covalent interactions that are presumed to be stronger also play a pivotal role in molecular recognition and albeit structural functions, however their role was not studied in detail so far. The cation neutral molecules interaction can be classified as (a) cation-hydrocarbon (saturated) interactions, (b) cation-π interaction, and (c) cation lone pair. In controlling the structure and function of macromolecular system, these three interactions are said to play the central role.

#The significant role of cations have been studied extensively in material sciences, host-guest complexes in biology and in inorganic.[99] The magnitude, strength, and the nature

of cation interaction with the neutral molecules are very sensitive to the neutral molecule involved and nature of metal. The π-system with mono-cation is electrostatic in nature and is quite different from the di-cationic interaction with the π-system.[100] With the increase in the π-system, from the earlier studies it can be concluded that the interaction energy increases.[101,102] For example, the energy of Li^+ with benzene, anthracene, tetracene, and naphthalene are 35.40, 41.40, 38.00, 39.60 and kcal/mol respectively.[101]

1.5.1 Hydrogen bonding

The Hydrogen bonding is said to be present between the electronegative atom and the intermolecular moieties of hydrogen. It is quite weak but the combination of several types of these interactions brings a required stability. Hydrogen bond among the noncovalent interactions is one of the most studied noncovalent interactions. There are a large number of studies based on hydrogen bonding and these depicts a large variety and variation in hydrogen bonding that depends on the acceptor and donor. In most of the cases, it is hugely controlled by the electrostatic forces and also with contributions from other components. The hydrogen bonding present in different clusters viz. linear, standard forms and circular forms was investigated and it is explored that the interaction energy depends on cluster size and not on the arrangement of the clusters.[103,104] The hydrogen bonds were categorized into strong (O-H.....O or F-H.....H) and these have interaction energies greater than 10 kcal/mol, normal with interaction energies of up to 5 kcal/mol and also the non-classical hydrogen bonds (X-H.....M,X-H.....H-M,X-H.....H-B).[105-107]

1. 5.2 Cation-π interactions

Cation-π interaction is a strong noncovalent interaction which exists between a cation and a π-system.[108,109] Kebarle and co-workers made the first evaluation of K^+ ion interaction with benzene and have effectively manifested that K^+ ion shows a small preference to bind to benzene in comparison to the water molecule.[110] The presence of cation-π interactions in biological systems and their relevance was demonstrated by many groups.[108,109,111-113] The analysis based on protein database performed by Petsko and co-workers [113] on 33 high resolution protein structures indicated that the positively charged side chain of amino groups of lysine (Lys), glutamine (Glu), histidine (His), asparagines (Asp) and arginine (Arg) are likely to have good interaction. These cation-π interaction also accord to the stability of protein-ligand and protein-DNA complexes.[114-116]

Rodgers, Armentrout and their co-workers have contributed enormously in comprehending the role of cation-π interactions by some important studies.[117-122] The calculated binding energies obtained theoretically were found to be in good agreement with the experimentally obtained results.[117,122]

Zhu et al. have carried out a theoretical study to elucidate the cation-π and cation-σ interactions of nucleobases (A, C, G, T, U) with alkali and alkaline earth metals.[123] A similar work was carried out by Munoz et al. that uses the Hartree Fock (HF) and MP2 calculations to study the interaction of divalent and mono metal ions with nucleobases.[124] Ryzhov and Dunbar studied the Na^+ and K^+ affinities with phenylalanine, tyrosine and tryptophan using kinetic method.[125] Sastry and co-workers carried a systematic and by far the most comprehensive survey of binding of alkali and alkaline earth metals with the aromatic side chain motifs with a special attention to

cation-π interactions.[126] The predilection of binding of metal ion to π-systems, such as aromatic amino acids[129,130] benzene and substituted benzenes,[130-132] poly-aromatic hydrocarbons[127,128,134-136] and heteroaromatics[137,138] were studied thoroughly.

Also of interest are implicit and explicit metal ion solvation processes [139-142] that involve a healthy competition between the π and non-π cation binding site, cooperativity of the cation-π interaction,[143,144] are also studied extensively in great detail. A comprehensive review on cation-interaction written by Sastry et al.[145] narrates the significant role and importance of cation-interaction in different branches of science.

1.5.3 Stacking interaction

When the two aromatic entities are placed parallel or in perpendicular orientation then the interaction that exists between these two moieties are said to exhibit the stacking interaction (π- π) and CH- π type of interaction[146-151]. Few examples that illustrate that the stacking interaction plays a role of central importance are: (a) Vertical base-base interaction which stabilizes the double helical structure of DNA[152], (b) Conformational preference and binding of macrocyclic compounds like diarylnaphthalenes[153-155], (c) Complexation in host-guest systems, (d) Catalytic hydroformylation[156], (e) Catalytic formation of elastomeric polypropylene[157], (f) Asymmetric cis dihydroxylation of olefins[158] (g) Drug-receptor interactions.[159] etc.

Thus, it may be conclusively said that this subtle but very important interaction is ubiquitous in multifarious fields of science ranging from structural biology,

supramolecular science, drug design, conformational analysis, asymmetric catalysis etc. and also it has become an independent area of research.[146-159]

In condensed phase, the aromatic moieties orient themselves in different fashion however it is very difficult to say a confirmed geometrical orientation exhibited by the aromatic rings to have π-π interaction. Various methods are used to identify π-π interactions in chemical and biological systems.[160-165] The three most common orientations that can be observed in stacking interaction are:- (i) T-shape orientation, (ii) Offset or parallel displaced (PD) orientation and (iii) Sandwich or S type orientation.

The π-π interaction has also been analysed to confirm the thermal stability of thermophilic proteins.[166]

Although there are a large theoretical studies on π-π interactions but these are limited to flat aromatic systems and few reports are available for curved aromatic systems like corannulene.[167] So there is a scope for both the experimentalists and theoreticians to explore this crucial interaction.

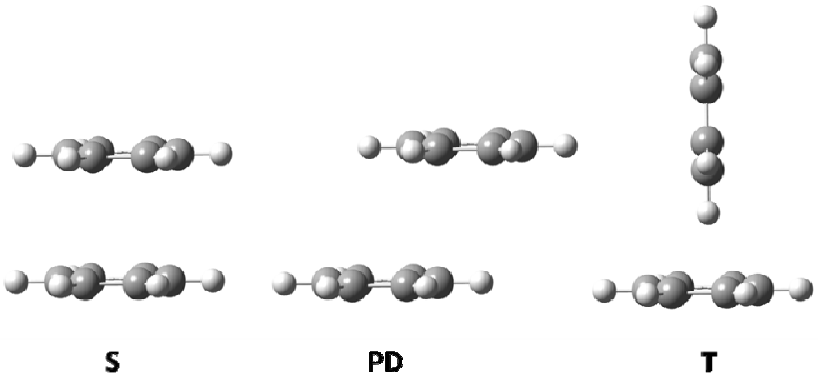

Figure 1.9: Three possible orientations in stacking interaction.

1.6 Review of Literature

Graphene is a planar form of carbon atoms designed in a two-dimensional hexagonal lattice fashion. It has emerged as the most dominating allotropes of carbon during the last few years. Its extended honeycomb network is the basic building block of other important allotropes such as 3D graphite formed by the stacking of several layers of graphene; 1D nanotube, obtained by rolling the graphene and the 0D fullerene prepared by wrapped graphenes.[168] Graphene is being used in the designing of new nanomaterials for energy storage devices, fuel cells and biosensors owing to its high stability, elasticity and electromechanical modulation.[169-171] Also, graphene exhibits extraordinary electronic properties in comparison to many of the conventional materials; the highly conductive graphene becomes an insulator after hydrogenation. This hydrogenation of graphene is highly reversible; the intrinsic conductivity as well as the structure of graphene can be restored on annealing.[172-174] Graphene is also an important material in nanoscale electronics due to its compatibility with industry standard lithographic processing. The electron mobilities are up to 150 times greater than Si, and the thermal conductivity is approximately twice that of diamond.[175] Thus one can say that graphene has revolutionalized the technology.

Graphene sensors have emerged as another area of recent interest. The chemical and physical properties of graphene make it a promising candidate that can be used as a sensor to detect different gases such as H_2, NO_2 and NH_3.[176] Schedin et al., in their experimental results, illustrated that graphene based sensors allow the sensitivity levels such that the adsorption of individual gas molecules could be detected accurately.[177] Graphene-polyaniline nanocomposite is found to be a good sensor for H_2 gas while

nitrogen doped graphene find its application in electrochemical biosensing.[178] It is also shown that, through functionalization, properties of graphene can be modified. The functionalization of graphene with hydrogen, oxygen or other chemical groups is of prime importance as a way to engineer different properties of graphene. A recent study reveals that with controlled epoxide functionalization, graphene can be used as a starting material for diverse chemical functionalization by chemical modification of the epoxide group. The functionalization of graphene and single-walled carbon nanotubes (SWCNT) with individual 3d transition metal atoms were also modeled using density functional theory calculations (DFT).[179-186] The capability to detect single bio-molecules with high accuracy and efficiency is of prime importance in many areas of environmental science, biology and chemistry.[187-193] Efficient bio-sensors are expected to contribute to the improvement of medicine and medical treatment.[189]

Nano-materials, due to their extreme sensitivity of the electron-transport properties in confined materials to external perturbations, form an excellent technological platform for single-molecule recognition.[194-197] Recently, graphene nano-ribbon (GNR) has emerged as a suitable candidate for making sensors for single small molecules, such as H_2, H_2O and NO. This concept is based on measuring a variation in the source-drain current of a GNR based field-effect transistors (FETs) originating from the covalent bond formed between the molecule to be detected and a defect (or an edge) of GNR.

The interaction of the biomolecules such as nucleic bases on the surface of GNR and CNT has attracted many researchers. In particular, the DNA-CNT interaction has cast its spell in the research community due to its application in various fields such as DNA sensing, DNA sequencing and drug delivery.[198-201] It has also been found that the

determination of a patient's DNA sequence can even reveal his risk of falling ill with particular diseases and it also helps to design "personalized medicine", and it is therefore the DNA sequencing that appears to be one of the most potential applications for the carbon nanostructures.[202-204] Sensors for amplified detection methods based on CNT biomolecule composites is an area of recent interest, and such sensors can be efficiently used to detect various carbon nanostructures as well as different biomaterials such as DNA, protein, and so on.[205]

Also, DNA-functionalized carbon nanotubes (CNTs) form the basis for not only a new class of chemical sensors but also for the molecular electronic devices. An ultrasensitive graphene embedded nano channel device which effectively controls the motion of nucleobases via π-π interaction was also reported.[206] Zheng et al.,[207] constructed a carbon nanotube-based DNA biosensor for sensing the phenolic pollutants.

Many research groups have focused on determining the DNA-CNT interaction and tried to explore the strength of binding of different nucleosides, nucleobases, and nucleobases pairs on the carbon nanotubes and graphene, in both experimental and computational studies.[208-212] The different binding energy orders for different studies are found in many experimental studies and it is understood that this may be due to the different experimental conditions applied. For most cases, in computational studies, the order is G > A > T > C > U, and in some cases, the order is G~A~T~C > U.

The dispersion forces in the dispersion interaction are the most important interactions in molecular systems that are not addressed well in several DFT approaches. Efforts were made by the several research groups [213-225] to precisely incorporate dispersion in the correlation term of DFT. There were several studies of interaction of nucleic bases with

CNT or graphene which however did not consider the dispersion interaction into account. Some early works based on LDA scheme of DFT, also lack dispersion correction. However the recent studies adopted either classical FF (force field) or dispersion corrected DFTs to consider the dispersion factor. It is believed that the π-π stacking plays a key role in the binding of nucleobase to graphene or CNT, dispersion therefore can play a significant role in determining the binding structure and BE (Binding Energy). So, one can precisely say that different approaches lead to different results. Therefore the past studies can be broadly classified into two categories: those performed with methods that consider dispersion, and those which do not consider dispersion-corrected methods. Semi-empirical QM methods are based on ab initio methods but include empirical parameters to speed up the calculations, examples include AM1.[226-230] In computational quantum chemistry and physics, DFT has been widely used, due to its relatively low computational cost compared with high level ab initio methods and high accuracy compared with semi-empirical methods.

In 1964, Kohn and Hohenberg published the first paper on DFT in which they substituted the many electron wavefunction with the electron density and reduced the number of variables. One year later, Kohn and Sham in 1965 improved the Hohenberg and Kohn's theory by introducing effective potential that included external potential, exchange and correlation interactions.

Gowtham et al.,[231] studied the adsorption of nucleobases (A, C, G, T and U) on graphene using MP2 and local density approximation (LDA). In a later work, Gowtham et al.,[232] also studied the adsorption of the same nucleobases on a (5,0) CNT, using the same approach except that the BE calculation was only done with LDA only, and not

with MP2. The order of the BE was found to be the same, i.e., G>A>T>C>U with the values being 47.28, 37.63, 32.81, 27.98 and 27.02 kJ/mol, respectively. Their results confirmed that the BEs for CNT were much smaller than those for graphene, that was attributed to the larger curvature of the CNT and resulting smaller area of contact. Meng et al.[233] first optimized the structures using CHARMM FF which includes an empirical description of dispersion interaction, but dispersion was neglected again during the re-optimization step using LDA.

Meng et al.[234] used a different approach (time dependent LDA method) to study the binding between DNA nucleosides and a CNT (10,0). From these simulations, the optical absorbance spectrum for DNA nucleosides were obtained, which were used to determine the preferred orientation of the nucleosides on the CNT. The dependence of BE on CNT chirality was studied by Wang *et a*l.,[235] using LDA. They considered two connected adenosine monophosphates with the phosphate groups terminated by H atoms. The resulting molecule was neutral and was taken to interact with different CNTs, including five (m,0) zigzag tubes with m = 7,8,9,10,17 and four (n,n) armchair tubes with n=4,5,6,7. Periodic boundary condition using supercell approach and the linear combination of numerical atomic orbitals (LCAO) basis set with double-zeta polarizations were used. In another work, Wang [236] considered all four DNA nucleobases interacting with two types of CNTs: (5,5) and (10,0). Same as his first work (Wang *et al.*, 2007), for each type of CNT, only a small part was made to interact with the nucleobases. The BSSE-corrected BE for the C(5,5) CNT hybrid in vacuum was 46.46 kJ/mol which is quite different from Wang's former study (Wang *et al.*,[237] 2007) in which the BE for the same system was determined to be 32.76 kJ/mol. The order of the

BE between nucleobase and CNT in the gas phase was found to be G>A>T>C for both CNTs. This is in agreement with the DFT studies of Gowtham et al., on the interaction of nucleobases with graphene and (5,0) CNT (Gowtham et al., [231,232]), and also with the MM results of Meng et al.,[234] for the interaction of nucleosides with a (10,0) CNT.

Recent works using dispersion-corrected DFT also gave rise to different results, possibly due to the difference in ways of incorporating dispersion interaction in these methods. The choice of basis sets can affect the BE evaluation, even with the same method (Shukla et al.[238]). In addition, it is also found that basis set superposition (BSSE) can be large and has to be taken into account (Tournus et al.[239]). Performance of simulation methods and basis set are still being widely evaluated in the computational chemistry.

Though a large number of dispersion-corrected methods exist in literature however benchmarking has been performed by some of them.[240-242] Among these methods, Minnesota density functional developed by Truhlar's group, e.g., M05, M05-2X, M06, M06-L, M06-2X and M06-HF, are based on meta-GGA approximations [218,243-246].

Swathi and Chandra Shekar (with ωB97XD functional) examined physisorption of nucleobases on coronene as a model of graphene (Chandra Shekar et al.[247]). Different initial configurations (ICs) were considered while the separation distance was maintained at 3Å in all initial configurations (ICs). Geometry optimization was carried out at ωB97XD/6-31G(d,p) level followed by a single point energy (SPE) calculation at ωB97XD/6- 311+G (d,p). The order of the BSSE corrected BEs was determined to be G>T>A>C>U with the values of 75.73, 66.53, 65.27, 64.43 and 56.48 kJ/mol, respectively.

Antony and Grimme studied the influence of damping on various interactions in great detail.[222] Vovusha et al.[248], studied the interaction of nucleobases with graphene using M05-2X and M06-2X functional. Vovusha et al., in their study of graphene model, included 54 carbons with 18 hydrogen atoms capping the edge carbons. Geometry optimizations were all performed at M05-2X/6-31G(d) level and BEs were evaluated using both M05-2X and M06-2X methods with 6-31+G(d,p) and 6311++G(d,p) basis sets. The separation distance between nucleobases and graphene in the optimized structures was determined to be 3.2-3.5 Å which is close to previously reported results. Results (energies values) obtained using M06-2X were considerably larger than the ones obtained using M05-2X method. The order of the BE using M05-2X was determined to be G>C=T>A>U and G>C>T>A>U respectively with 6-31+G(d,p) and 6-311++G(d,p) basis sets. When M06-2X was used for the BE calculation, the order was changed to G>T>A>C>U and G>T>C>A>U respectively using 6-31+G(d,p) and 6-311++G(d,p) basis sets. This demonstrates the great effect of method and basis set on the value and order of the BE.

Umadevi et al.[249] studied in detail the interaction of aromatic amino acids, nucleic bases and other small molecules in detail and reported the order of binding for nucleobases with graphane in the order G > A > C > T > U.

Table 1.1: Some experimental studies based on different types of analyte and carbon nanostructures involved.

Types of Analyte	Carbon nanostructures	Target analyte	Reference Number
Protein	SWCNT	H63D mutation in the HFE gene	[250]
Protein	SWCNT	Immunoglobulin E (IgE)	[251]
Protein	Graphene	Bovine Serum Albumin (BSA)	[252]
Protein	(rGO)	Matrilysin	[253]
Nucleic acid	SWCNT	ssRNA	[254]
Nucleic acid	SWCNT	ssDNA	[255]
Nucleic acid	SWCNT	miRNA	[256]
Nucleic acid	GO	ssDNA	[257]
Nucleic acid	GO	SsDNA	[258]
Nucleic acid	GO	ssDNA	[259]
Nucleic acid	GO	ssDNA	[260]
Nucleic acid	GO	ssDNA	[261]
Nucleic acid	GO	ssDNA/miRNA	[262]
Nucleic acid	GO	SNP	[263]
Nucleic acid	GO	SNP B	[264]

Table1.2: Different types of sensors based on various carbon nanostructures with linear range.

S.N.	Analyte detected	Sensor type	Sensing materials	Linear range	Ref. No.
1	Clinical applications Glucose	Electrochemical sensor	Graphene copper NP	0.45 mM	[265]
2	Cholesterol	Electrochemical biosensor	Graphene	50-300μM	[266]
3		Electrochemical biosensor	Platinum-palladium-chitosan-graphene hybrid nanocomposite	2.2-520 μM	[267]
4		Optical biosensor	Cerium-oxide graphene composite	12 mM to 7.2 mM	[268]
5		Electrochemical biosensor	Graphene-PVP-PANi	50 mM to 10 mM	[269]
6	H_2O_2	Electrochemical sensor	Palladium NP-graphene nanosheet film	0.1-1000 μM	[270]
7		Electrochemical biosensor	Graphen-palladium -horseradish peroxidase	25-3500 μM	[271]
8		Electrochemical biosensor	Gold NP-graphene nanosheet film	0.3 μM to 1.8 mM	[272]
9	DNA	Magnetic field (Hall effect)	Graphene-PMMA	1×10^{-3} to 10 nM	[273]
10	Dopamine	Electrochemical sensor	Graphene and PVP	5×10^{-10} to 1×10^{-3} M	[274]
11		Electrochemical sensor	Amino-group functionalized Fe3O4 nanoparticles on graphene	0.2-38 μM	[275]

			sheets		
12		Electrochemical sensor	Graphene	5.00-710 μM	[276]
13	Ascorbic acid	Electrochemical sensor	Amino-group functionalized Fe_3O_4 nanoparticles on graphene sheets	5-1600 μM	[275]
14		Electrochemical sensor	Graphene	9.00-2314 μM	[276]
15	Uric acid	Electrochemical sensor	Amino-group functionalized Fe_3O_4 nanoparticles on graphene sheets	1-850 μM	[275]
16		Electrochemical sensor	Graphene	6-1330μM	[276]
17	CEA	Electrochemical immunosensor	Graphene-gold NP -carboxyl groups	0.010-50 ng mL^{-1}	[277]
18		Electrochemical immunosensor	Graphene-gold NP-silver NP	0.010-120 ng mL^{-1}	[278]
19	α-fetoprotein	Electrochemical immunosensor	Graphene-gold NP -carboxyl groups	0.016-50 ng mL^{-1}	[277]
20		Electrochemical immunosensor	Doped graphene sheets	0.05-30 ng mL^{-1}	[279]
21	Thrombin	Optical biosensor	Aptamer and graphene nanocomposite	1-100 fM	[280]
22		Optical aptasensor	Graphene	62.5-187.5 pM	[281]
23	PSA	Electrochemical immunosensor	Graphene-methylene blue/ chitosan nanocomposite	0.05-5.0 ng mL^{-1}	[282]
24		Electrochemical immunosensor	Graphene-silver hybridized mesoporous silica NP	0.01-10 ng mL^{-1}	[283]
25		Electrochemical biosensor	Graphene nanosheets	2 pg mL^{-1} to	[284]

			-horseradish peroxidase functionalized with gold NP	2 μg mL^{-1}	
26	IL-6	Electrochemical immunosensor	Graphene-gold NP	1-40 pg mL^{-1}	[285]
27	MMP-2	Electrochemical immunosensor	Gold NP-nitrogen doped graphene composites	0.5 -50,000 pg mL^{-1}	[286]
28	cTnI	Electrochemical immunosensor	Platinum NP/graphene composite	0.01-10 ng mL^{-1}	[287]
29	Environmental applications Malachite green	Electrochemical sensor	Graphene quantum dots -gold NP	4.0×10^{-7} to 1.0×10^{-5} mol L^{-1}	[288]
30	Pb^{2+}	Electrochemical sensor	Graphene-poly(sodium 4-styrenesulfonate) composite	0.5-120 μg L^{-1}	[289]
31		Electrochemical sensor	Graphene-poly(crystal violet)	2.00×10^{-8} to 1.95 _ 10^{-5} mol L^{-1}	[290]
32		Electrochemical sensor	Graphene-Nafion	0.1-100 ng L^{-1}	[291]
33	Cd^{2+}	Electrochemical sensor	Graphene-poly(sodium 4-styrenesulfonate) composite	0.5-120 μg L^{-1}	[289]
34		Electrochemical sensor	Graphene-poly(crystal violet)	9.00×10^{-8} to 5.58×10^{-5} mol L^{-1}	[290]
35		Electrochemical sensor	Graphene-Nafion	0.1-100 ng L^{-1}	[291]
36	Methyl parathion	Electrochemical biosensor	Carboxylic graphene-NiO	10^{-13} to 10^{-8}M	[292]

37	Chlorpyrifos		NP-Nafion		
38	Carbofuran			10^{-12} to 10^{-8} M	
39	Paraoxon	Photoelectrochemical sensor	Graphene-MIP-CdSe-ZnS quantum dots	10^{-12} to 10^{-6} M	[293]
40	Dichlorvos				
41	4-aminophenol	Photoelectrochemical sensor	Graphene-MIP-CdS quantum dots	5.0×10^{-8} to 3.5×10^{-6} M	[294]
42	Hydrogen	Electrochemical sensor	Graphene-palladium NP	20-1000 ppm	[295]
43		Magnetic field (Hall effect)	Graphene-palladium NP	25-1000 ppm	[296]
44	Acetylene	Optical sensor	Graphene		[297]
45	Hexachlorobenzene	Electrochemical sensor	Nitrogen-doped graphene -chitosan	3 μg L^{-1} to 10 mg L^{-1}	[298]
46	Food applications Erythromycin	Electrochemical sensor	Graphene-MIP-gold NP -chitosan-platinum NP	7.0×10^{-8} to 9.0×10^{-5} M	[299]
47	Tryptamine	Electrochemical sensor	Graphene-MIP-MWCNT	9.0×10^{-8} to 7.0×10^{-5} M	[300]
48	Staphylococcus aureus	Piezoelectric sensor	Graphene-aptamer	4.1×10^{1} to 4.1×10^{5} cfu mL^{-1}	[301]

References

[1] E. H. L. Falcao and F. Wudl, *J. Chem. Tech. & Biotech.*, **82**, 524 (2007).

[2] H.-S. P. Wong and D. Akinwande, *Carbon nanotube and graphene device physics*. New York: Cambridge University Press, (2011).

[3] M. J. Allen, V. C. Tung, R. B. Kaner, *Chem. Rev.*, **110**, 132 (2009).

[4] "The Nobel Prize in Chemistry 2010". Nobelprize.org. Nobel Media AB http://www.nobelprize.org/nobel_prizes/chemistry/laureates/2010/

[5] J. C. Charlier, *Acc. Chem. Res.*, **35**, 1063 (2002).

[6] H. W. Kroto, *Nature*, **329**, 529 (1987).

[7] H. W. Kroto, J. R. Heath, S. C. O'Brien, R. F. Curl, R. E. Smalley, *Nature*, **318**, 162 (1985).

[8] "The Nobel Prize in Chemistry 1996". Nobelprize.org. Nobel Media AB http://www.nobelprize.org/nobel_prizes/chemistry/laureates/1996/

[9] G. Mehta, M. B.Viswanath, G. N. Sastry, E. D. Jemmis, D. S. K. Reddy, A. C. Kunwar, *Angew. Chem. Int. Ed.*, **31**, 1488 (1992).

[10] G. N. Sastry, E. D. Jemmis, G. Mehta, S. R. Shah, *J. Chem. Soc., Perk. Trans.*, **2**, 1867 (1993).

[11] E. D. Jemmis, G. N. Sastry, G. Mehta, *J. Chem. Soc., Perk. Trans.*, **2**, 437 (1994).

[12] H. Sakurai, T. Daiko, T. Hirao, *Science*, **301**, 1878 (2003).

[13] E. D. Jemmis, G. Subramanian, G. N. Sastry, G. Mehta, R. N. Shirsat, S. R. Gadre, *J. Chem. Soc., Perk. Trans. 2*, **11**, 2343 (1996).

[14] T. C. Dinadayalane and G. N. Sastry, *J. Org. Chem.*, **67**, 4605 (2002).

[15] T. C. Dinadayalane, S. Deepa, G. N. Sastry, *Tetrahedron Lett.*, **44**, 4527 (2003).

[16] U. D. Priyakumar and G. N. Sastry, *Tetrahedron Lett.*, **42**, 1379 (2001).

[17] K. S. Novoselov, A. K. Geim, S. V. Morozov, D. Jiang, Y. Zhang, S. V. Dubonos, I. V. Grigorieva, A. A. Firsov, *Science*, **306**, 666 (2004).

[18] K. S. Novoselov, D. Jiang, F. Schedin, T. J. Booth, V. V. Khotkevich, S. V. Morozov, A. K. Geim, *Proc. Natl. Acad. Sci. U. S. A.*, **102**, 10451 (2005).

[19] K. S. Novoselov, A. K. Geim, S. V. Morozov, D. Jiang, M. I. Katsnelson, I. V. Grigorieva, S. V. Dubonos , A. A. Firsov, *Nature*, **438**, 197 (2005).

[20] V. P. Gusynin and S. G. Sharapov, *Phys. Rev. Lett.*, **95**, 146801 (2005).

[21] K. S. Novoselov, Z. Jiang, Y. Zhang, S. V. Morozov, H. L. Stormer, U. Zeitler, J. C. Maan, G. S. Boebinger, P. Kim , A. K. Geim, *Science*, **315**, 1379 (2007).

[22] N. M. R. Peres, F. Guinea, A. H. C. Neto, *Phys. Rev. B*: *Condens. Matter Mater. Phys.*, **73**, 125411 (2006).

[23] Y. B. Zhang, Y. W. Tan, H. L. Stormer , P. Kim, *Nature*, **438**, 201 (2005).

[24] S. Latil and L. Henrard, *Phys. Rev. Lett.*, **97**, 036803 (2006).

[25] R. R. Nair, P. Blake, A. N. Grigorenko, K. S. Novoselov,T. J. Booth, T. Stauber, N. M. R. Peres, A. K. Geim, *Science*, **320**, 1308 (2008).

[26] G. Eda, G. Fanchini and M. Chhowalla, *Nat. Nanotechnol.*, **3**, 270 (2008).

[27] A. B. Kuzmenko, E. van Heumen, F. Carbone, D. van der Marel, *Phys. Rev. Lett.*, **100**, 117401 (2008).

[28] X. Du, I. Skachko, A. Barker, E. Y. Andrei, *Nat. Nanotechnol.*, **3**, 491 (2008).

[29] A. A. Balandin, S. Ghosh, W. Z. Bao, I. Calizo, D. Teweldebrhan, F. Miao, C. N. Lau, *Nano Lett.*, **8**, 902 (2008).

[30] J. N. Hu, X. L. Ruan, Y. P. Chen, *Nano Lett.*, **9**, 2730 (2009).

[31] I. Jung, D. A. Dikin, R. D. Piner, R. S. Ruoff, *Nano Lett*., **8**, 4283 (2008).

[32] V. Ryzhii, *Jpn. J. Appl. Phys*., **45**, L923 (2006).

[33] A. R. Wright, X. G. Xu, J. C. Cao, C. Zhang, *Appl. Phys. Lett*., **95**, 072101 (2009).

[34] F. Rana, IEEE Trans. *Nanotechnol*., **7**, 91 (2008).

[35] C. N. R. Rao, K. Biswas, K. S. Subrahmanyam, A. Govindaraj, *J. Mater. Chem*., **19**, 2457 (2009).

[36] C. N. R. Rao, A. K. Sood, K. S. Subrahmanyam, A. Govindaraj, *Angew. Chem., Int. Ed*., **48**, 7752 (2009).

[37] M. J. Allen, V. C. Tung, Richard B. Kaner, *Chem. Rev*., **110**, 132 (2010).

[38] D. S. L. Abergel, V. Apalkov, J. Berashevich, K. Ziegler, T. Chakraborty, *Adv. Phys*., **59**, 261 (2010).

[39] M. J. Allen, V. C. Tung, R. B. Kaner, *Chem. Rev*., **110**, 132 (2010).

[40] M. F. Craciun, S. Russo, M. Yamamoto, S. Tarucha, *Nano Today*, **6**, 42 (2011).

[41] C. N. R. Rao, K. Biswas, K. S. Subrahmanyam, A. Govindaraj, *J. Mater. Chem*., **19**, 2457 (2009).

[42] V. Singh, D. Joung, L. Zhai, S. Das, S. I. Khondaker, S. Seal, *Prog. Mater. Sci*., **56**, 1178 (2011).

[43] Y. Q. Wu, Y. M. Lin, A. A. Bol, K. A. Jenkins, F. N. Xia, D. B. Farmer, Y. Zhu, P. Avouris, *Nature*, **472**, 74 (2011).

[44] F. S. F. Schwierz, *Nat. Nanotechnol*., **5**, 487 (2010).

[45] J. S. Wu, W. Pisula, K. Mullen, *Chem. Rev*., **107**, 718 (2007).

[46] Y. Q. Sun, Q. O. Wu, G. Q. Shi, *Energy Environ. Sci*., **4**, 1113 (2011).

[47] D. A. C. Brownson, D. K. Kampouris, C. E. Banks, *J. Power Sources*, **196**, 4873 (2011).

[48] C. K. Huang, Y. X. Ou, Y. Q. Bie, Q. Zhao, D. P. Yu, *Appl. Phys. Lett*., **98**, 263104 (2011).

[49] Z. S.Wu, S. F. Pei, W. C. Ren, D.M. Tang, L. B. Gao, B. L. Liu, F. Li, C. Liu, H.M. Cheng, *Adv. Mater*., **21**, 1756 (2009).

[50] J. K. Wassei, R. B. Kaner, *Mater. Today*, **13**, 52 (2010).

[51] D. C. Wei, Y. Q. Liu, Y. Wang, H. L. Zhang, L. P. Huang, G. Yu, *Nano Lett*., **9**, 1752 (2009).

[52] T. B. Martins, R. H. Miwa, A. J. R. da Silva, A. Fazzio, *Phys. Rev. Lett*., **98**, 196803 (2007).

[53] D. Gunlycke, J. Li, J. W. Mintmire, C. T. White, *Appl. Phys. Lett*., **91**, 112108 (2007).

[54] F. Cervantes-Sodi, G. Csányi, S. Piscanec, A. C. Ferrari, *Phys. Rev. B: Condens. Matter Mater. Phys*., **77**, 165427 (2008).

[55] Y. X. Huang and P. Chen, *Adv. Mater*., **22**, 2818 (2010).

[56] T. Asefa, C. T. Duncan, K. K. Sharma, *Analyst*, **134**, 1980 (2009).

[57] Y. X. Huang, D. Cai, P. Chen, *Anal. Chem*., **83**, 4393 (2011).

[58] S. Roy and Z. Q. Gao, *Nano Today*, **4**, 318 (2009).

[59] M. F. Frasco and N. Chaniotakis, *Sensors*, **9**, 7266 (2009).

[60] C. P. Han and H. B. Li, *Anal. Bioanal. Chem*., **397**, 1437 (2010).

[61] H. Haick, *J. Phys. D: Appl. Phys*., **40**, 7173 (2007).

[62] X. L. Luo, A. Morrin, A. J.Killard, M. R. Smyth, *Electroanalysis*, **18**, 319 (2006).

[63] K. I. Chen, B. R. Li, Y. T. Chen, *Nano Today*, **6**, 131 (2011).

[64] F. Patolsky, G. Zheng, C. M. Lieber, *Nanomedicine*, **1**, 51 (2006).

[65] N. S. Ramgir, Y. Yang, M. Zacharias, *Small*, **6**, 1705 (2010).

[66] A. K. Wanekaya, W. Chen, N. V. Myung, A. Mulchandani, *Electroanalysis*, **18**, 533 (2006).

[67] C. B. Jacobs, M. J. Peairs, B. J. Venton, *Anal. Chim. Acta*, **662**, 105 (2010).

[68] K. Maehashi and K. Matsumoto, *Sensors*, **9**, 5368 (2009).

[69] N. Sinha, J. Z. Ma, J. T. W. Yeow, *J. Nanosci. Nanotechnol*., **6**, 573 (2006).

[70] T. Zhang, S. Mubeen, N. V. Myung, M. A. Deshusses, *Nanotechnology*, **19**, 332001(2008).

[71] G. S. Wilson, R. Gifford, *Biosens. Bioelectron*., **20**, 2388 (2005).

[72] B. D. Malhotra, R. Singhal, A. Chaubey, S.K. Sharma, A. Kumar, *Curr. Appl. Phys.*, **5**, 92 (2005).

[73] P. Kang, M. C. Wang, S. Nam, *Microelectron. Eng*., **161**, 18 (2016).

[74] J. N. Tiwari, V. Vij, K. C. Kemp, K. S. Kim, *ACS Nano*, **10**, 46 (2016).

[75] K. J. Huang, D. J. Niu, J. Y. Sun, C. H. Han, Z. W. Wu, Y. L. Li, X. Q. Xiong, *Colloids and Surfaces B: Biointerfaces*, **82**, 543 (2011).

[76] H. S. Yin, Y. L. Zhou, Q. A. Ma, S. Y. Ai, Q. P. Chen, L. S. Zhu, *Talanta*, **82**, 1193 (2010).

[77] J. Zhang, J. P. Lei, R. Pan, Y. D. Xue, H. X. Ju, *Biosens. Bioelectron*., **26**, 371 (2010).

[78] Y. Wang, Y. M. Li, L. H. Tang, J. Lu, J. H. Li, *Electrochem. Commun*., **11**, 889 (2009).

[79] J. Zhang, R. H. Xue, W. Y. Ong, P. Chen, *Biophys. J.*, **97**, 1371 (2009).

[80] R. S. Dey and C. R. Raj, *J. Phys. Chem. C*, **114**, 21427 (2010).

[81] S. Iijima, *Nature*, **354**, 56 (1991).

[82] S. Iijima and T. Ichihashi, *Nature*, **363**, 603 (1993).

[83] P. R Bandaru, C. Daraio, S. Jin, A.M. Rao, *Nat. Mater*., **4**, 663 (2005).

[84] T. W. Ebbesen, H. J. Lezec, H. Hiura, J. W. Bennett, H. F. Ghaemi, T. Thio, *Nature*, **382**, 54 (1996).

[85] M. M. J. Treacy, T.W. Ebbesen, J. M. Gibson, *Nature*, **381**, 678 (1996).

[86] M. F. Yu, O. Lourie, M. J. Dyer, K. Moloni, T. F. Kelly, R. S. Ruoff, *Science*, **287**, 637 (2000).

[87] S. B. Sinnott, O. A. Shenderova, C. T. White, D. W. Brenner, *Carbon*, **36**, 1 (1998).

[88] B. N. Shobha and N. J. R Muniraj, *Microsyst.Technol*., **21**,791 (2015).

[89] G. N. Lewis, Valence and the Structure of Atoms and Molecules, American Chemical Society Monograph Series: New York, (1923).

[90] W. Heitler and F. Z. London, *Physik*, **44**, 455 (1927).

[91] L. Pauling, *The Nature of the Chemical Bond*, Cornell University Press: Ithaca, NY, (1939).

[92] J. D. van der Waals, *Doctoral Dissertation*, Leiden, (1873).

[93] K. M.-D, P. Hobza, *Chem. Rev*., **100**, 143 (2000).

[94] "The Nobel Prize in Chemistry 1987". Nobelprize.org. Nobel Media AB http://www.nobelprize.org/nobel_prizes/chemistry/laureates/1987.

[95] J. D. van der Waals, "*On the continuity of the gas and liquid state*", Leiden, The

Netherlands, (1873).

[96] R. Eisenschitz and F. London, *Zeitschrift für Physik*, **60**, 491 (1930).

[97] D. Vijay, H. Zipse, G. N. Sastry, *J. Phys. Chem. B*, **112**, 8863 (2008).

[98] D. Vijay and G. N. Sastry, *Chem. Phys. Lett*., **485**, 235 (2010).

[99] J. M. Lehn, *Angew. Chem. Int. Ed. Engl*., **27**, 89 (1988).

[100] W. Zhu, X. Tan, J. Shen, X. Luo, F. Cheng, P. C. Mok, R. Ji, K. Chen, H. Jiang, *J. Phys. Chem. A*, **107**, 2296 (2003).

[101] D. Vijay and G. N. Sastry, *Phys. Chem. Chem. Phys*., **10**, 582 (2008).

[102] J. F. Gal, P. C. Maria, M. Decouzon, O. Mo, M. Yanez, J. L. M. Abboud, *J. Am. Chem. Soc*., **125**, 10394 (2003).

[103] A. S. Mahadevi, Y. I. Neela, G. N. Sastry, *Phys. Chem. Chem. Phys*., **13**, 15211 (2011).

[104] Y. I. Neela, A. S. Mahadevi, G. N. Sastry, *J. Phys. Chem. B*, **114**, 17162 (2010).

[105] R. H. Crabtree, *Science*, **283**, 2000 (1998).

[106] R. Custelcean and J. E. Jackson, *Chem. Rev*., **101**, 1963 (2001).

[107] T. B. Richard, S. de Gala, R. H. Crabtree, P. E. M. Siebahn, *J. Am. Chem. Soc*., **117**, 12875 (1995).

[108] D. A. Dougherty, *Science*, **271**, 163 (1996).

[109] C. J. Ma and D. A. Dougherty, *Chem. Rev*., **97**, 1303 (1997).

[110] J. Sunner, K. Nishizawa, P. Kebarle, *J. Phys. Chem*., **85**, 1814 (1981).

[111] S. K. Burley and G. A. Petsko, *J. Am. Chem. Soc*., **108**, 7995 (1986).

[112] S. K. Burley and G. A. Petsko, *Science*, **229**, 23 (1985).

[113] S. K. Burley and G. A. Petsko, *FEBS Lett*., **203**, 139 (1986).

[114] J. P. Gallivan, D. A. Dougherty, *Proc. Natl. Acad. Sci. USA*, **96**, 9459 (1996).

[115] R. Wintjens, J. Lievin, M. Rooman, E. Buisine, *J. Mol. Biol*., **302**, 395 (2000).

[116] M. M. Gromiha, C. Santosh, M. Suwa, *Polyme*r, **45**, 633 (2004).

[117] J. C. Amicangelo, P. B. Armentrout, *J. Phys. Chem*. A, **104**, 11420 (2000).

[118] R. Amunugama, M. T. Rodgers, *Int. J. Mass. Spectrom*., **222**, 431(2003).

[119] H. Huang, M. T. Rodgers, *J. Phys. Chem. A*, **106**, 4277 (2002).

[120] M. T. Rodgers, P. B. Armentrout, *Int. J. Mass. Spectrom*., **359**, 185 (1999).

[121] R. Amunugama and M. T. Rodgers, *Int. J. Mass. Spectrom*., **439**,195 (2000).

[122] R. Amunugama and M. T. Rodgers, *J. Phys. Chem. A*, **106**, 5529 (2002).

[123] W. Zhu, X. Luo, C. M. Puah, X. Tan, J. Shen, J. Gu, K. Chen, H. Jiang, *J. Phys. Chem. A*, **108**, 4008 (2004).

[124] J. Munoz, J. Sponer, P. Hobza, M. Orozco, F. I. Luque, *J. Phys. Chem. B*, **105**, 6051 (2001).

[125] V. Ryzhov and R. C. Dunbar, *J. Am. Soc. Mass Spectrom*., **11**, 1037 (2000).

[126] A. S. Reddy and G. N. Sastry, *J. Phys. Chem. A*, **109**, 8893 (2005).

[127] U. D. Priyakumar and G. N. Sastry, *Tetrahedron Lett*., **44**, 6043 (2003).

[128] U. D. Priyakumar, M. Punnagai, G. P. Krishnamohan, G. N. Sastry, *Tetrahedron*, **60**, 3037 (2004).

[129] F. M. Siu, N. L. Ma, C. W. Tsang, *J. Am. Chem. Soc*., **123**, 3397 (2001).

[130] F. M. Siu, N. L. Ma, C. W. Tsang, *Chem.Eur. J*., **10**, 1966 (2004).

[131] H. B. Yi, H. M. Lee, K. S. Kim, *J. Chem. Theory Comput*., **5**, 1709 (2009).

[132] M. Watt, J. Hwang, K. W. Cormier, M. Lewis, *J. Phys. Chem. A*, **113**, 6192 (2009).

[133] J. S. Rao and G. N. Sastry, *J. Phys. Chem. A*, **113**, 5446 (2009).

[134] D. Vijay, H. Sakurai, V. Subramanian, G. N. Sastry, *Phys. Chem. Chem. Phys*., **14**, 3057 (2012).

[135] B. Satheesh, Y. Soujanya, G. N. Sastry, *J. Chem. Sci*., **119**, 509 (2007).

[136] D. Umadevi and G. N. Sastry, *J. Phys. Chem. C*, **115**, 9656 (2011).

[137] D. Vijay and G. N. Sastry, *J. Phys. Chem. A*, **110**, 10148 (2006).

[138] B. Sharma, D. Umadevi, G. N. Sastry, *Phys. Chem. Chem. Phys*., **14**, 13922 (2012).

[139] J. S. Rao, H. Zipse, G. N. Sastry, *J. Phys. Chem. B*, **113**, 7225 (2009).

[140] A. S. Reddy, H. Zipse. G. N. Sastry, *J. Phys. Chem. B*, **111**, 11546 (2007).

[141] A. S. Mahadevi, G. N. Sastry, *J. Phys. Chem. B*, **115**, 703 (2011).

[142] B. Sharma, J. S. Rao, G. N. Sastry, *J. Phys. Chem. A*, **2011**, 115 (1971).

[143] D. Vijay and G. N. Sastry, *Chem. Phys. Lett*., **485**, 235 (2010).

[144] D. Vijay, H. G. Zipse, G. N. Sastry, *J. Phys. Chem. B*, **112**, 8863 (2008).

[145] A. S. Mahadevi and G. N. Sastry, *Chem. Rev*., **113**, 2100 (2013).

[146] C. A. Hunter and J. K. M. Sanders, *J. Am. Chem. Soc*., **112**, 5525 (1990).

[147] D. D. Boehr, A. R. Farley, G. D. Wright, J. R. Cox, *Chem. and Biol*., **9**, 1209 (2002).

[148] G. B. Mc Gaughey, M. A. Gagne´, K. Rappe´, *J. Biol. Chem*., **273**, 15458 (1998).

[149] R. Bhattacharyya, U. Samanta, P. Chakrabarti, *Protein Eng*., **15**, 91 (2002).

[150] M. O. Sinnokrot and C. D. Sherril, *J. Phys. Chem. A*, **108**, 10200 (2004).

[151] P. Hobza and Z. Havlas, *Theor. Chem. Acc*., **99**, 372 (1998).

[152] W. Saenger, *Principles of Nucleic Acid Structure*, Springer-Verlag: New York, 132 (1984).

[153] F. Cozzi, M. Cinquini, R. Annuziata, J. S. Siegel, *J. Am. Chem. Soc*., **115**, 5330 (1993).

[154] C. A. Hunter, P. Leighton, J. K. M. Sanders, *J. Chem. Soc. Trans. Perkin I*, 547 (1989).

[155] R. J. Abraham, F. Eivazi, H. Pearson, K. M. Smith, J. Chem. Soc. Chem. Comm., 699 (1976).

[156] A. E. Alexander, *J. Chem. Soc*., **0**, 1813 (1937).

[157] L. A. Castonguay, A. K. Rappe, C. J. Casewit, *J. Am. Chem. Soc*., **113**, 7177 (1991).

[158] M. A. Pietsch and A. K. Rappe, *J. Am. Chem. Soc*., **118**, 10908 (1996).

[159] H. C. Kolb, P. G. Andersson, K. B. Sharpless, *J. Am. Chem. Soc*., **116**, 1278 (1994).

[160] A. G. Gilman, T. W. Rall, A. S. Mies, P. Taylor, *The Pharmaceutical Basis of Therapeutics*, McGraw Hill, Inc.: New York, (1993).

[161] S. K. Burley and G. A. Petsko, *Science*, **229**, 23 (1985).

[162] C. A. Hunter, J. Singh, J. M. Thornton, *J. Mol. Biol*., **218**, 837 (1991).

[163] J. Singh, J. M. Thornton, *J. Mol. Biol*., **211**, 595 (1990).

[164] C. A. Hunter and J. K. M. Sanders, *J. Am. Chem. Soc*., **112**, 5525 (1990).

[165] C. Janiak, *J. Chem. Soc. Dalton Trans*., **38**, 85 (2000).

[166] N. Kannan and S. Vishveshwara., *Protein Eng*., **13**, 753 (2000).

[167] S. Tsuzuki, T. Uchimaru, K. Tanabe, *J. Phys. Chem. A*, **102**, 740 (1998).

[168] M. J. Allen, V. C. Tung, R. B. Kaner, *Chem. Rev*., **110**, 132 (2010).

[169] M. Pumera, A. Ambrosi, A. Bonanni, E. L. K. Chng, H.L. Poh, *Trends in Analytical Chemistry*, **29**, 954 (2010).

[170] M. D. Stoller, S. Park, Y. Zhu, J. An, R. S. Ruoff, *Nano letters*, **8**, 3498 (2008).

[171] Y. Si and E. T. Samulski, *Chem. Mater*., **20**, 6792 (2008).

[172] L. Chen, A. C. Cooper, G. P. Pez, H. Cheng, *J. Phys. Chem. C*, **111**, 18995 (2007).

[173] P. A. Denis and F. Iribarne, *Theochem*., **907**, 93 (2009).

[174] M. Rubes and O. Bludsky, *ChemPhysChem*, **10**, 1868 (2009).

[175] K. A. Ritter and J. W. Lyding, *Nature materials*, **8**, 235 (2009).

[176] C. N. R. Rao, A. K. Sood, K. S. Subrahmanyam, A. Govindaraj, *Angewandte Chemie*, **48**, 7752 (2009).

[177] F. Schedin, A. K. Geim, S. V. Morozov, E. W. Hill, P. Blake, M. I. Katsnelson, K. S. Novoselov, *Nature Materials Lett*., **6**, 652 (2007).

[178] L. Al-Mashat, K. Shin, K. K.-zadeh, J. D. Plessis, S. H. Han, R. W. Kojima, R. B. Kaner, D. Li, X. Gou, S. J. Ippolito, W. Wlodarski, *J. Phys. Chem. C*, **114**, 16168 (2010).

[179] G. Lee, B. Lee, J. Kim, K. Cho, *J. Phys. Chem. C*, **113**, 14225 (2009).

[180] V. Hubert, A. Gil, G. Frapper, *J. Phys. Chem. C*, **114**, 14141 (2010).

[181] N. Ghaderi and M. Peressi, *J. Phys. Chem. C*, **114**, 21625 (2010).

[182] S. Park, K-S. Lee, G. Bozoklu, W. Cai, S. T. Nguyen, R. S. Ruoff, *ACS Nano*, **3**, 572 (2008).

[183] D. Wang, R. Kou, D. Choi, Z. Yang, Z. Nie, J. Li, L. V. Saraf, D. Hu, J. Zhang, G. L. Graff, J. Liu, M. A. Pope, I. A. Aksay, *ACS Nano*, **4**, 1587 (2010).

[184] M. Quintana, K. Spyrou, M. Grzelczak, W. R. Browne, P. Rudolf, M. Prato, *ACS Nano*, **4**, 3527 (2010).

[185] H. Tachikawa and T. Iyama, *Jap. J. Appl. Phys.*, **49**, 06GJ12-1 (2010).

[186] N. Al-Aqtash and I. Vasiliev, *J. Phys. Chem. C*, **113**, 1290 (2009).

[187] S. H. Lim, L. Feng, J. W. Kemling, C. J. Musto, K. S. Suslick, *nature chemistry*, **1**, 562 (2009).

[188] F. Bano, L. Fruk, B. Sanavio, M. Glettenberg, L. Casalis, C. M. Niemeyer, G. Scoles, *Nano Letters*, **9**, 2614 (2009).

[189] M. Zwolak and M. Di Ventra, *Rev. Mod. Phys.*, **80**, 141 (2008).

[190] C. P. Fredlake, D. G. Hert, E. R. Mardis, A. E. Barron, *Electrophoresis*, **27**, 3689 (2006).

[191] P. Jonkheijm, D. Weinrich, H. Schrçder, C. M. Niemeyer, H. Waldmann,. *Angew. Chem. Int. Ed.*, **47**, 9618 (2008).

[192] F. Patolsky, G. Zheng, C. M. Lieber, *Nature protocols*, **1**, 1711 (2006).

[193] J. M. Vidic, J. Grosclaude, M-A Persuy, J. Aioun, R. Salessea, E. P.-Augy, *Lab chip*, **6**, 1026 (2006).

[194] G. Zhang, P. Qi, X. Wang, Y. Lu, X. Li, R. Tu, S. Bangsaruntip, D. Mann, L. Zhang, H. Dai, *Science*, **314**, 974 (2006).

[195] J. C. Meyer, A. K. Geim, M. I. Katsnelson, K. S. Novoselov, T. J. Booth, S. Roth, *Nature Letters*, **446**, 60 (2007).

[196] E. Shapir, H. Cohen, A. Calzolari, C. Cavazzoni, D. A. Ryndyk, G. Cuniberti, A. Kotlyar, R. D. F. Felice, D. Porath, Nature Materials, **7**, 68 (2008).

[197] N. Kang, A. Erbe, E. Scheer, *New Journal of Physics*, **10**, 023030 (1-9) (2008).

[198] X. Zhao, *J. Phys. Chem. C*, **115**, 6181 (2011).

[199] A. Paul and B. Bhattacharya, *Materials and Manufacturing Processess*, **25**, 891 (2010).

[200] Z. Liu, K. Yang, S.T. Lee , *J. Mater. Chem.*, **21**, 586 (2011).

[201] D. A. Yarotski, S. V. Kilina, A. A. Talin, S. Tretiak, O. V. Prezhdo, A. V. Balatsky, A. J. Taylor, *Nano Letters*, **9**, 12 (2009).

[202] G. S-Jimenez, B. Childs, D. Valle, *nature analysis*, **409**, 853 (2001).

[203] T. Nelson, B. Zhang, O. V. Prezhdo, *Nano Letters*, **10**, 3237 (2010).

[204] J. Prasongkit, A. Grigoriev, B. Pathak, R. Ahuja, R. H. Scheicher, *Nano Letters*, **11**, 1941 (2011).

[205] P. W. Barone, S. Baik, D. A. Heller, M. S. Strano, *Nature Materials*, **4**, 86 (2005).

[206] S. K. Min, W. Y. Kim, Y. Cho, K. S. Kim, *Nature nanotechnology*, **6**, 162 (2011).

[207] Y. Zheng, C. Yang, W. Pu, J. Zhang, *Microchim. Acta*, **166**, 21 (2009).

[208] R. J. Chen, S. Bangsaruntlp, K. A. Drouvalakls, N. W. S. Kam, M. Shim, Y. Li, W. Kim, P. J. Utz, H. Dai, *PNAS*, **100**, 4984 (2003).

[209] S. G. Stepanian, M. V. Karachevtsev, A. Y. Glamazda, V. A. Karachevtsev, L. Adamowicz, *Chem. Phys. Lett.*, **459**, 153 (2008).

[210] Y. V. Shtogun, L. M. Woods, G. I. Dovbeshko, *J. Phys. Chem. C*, **111**, 18174 (2007).

[211] H. Wang and A. Ceulemans, *Phys. Rev. B*, **79**,195419 (1-6) (2009).

[212] P. Wang, H. Wu, Z. Dai, X. Zou, *Biosens. & Bioelec*., **26**, 3339 (2011).

[213] L. R. Rutledge, H. F. Durst, S. D. Wetmore, *J. Chem. Theory Comput*., **5**, 1400 (2009).

[214] L. R. Rutledge and S. D. Wetmore, *Can. J. of Chem*., **88**, 815 (2010).

[215] E. R. Johnson, R. A. Wolkow, G. A. Di Labio, *Chem. Phys. Lett.*, **394**, 334 (2004).

[216] E. R. Johnsona, I. D. Mackieb, G. A. DiLabio, *J. Phys. Org. Chem*., **22**, 1127 (2009).

[217] M. Dion, H. Rydberg, E. Schrçder, D. C. Langreth, B. I. Lundqvist, *Phy. Rev. Lett.*, **92**, 246401 (1-4) (2004a).

[218] Y. Zhao and D. G. Truhlar, *J. Chem. Theory Comput*., **1**, 415 (2005).

[219] Y. Zhao and D. G. Truhlar, *Chem. Phys. Lett*., **502**, 1 (2011).

[220] E. J. Meijer and M. Sprik , *J. Chem. Phys*., **105**, 8684 (1996).

[221] A. Tkatchenko and M. Scheffler, *Phy. Rev. Lett.*, **102**, 073005(1-4) (2009).

[222] S. Grimme, *J. Comp. Chem*., **25**, 1463 (2004).

[223] S. Grimme, *J. Comp. Chem*., **27**, 1787 (2006).

[224] S. Grimme, J. Antony, S. Ehrlich, H. Krieg, *J. Chem. Phys*., **132**, 154104 (1-19) (2010).

[225] S. Grimme, S. Ehrlich, L. Goerigk, *J. Comp. Chem*., **32**, 1456 (2010).

[226] M. J. S. Dewar, E. G. Zoebisch, E. F. Healy, J. J. P. Stewart, *J. Am. Chem. Soc.*, **107**, 3902 (1984).

[227] J. J. P. Stewart, *J. Comp. Chem*., **10**, 221(1988).

[228] J. J. P. Stewart, *J. Comp. Chem*., **10**, 209 (1989).

[229] J. J. P. Stewart, *J. Comp. Chem*., **12**, 320 (1990).

[230] J. J. P. Stewart, *J. Mol. Model*., **13**, 1173 (2007).

[231] S. Gowtham, R. H. Scheicher, R. Ahuja, R. Pandey, S. P. Karna, *Phy. Rev. B*, **76**, 033401(1-4) (2007).

[232] S. Gowtham, R. H. Scheicher, R. Pandey, S. P. Karna, R. Ahuja, *Nanotechnology*, **19**, 125701 (1-6) (2008).

[233] S. Meng, P. Maragakis, C. Papaloukas, E. Kaxiras, *Nano Lett*., **7**, 45 (2007a).

[234] S. Meng, W. L. Wang, P. Maragakis, E. Kaxiras, *Nano Lett*., **7**, 2312 (2007b).

[235] H. Wang and A. Ceulemans, *Phys. Rev. B*, **79**, 195419 (1-6) (2009).

[236] Y. Wang, *J. Phys. Chem. C: Nanomater Interfaces*, **112**, 14297-14305 (2008).

[237] Yi. Wang and Y. Bu, *J. Phys. Chem. B*, **111**, 6520 (2007).

[238] M. K. Shukla, M. Dubey, E. Zakar, R. Namburu, Z. Czyznikowsk, J. Leszczynski, *Chem. Phy. Lett*., **480**, 269 (2009).

[239] F. Tournus and J. C. Charlier, *Phy. Rev. B.*, **71**, 165421 (1-8) (2005).

[240] M. Dion, H. Rydberg, E. Schrçder, D.C. Langreth, B.I. Lundqvist, *Phy. Rev. Lett*., **92**, 246401 (1-4) (2004a).

[241] E. G. Hohenstein, S. T. Chill, C. D. Sherrill, *J. Chem. Theory Comput*., **4**, 1996 (2008).

[242] S. Ehrlich, J. Moellmann, *S. Grimme, Acc. Chem. Res*., **46**, 916 (2013).

[243] Y. Zhao and D. G. Truhlar, *J. Chem. Phys*., **125**, 194101 (1-18) (2006a).

[244] Y. Zhao and D. G. Truhlar, *J. Phys. Chem. A*, **110**, 13126 (2006b).

[245] Y. Zhao and D. G. Truhlar, *Theor. Chem. Acc*., **120**, 215 (2008).

[246] Y. Zhao and D. G. Truhlar, *Acc. Chem. Res.*, **41**, 157 (2008).

[247] S. Chandra and R. S. Swathi, *J. Phys. Chem. C*, **118**, 4516 (2014).

[248] H. Vovusha, S. Sanyal, B. Sanyal, *J. Phys. Chem. Lett*., **4**, 3710 (2013).

[249] D. Umadevi and G. N. Sastry, *Phys. Chem. Chem. Phys*., **17**, 30260 (2015).

[250] A. Star, E. Tu, J. Niemann, J.-C. P. Gabriel, C. S. Joiner, C. Valcke, *Proc. Natl. Acad. Sci. U. S. A*., **103**, 921 (2006).

[251] K. Maehashi, T. Katsura, K. Kerman, Y. Takamura, K. Matsumoto, E. Tamiya, *Anal. Chem*., **79**, 782 (2007).

[252] Y. Ohno, K. Maehashi, Y. Yamashiro, K. Matsumoto, *Nano Lett*., **9**, 3318 (2009).

[253] H. Chen, P. Chen, J. Huang, R. Selegard, M. Platt, A. Palaniappan, D. Aili, A. I. Tok, B. Liedberg, *Anal. Chem*., **88**, 2994 (2016).

[254] M. T. Martı´nez, Y.-C. Tseng, N. Ormategui, I. Loinaz, R. Eritja, J. Bokor, *Nano Lett*., **9**, 530 (2009).

[255] S. Sorgenfrei, C.-Y. Chiu, R. L. Gonzalez, Y.-J. Yu, P. Kim, C. Nuckolls, K. L. Shepard, *Nat. Nanotechnol*., **6**, 126 (2011).

[256] P. Ramnani, Y. Gao, M. Ozsoz, A. Mulchandani, *Anal. Chem*., **85**, 8061 (2013).

[257] R. Stine, J. T. Robinson, P. E. Sheehan, C. R. Tamanaha, *Adv. Mater*., **22**, 5297 (2010).

[258] B. Cai, S. Wang, L. Huang, Y. Ning, Z. Zhang, G.-J. Zhang, *ACS Nano*, **8**, 2632 (2014).

[259] Z. Yin, Q. He, X. Huang, J. Zhang, S. Wu, P. Chen, G. Lu, P. Chen, Q. Zhang, Q. Yan, H. Zhang, *Nanoscale*, **4**, 293 (2012).

[260] C. Zheng, L. Huang, H. Zhang, Z. Sun, Z. Zhang, G.-J. Zhang, *ACS Appl. Mater. Interfaces*, **7**, 16953 (2015).

[261] Q. Zhao, Y. Zhou, Y. Li, W. Gu, Q. Zhang, J. Liu, *Anal. Chem*., **88**, 1892 (2016).

[262] F. Li, J. Chao, Z. Li, S. Xing, S. Su, X. Li, S. Song, X. Zuo, C. Fan, B. Liu, W. Huang, L. Wang, L. Wang, *Anal. Chem.*, **87**, 3877 (2015).

[263] Y. Huang, H. Y. Yang, Y. Ai, *Anal. Chem*., **87**, 9132 (2015).

[264] J. Huang, Z. Wang, J. K. Kim, X. Su, Z. Li, *Anal. Chem*., **87**, 12254 (2015).

[265] J. Luo, S. Jiang, H. Zhang, J. Jiang, X. Liu, *Analytica Chimica Acta* , **709**, 47 (2012).

[266] R. Manjunatha, G. S. Suresh, J. S. Melo, S. F. D'Souza, Thimmappa V.Venkatesha, *Talanta*, **99**, 302 (2012).

[267] S. Cao, L. Zhang, Y. Chai, R. Yuan, *Talanta*, **109**, 167 (2013).

[268] M. Zhang, R. Yuan, Y. Chai, C. Wang, X. Wu, *Analy. Biochem*., **436**, 69 (2013).

[269] N. Ruecha, R. Rangkupan, N. Rodthongkum, O. Chailapakul, *Biosens. & Bioelec*., **52**, 13 (2014).

[270] X.-M Chen, Z.-X Cai, Z-Y Huang, M. Oyama, Y-Qi Jiang, X. Chen, *Electrochimica Acta*, **97**, 398 (2013).

[271] S. Nandini, S. Nalini, R. Manjunatha, S. Shanmugam, J. S. Melo, G. S. Suresh, *J. Electroanal. Chem.*, **689**, 233 (2013).

[272] H. Songa, Y. Nia, S. Kokotc, *Analytica Chimica Acta*, **788**, 24 (2013).

[273] C.-T. Lin, P.T.K. Loan, T.-Y. Chen, K.-K. Liu, C.-H. Chen, K.-H. Wei, L.-J. Li, *Adv. Funct. Mater*., **23**, 2301 (2013).

[274] Q. Liu, X. Zhu, Z. Huo, X. He, Y. Liang, M. Xu, *Talanta,* **97**, 557 (2012).

[275] D. Wu, Y. Li, Y. Zhang, P. Wang, Q. Wei, B. Du, *Electrochimica Acta*, **116**, 244 (2014).

[276] S. Qi, B. Zhao, H. Tang, X. Jiang, *Electrochimica Acta*, **161**, 395 (2015).

[277] Q. Zhu, Y. Chai, R. Yuan, Y. Zhuo, J. Han, Y. Li, N. Liao, *Biosens. & Bioelec.*, **43**, 440 (2013).

[278] J. Huang, J. Tian, Y. Zhao, S. Zhao, *Sens.& Actuat. B*, **206**, 570 (2015).

[279] L. Zhao, S. Li, J. He, G. Tian, Q. Wei, H. Li, *Biosens. & Bioelec.*, **49**, 222 (2013).

[280] Y. Wang, Y. Xiao, X. Ma, N. Li, X. Yang, *Chem. Commun*., **48**, 738 (2012).

[281] H. X. Chang, L. H. Tang, Y. Wang, J. H. Jiang, J. H. Li, *Anal. Chem*., **82**, 2341 (2010).

[282] K. Mao, D. Wu, Y. Li, H. Ma, Z. Ni, H. Yu, C. Luo, Q. Wei, B. Du, *Analy. Biochem*., **422**, 22 (2012).

[283] Y. Li, J. Han, R. Chen, X. Ren, Q. Wei, *Analy. Biochem*., **469**, 76 (2014).

[284] M. Yan, D. Zang, S. Ge, L. Ge, J. Yu, *Biosens. & Bioelec*., **38**, 355 (2012).

[285] G. Wang, X. Hea, L. Chena, Y. Zhua, X. Zhanga, *Colloids and Surfaces B: Biointerfaces*, **116**, 714 (2014).

[286] G. Yang, L. Li, R. K. Rana, J.-J. Zhu, *Carbon*, **61**, 357 (2013).

[287] S. Singal, A.K. Srivastava, A.M. Biradar, A. Mulchandani, Rajesh, *Sens. & Actuators B*, **205**, 363 (2014).

[288] J. Hou, F. Bei, M. Wang, S. Ai, *J. Appl. Electrochem*, **43**, 689 (2013).

[289] C. Huangfu, L. Fu, Y. Li, X. Li, H. Du, J. Ye, *Electroanalysis,* **25**, 2238 (2013).

[290] M. Chen, M. Chao, X. Ma, *J. Appl. Electrochem*., **44**, 337 (2014).

[291] S. Chaiyo, E. Mehmeti, K. Zagar, W. Siangproh, O. Chailapakul, K. Kalcher, *Anal. Chim. Acta*, **918**, 26 (2016).

[292] L. Yang, G. Wang, Y. Liu, M. Wang, *Talanta*, **113**, 135 (2013).

[293] X. Li, Z. Zheng, X. Liu, S. Zhao, S. Liu, *Biosens. & Bioelec.*, **64**, 1 (2015).

[294] R. Wang, K. Yan, F. Wang, J. Zhang, *Electrochimica Acta*, **121**, 102 (2014).

[295] M. G. Chung, D.-H. Kim, D. K. Seo, T. Kim, H. U. Im, H. M. Lee, J.-B. Yoo, S.-H Hong, T. J. Kanga, Y. H. Kima, *Sens.& Actuat. B*, **169**, 387 (2012).

[296] L. Huang, Z. Zhang, Z. Li, B. Chen, X. Ma, L. Dong, L.-M. Peng, *ACS Appl. Mater. Interf.*, **7**, 9581 (2015).

[297] Y. Tan, C. Zhang, W. Jin, F. Yang, H.L. Ho, J. Ma, *IEEE J. Sel. Top. Quant. Electron.*, **99**, 1 (2016).

[298] G. Yu, W. Zhang, Q. Zhao, W. Wu, X. Wei, Q. Lu, *Sens.& Actuat. B*, **235**, 439 (2016).

[299] W. Lian, S. Liu, J. Yu, X. Xing, J. Li, M. Cui, J. Huang, *Biosens. & Bioelec.*, **38** 163 (2012).

[300] X. Xing, S. Liu, J. Yu, W. Lian, J. Huang, *Biosens. & Bioelec.*, **31**, 277 (2012).

[301] Y. Lian, F. He, H. Wang, F. Tong, *Biosens. & Bioelec.*, **65**, 314 (2015).

Chapter 2

Methodology

CHAPTER 2

METHODOLOGY

2.1 Introduction

The interplay between the theory and experiment can well be experienced with the help of the computational power. The computational modelling has emerged as a new paradigm beside the theory and experiment. In the field of molecular sciences, computation has enabled us to provide basic insights at atomic level. The advances in recent computer software and hardware techniques enable to implement a range of computational methodologies in efficient and user friendly fashion. An attempt has been made to give a brief description of various theoretical methodologies employed. At the outset a brief introduction about the quantum mechanical principles, which provide the platform to build the computational techniques, has been discussed.

Unlike molecular mechanics (MM), quantum mechanics (QM) describes molecules in terms of interactions among nuclei and electrons. Quantum mechanics based methods are generally more accurate than MM methods, however, calculations are computationally more intensive than MM calculations.[1] Three major categories of quantum mechanics are: ab initio, semi-empirical and density functional theory (DFT) methods.

2.2 Ab-Initio Method

The classical mechanics is capable of predicting trajectory of atoms, it finds itself inadequate to explain most properties at atomic level; quantum mechanics comes to the rescue. Though former aims at describing trajectory of a particle under study, latter aims at finding not an accurate motion but probability distribution function. While earlier works of Born, Hartree, Pauli, Dirac etc. helped in formal development of the subject during early stage, Schrodinger is undoubtedly the premier who helped build the foundation of the mechanics that was to have severe influence in what science has become today.[2] Modern day science is indebted deeply to Schrodinger for his well known wave equation.[3]

$$H\psi = E\psi \qquad (2.1)$$

Here H represents Hamiltonian operator of the system-comprising of kinetic energy and potential energy term, E is eigen value representing energy and ψ represents eigen function. ψ is well behaved mathematical function such that $\psi^*\psi$ represents probability density.[4] While this equation is solvable for hydrogen or hydrogen-like atom easily- with little or no approximation- depending on property of interest. Howsoever simple equation it may be and capable of correctly describing the system fully, the only problem lies in solving it for a given system. In fact, it is beauty of this equation that almost any molecular system can be explained by merely solving it completely and yet, the basic problem lies with method of solving it.

Even for the simplest system like Hydrogen atom, the motion of constituents of system viz electrons and nucleus (the eigen function) may be represented by total wave function

comprising of electronic as well as nuclear wave function. The Hamiltonian may be expanded as:

$$H = -\sum_i \frac{\hbar^2}{2m_e}\nabla^2 - \sum_A \frac{\hbar^2}{2m_A}\nabla^2 - \sum_i \sum_A \frac{Z_A e^2}{r_{iA}} + \sum_{i<j} \frac{e^2}{r_{ij}} + \sum_{A<B} \frac{Z_A Z_B e^2}{r_{AB}} \qquad (2.2)$$

where i, j represent summation over electrons while A, B stand for nucleus. First and second terms represent kinetic energy of electrons and nucleus, third term stands for electron-nucleus potential energy, while fourth and fifth terms denote inter-electron and inter-nucleon interaction energy. After Born-Oppenheimer's realization that electrons adjust instantaneously with any changes in nucleus, the Schrodinger's equation was resolved by variable separable method, it got solvable for electronic wave function separately for a given arrangement of nucleus.[5-7]

Changing nuclear positions necessitates addition of nuclear repulsion term to electronic energy to get correct total energy of new configuration. Although variation in nuclear position may be dealt-with easily in atoms, scenario complicates in energy levels of even the simplest molecule (e.g. diatomic or linear multi-atomic etc.). As has been discussed earlier that Hamiltonian comprises of (a) kinetic energy as well as (b) potential energy term also, which is sub-divided into (i) nucleus-nucleus interactions (ignored due to Born-Oppenheimer approximation), (ii) electron-nucleus potential energy and (ii) inter-electron interaction energy; it is this last term that creates complexity. Hamiltonian due to electrons only is written as:

$$H_e = -\sum_i \frac{1}{2}\nabla_i^2 - \sum_A \sum_i \frac{Z_A}{r_{iA}} + \sum_{i<j} \frac{1}{r_{ij}} \qquad (2.3)$$

Here first term is kinetic energy, second term is nucleus-electron potential energy and last term is electron-electron interaction energy. With this H_e in hand, one gets E_e and ψ_e as solution. Thus the modified Schrodinger wave equation for n electron system is written as:[8]

$$H_e(1,2,...,n)\psi_e(1,2,...,n) = E_e\psi_e(1,2,...,n) \qquad (2.4)$$

It should be noted, this gives only the electronic part and not the nuclear part. The results obtained at electronic equation are used to get total energy and total wave function of given system. Nuclear interactions do not play important role in atomic wave functions but become important in molecular wave functions (commonly called as molecular orbitals).

Multi-electron systems are solvable only with approximation methods and many workers have proposed numerous methods for solving it. D. R. Hartree made earliest attempts in 1928 by assuming the total wave function to be product of wave functions of individual electrons (assuming Z-electron atom):[9]

$$\psi_e(r_1,\theta_1,\phi_1;r_2,\theta_2,\phi_2;...;r_z,\theta_z,\phi_z) = \psi_1(r_1,\theta_1,\phi_1)\psi_2(r_2,\theta_2,\phi_2)...\psi_z(r_z,\theta_z,\phi_z) \quad (2.5)$$

As Schrodinger's equation involves potential energy operator which if known will provide wave function and eigen value. But potential energy term is not known fully for such system. Also wave function must carry coordinates for all Z-electrons. Variable separable method would guarantee Z-independent linear differential equations from a single Schrodinger's equation for Z-electron atom (ignoring electron-electron potential term), which may later be solved by beginning with an approximate trial solution and solving for a field which converges to certain value after substantial number of iterations,

commonly called as self consistent field. Alternatively, variational principle may be used to get desired solutions. However application of such trial wave function was soon discarded due to such total wave function not being anti-symmetric- a condition imposed by Pauli's exclusion principle. After Fermi-Dirac statistics,[10] electrons were assumed to possess spatial as well as spin functions:

$$\Psi_{tot} = \psi(\vec{r}) \times \xi(s) \tag{2.6}$$

Here $\psi(\vec{r})$ represents spatial wave function while $\xi(\vec{s})$ stands for spin wave function (commonly represented by α or β).[11] Slater devised a method for obtaining such total electron wave functions (anti-symmetric)[12] from spatial and spin coordinates with the help of so-called Slater determinant:[13]

$$\psi = \frac{1}{\sqrt{N!}} \begin{vmatrix} \phi_1(r_1)\alpha(s_1) & \phi_2(r_1)\beta(s_1) & \ldots & \ldots & \ldots & \phi_n(r_1)\beta(s_1) \\ \phi_1(r_2)\alpha(s_2) & \phi_2(r_2)\beta(s_2) & \ldots & \ldots & \ldots & \phi_n(r_2)\beta(s_2) \\ \ldots & \ldots & \ldots & & & \ldots \\ \ldots & \ldots & & \ldots & & \ldots \\ \ldots & \ldots & & & \ldots & \ldots \\ \phi_1(r_n)\alpha(s_n) & \phi_2(r_n)\beta(s_n) & & & & \phi_n(r_n)\beta(s_n) \end{vmatrix} \tag{2.7}$$

Alternatively,

$$\psi = \frac{1}{\sqrt{N!}} \begin{vmatrix} \chi_1(1) & \chi_2(1) & \ldots & \ldots & \ldots & \chi_N(1) \\ \chi_1(2) & \chi_2(2) & \ldots & \ldots & \ldots & \chi_N(2) \\ \ldots & \ldots & \ldots & & & \ldots \\ \ldots & \ldots & & \ldots & & \ldots \\ \ldots & \ldots & & & \ldots & \ldots \\ \chi_1(N) & \chi_2(N) & & & & \chi_N(N) \end{vmatrix} \tag{2.8}$$

Using Slater's method, Hartree and Fock improvised the method of Self-consistent field theory, whereby each electron is assumed as moving in a fixed field arising due to

nucleus and remaining electrons. This method proved to be a great success as the electron-electron interaction term posed a severe hindrance in variable separation method. The energy of the atom or molecule is given by:

$$E = \frac{\int \psi^* H \psi d\tau}{\int \psi^* \psi d\tau} \tag{2.9}$$

or, in Dirac Notation,[14-16]

$$E = \frac{\langle \psi \mid H \mid \psi \rangle}{\langle \psi \mid \psi \rangle} \tag{2.10}$$

Besides being anti-symmetric, the wave functions are assumed to be ortho-normal:

$$\int \psi_m^* \psi_n d\tau = \delta_{mn} \qquad \text{OR} \qquad \langle \psi_m \mid \psi_n \rangle = \delta_{mn} \tag{2.11}$$

2.3 Hartree Self-Consistent Field Method

As stated earlier, nucleus is much heavier than electron, hence nuclear contribution in Hamiltonian does not play important role in atoms. However in molecules, configuration of nucleus of atoms adds to nuclear potential. Though Born-Oppenheimer helped in resolving such problem, this field (having constant value for a given geometry) must be added appropriately to get total energy and total wave function of the molecule.[17,18]

The Hamiltonian for N-electron system may be re-written as:

$$H_e = \sum_i h_i + \sum_i \sum_{j>i} g_{ij} + V_{nn} \tag{2.12}$$

where

$$h_i = -\frac{1}{2}\nabla^2 - \sum_A \frac{Z_A}{|R_A - r_i|} \tag{2.13}$$

and

$$g_{ij} = \frac{1}{|r_i - r_j|} \tag{2.14}$$

Note that one electron operator h_i describes the motion of the ith electron in the field of all nuclei of given molecule and must be the only operator in absence of any inter electronic or inter nuclear interaction, g_{ij} is two electron operator giving mutual repulsion between two electrons while V_{nn} is nuclear-nuclear interaction energy. From Dirac's notation for energy,

$$E = \sum_i \langle \chi_i \mid h_i \mid \chi_i \rangle + \frac{1}{2}\sum_{i,j} \left(\langle \chi_i \chi_i \mid g_{ij} \mid \chi_j \chi_j \rangle - \langle \chi_i \chi_j \mid g_{ij} \mid \chi_i \chi_j \rangle \right) + V_{nn} \tag{2.15}$$

Alternatively, it may be written as

$$E = \sum_i \langle \chi_i \mid h_i \mid \chi_i \rangle + \sum_{i<j} \left(J_{ij} - K_{ij} \right) + V_{nn} \tag{2.16}$$

Here first term represents energy due to core Hamiltonian operator in absence of any interaction, J_{ij} represents Coulomb operator (classically it is repulsion between two charge distributions), K_{ij} represents exchange operator (for which there is no classical analogue and is a result of Pauli's exclusion principle).[19] Evidently, this is many body problem (unlike Hydrogen atom, which is at most a two body problem) for which there is no 'exact' solution. Hence one solution can only be 'better' than another. To determine

the Molecular Orbital (MO) which has minimum energy (stable configuration), variational principle is used. A better wave function will have minimum energy lesser than a less 'correct' one. Such type of optimization is obtained subject to constraint that MOs should remain orthogonal and normalized. For this, Lagrange's method of undetermined multipliers may be used.[17,20] Thus the problem is minimization of energy subject to orthonormality constraint:

$$S_{ij} = \int \chi_i \chi_j d\tau = \left\langle \chi_i \mid \chi_j \right\rangle = \delta_{ij} \tag{2.17}$$

The Lagrange function will now be stationary with respect to variations in orbitals:

$$L = E - \sum_{i,j} \lambda_{ij} \left(\left\langle \chi_i \mid \chi_j \right\rangle - \delta_{ij} \right) \tag{2.18}$$

For extremum of Lagrange function:

$$\delta L = \delta E - \delta \sum_{i,j} \lambda_{ij} \left(\left\langle \chi_i \mid \chi_j \right\rangle - \delta_{ij} \right) = 0 \tag{2.19}$$

Here λ_{ij} is often identified as energy and related to molecular orbital energies. Under such formulation, one is now forced to find solution which takes into consideration motion of all electrons simultaneously, which in turn are so interconnected that change in one's coordinates (spatial or spin) is bound to affected others as well. To avoid such difficulty, one is forced to consider motion of one electron under the influence of field of nuclei and other electrons in their fixed orbitals χ_j. The resulting equation may then be tidied up as follows:[17,21]

$$F_i \chi_i = \sum_j \varepsilon_{ij} \chi_j \tag{2.20}$$

where F_i is called Fock operator:

$$F_i(1) = h_i(1) + \sum_j \left(J_j(1) - K_j(1) \right) \tag{2.21}$$

Here 1 in parentheses denotes operator for one particular electron, J is Coulomb operator (electron repulsion term) and K is exchange operator (spin correlation term). If Lagrangian multipliers are chosen zero unless indices i and j are same, one gets standard eigen value problem:

$$F_i \chi_i = \varepsilon_i \chi_i \tag{2.22}$$

It should be noted that solutions of above equations are not unique as determinant is unaffected by row/column transformations. Also, Fock operator is evaluable only if orbitals of remaining electrons are known. To counteract this vicious cycle, iterative method is employed which assumes trial solutions to get Fock operator (via Coulomb and Exchange operators) till solutions are 'self-consistent'. The Hartree Fock method is also known as mean field approximation method in which average electron-electron repulsion is taken into account.[22]

2.4 Roothaan Hall Equation

Fock proposed extension of Hartree's SCF procedure by introducing Slater's determinantal wave functions (obeying Pauli's exclusion principle). Although very elegant method for solving atoms, direct solution of Hartree Fock equation was not so practical for molecules. Roothaan and Hall independently recast the HF equation in matrix form by expanding MOs in terms of basis functions, conveniently called as atomic orbitals. This method is advantageous as it also helps in interpretability of results as

properties of molecules are commonly traced back to those of constituent atoms. In this scheme, spatial wave function is expressed as linear combination of basis functions:

$$\phi_i = \sum c_{\mu i}\theta_\mu \tag{2.23}$$

Energy minimization techniques help in evaluation of coefficients $c_{\mu i}$. Thus one gets a set of self consistent LCAO molecular orbitals ϕ_i. Such orbital will be best for any particular set of basis function. Roothaan Hall equation is obtained after variational technique:[23]

$$\sum_{\nu}\left(F_{\nu\mu} - \varepsilon_i S_{\nu\mu}\right)C_{\nu i} = 0 \tag{2.24}$$

where $F_{\nu\mu}$ is the Fock operator and $S_{\nu\mu}$ is the overlap integral:

$$F_{\nu\mu} = \left\langle \theta_\nu \mid h \mid \theta_\mu \right\rangle + \sum_{\gamma}^{AO}\sum_{\delta}^{AO} D_{\gamma\delta}\left(\left\langle \theta_\nu\theta_\gamma \mid g \mid \theta_\mu\theta_\delta \right\rangle - \left\langle \theta_\nu\theta_\gamma \mid g \mid \theta_\delta\theta_\mu \right\rangle\right) \tag{2.25}$$

$$S_{\nu\mu} = \left\langle \theta_\nu \mid \theta_\mu \right\rangle \tag{2.26}$$

The density matrix is defined as

$$D_{\gamma\delta} = \sum_{j}^{occ.MO} C_{\gamma j}C_{\delta j} \tag{2.27}$$

These equations were originally developed by Roothaan [23] and Hall [24] independently. Equations as mentioned above are a set of algebraic equations conveniently written as a matrix equation:

$$FC = SCE \tag{2.28}$$

The Fock matrix and C matrix are square matrix while E is a diagonal matrix whose elements are the orbital energies. Here the elements of Fock matrix depend on orbital coefficients $c_{\mu i}$ which appears on both sides of matrix equation, hence iterative procedure is adopted.[17]

Roothaan-Hall equation can be simplified to a form solvable by standard methods:

$$F'C' = C'E \tag{2.29}$$

where $F' = S^{-1/2} F S^{-1/2}$ and $C' = S^{1/2} C$ (2.30)

and solution exists only if determinant $|F' - EI|$ is zero. For larger matrices, diagonalization of matrix F' is preferred. The matrix of coefficients C' gives eigen vectors of F'.

Schrodinger equation is solved in Hartree-Fock method by setting up equations to solve all individual one-electron wavefunctions:

$$F_i(1)\phi_i(1) = \varepsilon_i \phi_i(1) \tag{2.31}$$

where 1 within parenthesis represents one electron equation. With certain basis set at hand, trial wave functions are formulated to get overlap matrix S_{ij} and Fock matrix F_{ij}. These are then used to calculate energy ε_i and coefficients $c_{\nu i}$ and iteration is followed until desired convergence is achieved. The motion of electrons is not correlated in HF equations.[25] The electron correlation is included in configuration interaction (CI) [26,27] and Møller-Plesset[28] perturbation theory.

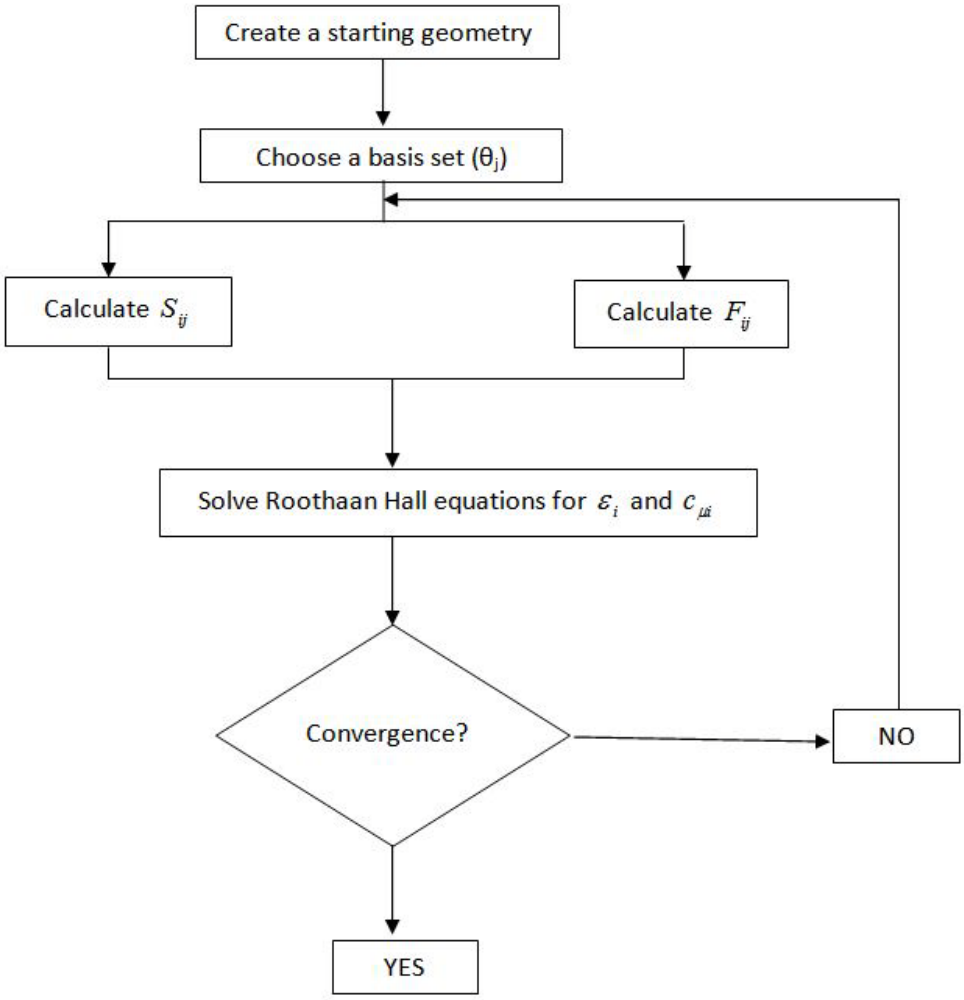

Figure 2.1: Algorithm for solving Roothaan Hall equation.

2.5 Basis Sets

Molecular orbitals can be expressed as a linear expansion of a combination of atomic orbitals termed as called basis functions. The basis set is a finite set of the basis functions. There are mainly two types of orbitals that are commonly used in the computing the electronic structure calculation: Slater Type Orbitals (STOs) and Gaussian Type Orbitals (GTOs). In 1930, the Slater type of orbitals (STOs) was first introduced by J. S. Slater and was addressed after his name.[29] The results obtained using these STOs were found

to be in good agreement for the simpler linear molecules, atomic and diatomic. The calculations of two electron integrals for other type of molecule is quite tedious and computationally expensive. This difficulty was handled with the use of Gaussian Type Orbital (GTO) proposed by S. F. Boys in 1950.[30]

2.5.1 Types of Basis Set

2.5.1.1 Minimal Basis Set

The minimal basis set was developed by Pople and co-workers and therefore are also termed as Pople basis set. A minimal basis set usually consists of a minimum number of basis function required to represent the electrons on each atoms. For example: to represent a H and He, only single s-function is used whereas to represent from Li to Ne, 1s, 2s, and 2p functions are used. The STO-nG is the most commonly used abbreviation to represent a minimal basis set where *n* is the number of Gaussian primitive functions to represent each orbital. In this bass set, the core and the valence orbitals are comprised of same number of Gaussian primitives. The main limitation of this basis set is its lack of flexibility. During the formation of the bond, orbital may vary (contract or expand) and the same cannot be well described by this minimal basis set. This problem can be rectified by representing each orbital with two or more functions. With the increase in the basis function, the accuracy in describing the orbital increases. Some commonly used minimal basis sets are: STO-3G, STO-4G, STO-6G, and STO-3G* (polarised version of the STO-3G).

2.5.1.2 Double-ζ and Extended Basis Sets

In the case of double-ζ basis sets two basis functions are assigned for each orbital. When more than two basis functions are assigned for each orbital, then they are known as extended basis sets. The extended basis sets provides a better description about the orbitals by allowing higher flexibility for the orbital exponents and also for the size of the orbitals. Few examples of this basis set are Dunning DZ, TZV, Dunning DZP, TZVPP (Valence triple- ζ plus polarization), QZVPP (Valence quadruple- plus polarization).

2.5.1.3 Split–Valence Basis Set

Calculating the double- ζ for every orbital is a tedious process. So, one should be concerned more for the valence orbital since the valence electrons mainly participate in bonding so double- ζ is calculated only for valence orbital electrons. The less important inner-shell electrons are described with a single Slater orbital. This method is called as split–valence basis set.[31,32] The split valence basis set 6-31G is represented as: X-YZG.

In the above mentioned case, the two numbers just after the hyphen (-) represent that it is a split valence double ζ .The split valence triple ζ, and quadrupole ζ are represented as X-YZWG and X-YZWVG respectively. Some of the commonly used basis sets are 3-21G, 6-31G, 6-311G etc.

2.5.1.3.1 Polarization Function

The polarization function is represented by the Pople notation and is denoted by an asterisk (*). A single asterisk denotes the addition of d-type polarization functions to the heavy atoms and the addition of second asterisk imply the inclusion of p-type functions to

the hydrogen atoms as in 3-21G*, 6-31G* or 6-311G** basis sets. In 6-311G basis set, the core orbital are modeled by the single function which is comprised of six primitive GTOs and the valence part is modeled by the 3 basis functions which consists of 3, 1 and 1 primitive GTOs. It is also quite noteworthy that 6-31G (d,p) is the same as 6-31G**.

2.5.1.3.2 Diffuse Function

Diffuse basis set adds the s and p type functions to heavy and H atoms to provide large region of space orbital. The basis sets described so far fail to deal with the anions and molecules containing the lone pairs which do have large amount of electron density away from the nuclear centres. This is necessary for describing the systems where electrons are far away from nucleus such as in anions, molecules with lone pairs, systems with excited states and low ionization potential etc. In order to overcome this problem, highly diffuse functions are added to the basis set. These basis sets are denoted using a "+" sign, i.e. 3-21+G. A single "+" sign denotes p orbital, "++" indicates accounts for p and s orbitals as in 6-31+G* or 6-311++G** basis sets.

The choice of DFT functional and basis set primarily depends on the type of system, the required accuracy of the results as well as computational resources available. There are a large variety of DFT functionals and basis sets implemented in the Gaussian 09. We have used various functionals and basis sets in the work described in this thesis. In the chapter three of the present thesis, the geometries of all the modeled systems were optimized using the 6-31G basis sets thereby the geometries were subjected for the single point energy calculations using 6-31++G**. The fourth chapter of the thesis deals with the various doped graphene models. In this chapter the geometries of the systems were optimized with 6-31+G** basis set followed by the single point energy calculations with

6-311+G** basis set. The chapter five discusses the role of metal ions in SWCNT. In this chapter, the geometries were initially optimized using the 6-31G* basis set. Further details and justification of the computational scheme adopted can be found in respective chapters along with references.

2.6 Density Functional Theory

For the development of DFT, Walter Kohn, in 1998 was conferred with the Nobel prize in chemistry. Since then, this theory became a powerful computational tool to handle the many-electron system.

Since the last two decades, the DFT based computation became very popular and drew the attention of the researchers as it provided a lot of relevant information pertaining to the important properties of the system at a lower cost in comparison to the wave function based methods. The energy functional in case of DFT can be studied by using the following equation:

$$E_{DFT}[\rho] = T[\rho] + E_{ne}[\rho] + E_{ee}[\rho] \qquad (2.32)$$

Where, T [ρ] is the kinetic energy, $E_{ne}[\rho]$ represents the attraction between the nucleic and electrons and $E_{ee}[\rho]$ denotes the electron-electron repulsion. The third term i.e. the electron repulsion term can further be divided into coulomb J[ρ] and exchange parts K[ρ]. The equation now may be written by incorporating the correlation term implicitly in all the terms. Thus, the equation takes the form:

$$E_{DFT}[\rho] = T[\rho] + E_{ne}[\rho] + J[\rho] + K[\rho] \qquad (2.33)$$

The $E_{ne}[\rho] + J[\rho]$ term may be expressed in classical expression as:

$$E_{ne}[\rho] = -\sum_{\alpha}^{n} \int \frac{Z_{\alpha}(R_{\alpha})\alpha(r)}{|R_{\alpha} - r|} dr \tag{2.34}$$

Where n correspond to the number of nuclei.

$$J[\rho] = \frac{1}{2} \iint \frac{\rho(r)\rho(r')}{|r - r'|} dr dr' \tag{2.35}$$

Thomas and Fermi[33] made an attempt to calculate some important properties of the molecules instead of using the conventional wavefunction. In the year 1927, they proposed the following kinetic energy term $T_{TF}[\rho]$,

$$T_{TF}[\rho] = \frac{3}{10}\left(3\pi^2\right)^{\frac{2}{3}} \int \rho^{\frac{5}{3}}(r) dr \tag{2.36}$$

Where $T_{TF}[\rho]$ resembles the kinetic energy functional of the Thomas-Fermi (T-F) model. With incorporation of the exchange term, the model now is termed as T-F model where:

$$K[\rho] = -\frac{3}{4}\left(\frac{3}{\pi}\right)^{\frac{1}{3}} \int \rho^{\frac{4}{3}}(r) dr \tag{2.37}$$

The total energy functional of the system $E_{TFD}[\rho]$ can be expressed as:

$$E_{TFD}[\rho] = \frac{3}{10}(3\pi^2)^{\frac{2}{3}} \int \rho^{\frac{5}{3}}(r) dr - \sum_{\alpha}^{N_{nuclei}} \int \frac{Z_{\alpha}(R_{\alpha})\rho(r)}{|R_{\alpha} - r|} dr$$
$$+ \frac{1}{2} \iint \frac{\rho(r)\rho(r')}{|r - r'|} dr dr' - \frac{3}{4}\left(\frac{3}{\pi}\right)^{\frac{1}{3}} \int \rho^{\frac{4}{3}}(r) dr \tag{2.38}$$

The F-D model owes a drawback, since to represent the atoms and molecules, the assumptions made pertaining to the uniform electron gas model is very poor. The striking

feature of this T-F model is that the energy can be calculated considering the electron density and not how efficiently can one calculate the ground state energy.

In 1964, it was well established by Hohenberg and Kohn that, of a particular system, the ground state energy is a functional of electron density. In 1965, the formalism of DFT was put forwarded by Kohn- Sham. The superiority of the DFT approach over the SCF procedure can well be understood by the fact that the conventional SCF procedure has a wave function which is a function of 3N variables, N being the number of electrons present in the system.

2.6.1 Hohenberg−Kohn Theorems

In the year 1964, Hohenberg and Kohn proposed two fundamental theorems that laid down the formulation of the DFT. These two theorems led to the beginning of the Modern DFT at that time.

First Hohenberg-Kohn theorem (HK-I)[34] states that all the properties of a molecule in a ground electronic state can be determined by the ground state electron density. In other words, ground state energy (E_0) is a functional of ground electron density, $\rho_0(x, y, z)$.

$$E_0 = E_0[\rho_0] \tag{2.39}$$

So, the electron density can be integrated over all space to obtain the total number of electrons of the system (N).

$$\int \rho_0(r)dr = N \tag{2.40}$$

The second Hohenberg-Kohn theorem (HK-II) states that the ground state energy E_0 can be obtained by applying variational principle. Accordingly, for every trial density

function that satisfies the equation and $\rho_{tr}(r)\geq 0$ for all r, the following inequality holds, where, E_υ is the energy functional.

$$E_0[\rho_0] < E_\upsilon[\rho_{tr}(r)] \tag{2.41}$$

Later Kohn- Sham gave an approach that was popularly known as K-S approach. In this approach, the iterative processes which were similar to the single-electron wavefunction in HF is considered to attain the self-consistency, which is known as Kohn-Sham approach.

In this approach, the energy of the system is considered to be the sum of the kinetic energy functional of non-interacting system (T_s), the energy functional due to the nuclei (E_{ne}), the Coulomb electron-electron repulsion (J) and the term E_{xc} which includes the effects of exchange and correlation. The noteworthy feature in this equation is that all the terms are functional of the electron density (ρ).

$$E_{DFT}[\rho] = T_S[\rho] + E_{ne}[\rho] + J[\rho] + E_{XC}[\rho] \tag{2.42}$$

The accuracy of KS method depends on the quality of the exchange-correlation functional, which is defined as,

$$E_{XC}[\rho] = \Delta T[\rho] + \Delta V_{ee}[\rho] \tag{2.43}$$

ΔT and ΔV_{ee} are the difference in average electronic kinetic energy and electron-electron repulsion terms in comparison to non-interacting reference system. The functional derivatives of E_{XC} is the exchange-correlation potential (V_{XC}).

$$V_{XC}(r) = \frac{\delta E_{XC}[\rho(r)]}{\delta\rho(r)} \tag{2.44}$$

E_{XC} is the unknown term and approximations have to be explored to get the correct values for the exchange-correlation energy.

2.6.2 Local Density Approximation (LDA)

The LDA approach considers that the density may be dealt with locally just like a uniform homogeneous electron gas as this is the only system for which the exchange-corelation energy is accurately known. At every point in the system, this exchange correlation energy is comparable with the uniform electron gas owing the similar density. The exchange electron density is governed by the Dirac formula and is given as:

$$E_X^{LDA}[\rho] = -\frac{3}{4}\left(\frac{3}{\pi}\right)^{1/3}\int \rho^{\frac{4}{3}}(r)dr \tag{2.45}$$

$$E_X^{LDA} = -\frac{3}{4}\left(\frac{3}{\pi}\right)^{1/3}\rho^{\frac{1}{3}} \tag{2.46}$$

Where E_X^{LDA} is the exchange energy per particle. Kohn-Sham originally proposed the key idea of this approximation and this is true for the slowly varying density. This correlation energy may be acquired by adapting to many body studies of Gell-Mann and Brueckner and Ceperly and Alder.[35,36] However, there are various remarkable density functionals that were developed based on the LDA approximation like Vosko-Wilk-Nusair (VWN),[37] Perdew-Zunger (PZ81),[38] and Perdew-Wang (PW92).[39] In LSDA, the electron density is replaced with the spin electron density, therefore are termed as local spin density approximation (LSDA).

2.6.3 Generalised Gradient Approximation (GGA)

It is only after the introduction of the gradient corrections that the DFT methods have been extensively used for the molecular systems. When the exchange and the correlation functionals are made dependent on both electron densities and their gradients, the procedure seems to model the inhomogeneous (interacting) nature of the electrons. These methods are known as the gradient corrected methods, non-local methods or the generalized gradient approximation (GGA). Inclusion of the electron density gradients takes into account the interacting nature of the electrons, which is not the case in the LDA based approaches. The electron density in an atom or molecule varies greatly from place to place, so it is not surprising that the uniform electron gas model has serious shortcomings. Most DFT calculations nowadays use exchange-correlation energy functionals that utilize both the electron density and its gradient or slope (first derivatives with respect to position). These functionals are called gradient corrected, or said to use the generalized-gradient approximation (GGA). They are also called nonlocal functionals, in contrast to the LDA functionals.

The exchange and correlation terms in GGA is given as,

$$E_{XC} = E_X^{GGA} + E_C^{GGA} \tag{2.47}$$

Based on the GGA, some of the important exchange functionals are are Becke88 (B), Perdew-Wang (PW91), Modified Perdew-Wang (MPW), Gill96 (G96) and Perdew-Burke-Ernzerhof (PBE).[40-43] The correlation functionals based on GGA are Lee, Yang, and Parr (LYP), Perdew-Wang (PW91) , Perdew 86 (P86), Becke 96 (B96) and Perdew-Burke- Ernzerhof (PBE).[39,44-46]

2.6.4 Hybrid Functional

Both the approximations viz. LDA and GGA donot describe well the exchange term. The HF method yields an exact exchange term, the hybrid DFT involves mixing various amounts of Hartree-Fock (HF) nonlocal exchange operator with DFT exchange correlation functional. Axel, Becke in the year 1993, proposed the novel approach of constructing the density functional approximation. The hybrid exchange-correlation energy may be written as:

$$E_{XC}^{hyb} = \frac{X}{100} E_X^{HF} + \left(1 - \frac{X}{100}\right) E_X^{DFT} + E_C^{DFT} \tag{2.48}$$

where E_X^{HF} resembles the nonlocal Hartree-Fock (HF) exchange energy, X denotes the percentage of Hartree-Fock exchange in Hybrid functional, E_X^{DFT} gives the local DFT exchange energy and E_C^{DFT} informs about the local DFT correlation energy. The parameter X is optimized so as to obtain a better hybrid functional by adopting various methods. Among all the hybrid DFT methods, B3LYP is the most popular one that uses a totally different scheme. In this scheme three mixing parameters are noteworthy[44,47] as given below:

$$E_{XC}^{B3} = (1-a)E_X^{LSDA} + aE_X^{exact} + b\Delta E_X^{B88} + E_C^{LSDA} + cE_C^{GGA} \tag{2.49}$$

By comparing the experimental evidences in the form of data these 3 parameters, a, b, and c were calculated. Therefore, these are termed as the Becke3 parameter functional. PBE0 is also an important hybrid functional. In this functional, 1:3 ratio is considered of DFT and exchange energies.

Truhlar developed the Minesota functional which are based on meta-GGA approximation. These functional have empirical fitting and can be applied to the uniform electron gas.[48] B2LYP [49] is an example of the most widely used double hybrid DFT functional.

2.7 Dispersion Correction

Dispersion forces are important attractive forces that are generally of long range order. This type of forces acts between induced dipole and instantaneous dipole which arise due to the electron correlation between the interacting systems. Dispersion based first modern theory was proposed by London. According to London, these dispersion forces are an outcome of the subsystems separated. The main cause of dispersion forces is correlation effect and so these cannot be reproduced at HF level. The main drawback of DFT is primarily the lack of an exact and explicit form of the exchange -correlation functional.

In order to handle the issues concerned with the dispersion correction, various approaches were taken into consideration like nonlocal vdW density functional, conventional and parametrized density functional and the well known semi classical corrections DFT-D methods. Dion et al.[50] in the year 2004, propounded the vDW-DF, a non local correlation functional related to dispersion interactions. To overcome certain problems and propounded a second version vDW-DF2 by incorporating a more accurate semi local functional PW86.

Parametrization of the DFT functionals (standard) related to the exchange-correlation energy is another approach to obtain the developed functionals. The Wilson-Levy functional coupled with Hartree Fock theory is used to obtain the interaction energies of

weakly bonded systems.[51] Tao Perdew-Staroverov-Scuseria (TPSS) is a meta GGA functional for exchange-correlation energy without empirical parameters.[52,53]

Using the Semi classical approach, Truhlar et al. established the M05 class of functional. From the Minesota fnctional series, the M06-2X is found to deliver accurate results for various non-covalent interactions. DFT-D is the Grimme's approach that is subjected to the semiclassical treatement of various strenuous dispersion interaction. With the pace of time and advancement, DFT-D3 came to existence, removing certain drawbacks of the former. Also some other commonly used functional are B97D, B3LYP-D3, WB97XD, and B2LYPD.

2.8 Basis Set Superposition Error (BSSE)

An in-depth knowledge pertaining to the interaction energy is very crucial to the chemists as it signifies the stability of the complex system. In the chapter 4 of the present thesis, the interaction energies were calculated using the supramolecular approach. The term Basis Set Superposition Error" (BSSE) was coined by Liu and McLean to represent this error.[54] In weakly bound intermolecular interactions when monomer A approaches monomer B, the dimer is stabilized and as a result there is an artificial shortening of intermolecular distance and concomitant artificially strengthening the intermolecular interaction. Such error arises from the inconsistent treatment of the monomers and termed as basis set superposition error (BSSE).[55] To eliminate this error Boys and Bernardi proposed a technique called counterpoise correction and a brief overview has been given below.[56] Intermolecular interaction energy for a typical dimer AB from supramolecular approach can be computed as:

$$\Delta E_{CP}(AB) = E_{AB}^{\alpha\cup\beta}(AB) - E_{AB}^{\alpha\cup\beta}(A) - E_{AB}^{\alpha\cup\beta}(B) \tag{2.50}$$

In this case, $E_{AB}^{\alpha\cup\beta}(A)$ is the energy of monomer A, whose geometry is that found in the AB complex and calculated with the dimer basis set, and $E_{AB}^{\alpha\cup\beta}(B)$ is the energy of the monomer B. It is noteworthy that the subscript on the ΔE signifies the method adopted in the calculation. In this type of method, the same numbers of basis functions are utilized in each component.

2.9 Quantum Theory of Atoms in Molecules (QTAIM) Analysis

One of the main objectives of the quantum chemistry is the classification of chemical bonds. However, the main notion of the chemical bond can be easily comprehended by the chemist. There are various procedures that define the criteria how to classify the chemical bonds using the quantum mechanical approach. These methods are mostly based on either orbital picture[57,58] (such as orbital localization) or electron density (ρ(r)) bases analysis.[59,60] One of the well established and popular methods is based upon the electron density and is known as QTAIM analysis. In this analysis, the critical points are considered for the study and play the central role in classifying the electron density. The critical points (CPs) are the points at which the first derivative of the electron density vanishes and play significant role in the characterization of electron density topology in QTAIM.[61]

$$\nabla\rho = i\frac{dp}{dx} + j\frac{dp}{dx} + k\frac{dp}{dx}\begin{cases} = 0(\,forCPs) \\ Generally \neq 0(\,forotherpo\,\text{int}\,s) \end{cases} \tag{2.51}$$

This critical points are categorized as per their rank and signature which represented as (ω, σ). The number of non-zero curvatures of ρ(r) at the critical points is termed as the rank. A critical point which has rank <3 is said to be unstable mathematically.

The presence of such a CP (with a rank less than three) indicates a change in the topology of the density thereby producing a change in the molecular structure. For this reason, critical points with ω < 3 are generally not found in equilibrium charge distributions and one nearly always finds ω = 3. However, the signature is the algebraic sum of the signs of the curvatures, i.e. each of the three curvatures contributes ±1 depending on whether it is a positive or negative curvature. There are four types of stable critical points that have three non-zero eigenvalues:

- (3, 3) Three negative curvatures: is a local maximum.
- (3, 1) Two negative curvatures: is a maximum in the plane defined by the corresponding eigenvectors but is a minimum along the third axis which is perpendicular to this plane.
- (3,+1) Two positive curvatures: is a minimum in the plane defined by the corresponding eigenvectors and a maximum along the third axis which is perpendicular to this plane.

Depending upon the chemical structures, the critical points can be categorised: (3, -3) nuclear critical point (NCP); (3,+3) cage critical point (CCP), (3,+1) ring critical point (RCP) and (3, -1) bond critical point (BCP).

According to the QTAIM analysis, the interactions that prevail between the two atoms can be classified using the corresponding BCPs. It has been confirmed that the electron density at these BCPs has some correlation with the strength for the covalent bond.

The Laplacian of the electron density at this point ($\nabla^2\rho(r)$) reflects sharing character of the bond. Positive values for ($\nabla^2\rho(r)$) are generally attributed to closed shell interactions, such as the interatomic interaction between noble gas atoms, whereas negative values denote covalent bonding. The $\rho(r)$ values particularly for the covalent bonds ranges 0.200-0.400 au with the larger negative of ($\nabla^2\rho(r)$). Thus lower $\rho(r)$ values along with the positive ($\nabla^2\rho(r)$) values are indicative of interactions of van der Waals complexes.

2.10 Softwares Used

We have used Gaussian program along with GaussView software package for all DFT calculations. Gaussian is the most popular commercial quantum chemistry package, currently distributed by Gaussian Inc. Wallingford, USA. The current version of the program is Gaussian 09.[62] Gauss-View is popular modeling and visualization software of Gaussian. This program was developed by Semichem Inc., but distributed with Gaussian. Gauss-View is used to model the molecular system, create the input and visualize the output. Gaussian processes the input created by Gauss View and is used to perform all calculations and produces an output. There are several other packages that can be used to visualize Gaussian outputs apart from Gauss View, some of them are Avogadro, Chemcraft etc.

AIM2000 is a user friendly and efficient program, based on quantum theory of atoms in molecules. It uses the output generated by Gaussian09 as an input and automatically performs QTAIM analysis on the system under study. The QTAIM theory efficiently describes the nature and strength of various types of hydrogen-bonded interactions. It exploits some topological parameters viz. electron density (ρ) and its Laplacian ($\nabla 2\rho$),

kinetic energy density (G), potential energy density (V) and total electron energy density (H) at the bond critical point (BCP) of interaction atoms or fragments. The QTAIM analysis can also give insights on the strength of hydrogen bond as proposed by Koch and Popelier criterion.[63]

References

[1] W. J. Hehre, J. Yu, P. E. Klunzzinger, L. Lou, *A Brief Guide to Molecular Mechanics and Quantum Chemical Calculations, Wavefunction, Inc., U.S.A.*,(1998).

[2] L. I. Shiff, *Quantum Mechanics, 3rd edition, McGraw- Hill*, New York (1968).

[3] E. Schroedinger, *Ann. Physik*, **79**, 361 (1926).

[4] L. Pauling, E. B. Wilson, *Introduction to Quantum Mechanics, McGraw-Hill*, New York (1935).

[5] M. Born and J. R. Oppenheimer, *Ann. Physik*, **84**, 458 (1927).

[6] W. Kolos and L.Wolniewicz, *J. Chem. Phys.*,**41**, 3663 (1964).

[7] B. T. Sutsliffe, *Adv. Quantum. Chem.*, **28**, 65 (1997).

[8] J. A. Pople , D. L. Beveridge, *Approximate Molecular Orbital Theory, McGraw-Hill Book Co.*, New York (1970).

[9] D. R. Hartree, *Proc. Cambridge Phil. Soc.*, **24**, 426 (1928).

[10] G. Uhlenbeck and S. A. Goudsmit, *Nature wissenschaften*, **13**, 953 (1925).

[11] J. A. Pople, D. L. Beveridge, P. A. Dobosh, *J. Chem. Phys.*, 47, 2026 (1967).

[12] W. Pauli, *Physik.*, **31**, 765 (1925).

[13] J. C. Slater, *Phys. Rev.*, **35**, 509 (1930) and **34**, 1239 (1959).

[14] P. A. M. Dirac, *The Principle of Quantum Mechanics, Oxford University Press*, London (1958).

[15] J. K. L. McDonald, *Phys. Rev.*, **43**, 830 (1933).

[16] R. H. Young, *Int. J. Quant. Chem.*, **6**, 596 (1972).

[17] F. Jenson, *Introduction to Computational Chemistry, 2nd Edition, John Wiley & Sons Ltd.*, Chichester (2007).

[18] I. N. Levine, *Quantum Chemistry; Chapter-11, "The HartreeFock Self-Consistent Method", 5th Edition, Pearson*, (2000).

[19] I. N. Levine, *Quantum Chemistry., Chapter-8, "Perturbation Theory", 5th Edition* Pearson, (2000).

[20] J. A. Pople and D. L Beveridge, *Physik.*, **61**, 126 (1930).

[21] J. E. Lennard-Jones, *Proc. Roy. Soc*. (London), **A198**, 14 (1949).

[22] C. Edimiston, K. Ruedenberg, *Rev. Mol. Phys.*, **34**, 457 (1963); *J. Chem. Phys.*, **43**, 597 (1965).

[23] C. C. Roothan, *J. Rev. Mod. Phys.*, **23**, 69 (1951).

[24] G. G. Hall, *Proc. Roy. Soc., (London)*, **A205**, 541 (1951).

[25] W. J. Hehre, L. Radom, J. A. Pople, P.v.R. Schleyer, *Ab Initio Molecular Orbital Theory*, Wiley (1986).

[26] B. O. Roos, (Ed.) *Lecture Notes in Quantum Chemistry*, Springer -Verleg (1992).

[27] J. Olsen, O. Christiansen, H. Koch, P. Jorgensen, *J. Chem. Phys. Lett.*, **261**, 369 (1996).

[28] C. Moller and M. S. Plesset, *Phys. Rev.*, **46**, 618 (1934).

[29] J. C. Slater, *Phys. Rev.*, **36**, 57 (1930).

[30] S. F. Boys, *Proc. R. Soc. London A*, **200**, 542 (1950).

[31] J. S. Binkley, J. A. Pople, W. J. Hehre, *J. Am. Chem. Soc.*, **102**, 939 (1980).

[32] M. S. Gordon, J. S. Binkley, J. A. Pople, W. J. Pietro, W. J. Hehre, *J. Am. Chem. Soc.*, **104**, 2797 (1982).

[33] L. H. Thomas, *Math. Proc. Cambridge*, **23**, 542 (1927).

[34] P. Hohenberg and W. Kohn, *Phys. Rev.*, **136**, B864 (1964).

[35] D. M. Ceperley and B. Alder, *J. Phys. Rev. Lett.*, **45**, 566 (1980).

[36] M. Gell-Mann and K. A.Brueckner, *Phys. Rev.*, **106**, 364 (1957).

[37] S. H. Vosko, L. Wilk, M. Nusair, *Can. J. Phys.*, **58**, 1200 (1980).

[38] J. P. Perdew and A. Zunger, *Phys. Rev. B*, **23**, 5048 (1981).

[39] J. P. Perdew and Y. Wang, *Phys. Rev. B*, **45**, 13244 (1992).

[40] J. P. Perdew and K. Burke, Y. Wang, *Phys. Rev. B*, **54**, 16533 (1996).

[41] J. P. Perdew and K. Burke, M. Ernzerhof, *Phys. Rev. Lett.*, **77**, 3865 (1996).

[42] A. D. Becke, *Phys. Rev. A*, **38**, 3098 (1988).

[43] C. Adamo and V. Barone, *J. Chem. Phys.*, **108**, 664 (1998).

[44] C. Lee, W. Yang, R. G. Parr, *Phys. Rev. B*, **37**, 785 (1988).

[45] J. P. Perdew, *Phys. Rev. B*, **33**, 8822 (1986).

[46] A. D. Becke, *J. Chem. Phys.*, **104**, 1040 (1996).

[47] A. D. Becke, *J. Chem. Phys.*, **98**, 5648 (1993).

[48] Y. Zhao and D. Truhlar, *Theor. Chem. Acc.*, **120**, 215 (2008).

[49] S. J. Grimme, *Chem. Phys.*, **124**, 034108 (2006).

[50] M. Dion, H. Rydberg, E. Schröder, D. C. Langreth, B. I. Lundqvist, *Phys. Rev. Lett.*, **92**, 246401 (2004).

[51] L. C. Wilson and M. Levy, *Phys. Rev. B*, **41**, 12930 (1990).

[52] J. Tao and J. P. Perdew, *J. Chem. Phys.*, **122**, 114102 (2005).

[53] J. Tao, J. P. Perdew, V. N. Staroverov, G. E. Scuseria, *Phys. Rev. Lett.*, **91**, 146401 (2003).

[54] B. Liu and A. D. McLean, *J. Chem. Phys.*, **59**, 4557 (1973).

[55] H. B. Jansen, P. Ros, *Chem. Phys. Lett.*, **3**, 140 (1969).

[56] S. F. Boys and F. Bernardi, *Mol. Phys.*, **19**, 553 (1970).

[57] A. E. Reed, L. A. Curtiss, F. Weinhold, *Chem. Rev.*, **88**, 899 (1988).

[58] C. Edmiston and K. Ruedenberg, *Rev. Mod. Phys.*, **34**, 457 (1963).

[59] R. F. W. Bader, *Chem. Rev.*, **91**, 893 (1991).

[60] A. D. Becke and K. E. Edgecombe, *J. Chem. Phys.*, **92**, 5397 (1990).

[61] Bader, R. F. W. *Atoms in Molecules: A Quantum Theory*, Oxford University Press: Oxford, UK (1990).

[62] Gaussian 09, Revision D.01, M. J. Frisch, G. W. Trucks, H. B. Schlegel, G. E. Scuseria, M. A. Robb, J. R. Cheeseman, G. Scalmani, V. Barone, B. Mennucci, G. A. Petersson, H. Nakatsuji, M. Caricato, X. Li, H. P. Hratchian, A. F. Izmaylov, J. Bloino, G. Zheng, J. L. Sonnenberg, M. Hada, M. Ehara, K. Toyota, R. Fukuda, J. Hasegawa, M. Ishida, T. Nakajima, Y. Honda, O. Kitao, H. Nakai, T. Vreven, J. A. Montgomery, Jr., J. E. Peralta, F. Ogliaro, M. Bearpark, J. J. Heyd, E. Brothers, K. N. Kudin, V. N. Staroverov, T. Keith, R. Kobayashi, J. Normand, K. Raghavachari, A. Rendell, J. C. Burant, S. S. Iyengar, J. Tomasi, M. Cossi, N. Rega, J. M. Millam, M. Klene, J. E. Knox, J. B. Cross, V. Bakken, C. Adamo, J. Jaramillo, R. Gomperts, R. E. Stratmann, O. Yazyev, A. J. Austin, R.

Cammi, C. Pomelli, J. W. Ochterski, R. L. Martin, K. Morokuma, V. G. Zakrzewski, G. A. Voth, P. Salvador, J. J. Dannenberg, S. Dapprich, A. D. Daniels, O. Farkas, J. B. Foresman, J. V. Ortiz, J. Cioslowski, and D. J. Fox, Gaussian, Inc., Wallingford CT, (2013).

[63] U. Koch and P. L. A. Popelier, *J. Phys. Chem.*, **99**, 9747 (1995).

Chapter 3

Binding of nucleic bases adsorbed on graphene (GR) and boron nitride graphene (BNG)

CHAPTER 3

BINDING OF NUCLEIC BASES ADSORBED ON GRAPHENE (GR) AND BORON NITRIDE GRAPHENE (BNG)

3.1 Introduction

Graphene, the wonder material, since its discovery in 2004 by Andrew Geim and Novoselov has ignited the interest among the researchers due to its diverse chemical and physical properties that has led to a boom in the technological advancement. Some of the striking properties of graphene are high charge mobility, quasi-particles and quantum Hall effect that brings it ahead and becomes a preferred choice of material over the conventional materials.[1-13] Further electron confinement and some graphene nanostructures, such as one-dimensional graphene nanoribbons (GNRs) and zero dimensional graphene quantum dots (GQDs), have also attracted interest, which can provide a possibility to explore low dimensional transport and perspective for carbon-based nano electronics. Wei et al. successfully synthesized few layers of graphene for the application of high conductivity for nano-electromechanical switches.[15] Progress in preparing GNRs[12,14,16] and GQDs[4,11,13] has been reported with different approaches. First-principles calculations show that GNRs with hydrogen passivated edges mostly have non-zero and direct energy gaps.[22,23] Some very nice reviews[17-19,20,21] illustrate and focus on various aspects of graphene in detail. Fujita et al. studied

in detail the electronic properties of graphite particularly zig-zag and armchair graphite ribbons and explored the electronic property of the same.[18]

In the year 1962,[24] boron nitride graphene, generally termed as white graphene, was first fabricated in the laboratory and four years later it was patented.[25] It is a material with a range of noteworthy thermal, chemical and physical properties that may be used for a large number of applications, like genome editing,[26,27] drug delivery,[28,29] water treatment,[30] hydrogen storage,[31] cosmetics,[32] field effect transistors (FETs),[33] electronics [34-36], solar cells and photodectors.[37] etc.

Nucleic bases (NBs) are nitrogen-rich biomolecules, and are categorized as purines and pyrimidines. The Purines are adenine and guanine, adenine is generally denoted by single letter “A” while guanine is denoted by a single letter “G”. The pyrimidines are represented as thymine (T), cytosine (C), and uracil (U). Being the building blocks of deoxyribonucleic acid (DNA) and ribonucleic acid (RNA) these nucleic bases (NBs) play a very important role in transmission of genetic information, expression and storage. It is quite noteworthy that these nucleic bases (NBs) and their derivatives play a central role and are very important for studying the human metabolism, in clinical diagnosis and in the synthesis of anticancer drugs, etc.[38-41] Therefore, to have a deep understanding of their interaction with the carbon nanomaterials is crucial to develop novel sensors.

The interaction of biological molecules like DNA/RNA bases, amino acids using graphene and carbon nanotubes as the adsorbing material have been studied extensively both experimentally and theoretically. The studies illustrate that the nucleobases and amino complexes formed with the carbon nanostructures like graphene and carbon

nanotubes are stabilized by the non-covalent interactions like π-π stacking and X-π (X=NH,OH,CH).[42-49] The graphene oxide nanosheets are utilized for the removal of the toxins present in the drinking water in traces.[50] The graphene oxide is also capable of removing the antibiotics from water.[51] Also it is noticed that the cytotoxicity of small DNA intercalators are augmented in the presence of graphene oxide.[52] Recently, it is also explored that drug molecules tend to bind with greater affinity with the nanomaterials in the presence of different functional groups.[53,54]

For the molecular detection of the biological molecule (NBs) and to design a novel biosensor, the study and design of such adsorbing material is of paramount importance.[55-58] There has been a consistent endeavor for the development of some novel hybrid material that deals primarily with the interaction of NBs with nanomaterials which efficiently contributed to the life sciences.[59-65] Some contemporary studies explore the importance of doping particularly with Aluminium, Gallium, Nickel and Silicon on graphene which augments the adsorption strength of the NBs in comparison to the pristine graphene.[66-68] The strength of adsorption on the pristine graphene(G), Boron-doped graphene(BG), Nitrogen-doped graphene(NG), and Silicon-doped graphene(SG) has also been explored.[69] Experimental studies also reveal the synthesis of the NBs- graphene and carbon nanotubes materials.[70,71]

The dopants like Carbon, Silicon, Aluminium, Gallium on the Boron nitride nanotube (BNNTs) affects so much that the adsorption properties are increased such that they can be utilized for sensing, catalysis, drug delivery, and also for the removal of environmental pollutants.[72-77] Subramanian et al. suggested that for the nitrogen fixation, the boron-rich BNNTs could even act as catalysts.[78]

In the present work, a detailed comparison between the graphene and the boron nitride graphene has been performed, the interaction of the nucleic bases with boron nitride has been studied in two modes: (a) parallel mode and (b) perpendicular mode. The HOMO-LUMO gap is also calculated for the complex systems.

3.2 Methods

The graphene sheet considered in the study, consist of 72 carbon atoms which were passivated with 24 hydrogen atoms at the boundaries. The boron nitride graphene is obtained with the help of the Gauss View 5.0 by substituting the Nitrogen and Boron atoms alternatively. Initially the graphene sheets i.e. the graphene (GR) and the boron nitride graphene (BNG) were optimized by using the density functional theory (DFT)[79, 80] as implemented in the Gaussian 09 software package. The nucleic bases (NBs) were also optimized separately. The complex of the graphene and the nucleic bases were optimized at the same level using the B3LYP[81,82] method and 6-31G[83-92]basis set.

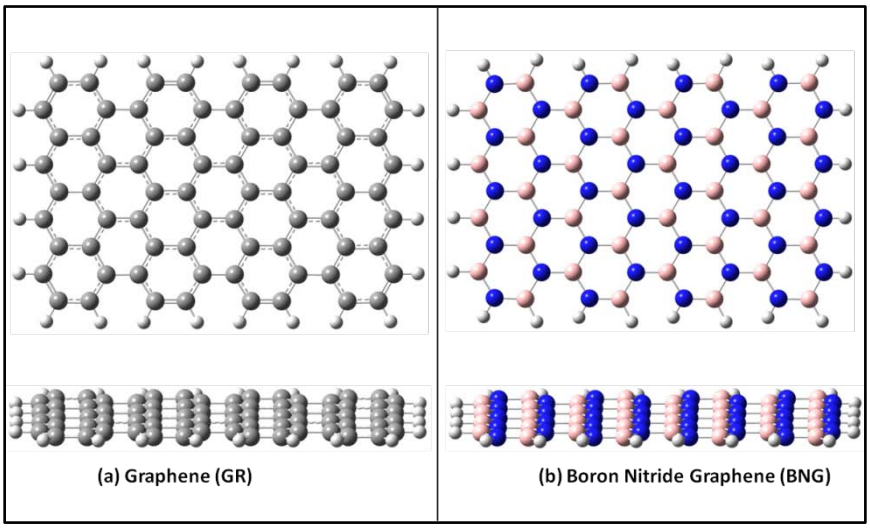

Figure 3.1: Optimized geometry of (a) GR and (b) BNG in top and side view at B3LYP/6-31G*

The nucleic bases Adenine, cytosine, guanine, thymine, and uracil were made to interact with the graphene (GR), boron nitride graphene (BNG), which were studied in detail.

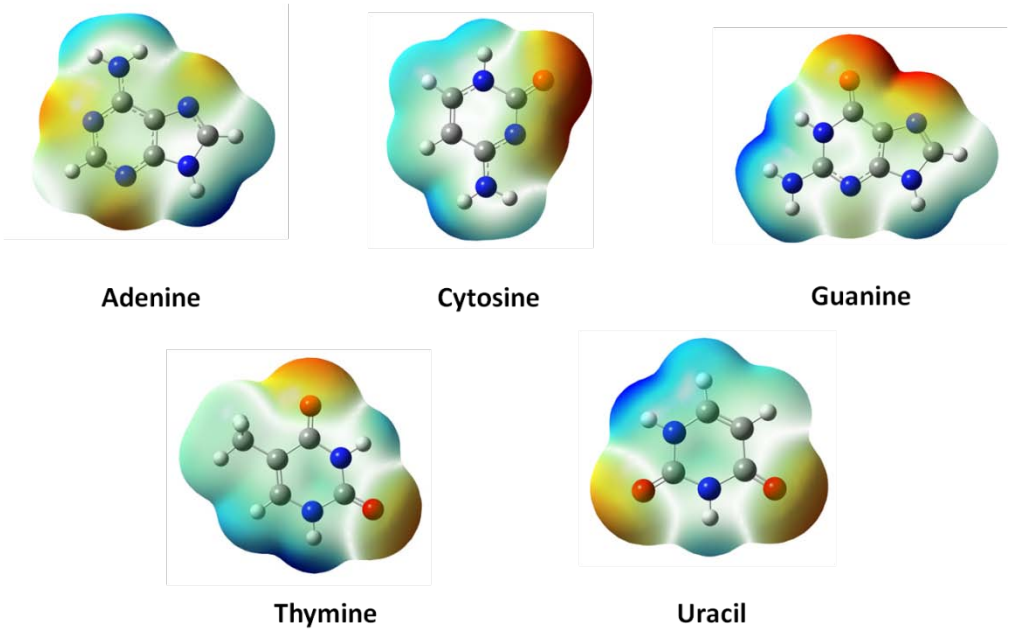

Figure 3.2: Nucleic bases with Molecular Electrostatic Potential (MESP).

All the geometries were optimized without any constraints. The full geometry optimizations and binding energy calculations using the graphene and boron nitride graphene (BNG) in the presence and absence of nucleic bases (Adenine, Cytosine, Guanine, Thymine and Uracil) were performed using the B3LYP functional and the 6-31G basis as implemented in the Gaussian 09 suite of program [93]. In the present chapter, two methods were chosen (a) B3LYP[81,82] and (b) ωB97XD[94]. The binding energy (BE) is calculated using the two basis sets: BS1 that corresponds to B3LYP/6-31++G** and BS2 pertains to ωB97XD/6-31++G**. The basis set for BS1 and BS2

remains the same i.e. 6-31++G**. The Homo-Lumo gaps of the interacting moieties were also calculated for each set of calculations.

3.3 Results and Discussion

The present chapter can be well understood into three schemes: (scheme 1 which is comprised of the graphene and the nucleic bases, scheme 2 consists of the boron nitride graphene and the nucleic bases that were made to interact in parallel configuration, while the scheme 3 deals with the boron nitride and the nucleic bases, in this scheme nucleic bases were made to interact in the perpendicular configuration).

The binding energy (B.E) was calculated using the given formula:

$$Binding\ Energy = \left[(E_A + E_B) - E_{AB}\right] \tag{3.1}$$

Where, E_{AB} is the energy of the complex system comprised of the nucleic bases and the graphene, E_A is the energy of the graphene while E_B is the energy of the nucleic bases (NBs).

Table 3.1: Calculated binding energy (in kcal/mol) of graphene (GR) and nucleic bases at BS1 (B3LYP/6-31++G** // B3LYP /6-31G) and BS2 (ωB97XD/ 6-31++G** // B3LYP /6-31G).

Model System	**Nucleic bases (NBs)**	**Binding Energy (BS1, B3LYP/ 6-31++G**)**	**Binding Energy (BS2, ωB97XD/ 6-31++G**)**
(GR)	Adenine (A)	1.580	12.700
	Cytosine (C)	2.177	12.695
	Guanine (G)	2.858	11.556
	Thymine (T)	1.141	9.450
	Uracil (U)	3.449	9.962

Table 3.2: Calculated binding energy (in kcal/mol) of Boron Nitride Graphene (BNG) and nucleic bases in parallel mode of interaction at BS1 (B3LYP/6-31++ G** // B3LYP /6-31G) and BS2 (ωB97XD/ 6-31++G** // B3LYP /6-31G).

Model System	**Nucleic bases (NBs)**	**Binding Energy (BS1, B3LYP/ 6-31++G**)**	**Binding Energy (BS2, ωB97XD/ 6-31++G**)**
(BNG)	Adenine (A)	0.123	14.863
	Cytosine (C)	2.430	13.375
	Guanine (G)	0.572	17.689
	Thymine (T)	0.552	13.603
	Uracil (U)	0.003	12.183

Table 3.3: Calculated binding energy (in Kcal/mol) of Boron Nitride Graphene (BNG) and nucleic bases in perpendicular mode of interaction at BS1 (B3LYP/6-31++ G** // B3LYP /6-31G) and BS2 (ωB97XD/ 6-31++G** // B3LYP /6-31G).

Model System	**Nucleic bases (NBs)**	**Binding Energy (BS1, B3LYP/ 6-31++G**)**	**Binding Energy (BS2, ωB97XD/ 6-31++G**)**
(BNG)	Adenine (A)	1.121	9.176
	Cytosine (C)	2.945	12.433
	Guanine (G)	3.283	13.519
	Thymine (T)	0.882	9.379
	Uracil (U)	0.927	9.238

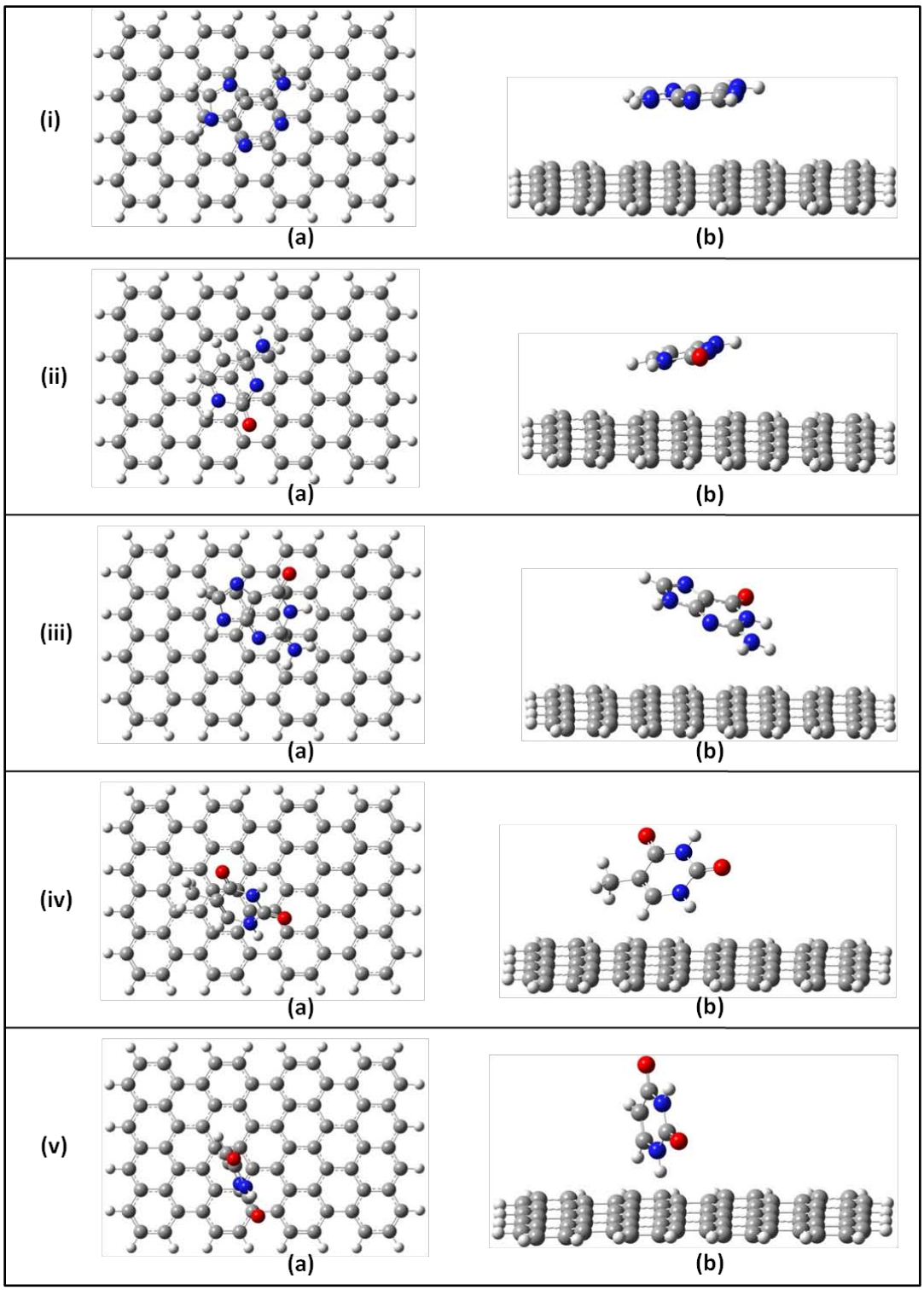

Figure 3.3: Optimized geometries showing interaction of graphene (GR) with nucleic bases (i) Adenine (A), (ii) Cytosine (C), Guanine (G), Thymine (T), and Uracil (U) in parallel position with (a) top (b) side view at B3LYP/6-31G.

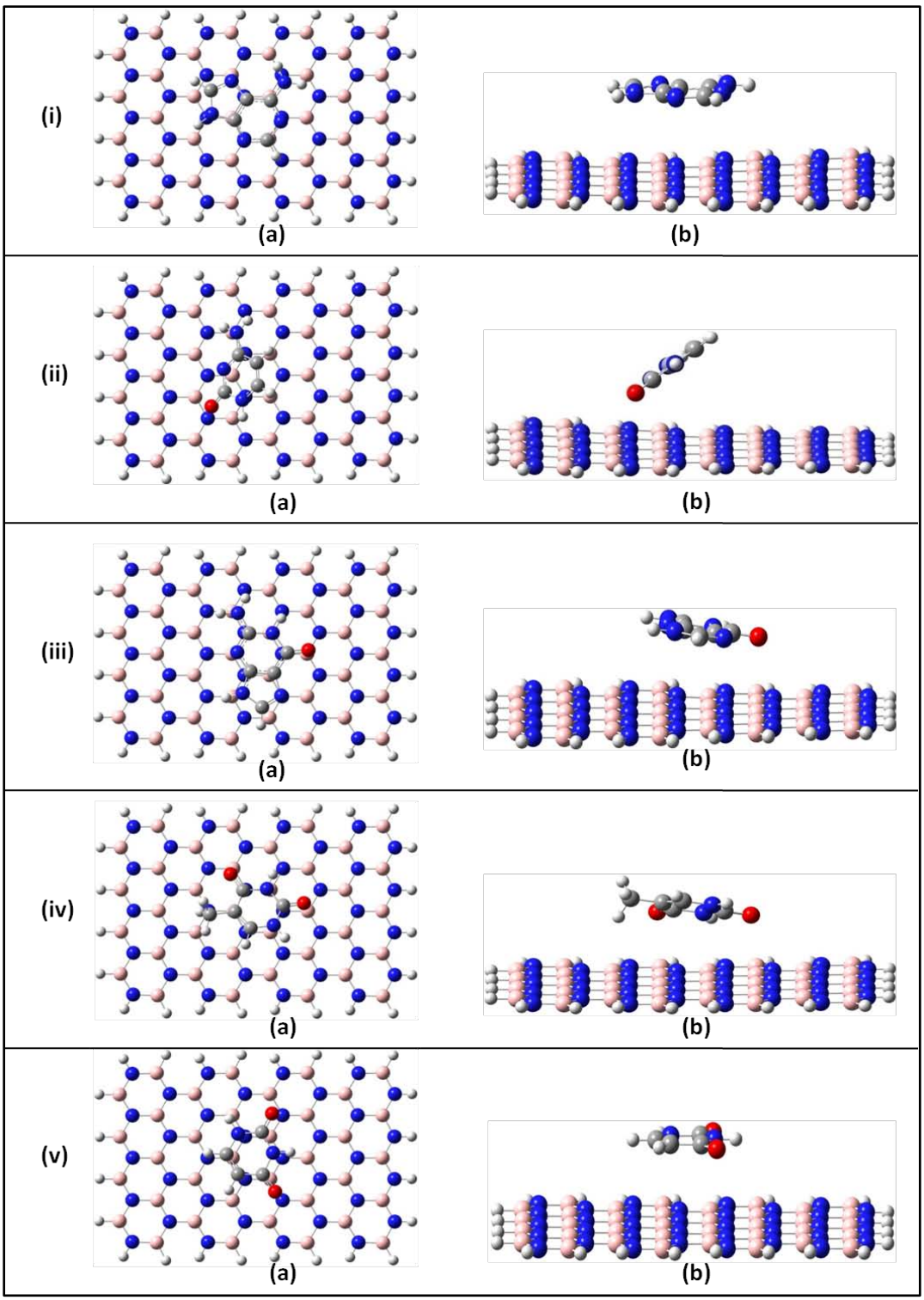

Figure 3.4: Optimized geometries showing interaction of boron nitride graphene (BNG) with nucleic bases (i) Adenine (A), (ii) Cytosine (C), Guanine (G), Thymine (T), and Uracil (U) in parallel position with (a) top view (b) side view at B3LYP/6-31G.

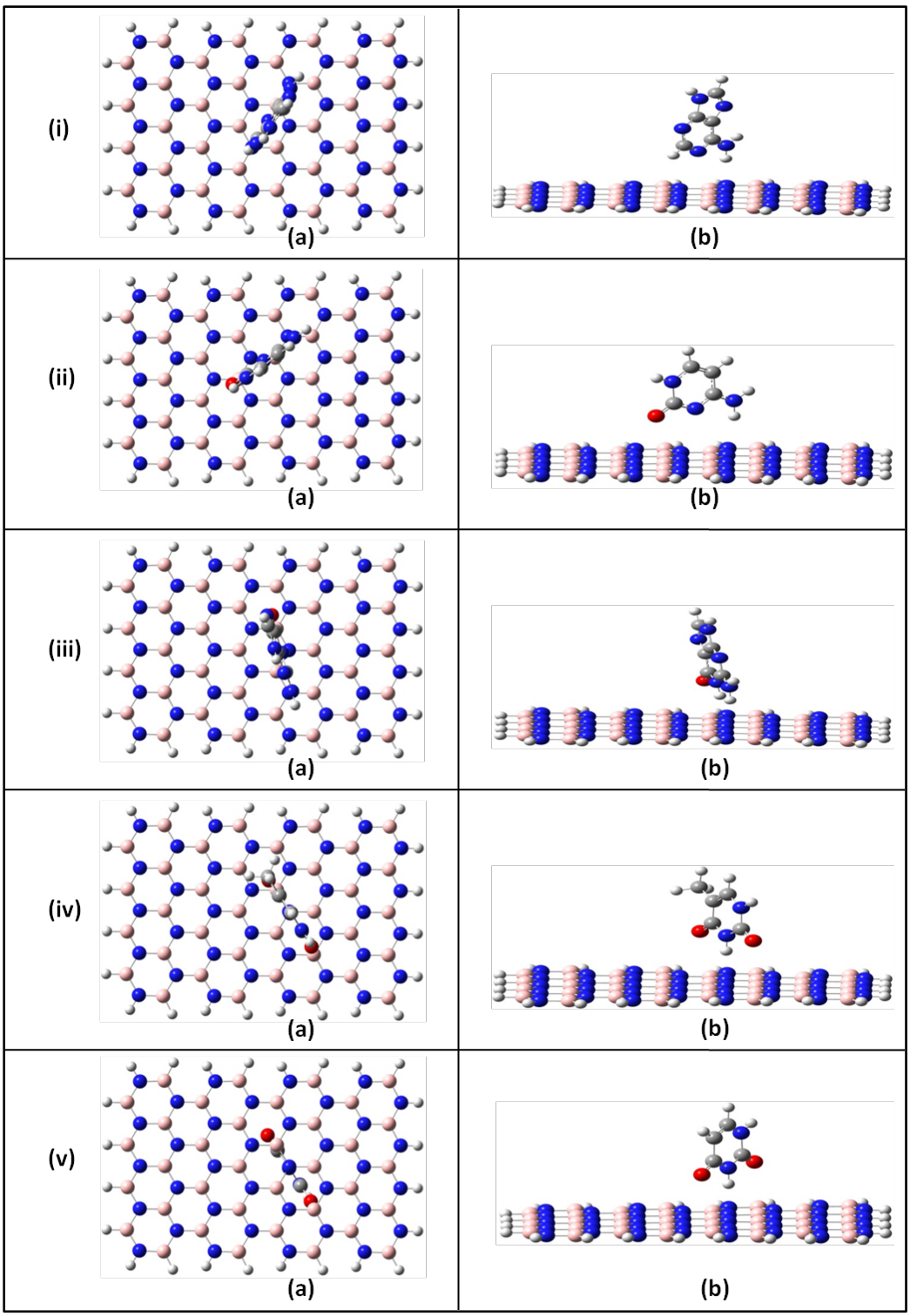

Figure 3.5: Optimized geometries showing interaction of boron nitride graphene (BNG) with nucleic bases (i) Adenine (A), (ii) Cytosine (C), Guanine (G), Thymine (T), and Uracil (U) in perpendicular position with (a) top view (b) side view at B3LYP/6-31G.

3.4 Binding Energy

Generally, the magnitude of physisorption energy is defined as lower than ~5 kcal/mol, whereas for chemisorptions energy it is higher than ~12 kcal/mol. Recently, Chung et al.[95] explored a method to link reversibly DNA with SWNT, and this methodology is very important for its application to behave as sensors to detect DNA. Our calculations show that all three different schemes possess adsorption energy within the range of~5 to13 kcal/mol, except for the Guanine in scheme 3. Thus, they are within the range of physisorption and chemisorption. Hence it appears from our study that for the graphene and boron nitride graphene complexes the adsorption and desorption are reversible at room temperature. Thereafter, we also investigated the HOMO- LUMO gap in detail for all the three schemes with complexes.

3.5 HOMO-LUMO and MESP (Molecular Electrostatic Surface Potential)

The frontier molecular orbitals of molecules play a key role in the chemical reactivity of molecules. These are the orbitals that participate in chemical reactions or interactions with other moieties and their energy difference (termed as gap) helps to quantify the chemical reactivity of the molecule.[96] The frontier orbitals viz. the highest occupied molecular orbital (HOMO) and lowest unoccupied molecular orbital (LUMO) were analyzed in order to further explain their chemical reactivity. The HOMO, in general, acts as an electron donor and LUMO acts as an electron acceptor, and the HOMO-LUMO energy gap is an important measure for stability of the system.

The molecular electrostatic potential (MESP) is a coloured map of electrostatic potential over constant electron density of molecules. The significance of MESP lies in the fact that it not only simultaneously displays the molecular size and shape but also it displays a positive, negative, and neutral electrostatic potential regions in terms of the color coding scheme which is very useful to investigate the most probable binding receptor site along with the size and shape of the molecules.[97]

The Homo-Lumo gap is calculated for all the three schemes and shown in the Table 4.1. The Homo-Lumo gap for the scheme 1 is found to exhibit a constant value of 0.25 eV for the BS1, while for the BS2 it is found to be 1.28 eV for all the complexes associated with the graphene. The Homo-Lumo gap for the scheme 2 which involves the boron nitride graphene with nucleic bases interacting in parallel mode ranges from 4.73 eV to 5.21 eV for basis set BS1 and 8.48 eV to 9.06 eV for BS2. For the scheme 3, the Homo-Lumo gap ranges from 4.71 eV to 5.23 eV for BS1 and for BS2 it ranges from 8.74 eV to 8.99 eV.

Table 3.4: Comparison of the Homo-Lumo gap (in eV) of various graphene models using two basis sets viz. BS1 (B3LYP/6-31++ G**) and BS2 (ωB97XD/ 6-31++G**).

Model system	Nucleic Bases (NBs)	Homo-Lumo gap (BS1)	Homo-Lumo gap (BS2)
GR		0.25	1.28
GR	A	0.25	1.28
	C	0.25	1.28
	G	0.25	1.28
	T	0.25	1.28
	U	0.25	1.28
BNG		5.75	9.55
(BNG+NBs)$_{\parallel}$	$A^{\parallel}$	5.21	8.96
	$C^{\parallel}$	5.06	9.06
	$G^{\parallel}$	5.01	8.48
	$T^{\parallel}$	4.80	8.83
	$U^{\parallel}$	4.74	8.78
(BNG+NBs)$^{\perp}$	$A^{\perp}$	5.24	8.99
	$C^{\perp}$	5.09	8.98
	$G^{\perp}$	4.98	8.46
	$T^{\perp}$	4.84	8.85
	$U^{\perp}$	4.71	8.74

The optimized structure of graphene and their complexes with nucleic bases are shown in Figure 4.1, 4.2 and 4.3. The initial configuration of all nucleic bases (A,C,G,T,U) were placed initially above the graphene surface in parallel configuration such the the π-π stacking interaction may be observed. The nucleic bases in the scheme 1 and 2 was placed at a distance of approximately 3Å .

On the basis of the complex system considered in this study, following significant conclusions can be drawn:

(a) In the case of scheme 1, where the nucleic bases interact with the graphene in parallel mode, there is no significant change in the Homo-Lumo gap for the BS1 and BS2 where the gap remains the same with values 0.25 and 1.28 eV respectively.

(b) In case of scheme 2, where the nucleic bases are placed in parallel position above the boron nitride graphene surface, the Homo-Lumo gap ranges from 4.73 for Uracil to 5.21 for Adenine for BS1. For BS2, the Homo-Lumo gap is 8.48 for Guanine while for Cytosine it is 8.96 eV.

(c) In scheme third, the nucleic bases were placed perpendicular to the boron nitride graphene, the Homo-Lumo gap ranges from 4.71 for Uracil and for adenine it is 5.23 eV. For the BS2, the Homo-Lumo gap is 8.74eV for Uracil and for Adenine it is 8.99eV.

(d) The preferential order of binding of the Binding energy for scheme 1, where the nucleic bases interact with the graphene is U>G>C>A>T for BS1 while for BS2 it is A>C>G>U>T.

(e) The preferential order of binding for the scheme 2, where the boron nitride graphene interacts with the nucleic bases in parallel mode is C>G>T>A>U for BS1 while for BS2 it is G>A>T>C>U.

(f) For the third scheme, the preferential order of binding of the nucleic bases with boron nitride and nucleic bases in perpendicular mode is G>C>A>U>T for BS1 and G>C>T>U>A for BS2.

3.6 Conclusion

In the present chapter, a systematic study has been accomplished to examine the Binding energy values using highly reliable first principle calculations for the five known nucleobases with the graphene and boron nitride graphene. The analysis reveals that NBs seems to have a substantially high preference for binding in the π–π stacking fashion. The preferential order of binding of the nucleic bases performed in scheme 1 of this chapter with basis set B3LYP/631++G is in agreement with the experimental study performed by Albertorio et al.[44,98] It is also quite noteworthy that the calculations performed in the scheme 2 with basis set ωB97XD/631++G are in agreement with other computational studies performed earlier.[45,60,62,99,100] The electronic properties of these molecules are also evaluated with the help of reactive surfaces such as HOMO, LUMO and MESP. The observations obtained in this chapter encourage a more focused research on graphene for the possible applications for nucleic acid sensors and DNA sequencing.

References

[1] K. S. Novoselov, A. K. Geim, S. V. Morozov, D. Jiang, Y. Zhang, S. V. Dubonos, I. V. Grigorieva, A. A. Firsov, *Science*, **306**, 666 (2004).

[2] K. S. Novoselov, A. K. Geim, S. V. Morozov, D. Jiang, M. I. Katsnelson, I. V. Grigorieva, S. V. Dubonos, A. A. Firsov, *Nature*, **438**, 197 (2005).

[3] Y. Zhang, Y-W Tan, H. L. Stormer, P. Kim, *Nature*, **438**, 201 (2005).

[4] J. S. Bunch, Y. Yaish, M. Brink, K. Bolotin, P. L. McEuen, *Nano Lett.*, **5**, 287 (2005).

[5] H. J. Rader, A. Rouhanipour, A. M. Talarico, V. Palermo, P. Samor, K. M., *Nat. Mater.*, **5**, 276 (2006).

[6] J. C. Meyer, A. K. Geim, M. I. Katsnelson, K. S. Novoselov, T. J. Booth, S. Roth, *Nature*, **446**, 60 (2007).

[7] A. K. Geim and K. S. Novoselov, *Nat. Mater.*, **6**, 183 (2007).

[8] M. I. Katsnelson, *Mater. Today*, **10**, 20 (2007).

[9] K. S. Novoselov, Z. Jiang, Y. Zhang, S. V. Morozov, H. L. Stormer, U. Zeitler, J. C. Maan, G. S. Boebinger, P. Kim, A. K. Geim, *Science*, **315**, 1379 (2007).

[10] M. Y. Han, B. Ozyilmaz, Y. Zhang, P. Kim, *Phys. Rev. Lett.*, **98**, 206805 (2007).

[11] B. Ozyilmaz, P. J.-Herrero, D. Efetov, D. A. Abanin, L. S. Levitov, P. Kim, *Phys. Rev. Lett.*, **99**, 166804 (2007).

[12] Z. Chen, Y.-M. Lin, M. J. Rooks, P. Avouris, *Physica E*, **40**, 228 (2007).

[13] A. L. V. de Parga, F. Calleja, B. Borca, M. C. G. Passeggi, Jr., J. J. Hinarejos, F. Guinea, R. Miranda, *Phys. Rev. Lett.*, **100**, 56807 (2008).

[14] X. Li, X. Wang, L. Zhang, S. Lee, H. Dai, *Science*, **319**, 1229 (2008).

[15] D. Wei, Y. Liu, H. Zhang, L. Huang, B. Wu, J. Chen, G. Yu, *J. Am. Chem. Soc.*, **131**, 11147 (2009).

[16] M. Terronesa, A. R. Botello-Méndez, J. C.-Delgadoc, F. L.-Urías, Y. I. V. -Cantúd, F. J. R.-Macíasd, A. L. Elías, E. M.-Sandovald, A. G. C.-Márquezd, J.-C. Charlier, H. Terrones, *Nano Today*, **5**, 351 (2010).

[17] G. M. Rutter, N. P. Guisinger, J. N. Crain, P. N. First, J. A. Stroscio, *Phys. Rev. B*, **81**, 245408 (2010).

[18] M. Fujita, K. Wakabayashi, K. Nakada, K. Kusakabe, *J. Phys. Soc. Jpn.*, **65**, 1920 (1996).

[19] K. Wakabayashi, M. Fujita, H. Ajiki, M. Sigrist, *Phys. Rev. B*, **59**, 8271 (1999).

[20] M. Ezawa, *Phys. Rev. B*, **73**, 045432 (2006).

[21] K. Nakada and M. Fujita, *Phys. Rev. B*, **54**, 17954 (1996).

[22] S.S. Yu, Q.B. Wen, W.T. Zheng, Q. Jiang, *Mol. Simulat.*, **34**, 1085 (2008).

[23] Y.-W. Son, M. L. Cohen, S. G. Louie, *Phys. Rev. Lett.*, **97**, 216803 (2006).

[24] T. E. O'Connor, *J. Am. Chem. Soc.*, **84**, 1753 (1962).

[25] W. S. Lenihan, Jr. F. Park, R. W. Reidl, Finddlay, Ohio, Assignors, *U.S. Patent* 3241918, March 22, (1966).

[26] T. H. Ferreira, L. M. Hollanda, M. Lancellotti, E. M. B. de Sousa, *J. Biomed. Mater. Res., Part A*, **103**, 2176 (2015).

[27] Ö. Şen, Z. Çobandede, M. Emanet, Ö. F. Bayrak, M. Çulha, *Biochim. Biophys. Acta, Gen. Subj.*, **1861**, 2391 (2017).

[28] S. Roosta, S. J. Nikkhah, M. Sabzali, S. M. Hashemianzadeh, *RSC Adv.*, **6**, 9344 (2016).

[29] Q. Weng, B. Wang, X. Wang, N. Hanagata, X. Li, D. Liu, X. Wang, X. Jiang, Y. Bando, D. Golberg, *ACS Nano*, **8**, 6123 (2014).

[30] W. Lei, H. Zhang, Y. Wu, B. Zhang, D. Liu, S. Qin, Z. Liu, L. Liu, Y. Ma, Y. Chen, *Nano Energy*, **6**, 219 (2014).

[31] J. Li, Lin, J. Xu, X. Zhang, X. Xue, Y. Mi, J. Mo, Z. Fan, Y. Hu, L. Yang, X. Zhang, J. Meng, F. Yuan, S. C.Tang, *Nanotechnology*, **24**, 155603 (2013).

[32] Líliam Márcia Silva Ansaloni, Edésia Martins Barros de Sousa, *Mater. Sci. Appl.*, **4**, 22 (2013).

[33] C. R. Dean, A. F. Young, I. Meric, C. Lee, L. Wang, S. Sorgenfrei, K. Watanabe, T. Taniguchi, P. Kim, K. L. Shepard, *Nat. Nanotechnol.*, **5**, 722 (2010).

[34] K. H. Lee, H. J. Shin, J. Lee, I. Y. Lee, G. H. Kim, J. Y. Choi, S. W. Kim, *Nano Lett.*, **12**, 714 (2012).

[35] J. Lee, T. J. Ha, K. N. Parrish, S. F. Chowdhury, *IEEE Electron Device Lett.*, **34**, 172 (2013).

[36] M. Iqbal, X. Jin, J. Eom, C. Hwang, *J. Mater. Chem. C*, **2**, 7776 (2014).

[37] X. Li, S. Lin, X. Lin, Z. Xu, P. Wang, S. Zhang, H. Zhong, W. Xu, Z. Wu, F. Wei, *Opt. Express*, **24**, 134 (2016).

[38] G. J-Sanchez, B. Childs, D. Valle, *Nature*, **409**, 853 (2001).

[39] T. Nelson, B. Zhang, O. V. Prezhdo, *Nano Lett.*, **10**, 3237 (2010).

[40] H. Nihei, H. Kanemitsu, A. Tamura, H. Oka, K. Sano, *Neurosurgery*, **25**, 613 (1989).

[41] Y. Tetsuya, M. Yuji, T. Sumio, *Clin. Chim. Acta*, **356**, 35 (2005).

[42] D. Umadevi, G. N.Sastry, *J. Phys. Chem. Lett.*, **2**, 1572 (2011).

[43] R. J. Chen, S. Bangsaruntip, K. A. Drouvalakis, N. W. S. Kam, M. Shim, Y. Li, W. Kim, P. J. Utz, H. Dai, *Proc. Natl. Acad. Sci. U.S.A.*, **100**, 4984 (2003).

[44] N. Varghese, U. Mogera, A. Govindaraj, A. Das, P. K. Maiti, A. K. Sood, C. N. R. Rao, *ChemPhysChem*, **10**, 206 (2009).

[45] S. Gowtham, R. H. Scheicher, R. Ahuja, R. Pandey, S. P. Karna, *Phys. Rev. B*, **76**, 033401 (2007).

[46] C. Cazorla, *Thin Solid Films*, **518**, 6951 (2010).

[47] H. S. Kang, *J. Am. Chem. Soc.*, **127**, 9839 (2005).

[48] C. Cazorla, V. R-Cervellera, C. Rovira, *J. Mater. Chem.*, **22**, 19684 (2012).

[49] T. Roman, W. A. Dinyo, H. Nakanishi, H. Kasai, *Thin Solid Films*., **509**, 218 (2006).

[50] X. Hua, L. Mub, J. Wenb, Q. Zhoua, *J. Hazard. Mater.*, **213**, 387 (2012).

[51] Y. Gao, Y. Li, L. Zhang, H. Huang, J. Hu, S. M. Shah, X. Su, *J. Colloid Interface Sci*., **368**, 540 (2012).

[52] B. Zheng, C. Wang, C. Wu, X. Zhou, M. Lin, X. Wu, X. Xin, X.Chen, L. Xu,; H. Liu, et al. *J. Phys.Chem. C*, **116**, 15839 (2012).

[53] F. L. Chi, Y. N. Guo, J. Liu, Y. L. Liu, Q. S. Huo, *J. Phys. Chem. C*, **114**, 2519 (2010).

[54] M. Ferrari, *Nat. Rev. Cancer*, **5**, 161 (2005).

[55] N. Ding, X. Chen, C.-M. L. Wu, H. Li, *Phys. Chem. Chem. Phys.*, **15**, 10767 (2013).

[56] X. Tu, S. Manohar, A. Jagota, M. Zheng, *Nature*, **460**, 250 (2009).

[57] I. Bald, S. Weigelt, X. Ma, P. Xie, R. Subramani, M. Dong, C. Wang, W. Mamdouh, J. Wang, F. Besenbacher, *Phys. Chem. Chem. Phys.*, **12**, 3616 (2010).

[58] M. Pagliai, S. Caporali, M. Muniz-Miranda, G. Pratesi, V. Schettino, *J. Phys. Chem. Lett.*, **3**, 242 (2012).

[59] P. Wang, H. Wu, Z. Dai, X. Zou, *Biosens. Bioelectron.*, **26**, 3339 (2011).

[60] S. Gowtham, R. H. Scheicher, R. Pandey, S. P. Karna, R. Ahuja, *Nanotechnology*, **19**, 125701 (2008).

[61] H. Wang, A. Ceulemans, *Phys. Rev. B*, **79**, 195419 (2009).

[62] J. Antony, S. Grimme, *Phys. Chem. Chem. Phys.*, **10**, 2722 (2008).

[63] D. Umadevi, G. N. Sastry, *J. Phys. Chem. Lett.*, **2**, 1572 (2011).

[64] T. Hussain, H. Vovusha, T. Kaewmaraya, V. Amornkitbamrung, R. Ahuja, Sens. *Actuators B: Chem.*, **255**, 2713 (2018).

[65] S. Panigrahi, A. Bhattacharya, S. Banerjee, D. Bhattacharyya, *J. Phys. Chem. C*, **116**, 4374 (2012).

[66] S. Gholami, A. Shokuhi Rad, A. Heydarinasab, M. Ardjmand, *J. Alloys Compd.*, **686**, 662 (2016).

[67] S. K. Mudedla, K. Balamurugan, M. Kamaraja, V. Subramanian, *Phys. Chem. Chem. Phys.*, **18**, 295 (2016).

[68] A. S. Rad, D. Zareyee, M. Peyravi, M. Jahanshahi, *Appl. Surf. Sci.*, **390**, 444 (2016).

[69] S. K. Mudedla, K. Balamurugan, V. Subramanian, *J. Phys. Chem. C*, **118**, 16165 (2014).

[70] H. Cao, X. Wu, G. Yin, J. H. Warner, *Inorg. Chem.*, **51**, 2954 (2012).

[71] P. Singh, J. Kumar, F. M. Toma, J. Raya, M. Prato, B. Fabre, S. Verma, A. Bianco, *J. Am. Chem. Soc.*, **131**, 13555 (2009).

[72] R. J. Baierlea, T. M. Schmidt, A. Fazzio, *Solid State Commun.*, **142**, 49 (2007).

[73] R. Wang, R. Zhu, D. Zhang, *Chem. Phys. Lett.*, **467**, 131 (2008).

[74] A. Soltani, S. G. Raz, V. J. Rezaei, A. D. Khalaji, M. Savar, *Appl. Surf. Sci.*, **263**, 619 (2012).

[75] M. D. Esrafili, N. Saeidi, *Struct. Chem.*, **27**, 595 (2016).

[76] E. Shakerzadeh, S. Noorizadeh, *Physica E*, **57**, 47 (2014).

[77] Z. Mahdavifar, N. Abbasi, E. Shakerzadeh, *Sens. Actuators B Chem.*, **185**, 512 (2013).

[78] C. V. S. Kumar, V. Subramanian, *Phys. Chem. Chem. Phys.*, **19**, 15377 (2017).

[79] P. Hohenberg and W. Kohn, *Phys. Rev.*, **136**, B864 (1964).

[80] W. Kohn and L. Sham, *Phys. Rev.*, **140**, A1133 (1965).

[81] A. D. Becke, *J. Chem. Phys.*, **98**, 5648 (1993).

[82] C. Lee, W. Yang, R. G. Parr, *Phys. Rev. B*, **37**, 785, (1988).

[83] R. Ditchfield, W. J. Hehre, J. A. Pople, *J. Chem. Phys.*, **54,** 724 (1971).

[84] W. J. Hehre, R. Ditchfield, J. A. Pople, *J. Chem. Phys.*, **56** 2257 (1972).

[85] P. C. Hariharan and J. A. Pople, *Theor. Chem. Acc.*, **28**, 213 (1973).

[86] P. C. Hariharan and J. A. Pople, *Mol. Phys.*, **27** 209 (1974).

[87] M. S. Gordon, *Chem. Phys. Lett.*, **76** 163 (1980).

[88] M. M. Francl, W. J. Pietro, W. J. Hehre, J. S. Binkley, D. J. DeFrees, J. A. Pople, M. S. Gordon, *J. Chem. Phys.*, **77**, 3654 (1982).

[89] R. C. Binning Jr. and L. A. Curtiss, *J. Comp. Chem.*, **11**, 1206 (1990).

[90] J.-P. Blaudeau, M. P. McGrath, L. A. Curtiss, L. Radom, *J. Chem. Phys.*, **107** 5016 (1997).

[91] V. A. Rassolov, J. A. Pople, M. A. Ratner, T. L. Windus, *J. Chem. Phys.*, **109** 1223 (1998).

[92] V. A. Rassolov, M. A. Ratner, J. A. Pople, P. C. Redfern, L. A. Curtiss, *J. Comp. Chem.*, **22**, 976 (2001).

[93] M. J. Frisch, G. W. Trucks, H. B. Schlegel, G. E. Scuseria, M. A. Robb, J. R. Cheeseman, G. Scalmani, V. Barone, B. Mennucci, G. A. Petersson, H. Nakatsuji, M. Caricato, X. Li, H. P. Hratchian, A. F. Izmaylov, J. Bloino, G. Zheng, J. L. Sonnenberg, M. Hada, M. Ehara, K. Toyota, R. Fukuda, J. Hasegawa, M. Ishida, T. Nakajima, Y. Honda, O. Kitao, H. Nakai, T. Vreven, J. A. Montgomery, Jr., J. E. Peralta, F. Ogliaro, M. Bearpark, J. J. Heyd, E. Brothers, K. N. Kudin, V. N. Staroverov, T. Keith, R. Kobayashi, J. Normand, K. Raghavachari, A. Rendell, J. C. Burant, S. S. Iyengar, J. Tomasi, M. Cossi, N. Rega, J. M. Millam, M. Klene, J. E. Knox, J. B. Cross, V. Bakken, C. Adamo, J. Jaramillo, R. Gomperts, R. E. Stratmann, O. Yazyev, A. J. Austin, R. Cammi, C. Pomelli, J. W. Ochterski, R. L. Martin, K. Morokuma, V. G. Zakrzewski, G. A. Voth, P. Salvador, J. J. Dannenberg, S. Dapprich, A. D. Daniels, O. Farkas, J. B. Foresman, J. V. Ortiz, J. Cioslowski, and D. J. Fox, Gaussian 09, Revision D.01, Gaussian, Inc., Wallingford CT, (2013).

[94] J.-D. Chai and M. Head-Gordon, *Phys. Chem. Chem. Phys.*, **10**, 6615 (2008).

[95] C. Chung, C. Gautier, S. Campidelli, , A. Filoramo, *Chem. Commun.*, **46**, 6539 (2010).

[96] H. Sklenar and J. Jager, *Int. J. Quantum Chem.*, **16,** 467 (1979).

[97] J. S. Murray and K. Sen, Molecular Electrostatic Potentials: Concepts and Applications (Elsevier, Amsterdam, Netherlands) (1996).

[98] F. Albertorio, M. E. Hughes, J. A. Golovchenko, D. Branton, *Nanotechnology*, **20**, 395101 (2009).

[99] S. G. Stepanian, M. V. Karachevtsev, A. Y. Glamazda, V. A. Karachevtsev, L. Adamowicz, *J. Phys. Chem. A*, **113**, 3621 (2009).

[100] M. K. Shukla, M. Dubey, E. Zakar, R. Namburu, Z. Czyznikowska, J. Leszczynski, *Chem. Phys. Lett.*, **480**, 269 (2009).

Chapter 4

Interaction with modified nucleic bases (MNBs) with graphene (GR) and doped graphene

CHAPTER 4

INTERACTION OF MODIFIED NUCLEIC BASES (MNBs) WITH GRAPHENE (GR) AND DOPED GRAPHENES

4.1 Introduction

Graphene, a versatile material has opened new avenues to increase the technological advancement owing to its extraordinary properties and enormous application in various fields.[1-5] Therefore, the application of graphene and its derivatives in various fields like sensors, field effect transistors, nanoelectronics, engineering nanocomposite materials, energy storage, biology, catalysis, and medicine have been studied extensively.[6-14] From the conviction of graphene and its derivatives application in medicine, biology and its interaction with biomolecules, it has drawn considerable amount of interest. The small gas molecules and various biomolecules used to get adsorbed on the graphene surface due to its remarkable large surface area[15,17-21]. Umadevi et al. used the density functional theory (DFT) and validated that the binding energy of carbon nanotube and DNA/RNA nucleic bases complexes is inversely proportional to the curvature.[16] The DNA sequencing was observed successfully with the aid of functionalized graphene in order to distinguish various nucleic bases.[22] For the removal of pollutants and pesticides, graphene can be used effectively.[23,24] Graphene owes high conductivity and the associated charge transfer that occurred between the two interacting moieties made it convenient to detect the adsorbed

molecules.[25] In the present era, doping is considered to be an effective way to modulate and tune the adsorption strength and various other parameters of interest. Thus doping with elements like Sulphur, Phosphorus, Silicon, Nitrogen, Aluminium, and Boron lead to topological deformation.[26-31] In the field of catalysts, pristine as well as modified graphene made their significant contribution.[32,33] Sundar and Subramaniam proposed the novel mechanism and explored new paths to activate the benzyl alcohol using the graphene and N-doped graphene by using the DFT.[34] Kumar et al. studied the interaction of nucleic bases with the pristine carbon nanotube and explored the difference between the binding affinity of these nucleic bases inside and outside the carbon nanotube.[35] It is clear from the previous reports that the silicon-doped graphene is useful in sensing various gases.[36] Recently it has been reported by Junkaew et al. [37] that N_2O reduction and CO oxidation is feasible using silicon coordinated nitrogen doped graphene. The DFT calculations reveal that graphene doped with silicon can be used to convert the NO into NO_2 as it acts as a metal free catalyst [38] Beside graphene doping, carbon nanotube doping too can be used to detect the highly carcinogenic and persistent pollutants and biomolecules.[39,40] Singh et al. used the DFT to explore the adsorption of the harmful gases. In the same study, the Aluminium doped graphene was suggested and shown to have greater inclination to behave as a good sensor in comparison to the pristine graphene in order to detect the harmful gases.[41] Ao et al. studied the Aluminium doped graphene by employing the DFT and suggested it as a promising material for the hydrogen storage. In his work, mainly two modes were considered i.e. parallel and perpendicular to study the interaction of hydrogen with Aluminium doped graphene.[42] Chen et al. investigated the high adsorption capacity of the hemoglobin via

Nickel-doped reduced graphene oxide by using the experimental techniques like Raman spectroscopy, X-ray diffraction, X-ray photoelectron and Fourier transform infrared spectroscopy, etc.[43] Denis explored the chemical reactivity of the graphene doped with Gallium (Ga), Arsenic(As), Germanium (Ge), and Selenium (Se). He proposed that Gallium doping makes the graphene to behave as a semi-metal. In this study, the effect of formation energy with the mentioned dopants is also discussed.[44] Losurdo et al. studied the Gallium nanoparticles on graphene and elaborated various aspects to modulate the Fermi level that may aid to create a high performance Surface Enhanced Raman Scattering (SERS) platforms. He also compared the commonly used noble metals i.e. gold and silver with the Gallium and provided some useful suggestions.[45] Lv et al. addressed the effect of Aluminium or Gallium doping on the graphene using the first principle calculations and discussed the ways to dissociate N_2O into N_2 and O_2 that can protect the ozone layer and paved a step forward to mitigate the global warming. In this study, it is reported that Aluminium doped graphene may be used to tackle the N_2O.[46] Li et al. brought to light the effect of sulfur –doped graphene effectively that may be used to detect the Fe^{3+}. For the several physiological and pathological processes, this Fe^{3+} is the main metal ion in many biological systems.[47] Li et al. bring forth the noteworthy and remarkable criteria to tune the electronic properties of graphene. It is reported that the sulfur-doped graphene quantum dots (S-GQDs) may be utilized in a wide range of applications.[48] So, the interaction of the biomolecules with graphene and doped graphene (Aluminium, Sulfur, Nickel, Gallium, and Germanium) is quite significant. Thus these doped graphenes have been selected to study the interaction with MNBs in the present study. It is hoped that these molecular systems will efficiently interact with the

molecules, and they may also provide very good molecular systems for the development of sensors.

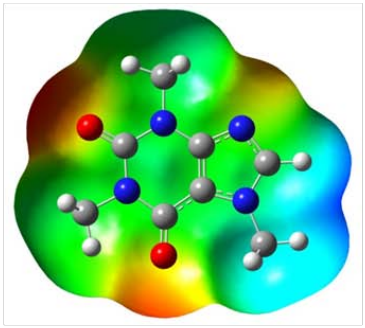

Caffeine (CAF)

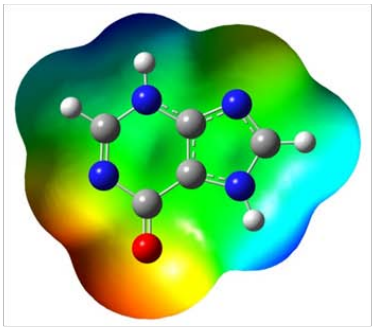

Hypoxanthine (HX)

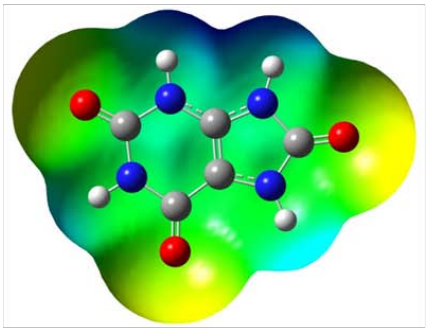

Uric Acid (UA)

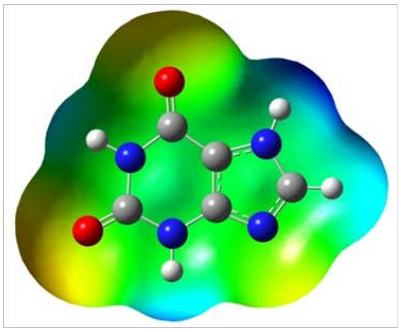

Xanthine (X)

Figure 4.1: The Modified nucleic bases (MNBs) and molecular electrostatic potential (MESP) at an isovalue of 0.0004a.u.

The building units of the DNA and RNA are the purine bases i.e. Adenine and Guanine. The compounds like hypoxanthine, uric acid and xanthine are the oxidation products that can be observed in the purines metabolism of the humans.[49] By drinking the coffee, tea and coca-cola, caffeine is introduced into our body which is a methyl derivative of xanthine.[50] For some serious problems like pneumonia, gout, hyperuricaemia, xanthinuria etc., the levels of the modified nucleic bases like uric acid, caffeine, hypoxanthine, and caffeine from the samples of blood and urine proved to be strong

indicators to detect such states.[51-55] So, for the clinical prediction of these indicator levels at an accurate level is very much required.[56] These MNBs can also be detected using the high pressure chromatography, electrochemistry methods, enzymatic methods etc.[57-64] However, in order to detect these MNBs, one requires fast sample preparation, expensive setup, and expensive material which limits the application of these methods. Therefore, electrochemical methods prove to be a better way in comparision to the above described methods. The modified electrodes have paved new ways to detect these important biomolecules.[65] It is quite clear from the previous works that carbon based materials can contribute enormously to develop the electrodes for different application.[66-67] Using the carbon nanotube and multi-walled carbon nanotube, the electrodes were fabricated and were used to detect the MNBs.[68-69] For the detection of caffeine, graphene was successfully used.[70,71] It is very much clear from the studies performed by Alwarappan and co-workers that the electrodes made by using graphene are much better than carbon nanotubes.[72] An improved electro catalytic activity was observed due to π-π interaction with MNBs using the reduced graphene oxide.[73] Thus, the understanding of these MNBs at molecular level is very much required in order to develop new sensors. In the present study, an effort has been made to study the interaction of the graphene and doped graphene (Aluminium doped graphene, sulfur doped graphene, Ni doped graphene, Gallium doped graphene, and Germanium doped graphene) with the modified nucleic bases (MNBs).

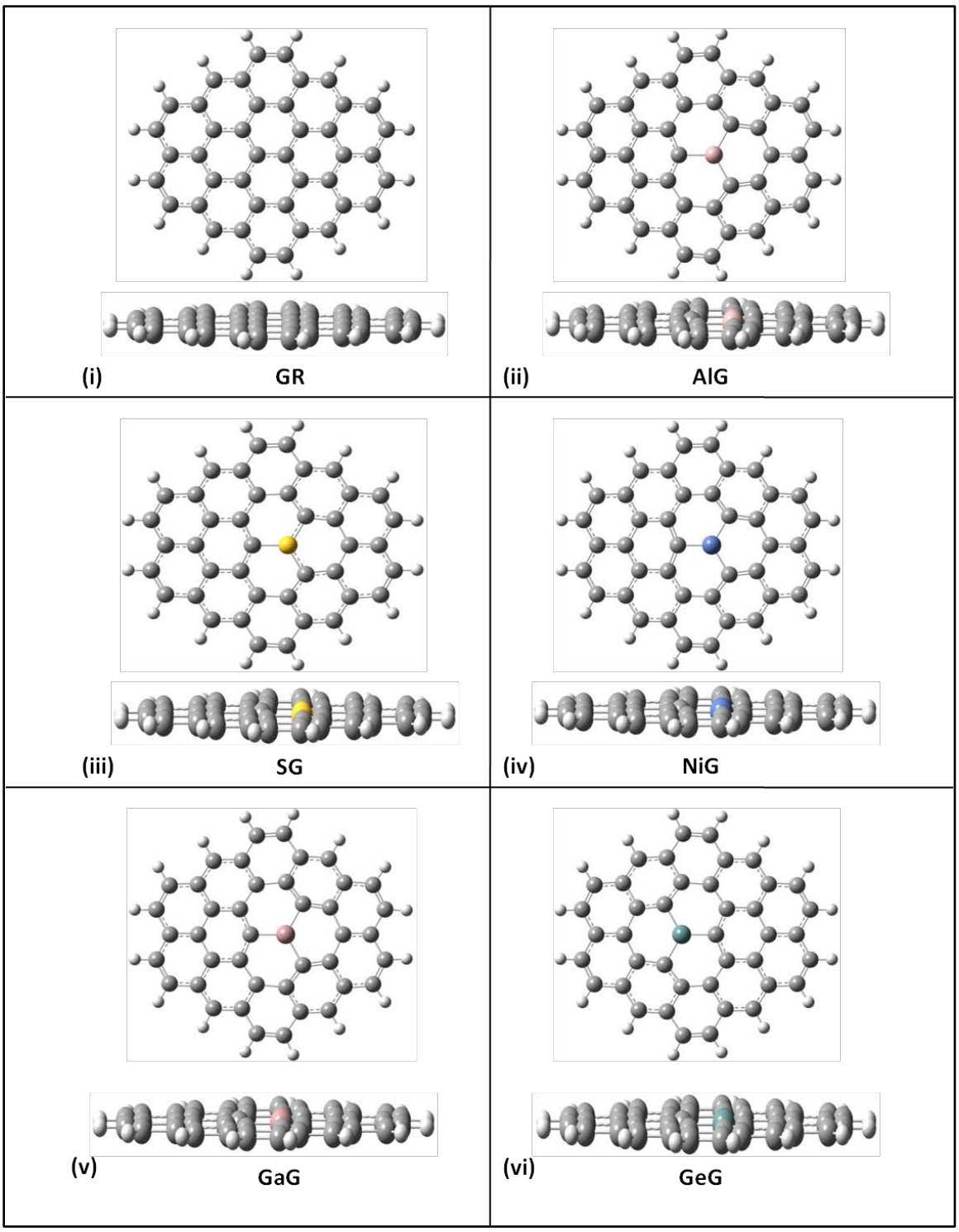

Figure 4.2: Optimized geometries of the graphene and doped graphenes at M06-2X/6-31+G** level: (a) top view and (b) side view.

The following points have been dealt with in detail in the present chapter:-

1) To evaluate the strength of the interaction between the MNBs and graphene (GR) along with doped graphenes (AlG, SG, NiG, GaG and GeG).
2) The study of the comparison of the adsorption energy of the MNBs on graphene and doped graphenes.
3) To study nature of the interaction among the two moieties (i.e. graphene, and MNBs).
4) Comprehending the changes in electronic structure after the adsorption of the MNBs with graphene and doped graphene.

4.2 Methods

The structure of the graphene model in the present study have been considered from the previous study.[74] The model of the graphene holds 42 carbon atoms that are passivated at the edges of the carbon atoms with hydrogen atoms. Thus, the molecular formula of graphene is $C_{24}H_{16}$. The density functional theory (DFT) methods like M06-2X and ωB97XD were extensively used methods to study the non-covalent interactions.[16,75] Therefore these functional are used for the present study. The geometry of the graphene is optimized at M06-2X/6-31+G** level of theory.

In the present study, the pristine graphene is doped with Aluminium, Sulfur, Nickel, Gallium, and Germanium atoms. The exact position of doping site is taken into consideration from the previous study.[76] The doped graphene models were also optimized at the same level of theory. The modified nucleic bases (MNBs) i.e. caffeine, hypoxanthine, uric acid, and xanthine are abbreviated as CAF, HX, UA and X

respectively in the following part of this chapter. The graphene models are abbreviated as pristine graphene (GR), Aluminium doped graphene (AlG), Sulfur doped graphene (SG), Nickel doped graphene (NiG), Gallium doped graphene (GaG), and Germanium doped graphene as (GeG).

The molecular complexes between the MNBs, graphene (GR) and doped graphenes (AlG, SG, NiG, GaG, GeG) were optimized at M06-2X/6-31+G** level of theory. The supramoleclar approach is used to calculate the interaction energies by employing the M06-2X/6-311+G** (BS1) and ωB97XD/6-311+G** (BS2) and B3LYP-D/6-311+G** (BS3) methods for the geometries obtained after optimization process at M06-2X/6-31+G**. The interaction energies were calculated by using the formula

$$I.E. = \left[E_{AB} - (E_A + E_B)\right] \qquad (4.1)$$

where E_{AB} is energy of the complex formed between MNBs and graphene, E_A is the energy of the graphene; E_B is the energy of the MNBs.

The interaction energies were corrected for the basis set superposition error (BSSE) employing the well known counterpoise method given by Boys and Bernadi.[77] All the calculations were performed using the Gaussian 09 software package.[78] The atoms in molecule (AIM) analysis was also performed which is used to identify both the covalent and non-covalent interactions.[79-81] In the present study, the AIM analysis is used to get a better understanding of the nature of interaction between graphene models and MNBs. The wave function generated from the M06-2X functional with 6-31+G** basis set is used for the AIM analysis using the AIM 2000 package.[82]

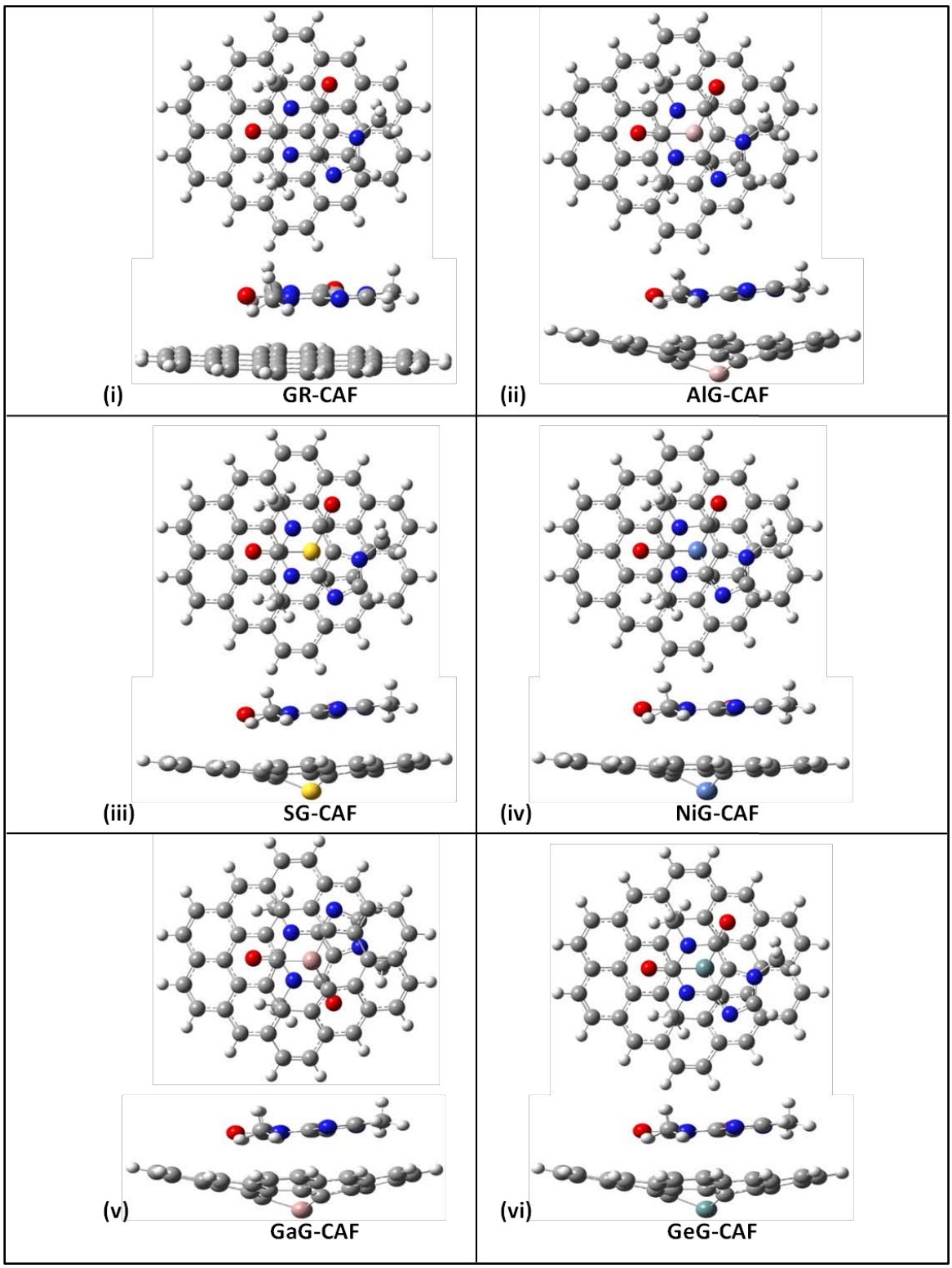

Figure 4.3: Optimized geometries of the complexes formed by caffeine with (i) graphene (GR), (ii) AlG, (iii) SG, (iv) NiG, (v) GaG and (vi) GeG at M06-2X/6-31+G** level shown in top view and side view.

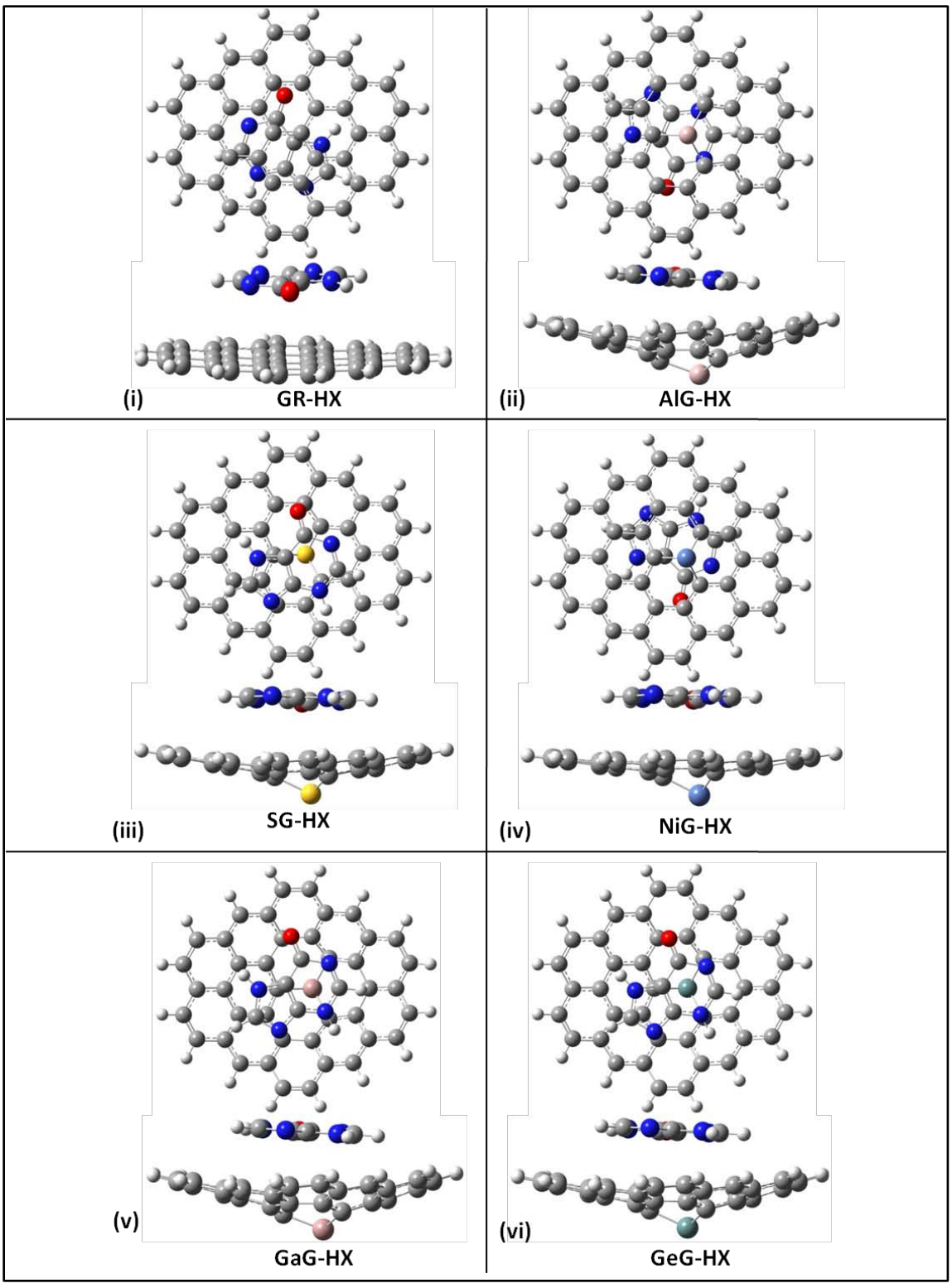

Figure 4.4: Optimized geometries of the complexes formed by hypoxanthine (HX) with (i) graphene (GR), (ii) AlG, (iii) SG, (iv) NiG, (v) GaG and (vi) GeG at M06-2X/6-31+G** level shown in top view and side view.

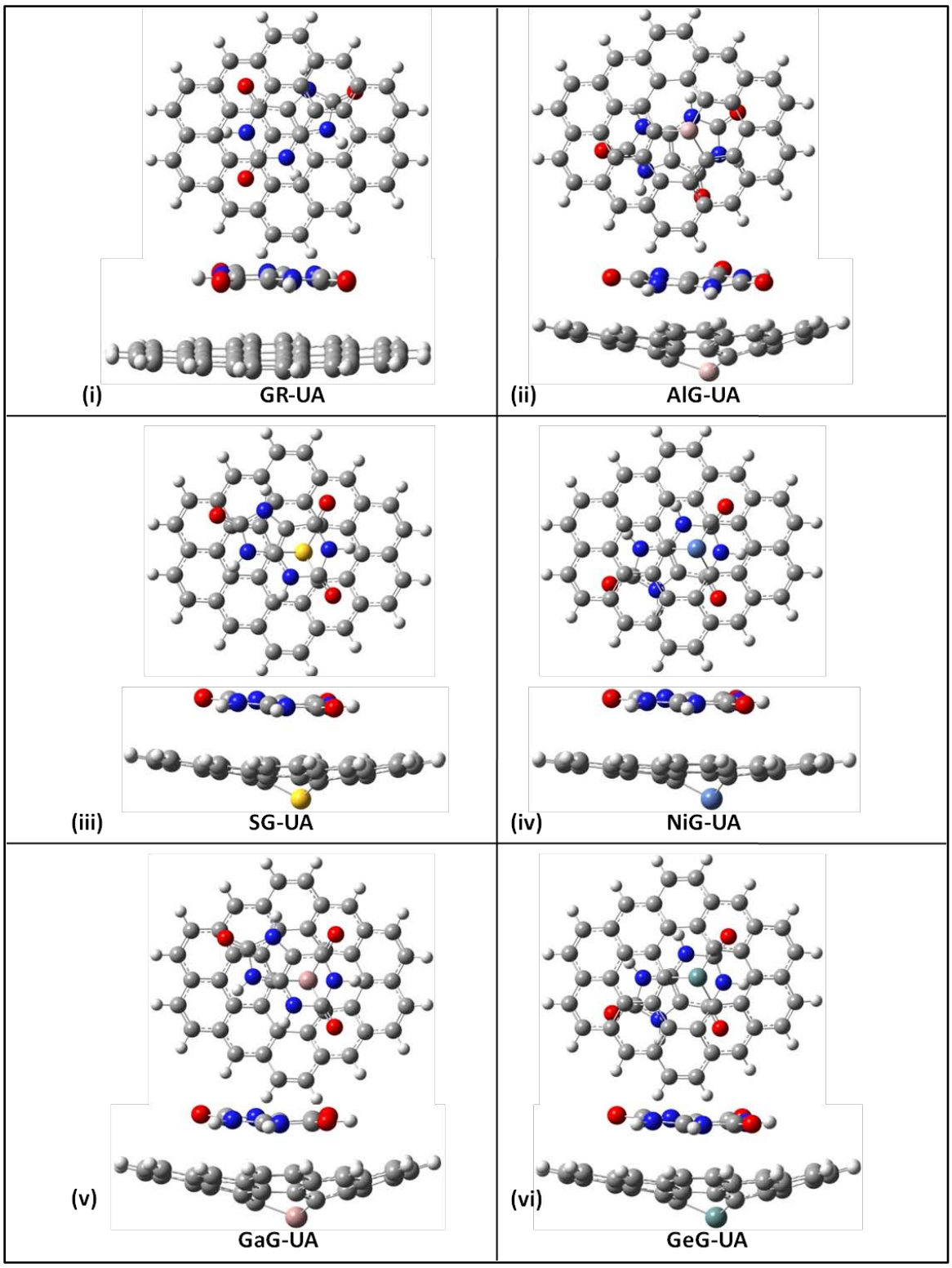

Figure 4.5: Optimized geometries of the complexes formed by uric acid (UA) with (i) graphene (GR), (ii) AlG, (iii) SG, (iv) NiG, (v) GaG and (vi) GeG at M06-2X/6-31+G** level shown in top view and side view.

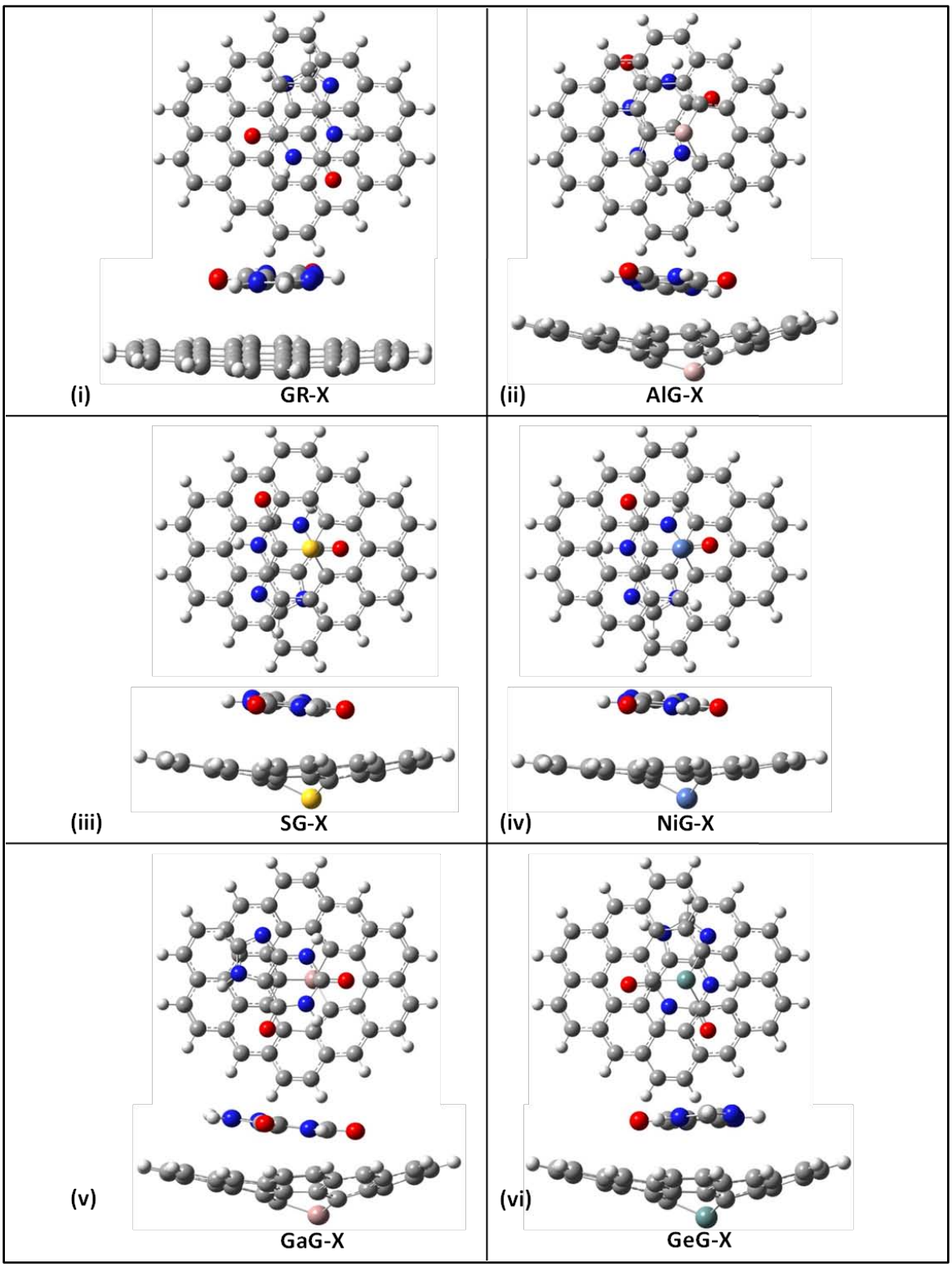

Figure 4.6: Optimized geometries of the complexes formed by xanthine (X) with (i) graphene (GR), (ii) AlG, (iii) SG, (iv) NiG, (v) GaG and (vi) GeG at M06-2X/6-31+G** level shown in top view and side view.

Table 4.1: Calculated interaction energy of MNBs (kcal/mol) with graphene models (GR, AlG, SG, NiG, GaG, GeG) at M06-2X/6-311++G** and ωB97XD/6-31++G** with and without basis set superposition error (BSSE).

Model	MNBs	BSSE Uncorrected M06-2X	BSSE corrected M06-2X	BSSE corrected ωB97XD	BSSE corrected B3LYPD
GR	CAF	-26.280	-20.11	-23.63	-21.50
	HX	-19.456	-14.32	-16.93	-15.43
	UA	-23.087	-17.38	-19.31	-18.27
	X	-20.266	-14.98	-16.99	-15.76
AlG	CAF	-52.104	-46.58	-50.71	-50.57
	HX	-52.437	-47.33	-49.86	-50.13
	UA	-54.401	-49.15	-50.70	-51.40
	X	-53.176	-48.21	-50.17	-50.62
SG	CAF	-85.799	-79.68	-82.78	-80.98
	HX	-82.050	-76.77	-78.98	-77.65
	UA	-85.138	-79.52	-81.06	-79.70
	X	-81.562	-76.26	-77.99	-76.82
NiG	CAF	-96.185	-90.40	-92.04	-86.11
	HX	-91.613	-86.54	-87.77	-82.04
	UA	-95.735	-90.35	-90.51	-85.25
	X	-91.309	-86.28	-86.39	-81.19
GaG	CAF	-55.307	-50.27	-50.07	-51.90
	HX	-55.980	-51.35	-49.21	-51.50
	UA	-56.644	-51.24	-49.29	-51.79
	X	-54.780	-49.59	-47.61	-49.91
GeG	CAF	-48.750	-43.04	-47.68	-43.04
	HX	-48.00	-42.90	-46.01	-48.15
	UA	-49.284	-43.83	-46.26	-48.44
	X	-45.721	-40.59	-43.54	-45.77

4.3 AIM Analysis

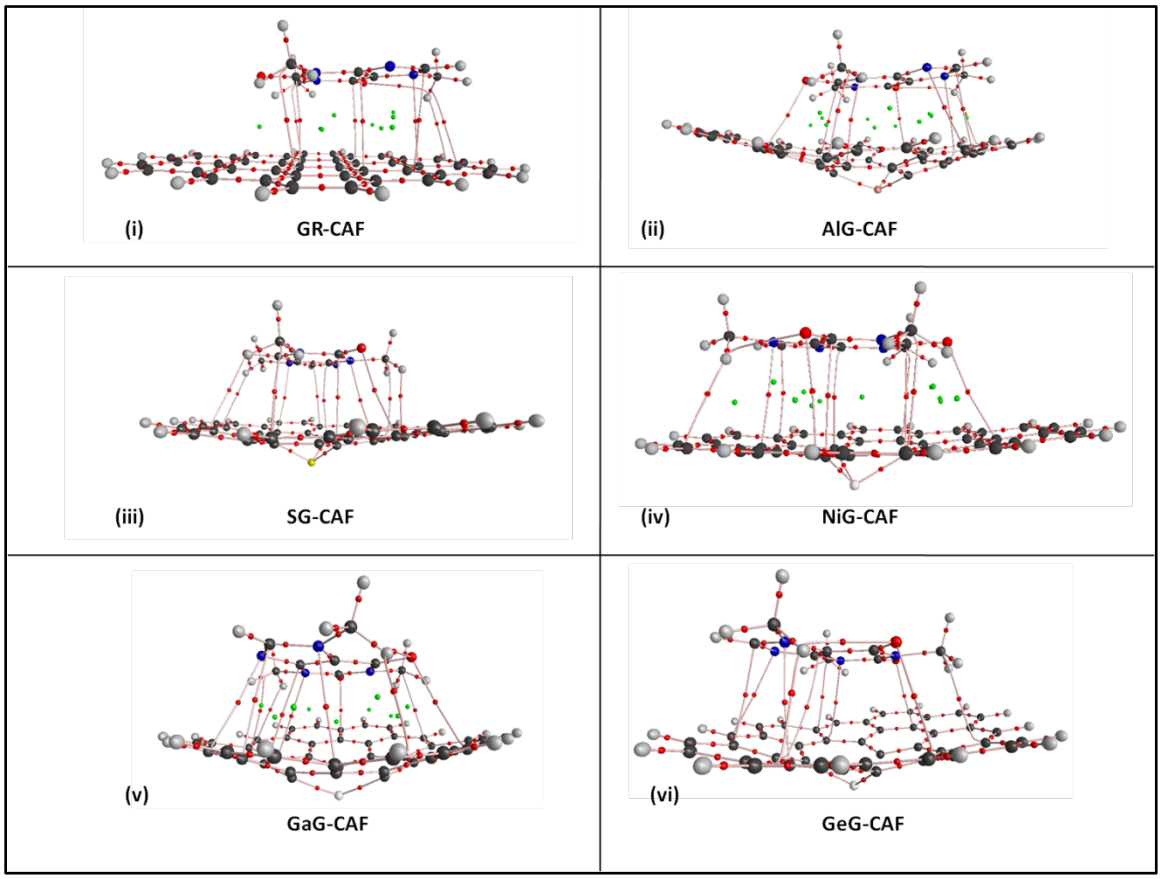

Figure 4.7: Molecular graphs of different complexes of graphene models with Caffeine. The bond critical points (BCPs) are represented by red dots.

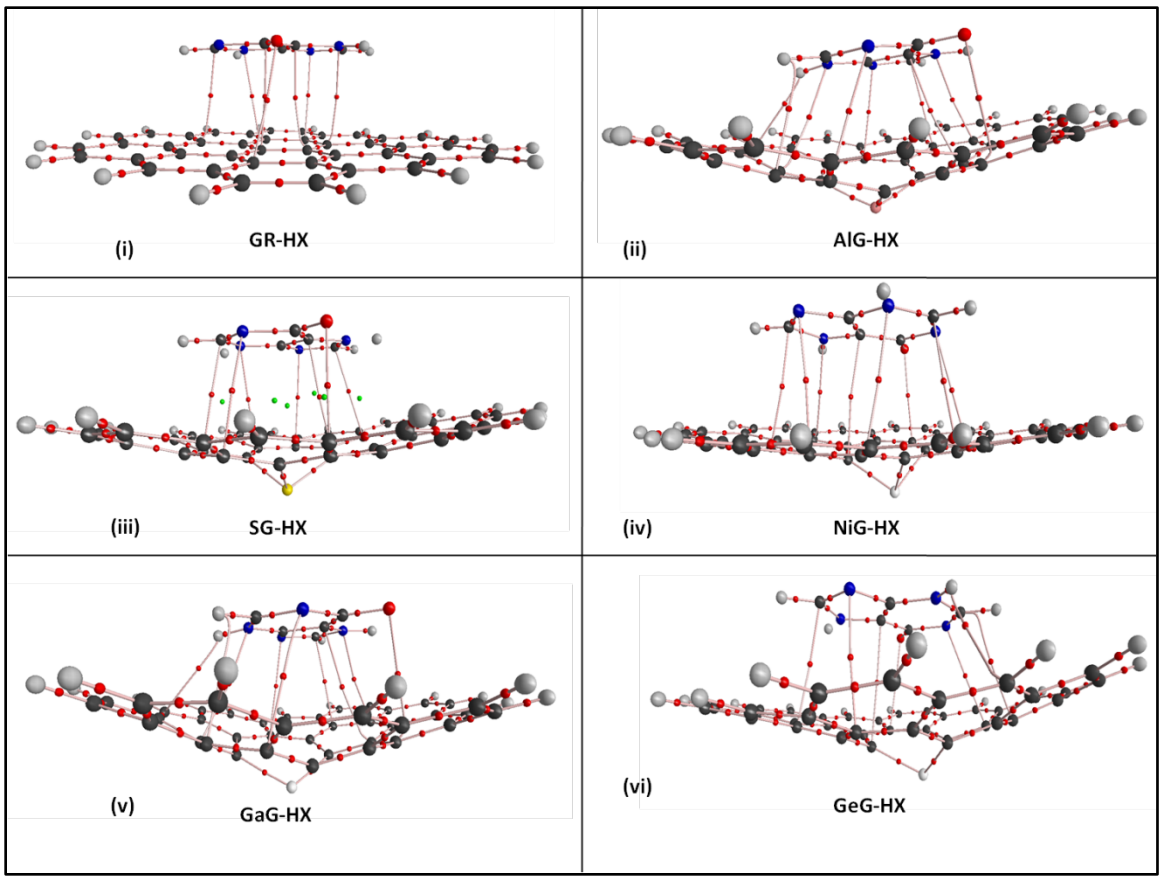

Figure 4.8: Molecular graphs of different complexes of graphene models with Hypoxanthine (HX). The bond critical points (BCPs) are represented by red dots.

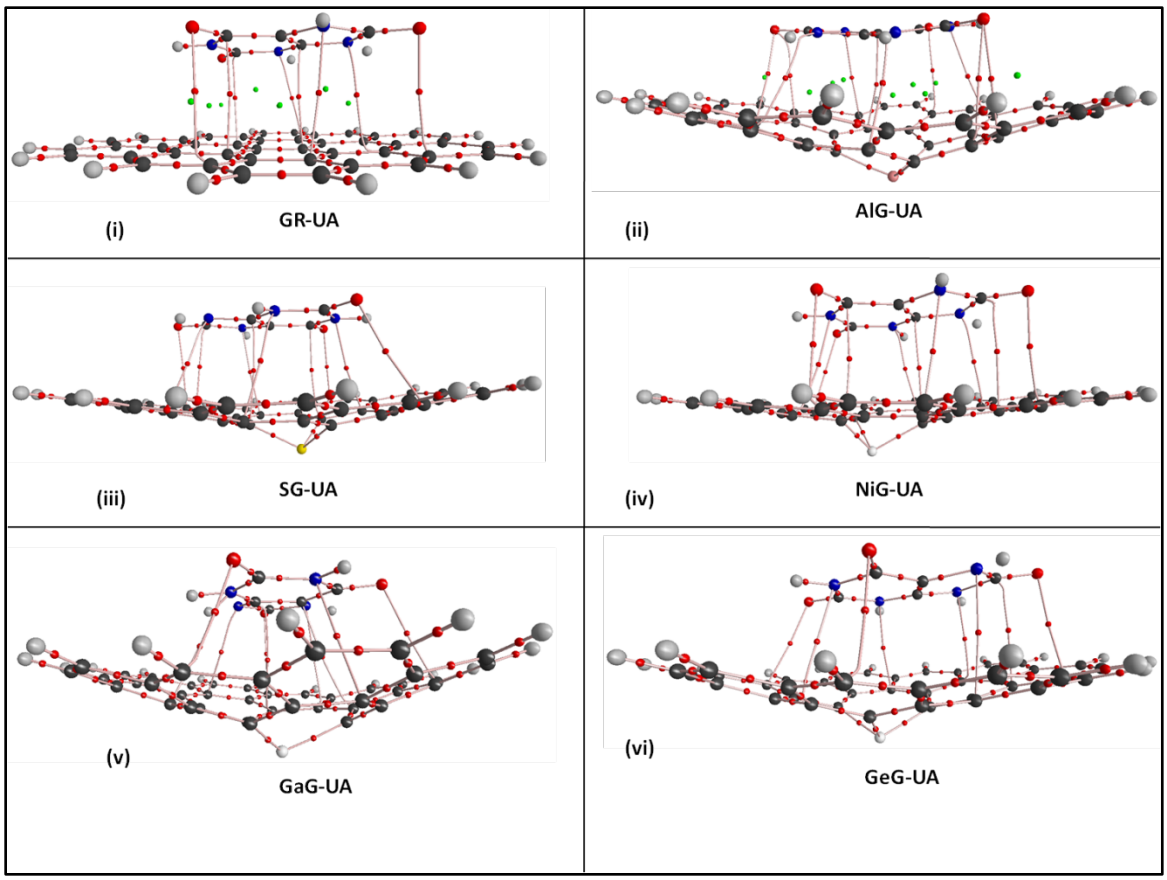

Figure 4.9: Molecular graphs of different complexes of graphene models with Uric Acid (UA). The bond critical points (BCPs) are represented by red dots.

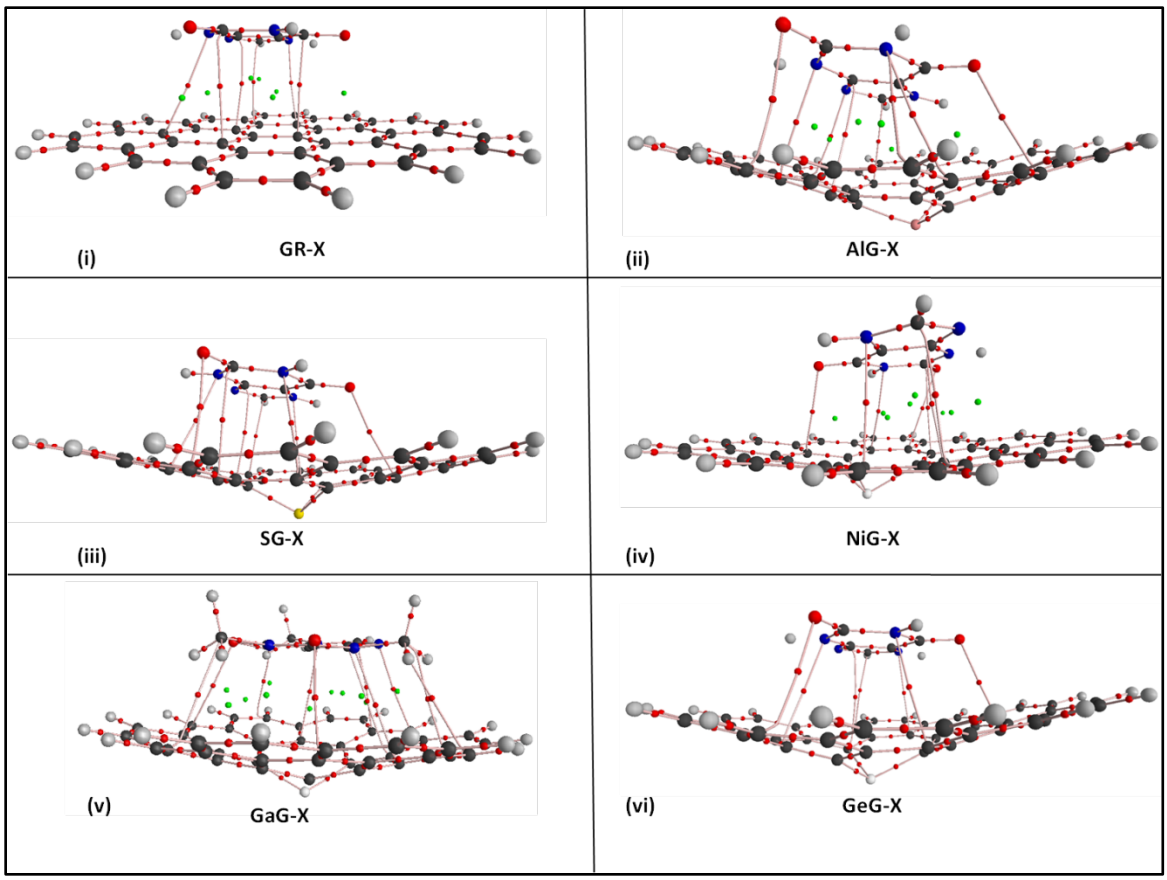

Figure 4.10: Molecular graphs of different complexes of graphene models with Xanthine (X). The bond critical points (BCPs) are represented by red dots.

4.4 Results and Discussion

The molecular electrostatic potentials for the MNBs are shown in Figure 1. The active centers of these MNBs like CO and N were made to interact with the graphene (GR) and doped graphene (AlG, SG, GaG and GeG). The active centers of the MNBs were placed parallel to the graphene surface at a certain distance around 3Å. The set of geometries obtained in this way were optimized at M06-2X/6-31+G** level. It is quite noteworthy that all the MNBs interacted with the different graphene models via the π-π (stacking) interaction. In almost all the complexes formed the doped atom protrudes out of the graphene surface. The interaction energies calculated at M06-2X/6-311+G** are shown in Table 1. The interaction energies were corrected for the basis set superposition error (BSSE). It is clear from the table that the BSSE uncorrected values are higher than the corrected values. Thus, clearly indicating the importance of the BSSE for the studied complexes. The BSSE corrected values for the BS1, BS2 and BS3 are also tabulated in the same table. Taking into consideration, the stacking pattern of the geometries, the dominant role of the dispersion interaction can be well understood. The Laplacian of the electron density $\left(\Delta^2\rho(r_c)\right)$ gives the important information pertaining to the nature of bonding. A negative value of $\left(\Delta^2\rho(r_c)\right)$ suggests that the concentration of the electron density along a particular bond pertains to covalent bond. A positive value of the $\left(\Delta^2\rho(r_c)\right)$ informs that the local depletion of the electron density exists at the BCPs, thereby suggesting the possibility of the closed shell interaction (i.e. electrostatic, hydrogen bond, and π-π stacking). The molecular graphs for the various complexes obtained from the AIM analysis are well shown in the Figures 4.7 to Figure 4.10. The BCPs are generally found between the two stacked entities. The calculated bond critical

points and the corresponding lagrangian at these points are shown in the Table 4.2. The important parameters like $\nabla^2\rho(r_c)$, potential energy density (V_c), kinetic energy density (G_c), and total energy density (H_c) are related to each other with the following equation. These parameters are related to each other as:

$$\frac{1}{4}\nabla^2\rho(r_c) = 2G_c + V_c \tag{4.2}$$

$$H_c = G_c + V_c \tag{4.3}$$

Table 4.2: Calculated sums of electron density ρ and Laplacian $\nabla^2\rho(r_c)$ at the BCPs.

Model	**MNBs**	**Charge Density (ρ)**	**Laplacian of (ρ)**
GR	CAF	0.07	-0.06
	HX	0.05	-0.04
	UA	0.06	-0.05
	X	0.05	-0.04
AlG	CAF	0.07	-0.05
	HX	0.07	-0.05
	UA	0.08	-0.06
	X	0.06	-0.05
SG	CAF	0.08	-0.07
	HX	0.06	-0.04
	UA	0.08	-0.06
	X	0.06	-0.05
NiG	CAF	0.07	-0.06
	HX	0.06	-0.05
	UA	0.07	-0.06
	X	0.05	-0.04
GaG	CAF	0.08	-0.06
	HX	0.07	-0.05
	UA	0.07	-0.05
	X	0.07	-0.05
GeG	CAF	0.07	-0.06
	HX	0.05	-0.04
	UA	0.06	-0.05
	X	0.06	-0.04

4.5 Interaction Energy

The interaction energies of all the complex systems were optimized and were corrected for the basis set superposition error (BSSE) for the three basis sets viz. M06-2X/6-311++G** (BS1), ωB97XD/6-311++G** (BS2), and B3LYP-D/6-311++G** (BS3).

The preferential order of binding for the three basis sets are as follows:

For BS1, the order is CAF>UA>X>HX, UA>X>HX>C, CAF>UA>HX>X, CAF>UA>HX>X, HX>UA>CAF>X, and UA>CAF>HX>X for the G, AlG, SG, NiG, GaG and GeG respectively.

For BS2, the order is CAF>UA>X>HX, CAF>UA>X>HX, CAF>UA>HX>X, C>UA>HX>X, CAF>UA>HX>X, CAF>UA>HX>X for the G, AlG, SG, NiG, GaG, GeG respectively.

For the BS3, the order is CAF>UA>X>HX, UA>X>CAF>HX, CAF>UA>HX>X, CAF>UA>HX>X, CAF>UA>HX>X, UA> HX >X> CAF.

4.6 Homo Lumo Gap

The highest occupied molecular orbital and the lowest unoccupied molecular orbital i.e. Homo Lumo gap is calculated for all the complex systems that involve the Graphene (GR), doped graphene models and the modified nucleic bases (MNBs). The Homo Lumo gap for the graphene complexes is the highest with maximum value of 4.0 eV. The trend of the Homo Lumo gap for the different doped graphenes is G>GeG NiG>SG AlG >GaG.

Table 4.3: Calculated Homo Lumo energy gap (eV) of various complex at M06-2X/6-31+G** Method.

Model	MNBs	Homo Lumo Energy gap (eV)
GR		4.0
GR	CAF	4.0
	HX	4.0
	UA	4.0
	X	4.0
AlG		2.7
AlG	CAF	2.5
	HX	2.5
	UA	2.5
	X	2.5
SG		2.8
SG	CAF	3.4
	HX	3.4
	UA	3.5
	X	3.4
NiG		3.4
NiG	CAF	3.5
	HX	3.6
	UA	3.6
	X	3.6
GaG		2.6
GaG	CAF	2.5
	HX	2.5
	UA	2.5
	X	2.5
GeG		3.7
GeG	CAF	3.4
	HX	3.4
	UA	3.4
	X	3.4

4.7 Conclusion

The present study elaborates in detail the adsorption mechanism of modified nucleic bases (MNBs) on graphene (GR) and various other models of doped graphenes (AlG, SG, NiG, GaG, GeG) considered in this study. The preferential order of interaction energy for the studied modified nucleic bases (MNBs) in general is CAF>UA>HX>X. The AIM analysis confirms that the MNBs interact with the π–π (stacking) interaction which is the main factor for the adsorption of MNBs on different doped graphenes. Significant changes in the HOMO-LUMO gap of the intermolecular complex are analyzed. These variations in the electronic structure and associated changes in the electronic properties will be helpful to design new sensors. Therefore, the findings of this study may spark experimental studies in this direction. This detailed study using electronic calculations and associated analysis tools have been used to explore the utilility of this study in the field of sensors.

References

[1] A. K. Geim and K. S. Novoselov, *Nat. Mater.*, **183**, 1476 (2007).

[2] A. K. Geim, *Science*, **324**, 1530 (2009).

[3] K. S. Novoselov, A. K. Geim, S. V. Morozov, D. Jiang, Y. Zhang, S. V. Dubonos, I. V. Grigorieva, A. A. Firsov, *Science*, **306**, 666 (2004).

[4] S. Latil and L. Henrard, *Phys. Rev. Lett.*, **97**, 036803 (2006).

[5] A. A. Balandin, S. Ghosh, W. Z. Bao, I. Calizo, D. Teweldebrhan, F. Miao, C. N. Lau, *Nano Lett.*, **8**, 902 (2008).

[6] Y. Xuan, Y. Q. Wu, T. Shen, M. Qi, M. A. Capano, J. A. Cooper, P. D. Ye, *Appl. Phys. Lett.*, **92**, 013101 (2008).

[7] X. M. Yang, Y. F. Tu, L. Li, S. Shang, X. M. Tao, *ACS Appl. Mater. Interfaces*, **2**, 1707 (2010).

[8] C. Liu, S. Alwarappan, Z. F. Chen, X. X. Kong, C. Z. Li, *Biosens. Bioelectron.*, **25**, 1829 (2010).

[9] M. D. Stoller, S. J. Park, Y. W. Zhu, J. H. An, R. S. Ruoff, *Nano Lett.*, **8**, 3498 (2008).

[10] X. Li, X. Wang, L. Zhang, S. Lee, H. Dai, *Science*, **319**, 1229 (2008).

[11] C. C. Lu, Y. C. Lin, C. H. Yeh, J. C. Huang, P. W. Chiu, *ACS Nano*, **6**, 4469 (2012).

[12] C. H. Lu, H. H. Yang, C. L. Zhu, X. Chen, G. N. Chen, *Angew. Chem., Int. Ed.*, **48**, 4785 (2009).

[13] L. T. Qu, Y. Liu, J. B. Baek, L. Dai, *ACS Nano*, **4**, 1321(2010).

[14] Z. Liu, J. T. Robinson, X. M. Sun, H. J. Dai, *J. Am. Chem. Soc.*, **130**, 10876 (2008).

[15] Wu. Qin, Xin. Li, W. W. Bian, X. J. Fan, J. Y. Qi, *Biomaterials*, **31**, 1007 (2010).

[16] D. Umadevi and G. N. Sastry, *J. Phys. Chem. Lett.*, **2**, 1572 (2011).

[17] C. Rajesh, C. Majumder, H. Mizuseki, Y. Kawazoe, *J. Chem. Phys.*, **130**, 124911 (2009).

[18] H. E. Romero, P. Joshi, A. K. Gupta, H. R. Gutierrez, M. W. Cole, S. A. Tadigadapa, P. C. Eklund, *Nanotechnology*, **20**, 245501 (2009).

[19] B. Huang, Z. Li, Z. Liu, G. Zhou, S. Hao, J. Wu, B. L. Gu, W. Duan, *J. Phys. Chem. C*, **112**, 13442 (2008).

[20] O. Leenaerts, B. Partoens, F. Peeters, *Phys. Rev. B: Condens. Matter Mater. Phys.*, **77**, 125416 (2008).

[21] J. Lee, Y. K. Choi, H. J. Kim, R. H. Scheicher, J. H. Cho, *J. Phys. Chem. C*, **117**, 13435 (2013).

[22] J. Prasongkit, A. Grigoriev, B. Pathak, R. Ahuja, R. H. Scheicher, *J. Phys. Chem. C* **117**, 15421 (2013).

[23] S. M. Maliyekkal, T. S. Sreeprasad, D. Krishnan, S. Kouser, A. K. Mishra, U. V. Waghmare, T. Pradeep, *Small*, **9**, 273 (2012).

[24] K. Balamurugan and V. Subramanian, *J. Phys. Chem. C*, **117**, 21217 (2013).

[25] N. Mohanty and V. Berry, *Nano Lett.*, **8**, 4469 (2008).

[26] J. Dai, J. Yuan, P. Giannozzi, *Appl. Phys. Lett.*, **95**, 232105 (2009).

[27] Z. Ao, S. Li, Q. Jiang, *Solid State Commun.*, **150**, 680 (2010).

[28] A. Kaniyoor, R. I. Jafri, T. Arokiadoss, S. Ramaprabhu, *Nanoscale*, **1**, 382 (2009).

[29] Y. H. Zhang, Y. B. Chen, K. G. Zhou, C. H. Liu, J. Zeng, H. L. Zhang, Y. Peng, *Nanotechnology*, **20**, 185504 (2009).

[30] Z. M. Ao, J. Yang, S. Li, Q. Jiang, *Chem. Phys. Lett.*, **461**, 276 (2008).

[31] Z. M. Ao, S. Li, Q. Jiang, *Phys. Chem. Chem. Phys.*, **11**, 1683 (2009).

[32] B. F. Machado and P. Serp, *Catal. Sci. Technol.*, **2**, 54 (2012).

[33] J. Pyun, *Angew. Chem., Int. Ed.*, **50**, 46 (2011).

[34] J. V. Sundar and V. Subramanian, *Org. Lett.*, **15**, 5920 (2013).

[35] A. Kumar, D. Singh, D. Kumar, D. Kumar, *J. Comp. Chem.*, **24**, 802 (2018).

[36] Y. Zou, F. Li, Z.H. Zhu, M.W. Zhao, X.G. Xu, X.Y. Su, *Eur. Phys. J. B*, **81**, 475 (2011).

[37] A.Junkaew, S. Namuangruk, P. Maitarad and M. Ehara, *RSC Adv.*, **8**, 22322 (2018).

[38] Y. Chen, Y.-J. Liu, H.-X. Wang, J.-X. Zhao, Q.-H. Cai, X.-Z. Wang, and Y.-H Ding, *ACS Appl. Mater. Interfaces*, 5, 5994 (2013).

[39] X. M. Feng, R. M. Li, Y. W. Ma, R. F. Chen, Q. B. Mei, Q. L. Fan, W. Huang, *Sci. China: Chem.*, **54**, 1615 (2011).

[40] H. Jiang, D. Zhang, R. Wang, *Nanotechnology*, **20**, 145501 (2009).

[41] D. Singh, A. Kumar, D. Kumar, *Bull. Mater. Sci.*, **40**, 1263 (2017).

[42] Z. M. Ao, Q. Jiang, R. Q. Zhang, T. T. Tan, and S. Li, *J. of Appl. Phys.*, **105**, 074307 (2009).

[43] L. Chen and Z.-R. Xu, *RSC Adv.*, **6**, 56278 (2016).

[44] P. A. Denis, *ChemPhysChem*, **15**, 3994 (2014).

[45] M. Losurdo, C. Yi, A. Suvorova, S. Rubanov, T-Ho Kim, M. M. Giangregorio, W. Jiao, I.Bergmair, G. Bruno, A. S. Brown, *ACS Nano*, **8**, 3031 (2014).

[46] Y-an Lv, G-L Zhuang, J-G Wang, Ya-bo Jia, Q. Xie, *Phys. Chem. Chem. Phys.*, **13**, 12472 (2011).

[47] S. Li, Y. Li, J. Cao, J. Zhu, L. Fan, X. Li, *Anal. Chem.*, **86**, 10201 (2014).

[48] X. Li, S. P. Lau, L. Tang, R. Ji, P. Yang, *RSC Nanoscale*, **6**, 5323 (2014).

[49] T. Yamamoto, Y. Moriwaki, S. Takahashi, *Clin. Chim. Acta.*, **356**, 35 (2005).

[50] I. Biaggioni, S. Paul, A. Puckett, C. Arzubiaga, *J. Pharmacol. Exp. Ther.*, **258**, 588 (1991).

[51] M. K. Kutzing and B. L. Firestein, *J. Pharmacol. Exp. Ther.*, **324**, 1 (2008).

[52] N. Turgan, B. Boydak, S. Habif, C. Guilter, B. Senol, I. Mutaf, D. Ozmen, O. Baymdlr, *Int. J. Clin. Lab. Res.*, **29**, 162 (1999).

[53] V. Fellman and K. O. Raivio, *Pediatr. Res.*, **41**, 599 (1997).

[54] N. Spataru, B. V. Sarada, D. A. Tryk, A. Fujishima, *Electroanalysis*, **14**, 721 (2002).

[55] A. Pizzariello, J. Švorc, M. Stred'ansky, S. Miertuš, *J. Sci. Food Agric.*, **79**, 1136 (1999).

[56] H. Nihei, H. Kanemitsu, A. Tamura, H. Oka, K. Sano, *Neurosurg.*, **25**, 613 (1989).

[57] S. Sumi, K. Kidouchi, S. Ohba, Y. Wada, *J. Chrom. B*, **670**, 376 (1995).

[58] K. Safranow, Z. Machoy, K. Ciechanowski, *Anal. Biochem.*, **286**, 224 (2000).

[59] Z. K. Shihabi, M. E. Hinsdale, A. J. Bleyer, *J. Chrom. B*, **669**, 163 (1995).

[60] T. Wessela, C. Lanversa, S. Fruend, G. Hempel, *J. Chrom. A*, **894** ,157 (2000).

[61] L. Mao, F. Xu, Q. Xu, L. Jin, *Anal. Biochem.*, **292**, 94 (2001).

[62] M. A. Carsol, G. Volpe, M. Mascini, *Talanta*, **44**, 2151 (1997).

[63] Y. Wang, Li.li Tong, *Sens. and Act. B*, **150**, 43 (2010).

[64] C. Yiting, Q. Bin, J. Yingyan, L. Zhenyu, S. Jianjun, Z. Lan, C. Guonan, *Electrochem. Commun.*, **11**, 2093 (2009).

[65] N. K. Chaki and K. Vijayamohanan, *Biosen. and Bioelec.*, **17**, 1 (2002).

[66] J. Wang, M. Musameh, Y. H. Lin, *J. Am. Chem. Soc.*, **125**, 2408 (2003).

[67] X. Kang, J. Wang, H. Wu, I. A. Aksay, J. Liu, Y. Lin, *Biosen. and Bioelec.*, **25**, 901 (2009).

[68] Z. Wang, X. Dong, J. Li, *Sens. and Act. B*, **131** 411 (2008).

[69] Y. Wang, *Coll. Surf. B: Biointer.*, **88**, 614 (2011).

[70] W Yu H. Khoo, M. Pumera, A. Bonanni, *Anal. Chem. Act.*, **804**, 92 (2013).

[71] J-Yong Sun, Ke -J Huang, S-Y Wei, Z-W Wu, F.-P. Ren, *Coll. Surf. B: Biointer.*, **84**, 421 (2011).

[72] S. Alwarappan, A. Erdem, C. Liu, C-Z. Li, *J. Phys. Chem. C*, **113**, 8853 (2009).

[73] M. A. Raj and S. A. John, *Anal. Chem. Act.*, **771**, 14 (2013).

[74] R. A. Sidik and A. B. Anderson, *J. Phys. Chem. B*, **110**, 1787 (2006).

[75] S. Panigrahi, A. Bhattacharya, S. Banerjee, D. Bhattacharyya, *J. Phys. Chem. C*, **116**, 4374 (2012).

[76] K. Xiangkai and S. Zhiyuan, *Phys. Chem. Chem. Phys.*, **14**, 13564 (2012).

[77] S. F. Boys and F. Bernardi, *Mol. Phys.*, **19**, 553 (1970).

[78] Gaussian 09, Revision A.02, M. J. Frisch, G. W. Trucks, H. B. Schlegel, G. E. Scuseria, M. A. Robb, J. R. Cheeseman, G. Scalmani, V. Barone, B. Mennucci,

G. A. Petersson, H. Nakatsuji, M. Caricato, X. Li, H. P. Hratchian, A. F. Izmaylov, J. Bloino, G. Zheng, J. L. Sonnenberg, M. Hada, M. Ehara, K. Toyota, R. Fukuda, J. Hasegawa, M. Ishida, T. Nakajima, Y. Honda, O. Kitao, H. Nakai, T. Vreven, J. A. Montgomery, Jr., J. E. Peralta, F. Ogliaro, M. Bearpark, J. J. Heyd, E. Brothers, K. N. Kudin, V. N. Staroverov, R. Kobayashi, J. Normand, K. Raghavachari, A. Rendell, J. C. Burant, S. S. Iyengar, J. Tomasi, M. Cossi, N. Rega, J. M. Millam, M. Klene, J. E. Knox, J. B. Cross, V. Bakken, C. Adamo, J. Jaramillo, R. Gomperts, R. E. Stratmann, O. Yazyev, A. J. Austin, R. Cammi, C. Pomelli, J. W. Ochterski, R. L. Martin, K. Morokuma, V. G. Zakrzewski, G. A. Voth, P. Salvador, J. J. Dannenberg, S. Dapprich, A. D. Daniels, O. Farkas, J. B. Foresman, J. V. Ortiz, J. Cioslowski, D. J. Fox, Gaussian, Inc., Wallingford CT, (2009).

[79] P. L. A. Popelier, *Atoms in Molecules*: An Introduction; Prentice Hall: New York, (2000).

[80] R. F. W. Bader, *Atoms in Molecules*: A Quantum Theory; Clarendon Press: Oxford, U.K., (1990).

[81] S. J. Grabowski, *Hydrogen Bonding-New Insights: Challenges and Advances in Computational Chemistry and Physics*; *Springe*r: Dordrecht, The Netherlands, **3** (2006).

[82] F. Biegler-Konig, J. Schonbohm, R. Derdau, D. Bayles, R. F. W. Bader, AIM2000, Version 1; Bielefeld: Germany, (2000).

Chapter 5

Interaction of alkali metal ions with single walled carbon nanotube (SWCNT)

CHAPTER 5

INTERACTION OF ALKALI METAL IONS WITH ZIG-ZAG SINGLE WALLED CARBON NANOTUBE (SWCNT)

5.1 Introduction

In the field of nanotechnology, the carbon nanotubes (CNTs) have contributed significantly at a large scale. For the last two decades or so, there has been a great deal of research for these carbon nanotubes in almost all possible areas but there are few yet to be explored. The word “nano” has been taken from the Greek which means “dwarf” (small) in English. During the last three decades, by utilizing the various scientific instruments, this branch of science “nanotechnology” has well established itself and has become a word of mouth among the entire research fields. The credit belongs to Norio Taniguchi, of Japan, who first named this famous branch of science, i.e. “Nanotechnology”. It is well known today that the credit goes to Sumio Iijima[1] for the discovery of carbon nanotube in 1991 but there is a very interesting story (incident) about it. In 1952, it was Radushkevich and Lukyanovich[2] who first brought to light the “worm-like” carbon formations at 600^0C which they discovered while studying the decomposition of carbon monoxide (CO) on iron particles during the formation of soot. Since then, these carbon nanotubes (CNTs) were unexplored and no one actually knew until 1991 that this carbon formation will lead to the technological advancement to a greater height in the forth coming future.

5.2 Carbon nanotube (CNT)

Depending upon the number of walls associated with the CNT, these structures are generally termed as single walled carbon nanotube (SWCNT) which may be obtained by wrapping a single layer of graphene. The length of this structures so formed may vary depending upon the methods followed to produce it. However, double walled carbon nanotubes also exist that are comprised of two concentric carbon nanotubes where the inner tube is enclosed by the outer tube. Also, the multi-walled carbon nanotube (MWCNTs) do exist that are made by wrapping more than two layers of graphene. The diameter of the MWCNTs ranges from 2 to 50 nm which depends upon the number of graphene. The distance between the two layers of MWCNTs is of 0.34nm approximately.

There is another well defined criterion i.e. “chirality” that successfully classifies the CNTs based on the chiral indices n and m. The chiral indices are represented as (n,m). When the chiral indices are same, i.e. n=m, the so called CNT is termed as armchair CNT and owes a metallic behavior. When n=n, and m=0, we have zig-zag CNT. These zig-zag CNTs generally behave as semiconductors. It is quite noteworthy that the semi-conducting SWCNTs behave as p-type semiconductors.[3]

When we have two different chiral indices, i.e. chirality is (n,m) then such CNT is said to behave as metallic if the difference between n and m is a multiple of 3, else they behave as semiconductors.

So, in general, it can be said that the carbon nanotubes show metallic or semi-metallic behavior (semi-conductors) depending on the chirality.[4-16]

By using the the chiral indices (n,m), the diameter of the SWCNTs can be calculated by the formula:

$$d = \frac{a}{\pi}\left[3\left(n^2 + m^2 + nm\right)\right]^{1/2} \qquad (5.1)$$

where d is diameter, a is C-C bond length and m and n are chiral indices of CNT.

The CNTs have some prominent properties like high mechanical strength, high surface areas, and large aspect ratio. Yu et al. reported that the tensile strength of steel is 20 times lower than SWCNTs; also the Young's modulus of CNTs is much greater than fibers of steel.[17] The thermal and electrical conductivity of CNT is reported to be comparable with that of copper.[27,28] These outstanding properties opened new avenues for the application of the carbon nanotubes in different fields. Guanghua et al.[18] reported that the mechanical strength of SWCNTs depends upon the diameter.

5.3 Importance of non-covalent interactions

In the present era of advanced computational techniques, the relevance of the non-covalent interactions can be well understood as they have brought themselves in lime light due to their commanding force in biological systems and various other important fields. Non-covalent interactions were conventionally thought to be as weak interactions but have proven their presence in different fields.[19-24] The hydrogen bonding is the most extensively examined interaction[25,26], yet the noteworthiness of the other noncovalent interactions like CH···π interactions, anion–π , cation–π, π–π stacking, and halogen bonding for a wide range of applications in material design, molecular recognition, catalysis, supramolecular interactions are well noticed.[19,23,27-35]

The importance of the cation−π interaction (the strongest among the noncovalent interactions) can be understood by the fact that these cation−π interactions play a central role in controlling the structure and function of macromolecules.[19,27,24]

The importance of cooperative or anticooperative effects in these noncovalent interactions are well studied.[36-40]

It is well reported that the metal ion pollutants residing in water could be removed by interaction of metal ion with carbon nanostructures, thereby making a significant contribution.[41] Some recent studies displayed the effect of the curvature on the cation-π interactions.[42-44] Li et al. revealed that in order to differentiate the metallic carbon nanotubes from semi-conducting materials, the non-covalent functionalization with alkali metals plays an important role.[45] There are some excellent studies performed which demonstrate the effect of solvation on cation-π interactions where different metal ions were used.[46-48] Thus these cation- π interaction are very crucial to study and will definitely open new doors for the unexplored applications in future.

In the present chapter, a detailed study to comprehend the behavior of monocations (K^+, Na^+) while it passes at different positions of SWCNT has been performed. Different parameters like interaction energy, homo-lumo energy gap, and the variation of charge between the two moieties has been analyzed at different positions. These parameters provide necessary information for tuning the electronic and conductivity properties via the formation of metal ion complex.

5.4 Methods

The structure of the SWCNT in the present study has been considered from the previous study.[49] There are 80 carbon atoms and 20 hydrogen atoms present in the model system. The dangling bonds at the truncated ends of the SWCNT were passivated with hydrogen atoms to stop spurious end effects. The calculations performed in this chapter were carried out by using density functional theory (DFT) method as implemented in the Gassian09 program package.[50] In this study, the geometries of alkali metal ions (K^+, and Na^+) with single walled carbon nanotube (SWCNT) were optimized using the well known B3LYP method[51,52] at 6-31G* basis set. The single point energy calculations were also performed by using B3LYP which is abbreviated as (BS1) and M06 abbreviated as (BS2) method at 6-31++G** basis set.

The interaction energy ΔE of the alkali metal ions (K^+ and Na^+) with SWCNT is calculated by using the following formula:

$$\Delta E = E_0 - E \qquad (5.1)$$

where E_0 is the total energy of the complex system for the initial position of the alkali metal ions with SWCNT, E represents the variation of the total energy at different position of alkali metal ion with SWCNT.

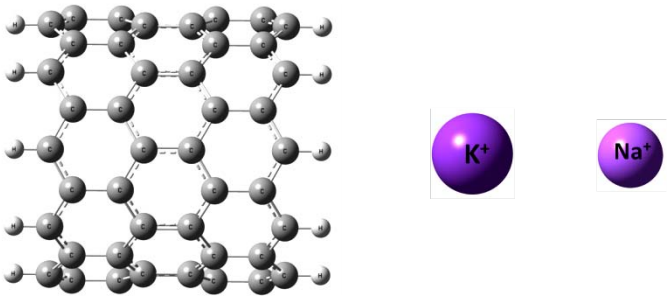

Figure 5.1: Optimized geometry of single walled carbon nanotube SWCNT (10, 0) and alkali metal ions (K^+ and Na^+) interaction.

5.5 Results and Discussion

In the present chapter, the alkali metal ions (K^+ and Na^+) and single walled carbon nanotube are considered for the study whose optimized geometries are shown in Figure 5.1. The optimized structures of alkali metal ions K^+ and Na^+ with complex structure are shown in Figure 5.2 and 5.9 respectively. It is quite noteworthy that the alkali metal ions (K^+ and Na^+) were subjected to pass right in the central positions from one end of the SWCNT to the other. There were total 18 positions which were considered in this study. At each position, the variation of interaction energy, homo lumo gap and associated charge transfer is calculated. The variation of important parameters like interaction energy, homo lumo gap and the associated charge transfer were calculated using the two basis sets BS1(B3LYP/6-31++G**) and BS2(M06/6-31++G**) considered in this study. The calculated total energy (kcal/mol), ΔE (kcal/mol), Homo Lumo Gap (eV) and Mulliken charge on alkali metal ion (K^+) and Single Walled Carbon Nanotube (SWCNT) can be observed from the Table 5.1(for BS1), Table 5.2 (for BS2), while for Na^+ it may be seen in Table 5.3 (for BS1) and Table 5.4 (for BS2). The variation of interaction energy, homo lumo gap and charge transfer for the K^+ ion can be depicted from the Figures 5.3 to Figure 5.8 for BS1 and BS2, however for Na^+, the same variations can be seen from Figure 10 to 15 for BS1 and BS2 respectively . The charge analysis among the two entities reveals significant information. The positive charge values indicate the transfer of charge from SWCNT to the metal ions while negative charge values indicate the transfer of charge from the metal ions to the SWCNT. The Mulliken charge analysis and HOMO-LUMO gap were also evaluated at various positions which provide relevant information.

5.6 Interaction energy and Homo Lumo gap

The interaction energy for BS1 and BS2 increases as the K^+ ion approaches the SWCNT and attains a maximum value at 7^{th} position, decreases to 10^{th} position and after the 13^{th} position, the interaction energy decreases sharply. The homo lumo gap remains almost constant from the 2^{nd} position to the 17^{th} position for the BS1 however for the BS2, the homo lumo gap increases as the K^+ ion approaches the SWCNT and decreases after the 6^{th} position till the 10^{th} position and increases to 16^{th} position followed by a decrease in homo lumo gap as the K^+ comes out of the SWCNT. Significant charge transfer can be observed as the K^+ ion approaches the central position of the benzene ring due to the cation-π interaction.

In the case of Na^+ ion, the interaction energy increases for BS1 and remains unchanged, however a gradual decrease in the interaction energy can be observed. For BS2, the interaction energy almost followed the same variation as observed in the case of K^+. For BS1, the homo lumo gap however increases as the metal ion approaches SWCNT, remains almost constant while the metal ion traverses inside the SWCNT and thereafter decreases as the metal ion comes out from the other side of the SWCNT. For BS2, the homo lumo gap does not remain constant as for BS1, it increases, and attains a minimum value at the 9^{th} position, increases and as it comes out of SWCNT, the gap decreases. The variation of charge transfer from the Mulliken charge analysis clearly shows how the transfer of the charge occurs with the movement of the metal ion.

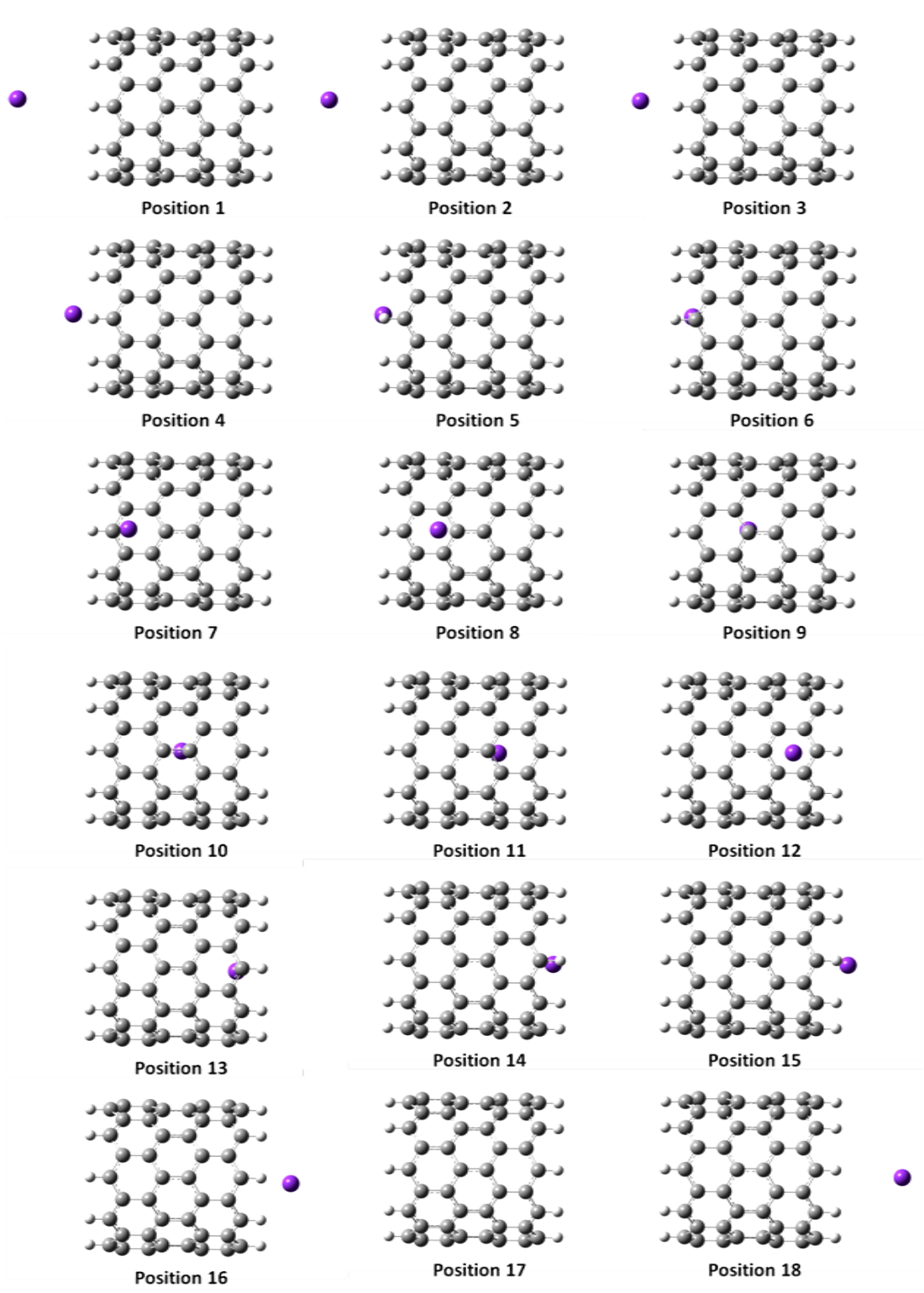

Figure 5.2: Optimized geometries of the complexes formed between the SWCNT(10,0) and alkali metal ion (K^+) at B3LYP/6-31G* method.

Table 5.1: Calculated Total Energy (kcal/mol), ΔE (kcal/mol), Homo Lumo Gap (eV) and Mulliken charge on alkali metal ion (K^+) and Single Walled Carbon Nanotube (SWCNT) at B3LYP/6-31++G** (BS1).

Metal ion	Various Positions	Total Energy (kcal/mol)	$\Delta E=E_0-E$ (kcal/mol)	Homo Lumo Gap (eV)	Charge on K^+	Charge on CNT
K^+	1	-2296876.185	0.000	0.121	1.015	-0.015
	2	-2296877.903	1.718	0.421	1.035	-0.035
	3	-2296881.36	5.175	0.427	1.035	-0.035
	4	-2296887.025	10.839	0.425	1.015	-0.015
	5	-2296894.603	18.418	0.425	1.005	-0.005
	6	-2296900.15	23.965	0.423	0.849	0.151
	7	-2296901.588	25.403	0.418	0.835	0.165
	8	-2296900.761	24.575	0.415	0.966	0.034
	9	-2296900.026	23.840	0.414	0.996	0.004
	10	-2296899.849	23.664	0.414	0.993	0.007
	11	-2296900.354	24.169	0.415	0.993	0.007
	12	-2296901.254	25.068	0.417	0.904	0.096
	13	-2296901.16	24.975	0.422	0.800	0.200
	14	-2296897.481	21.296	0.425	0.958	0.042
	15	-2296890.312	14.127	0.426	1.017	-0.017
	16	-2296883.419	7.234	0.425	1.025	-0.025
	17	-2296879.141	2.956	0.424	1.045	-0.045
	18	-2296876.707	0.522	0.244	1.023	-0.023

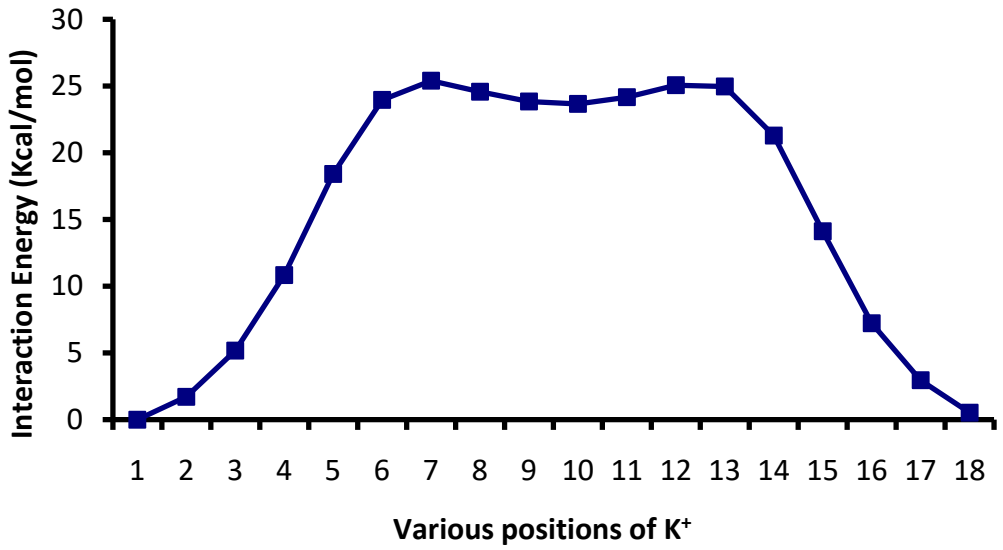

Figure 5.3: Variation of the interaction energy (kcal/mol) of complex system at different positions using B3LYP/6-31++G** (BS1).

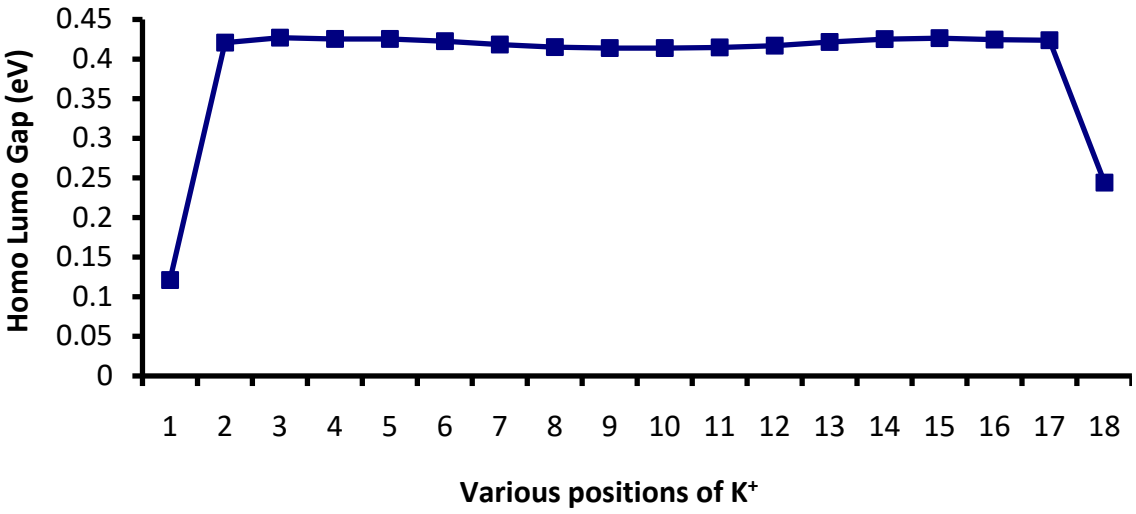

Figure 5.4: Variation of the Homo Lumo gap (eV) of complex system at different positions using B3LYP/6-31++G** (BS1).

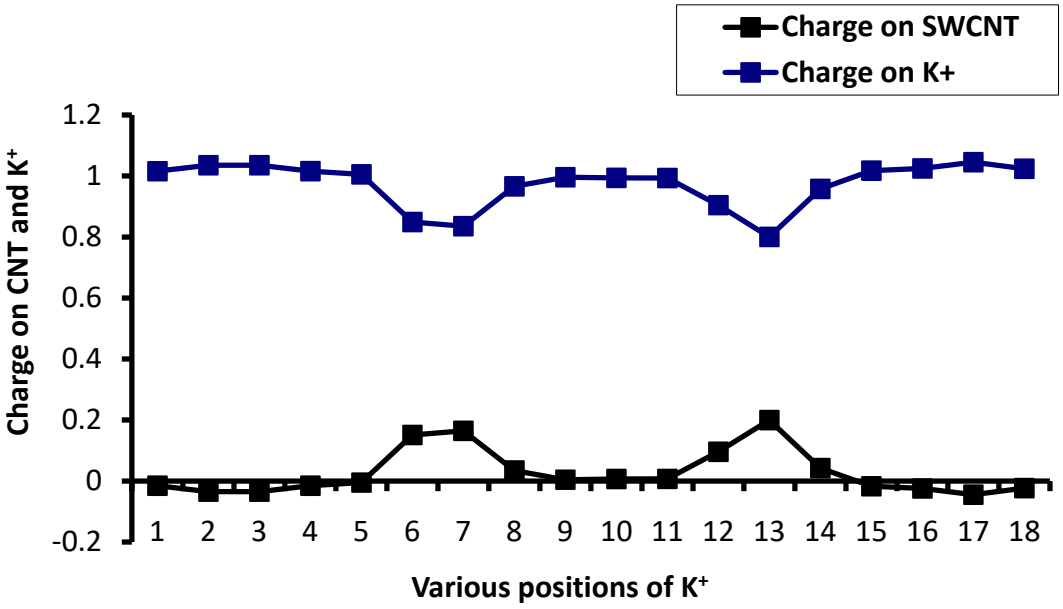

Figure 5.5: Mulliken charge analysis of SWCNT (10,0) and metal ion at different positions using B3LYP/6-31++G** (BS1)

Table 5.2: Calculated Total Energy (kcal/mol), ΔE (kcal/mol), Homo Lumo Gap (eV) and Mulliken charge on alkali metal ion (K^+) and Single Walled Carbon Nanotube (SWCNT) at M06/6-31++G** (BS2).

Metal ion	Various Positions	Total Energy (Kcal/mol)	$\Delta E=E_0-E$ (kcal/mol)	Homo Lumo Gap (eV)	Charge on K^+	Charge on CNT
K^+	1	-2295443.757	0.000	0.504	0.937	0.063
	2	-2295445.353	1.597	0.535	0.966	0.034
	3	-2295448.845	5.088	0.553	1.012	-0.012
	4	-2295455.72	11.963	0.553	1.041	-0.041
	5	-2295464.877	21.120	0.554	1.044	-0.044
	6	-2295471.319	27.562	0.548	0.904	0.096
	7	-2295474.138	30.381	0.538	0.829	0.171
	8	-2295473.127	29.371	0.531	0.903	0.097
	9	-2295472.435	28.679	0.529	0.909	0.091
	10	-2295472.209	28.453	0.528	0.943	0.057
	11	-2295472.923	29.166	0.530	0.897	0.103
	12	-2295473.86	30.103	0.534	0.880	0.120
	13	-2295473.181	29.424	0.544	0.836	0.164
	14	-2295468.155	24.398	0.552	1.013	-0.013
	15	-2295459.512	15.755	0.555	1.049	-0.049
	16	-2295451.343	7.586	0.549	1.026	-0.026
	17	-2295446.617	2.860	0.542	0.984	0.016
	18	-2295444.309	0.552	0.519	0.948	0.052

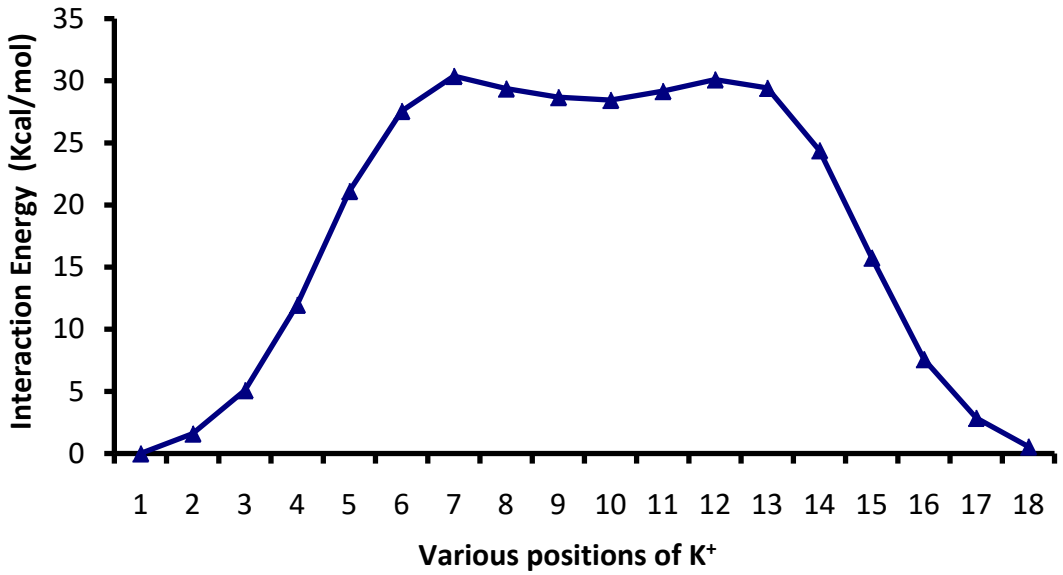

Figure 5.6: Variation of the interaction energy (kcal/mol) of complex system at different positions using M06/6-31++G** (BS2).

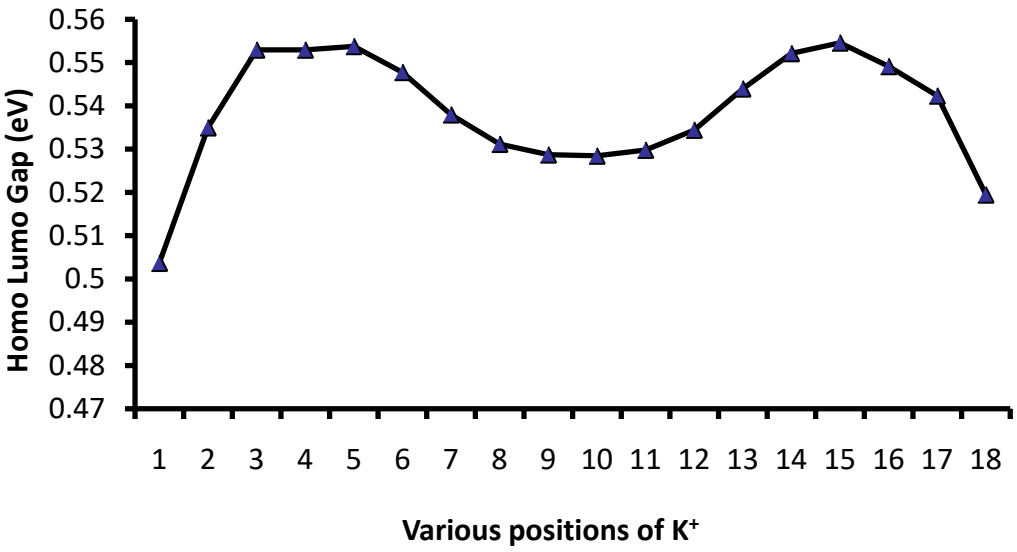

Figure 5.7: Variation of the Homo Lumo gap (eV) of alkali metal ion at different positions using M06/6-31++G** (BS2).

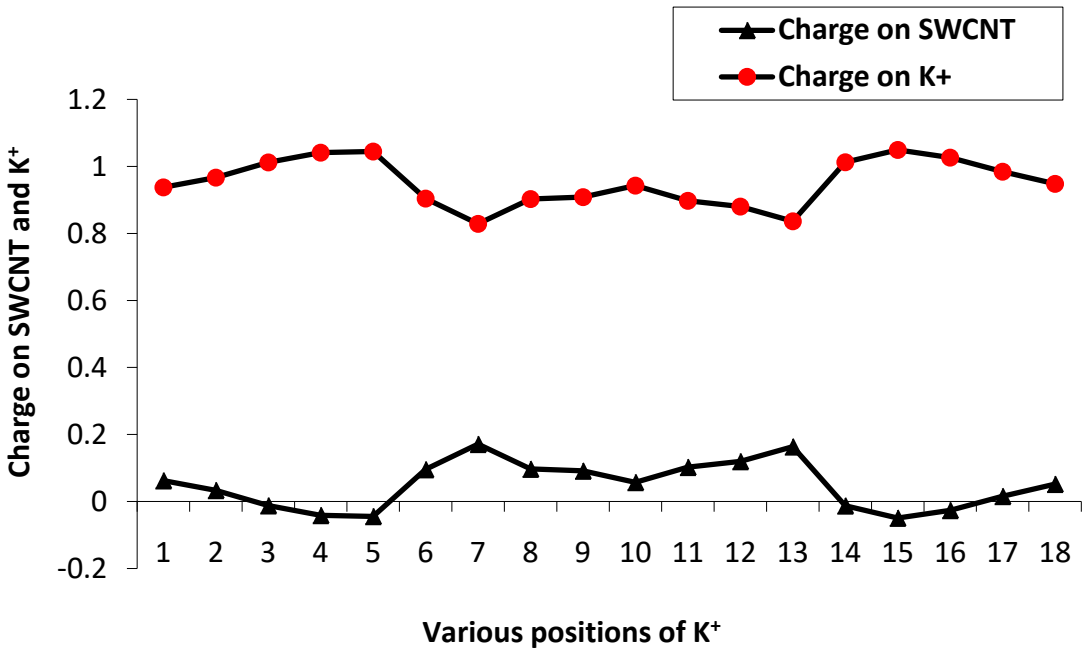

Figure 5.8: Mulliken charge analysis of SWCNT (10,0) and metal ion at different positions using M06/6-31++G** (BS2).

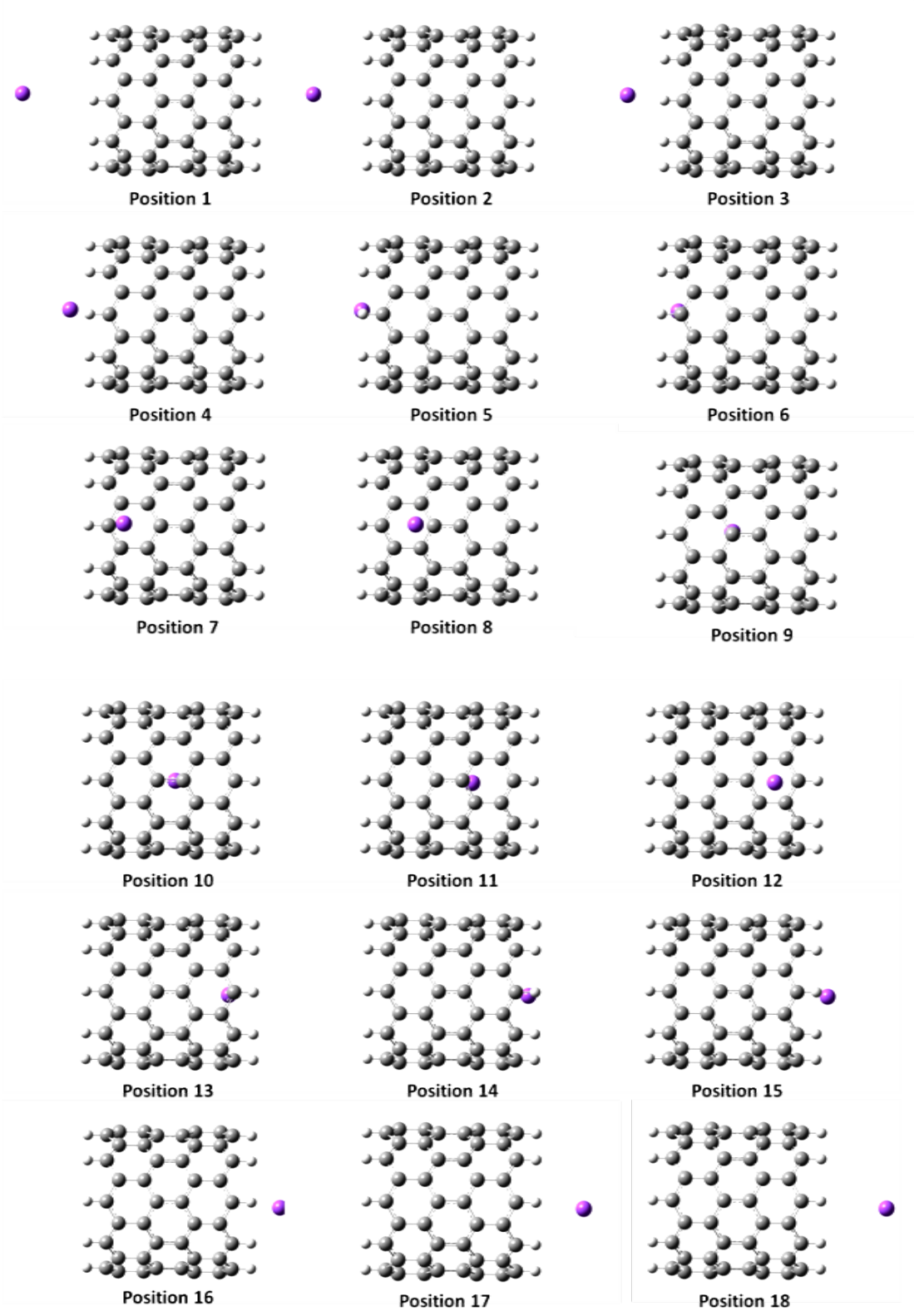

Figure 5.9: Optimized geometries of the complexes formed between the SWCNT(10,0) and alkali metal ion (Na^+) at B3LYP/6-31G* method.

Table 5.3: Calculated Total Energy (kcal/mol), ΔE (kcal/mol), Homo Lumo Gap (eV) and Mulliken charge on alkali metal ion (Na^+) and Single Walled Carbon Nanotube (SWCNT) at B3LYP/6-31++G** (BS1).

Metal ion	Various Positions	Total Energy (Kcal/mol)	$\Delta E=E_0-E$ (kcal/mol)	Homo Lumo Gap (eV)	Charge on Na^+	Charge on CNT
Na^+	1	-2022141.747	0.000	0.264	-1.000	2.000
	2	-2022263.729	121.982	0.369	0.465	0.535
	3	-2022264.086	122.339	0.393	0.498	0.502
	4	-2022266.478	124.731	0.414	0.713	0.287
	5	-2022273.14	131.393	0.425	1.025	-0.025
	6	-2022279.242	137.496	0.423	0.924	0.076
	7	-2022280.52	138.773	0.418	0.788	0.212
	8	-2022279.531	137.785	0.415	0.701	0.299
	9	-2022278.795	137.049	0.414	0.609	0.391
	10	-2022278.538	136.791	0.414	0.593	0.407
	11	-2022279.131	137.384	0.415	0.654	0.346
	12	-2022280.011	138.265	0.417	0.753	0.247
	13	-2022280.203	138.457	0.422	0.857	0.143
	14	-2022276.22	134.474	0.425	0.996	0.004
	15	-2022268.483	126.736	0.426	1.026	-0.026
	16	-2022264.758	123.011	0.403	0.567	0.433
	17	-2022263.726	121.979	0.380	0.465	0.535
	18	-2022263.924	122.178	0.355	0.472	0.528

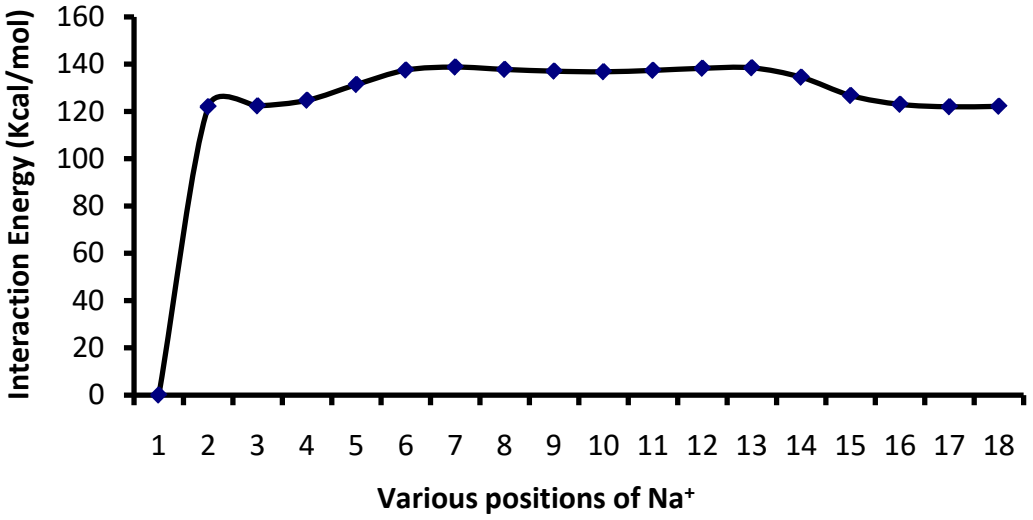

Figure 5.10: Variation of the interaction energy (kcal/mol) of complex system at different positions using B3LYP/6-31++G** (BS1).

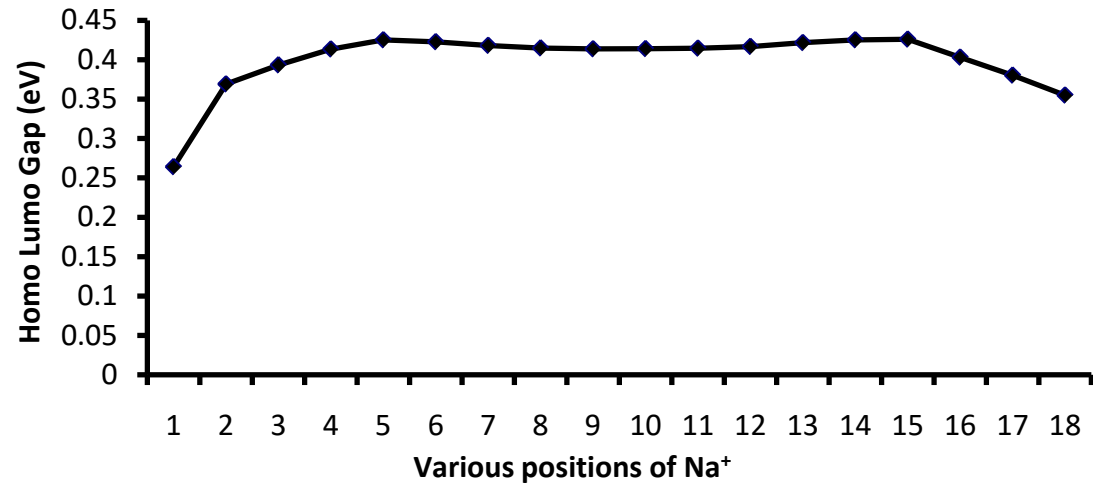

Figure 5.11: Variation of the Homo Lumo gap (eV) of alkali metal ion at different positions using M06/6-31++G** (BS1).

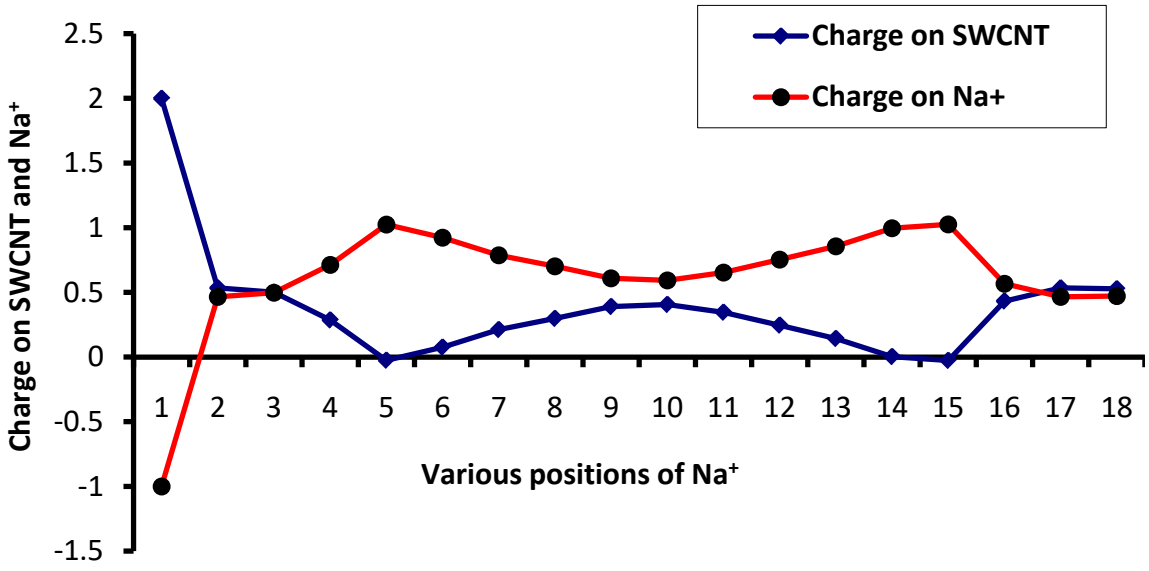

Figure 5.12: Mulliken charge analysis of SWCNT (10,0) and metal ion at different positions using M06/6-31++G** (BS1).

Table 5.4: Calculated Total Energy (kcal/mol), ΔE (kcal/mol), Homo Lumo Gap (eV) and Mulliken charge on alkali metal ion (Na^+) and Single Walled Carbon Nanotube (SWCNT) at M06/6-31++G** (BS2).

Metal ion	Various Positions	Total Energy (Kcal/mol)	ΔE=E0-E (kcal/mol)	Homo Lumo Gap (eV)	Charge on Na+	Charge on CNT
Na^+	1	-2020831.568	0.000	0.489	0.753	0.247
	2	-2020832.679	1.111	0.517	0.776	0.224
	3	-2020835.489	3.921	0.537	0.857	0.143
	4	-2020841.218	9.650	0.551	0.931	0.069
	5	-2020849.235	17.667	0.554	1.026	-0.026
	6	-2020855.999	24.431	0.548	0.914	0.086
	7	-2020857.848	26.280	0.538	0.742	0.258
	8	-2020856.457	24.889	0.531	0.661	0.339
	9	-2020855.649	24.081	0.504	0.571	0.429
	10	-2020855.42	23.852	0.528	0.559	0.441
	11	-2020855.896	24.328	0.530	0.610	0.390
	12	-2020857.22	25.652	0.534	0.704	0.296
	13	-2020857.186	25.618	0.544	0.824	0.176
	14	-2020852.552	20.984	0.552	1.026	-0.026
	15	-2020844.568	13.000	0.555	0.980	0.020
	16	-2020837.735	6.167	0.546	0.880	0.120
	17	-2020833.668	2.100	0.527	0.805	0.195
	18	-2020831.93	0.362	0.503	0.763	0.237

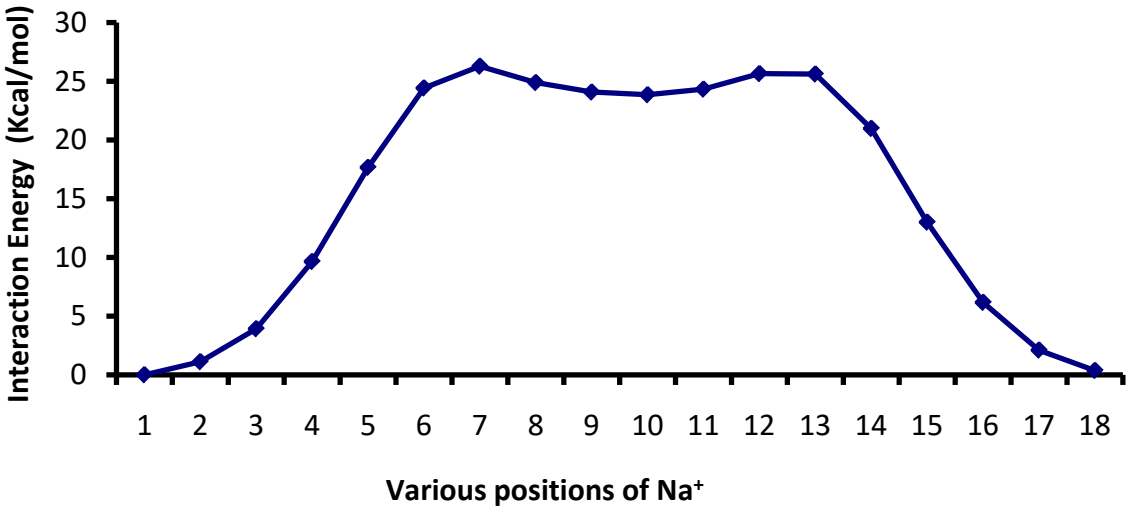

Figure 5.13: Variation of the interaction energy (kcal/mol) of complex system at different positions using M06/6-31++G** (BS2).

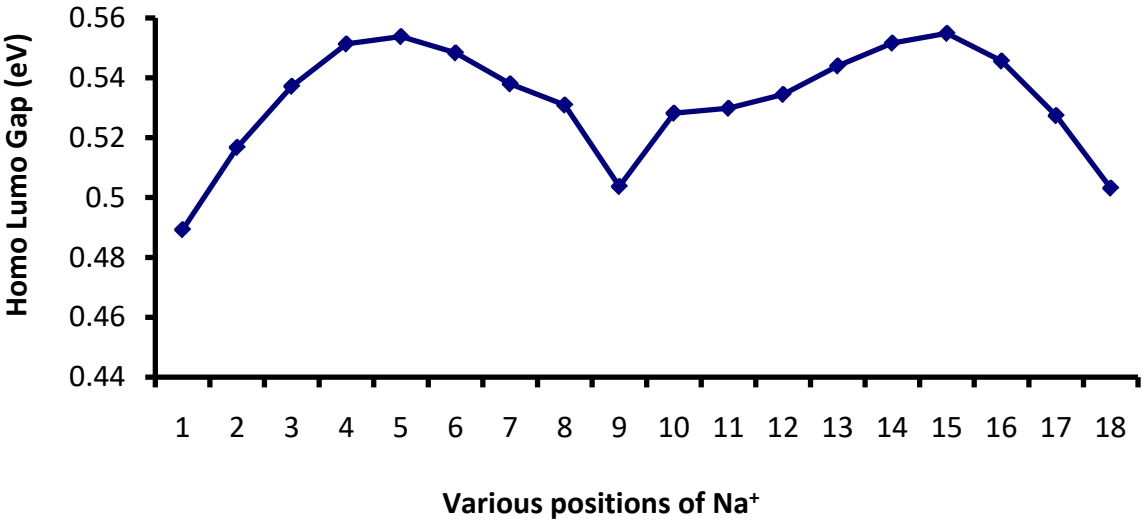

Figure 5.14: Variation of the Homo Lumo gap (eV) of alkali metal ion at different positions using M06/6-31++G** (BS2).

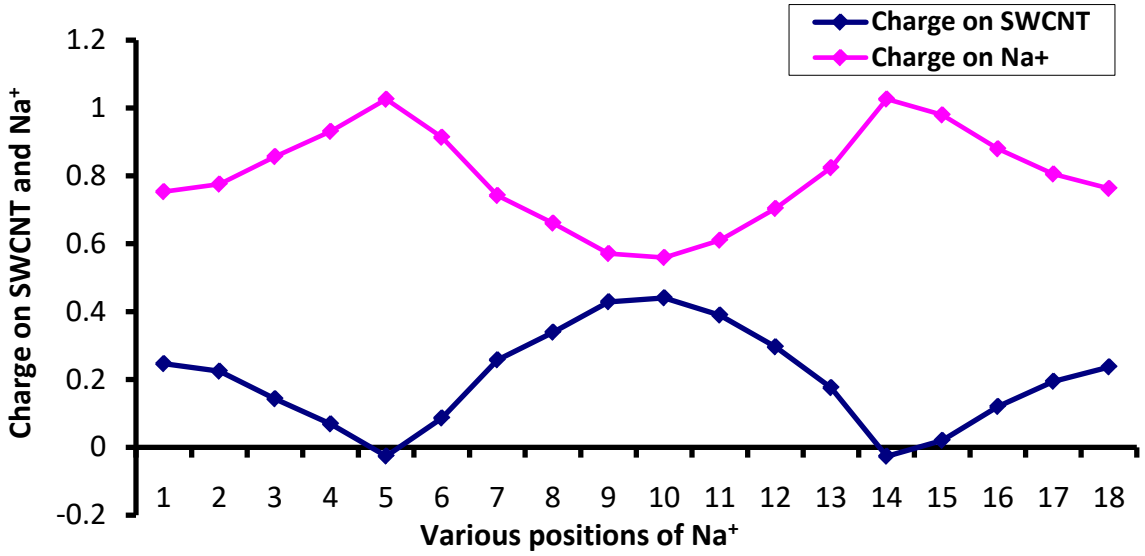

Figure 5.15: Mulliken charge analysis of SWCNT (10,0) and metal ion at different positions using M06/6-31++G** (BS2).

5.7 Conclusion

The present chapter is focussed upon the interaction of alkali metal ion, precisely K^+ and Na^+ ions with the single walled SWCNT. There were a total of 18 different positions at which the metal ions were allowed to pass from one end of the SWCNT to the other. Certain important parameters like interaction energy, homo lumo energy gap, Mulliken charge analysis were observed as the metal ion enters and comes out from the other side of the SWCNT. Significant changes occur in the homo lumo gap which may help to tune the electronic and conducting properties of the SWCNT.

References

[1] S. Iijima, *Nature*, **354**, 56 (1991).

[2] L. V. Radushkevich and V. M. Lukyanovich, *Zurn. Fisic, Chim*., **26**, 88 (1952).

[3] S. J. Tans and A. R. M Verschueren, *Nature*, **393**, 49 (1998).

[4] M. G. Hahm, D. P. Hashim, R. Vajtai, P. M Ajayan, *Carbon Lett*., **12**, 185 (2011).

[5] C. N. R Rao, A. Govindaraj, G. Gundiah, S. R. C Vivekchand, *Chem. Eng. Sci*., **59**, 4665 (2004).

[6] T. W. Ebbesen, H. J. Lezec, H. Hiura, J. W. Bennett, H. F. Ghaemi, *Nature*, **382**, 54 (1996).

[7] M. M. J. Treacy, T. W. Ebbesen, J. M. Gibson, *Nature*, **381**, 678 (1996).

[8] T. E. Chang, L. R. Jensen, A. Kisliuk, R. B. Pipes, R. Pyrz, A. P. Sokolov, *Polymer*, **46**, 439 (2005).

[9] F. L. Jin and S. J. Park, *Carbon Lett*., **14**, 1 (2013).

[10] K. A. Wepasnick, B. A. Smith, J. L. Bitter, D. Howard Fairbrother, *Anal Bioanal Chem*., **396**, 1003 (2010).

[11] B. Chandra, J. Bhattacharjee, M. Purewal, Y. W. Son, Y. Wu, M. Huang, H. Yan, T. F. Heinz, P. Kim, J. B. Neaton, J. Hone, *Nano Lett*., **9**, 1544 (2009).

[12] H. Dai, E. W. Wong, C. M. Lieber, *Science*, **272**, 523 (1996).

[13] H. Choo, Y. Jung, Y. Jeong, H. C. Kim, B. C. Ku, *Carbon Lett*., **13**, 191 (2012).

[14] K. S. Kim and S. J. Park, *Carbon Lett*., **13**, 51 (2012).

[15] J. W. Mintmire, B. I. Dunlap, C. T.White, *Phys Rev Lett*., **68**, 631 (1992).

[16] R. Saito, M. Fujita, G. Dresselhaus, M. S. Dresselhaus , *Appl Phys. Lett*., **60**, 2204 (1992).

[17] M.-F. Yu, O. Lourie, M. J. Dyer, K.Moloni, T. F. Kelly, R. S. Ruoff, *Science*, **287**, 637 (2000).

[18] G. Guanghua, C. Tahir, A.G. William, Nanotechnology, **9**, 184 (1998).

[19] A. S. Mahadevi and G. N. Sastry, *Chem. Rev*., **113**, 2100 (2013).

[20] K. S. Kim, P.Tarakeshwar, J. Y. Lee, *Chem. Rev*., **100**, 4145 (2000).

[21] K. M.-Dethlefs and P. Hobza, *Chem. Rev*., **100**, 143 (2000).

[22] H.-J. Schneider, *Angew. Chem., Int. Ed*., **48**, 3924 (2009).

[23] D. Umadevi, S. Panigrahi, G. N. Sastry, *Acc. Chem. Res*., **47**, 2574 (2014).

[24] R. Zahradnik, *Acc. Chem. Res*., **28**, 306 (1995).

[25] G. A. Jeffrey and W. Saenger, Springer: Berlin Heidelberg, 1991.

[26] Hydrogen Bonding-New Insights; Grabowski, S. J., Ed.; Challenges and Advances in Computational Chemistry and Physics; Leszczynski, J., Ser. Ed.; Springer: New York, 2006.

[27] A. S. Reddy, G. M. Sastry, G. N. Sastry, *Struct. Funct. Bioinf*. 2007, 67, 1179-1184.

[28] L. M. Salonen, M.Ellermann, F. Diederich, *Angew. Chem., Int. Ed*., **50**, 4808 (2011).

[29] H. Schneider, K. M. Vogelhuber, F. Schinle, J. M. Weber, *J. Am. Chem. Soc*., **129**, 13022 (2007).

[30] P. Gamez, T. J. Mooibroek, S. J. Teat, J. Reedijk, *Acc. Chem. Res*., **40**, 435 (2007).

[31] I. Geronimo, N. J. Singh, K. S. Kim, *J. Chem. Theo. Comput*., **7**, 825 (2011).

[32] R. R. Knowles and E. N. Jacobsen, *Proc. Natl. Acad. Sci. U. S. A.*, **107**, 20678 (2010).

[33] H. Xu, S. J. Zuend, M. G. Woll, Y. Tao, E. N. Jacobsen, *Science*, **327**, 986 (2010).

[34] A. S. Reddy and G. N. Sastry, *J. Phys. Chem. A*, **109**, 8893 (2005).

[35] M. Chourasia, G. M. Sastry, G. N. Sastry, *Int. J. Biol. Macromol*., **48**, 540 (2011).

[36] A. S. Reddy, D.Vijay, G. M. Sastry, G. N. Sastry, *J. Phys. Chem. B*, **110**, 2479 (2006).

[37] D. Vijay, H. Zipse, G. N. Sastry, *J. Phys. Chem. B*, **112**, 8863 (2008).

[38] D. Vijay and G. N. Sastry, *Chem. Phys. Lett*., **485**, 235 (2010).

[39] A. S. Mahadevi and G. N. Sastry, *Int. J. Quantum Chem*., **114**, 145 (2014).

[40] E. A. Orabi and G. Lamoureux, *J. Chem. Theor. Comput*., **8**, 182 (2012).

[41] G. P. Rao and C. Lu, F. Su, *Sep. Purif. Technol*., **58**, 224 (2007).

[42] U. D. Priyakumar and G. N. Sastry, *Tetrahedron Lett.*, **44**, 6043 (2003).

[43] U. D. Priyakumar, M. Punnagai, G. P. K. Mohan, G.N. Sastry, *Tetrahedron*, **60**, 3037 (2004).

[44] D. Vijay, H. Sakurai, V. Subramanian, G.N. Sastry, *Phys. Chem. Chem. Phys.*, **14**, 3057 (2012).

[45] N. Li, G. Lee, J. W. Yang, H. Kim, M. S. Yeom, R. H. Scheicher, J. S. Kim, K. S. Kim, *J. Phys. Chem. C*, **117**, 4309 (2013).

[46] J. S. Rao, T. C. Dinadayalane, J. Leszczynski, *J. Phys. Chem. A*, **112**, 12944 (2008).

[47] J. S. Rao, H. Zipse, G. N. Sastry, *J. Phys. Chem. B*, **113**, 7225 (2009).

[48] B. Sharma, J. S. Rao, G.N. Sastry, *J. Phys. Chem. A*, **115**, 1971 (2011).

[49] D. Umadevi, G. N. Sastry, *Chem. Phys. Lett.*, **549** 39 (2012).

[50] Gaussian 09, Revision D.01, M. J. Frisch, G. W. Trucks, H. B. Schlegel, G. E. Scuseria, M. A. Robb, J. R. Cheeseman, G. Scalmani, V. Barone, B. Mennucci, G. A. Petersson, H. Nakatsuji, M. Caricato, X. Li, H. P. Hratchian, A. F. Izmaylov, J. Bloino, G. Zheng, J. L. Sonnenberg, M. Hada, M. Ehara, K. Toyota, R. Fukuda, J. Hasegawa, M. Ishida, T. Nakajima, Y. Honda, O. Kitao, H. Nakai, T. Vreven, J. A. Montgomery, Jr., J. E. Peralta, F. Ogliaro, M. Bearpark, J. J. Heyd, E. Brothers, K. N. Kudin, V. N. Staroverov, T. Keith, R. Kobayashi, J. Normand, K. Raghavachari, A. Rendell, J. C. Burant, S. S. Iyengar, J. Tomasi, M. Cossi, N. Rega, J. M. Millam, M. Klene, J. E. Knox, J. B. Cross, V. Bakken, C. Adamo, J. Jaramillo, R. Gomperts, R. E. Stratmann, O. Yazyev, A. J. Austin, R. Cammi, C. Pomelli, J. W. Ochterski, R. L. Martin, K. Morokuma, V. G. Zakrzewski, G. A. Voth, P. Salvador, J. J. Dannenberg, S. Dapprich, A. D. Daniels, O. Farkas, J. B. Foresman, J. V. Ortiz, J. Cioslowski, and D. J. Fox, Gaussian, Inc., Wallingford CT, 2013.

[51] A. D. Becke, *J. Chem. Phys.*, **98**, 5648 (1993).

[52] C. Lee, W. Yang, R. G. Parr, *Phys. Rev. B*, **37**, 785 (1988).

Chapter 6

General conclusion and future prospects

CHAPTER 6

GENERAL CONCLUSION AND FUTURE PROSPECTS

The work done in the present thesis illustrates some striking focal points:

A. Technological advancements and recent developments in theory have enabled evolution of highly accurate, efficient and inexpensive methods applicable for designing novel sensors.

B. The extensively tested and highly benchmarked methods used by our research group were proven to be in congruence with experimental as well as theoretical studies accomplished in the past which proved be useful to study the interaction of graphene systems with nucleic bases presented in this thesis.

C. The studies present in this thesis work are expected to bridge the computational and experimental work being carried out with graphene and boron nitride graphene. Also they are expected to meet challenges of targeted drug delivery.

D. The focus of the study is to confirm the importance of DNA sequencing and specificity at molecular level. Thus, our study attempts to provide useful insights on the binding of nucleic base molecules to various carbon nanostructures.

E. Doping is an efficient way to tune the electronic properties of the graphene model system and its importance is highlighted in the present thesis.

Thus, the molecular modeling studies performed in the present thesis can be fruitful in designing novel sensors, to understand DNA sequencing and to aid targeted drug delivery.

List of publications

1. Interaction of amino acids with single walled carbon nanotube: a quantum mechanical study
   Dharmveer Singh, **Asheesh Kumar**, Devesh Kumar
   International journal of chemical and pharmaceutical analysis, **3**, 2, 1-7 (2016).

2. Assessing therapeutic potential of molecules: molecular property diagnostic suite for tuberculosis (MPDSTB)
   Anamika Singh Gaur, Anshu Bhardwaj, Arun Sharma, Lijo John, M Ram Vivek, Neha Tripathi, Prasad V Bharatam, Rakesh Kumar, Sridhara Janardhan, Abhaysinh Mori, Anirban Banerji, Andrew M Lynn, Anmol J Hemrom, Anurag Passi, Aparna Singh, **Asheesh Kumar**, Charuvaka Muvva, Chinmai Madhuri, Chinmayee Choudhury, D Arun Kumar, Deepak Pandit, Deepak R. Bharti, Devesh Kumar, Er Azhagiya Singam, Gajendra PS Raghava, Hari Sailaja, Harish Jangra, Kaamini Raithatha, Karunakar Tanneeru, Kumardeep Chaudhary, M Karthikeyan, M Prasanthi, Nandan Kumar, N Yedukondalu, Neeraj K Rajput, P Sri Saranya, Pankaj Narang, Prasun Dutta, R Venkata Krishnan, Reetu Sharma, R Srinithi, Ruchi Mishra, S Hemasri, Sandeep Singh, Subramanian Venkatesan, Suresh Kumar, UCA Jaleel, Vijay Khedkar, Yogesh Joshi and G Narahari Sastry.
   J. Chem. Sci. **129**, **5**, 515–531 (2017).

3. A review on QM/MM studies of nucleic bases interactions with graphene and carbon nanotubes
   Asheesh Kumar, Ruchi Mishra, Deep Kumar, Devesh Kumar
   International Journal of Science, Technology and Society, **3**, *2 (2017) 01-10 (2017)*

4. Adsorption of small gas molecules on pure and Al-doped graphene sheet: a quantum mechanical study
   Dharmveer Singh, **Asheesh Kumar** and Devesh Kumar**.**
   Bull. Mater. Sci., DOI 10.1007/s12034-017-1478-x (2017).

5. A review on theoretical studies of various types of Drug-DNA Interaction
   Ruchi Mishra, **Asheesh Kumar**, Ramesh Chandra, Devesh Kumar
   International Journal of Science, Technology and Society, **4**, *2 (2017) : 00-00 (2017)*

6. Structural Stability and Electronic Properties of $(Ga_nN_n)_m$ Micro Cluster by Using Ab-Initio and Tight-Binding Study
   Deep Kumar, **Asheesh Kumar**, Jitendra Kumar, and Devesh Kumar
   Advanced Science, Engineering and Medicine, **10**, 1-5, (2018).

7. Quantum Mechanical Study of Nucleic Acid Interaction with Carbon Nanotubes in Interior and at Exterior Positions
   Asheesh Kumar, Dharmveer Singh, Deep Kumar, Devesh Kumar
   Advanced Science Letters, **24**, *2 , 802-806(5) (2018)*

REVIEW ARTICLE

International Journal of Science, Technology and Society
Vol 3, No. 2 (2017) : 01-10

A review on QM/MM studies of nucleic bases interactions with graphene and carbon nanotubes

Asheesh Kumar, Ruchi Mishra, Deep Kumar, Devesh Kumar*

Department of Physics, School of Physical and Decision Sciences, Babasaheb Bhimrao Ambedkar University, Vidya Vihar, Rae Bareilly Road, Lucknow-226 025, India.

Publication Info

Article history:
Received : 10.12.2017
Accepted : 22.12.2017
DOI: https://doi.org/10.18091/ijsts.v3i02.11404

Key words:
Nucleic Acid (NA), Carbon nanotube (CNT), Graphene, Binding Energy, Initial Configurations (IC), QM (Quantum Mechanics) / MM (Molecular Mechanics).

Corresponding author:
Devesh Kumar

Email:
*dkclcre@yahoo.com

ABSTRACT

Nucleic bases interaction with carbonaceous materials finds significant attention due to their application in various fields such as DNA sequencing, DNA sensing and drug delivery. Nucleic bases, building blocks of nucleic acids interact with carbon nanotube and contribute significantly to the stability of the nucleic bases, carbon nanotube hybrids and their properties. In the present work, a thorough review of previous studies on the binding of nucleic bases with graphene and CNT is presented, with a focus on the simulation works that attempted to evaluate the structure and strength of binding. Dissimilitude among these works is noticed and factors that might contribute to such discrepancies are discussed in detail.

INTRODUCTION

Graphene and carbon-nanotubes have different applications for many reasons, but the differences can be ultimately attributed to the difference between one-dimensional materials and two dimensional materials. For example, a single walled carbon nanotube can be regarded as a single crystal with a high length–diameter ratio. However, the current synthesis and assembly technology cannot prepare the carbon nanotube crystals on a macroscopic scale, which limits their applications. While, graphene may be considered as a two-dimensional crystal structure, and its strength, conductivity and thermal conductivity are seen to be the best in two-dimensional crystal materials. It has a broad range of applications because of its ability to have a large area of continuous growth.

Graphene, is a planar form of carbon atoms designed in a two-dimensional hexagonal lattice fashion. It has emerged as the most dominating allotropes of carbon during the last few years. Its extended honeycomb network is the basic building block of other important allotropes such as 3D graphite formed by the stacking of several layers of graphene; 1D nanotube, obtained by rolling the graphene and the 0D fullerene prepared by wrapped graphenes (J. Allen Matthew *et al.,* 2010). Graphene is being used in the designing of new nanomaterials for energy storage devices, fuel cells and biosensors owing to its high stability, elasticity and electromechanical modulation (Stoller Meryl D *et al.*, 2008, Si Yongchao and T Samulski Edward, 2008, Pumera Martin *et al.,* 2010). Also, graphene exhibits extraordinary electronic properties in comparison to many of the conventional materials; the highly conductive graphene becomes an insulator after hydrogenation. This hydrogenation of graphene is highly reversible; the intrinsic conductivity as well as the structure of graphene can be restored on annealing (Chen Liang *et al., 2007;* Denis Pablo A *et al.,* 2009; Rubes Miroslav *et al.,* 2009). Graphene is also an important material in nanoscale electronics due to its compatibility with industry standard lithographic processing. The electron mobilities is up to 150 times greater than Si, and the thermal conductivity is approximately twice that of diamond (Ritter Kyle A *et al.,* 2009). Thus one can say that graphene has revolutionalized the technology.

Graphene sensors have emerged as another area of recent interest. The chemical and physical properties of graphene make it a promising candidate that can be used as a sensor to detect different gases such as H_2, NO_2, and NH_3. Schedin *et* al., in their experimental results, illustrated that graphene based sensors allow the sensitivity levels such that the adsorption of individual gas molecules could be detected accurately (Rao, C. N. R. *et al.,* 2009; Schedin F *et al.,* 2007). Graphene-polyaniline nanocomposite is found to be a good sensor for H_2 gas while nitrogen doped graphene find its application in electrochemical biosensing (Al-Mashat Laith *et al.,* 2010). It is also shown that, through functionalization, properties of graphene can be modified. The functionalization of graphene with hydrogen, oxygen, or other chemical groups is of prime importance as a way to engineer the different properties of graphene. A recent study reveals that with controlled epoxide functionalization, graphene can be used as a starting material for diverse chemical functionalization by chemical modification of the epoxide group. The functionalization of graphene and single-walled carbon nanotubes with individual 3d transition metal atoms were also modeled using density functional theory calculations.(Lee Geunsik *et al.,* 2009; Hubert Valencia *et al.,* 2010; Ghaderi Nahid *et al.,* 2010;Park Sungjin *et al.,*2008; Wang Donghai *et al.,2010;* Quintana Mildred *et al.*, 2010; Tachikawa Hirotoet *al.,* 2010; Al-Aqtash Nabil *et al.,* 2009).

The capability to detect single bio-molecules with high accuracy and efficiency is of prime importance in many areas of environmental science, biology, and chemistry (Lim Sung H. *et al.,* 2009; Bano Fouzia *et al.,* 2009; Zwolak Michael *et al.,* 2008; Fredlake P. Christopher *et al.,* 2006; Jonkheijm Pascal *et al.,* 2008; Patolsky Fernando *et al.,* 2006; Vidic Jasmina *et al.,* 2006). Efficient bio-sensors are expected to contribute to the improvement of medicine and medical treatment (Zwolak Michael, 2008). It is, quite uncertain whether traditional chemical techniques can be simultaneously fast and inexpensive which is another very important aspect that needs to be taken care of (Fredlake P. Christopher *et al.,* 2006). Nano-materials, due to their extreme sensitivity of the electron-transport properties in confined materials to external perturbations, form an excellent technological platform for single-molecule recognition (Zhang Guangyu *et al.,* 2006; Meyer Jannik C *et al.,* 2007; Shapir Errez *et al.,* 2008; N Kang *et al.,* 2007). Recently, graphene nano-ribbon (GNR) has emerged as a suitable candidate for making sensors for single small molecules, such as H_2, H_2O, and NO. This concept is based on measuring a variation in the source-drain current of a GNR based field-effect transistor originating from the covalent bond formed between the molecule to be detected and a defect (or an edge) of GNR. However, few reports exist on the use of GNRs as bio-sensors. One of the main reasons is that the biomolecules do not usually bind GNR via covalent bonds as a result of which the electrical perturbation induced by a biomolecule on a GNR is too weak to be detected. However the GNR is proposed to be used for the DNA sequence via π-π stacking in many reports.

Relevance of DNA bases and graphene/carbon nanotube interaction

The interaction of the biomolecules such as nucleic bases on the surface of GNR and CNT has attracted many researchers. In particular, the DNA-CNT interaction has cast its spell in the research community due to its application in various fields such as DNA sensing, DNA sequencing, and drug delivery (Zhao Xiongce 2011; Paul Ambarish 2010; Liu Zhuang *et al.,* 2011; Yarotski Dzmitry A *et al.,* 2009). It has also been found that the determination of a patient's DNA sequence can even reveal his risk of falling ill with particular diseases and it also helps to design "personalized medicine", and it is therefore the DNA sequencing that appears to be one of the most potential applications for the carbon nanostructures (Sanchez Jimenez Gerardo *et al.,* 2001; Nelson Tammie *et al.,* 2010; Prasongkit Jariyanee *et al.,* 2011). Sensors for amplified detection methods based on CNT-biomolecule composites is an area of recent interest, and such sensors can be efficiently used to detect various carbon nanostructures as well as different biomaterials such as DNA, protein, and so on (Barone Paul W *et al.*, 2005). Also, DNA-functionalized carbon nanotubes form the basis for not only a new class of chemical sensors but also for the molecular electronic devices. An ultrasensitive graphene-embedded nano channel device which effectively controls the motion of nucleobases via π-π interaction was also reported (Min Seung Kyu *et al.,* 2011).Weizmann *et al.,* 2011, recently reported that DNA-CNT nanowire networks can be used for DNA detection and Zheng Y*et al.,* 2009, constructed a carbon nanotube-based DNA biosensor for sensing the phenolic pollutants. Beside biomedical applications, comprehending the DNA-CNT interaction can also be used in the separation of carbon nanotubes as it has been shown that single-stranded DNA can be effectively used for the dispersion and separation of single-walled carbon nanotubes (Zheng M *et al.,* 2003). Some of the important conclusions can also be drawn from the studies (Wang X et al., (2011); Lu G et al.,(2009) ; Li J et al.,(2003)). Many research groups have focused on

determining the DNA-CNT interaction and tried to explore the strength of binding of different nucleosides, nucleobases, and nucleobases pairs on the carbon nanotubes and graphene, in both experimental and computational studies (Chen Robert J. *et al.,* 2003; Stepanian S.G. *et al.,* 2008; Shtogun Yaroslav V. *et al.,* 2007; Wang Hongming *et al.,* 2009; Wang Po *et al.,* 2011). The different binding energy orders for different studies are found in many experimental studies and it is understood that this may be due to the different experimental conditions applied. For most cases, in computational studies, the order is G > A > T > C > U, and in some cases, were found to be in the order as G~A~T~C > U. There are a number of theoretical and experimental studies on the nucleobases interaction with carbon nanotube and graphene surfaces as shown below:

Table 1. BE (kJ/mol) of nucleobases with SWCNT and graphene in theoretical and experimental studies.

Nucleic bases interaction with different Carbon nanomaterials			
Type	**Order**	**Method**	**Ref.**
SWCNT	T A ~C	Exp.	100
CNT(5,0)	G A T C U	Comp.	23
CNT(7,0)	G A ~T ~C U	Comp.	65
CNT (5,5), CNT(10,0)	G A T C	Comp.	86
GNR	G A ~T ~C U	Comp.	22

The binding energy of all the considered complexes illustrates that the binding energy increases as the curvature of SWCNT (single walled carbon nanotube) decreases and reaches the maximum for graphene. In general, the nucleobases tend to have π-π stacking (Zheng Y *et al.,* 2009) type of interaction with the carbon nanostructures. Hence, as the curvature of SWCNT decreases, there will be more efficient stacking between the carbon nanotube and the nucleobases surface, resulting in an increase in the binding energy of the complexes. The effect of size and curvature generally plays an important role in the non-bonded interactions (Zheng Ming *et al.,* 2003; Chen Robert J. *et al.,* 2003).

METHODS

First-Principles Methodology

In the QM methods, mostly DFT has been used in the computational chemistry and quantum physics due to their relatively low computational cost compared to high level *ab initio* methods and high accuracy in comparison to the semi- empirical methods.

The dispersion forces in the dispersion interaction are the most important interactions in molecular systems that are not addressed well in several DFT approaches. Efforts were made by the several research groups (Rutledge *et al.*, 2009; Rutledge and Wetmore, 2010; Johnson *et al.*, 2004, 2009; Dion *et al.*, 2004a; Zhao and Truhlar, 2005, 2011; Meijer and Sprik, 1996; Tkatchenko and Scheffler, 2009; Grimme, 2004, 2006; Grimme *et al.*, 2010, etc) to precisely incorporate dispersion in the correlation term of DFT. There were several studies of interaction of nucleic bases with CNT or graphene which however did not consider the dispersion interaction into account. Some early works based on LDA scheme of DFT, also lack dispersion correction. However the recent studies adopted either classical FF (force field) or dispersion corrected DFTs to consider the dispersion factor. It is believed that the π-π stacking plays a key role in the binding of nucleobase to graphene or CNT, dispersion therefore can play a significant role in determining the binding structure and BE (Binding Energy). So, one can precisely say that different approaches lead to different results. Therefore the past studies can be broadly classified into two categories: those performed with methods that consider dispersion, and those which do not consider dispersion-corrected methods.

Among the QM studies, there are also various methods with different levels of complexity and accuracy, including *ab initio* methods (HF, MP2 and CCSD (T)), DFT and semi-empirical methods. HF, originally named SCF method, is the first *ab initio* method and forms the basis of post- HF methods. Despite of having the correct description for the exchange energy, HF does not address the electron correlation precisely. Post-HF methods include MP2 (Møller and Plesset, 1934; Head- Gordon *et al.*, 1988), CI and CCSD (T) that were proposed to properly describe the correlation energy. These *ab initio* methods are usually employed for very small atomic systems due to their high computational cost. Semi-empirical QM methods are based on *ab initio* methods but include empirical parameters to speed up the calculations, examples include AM1 (Dewar *et al.*, 1985), PM3 (Stewart, 1989a,b, 1991) and PM6 (Stewart, 2007). In computational quantum chemistry and physics, DFT has been widely used, due to its relatively low computational cost compared with high level *ab initio* methods and high accuracy compared with semi-empirical methods. In 1964, Kohn and Hohenberg published the first paper on DFT in which they substituted the many electron wavefunction with the electron density and reduced the number of

variables. One year later, Kohn and Sham in 1965 improved the Hohenberg and Kohn's theory by introducing effective potential that included external potential, exchange and correlation interactions.

Methods lacking the dispersion correction

Gowtham *et al*., studied the adsorption of nucleobases (A, C, G, T and U) on graphene using MP2 and LDA (Gowtham *et al.*, 2007). Nucleobases in their work were attached to a methyl group. Plane wave basis set was used in the LDA calculations (Supercell approach), while in the MP2 calculations, 6-311++G(d,p) basis set was used with the graphene containing 28 carbon atoms terminated by hydrogen atoms at the edges. For each configuration of the nucleobase on the graphene, they initially performed a force relaxation to determine the preferred orientation and kept the bases at optimum separation distance. This was followed by a scan of the potential energy surface (PES) where the nucleobases were kept parallel to the graphene surface at a fixed distance. For each configuration, single point energy calculations were also performed and the minimum potential energy was determined. This configuration was subjected to a further optimization step in which all atoms were free to move and the final optimized structure was identified. Thereafter, BE was then calculated for the optimized structure using both MP2 and LDA. Table 2 shows the values of the obtained BEs. Among these two, MP2 predicted BE values that were almost doubled the LDA values. The BEs with respect to the different nucleobases almost remained in the same order: it was G>A=T=C>U using LDA and G>A>T>C>U using MP2. The final optimized nucleobases were found to be parallel to the graphene sheet with the separation distance being 3.5 Å.

Table 2. BE (kJ/mol) between nucleobases and graphene [Gowtham *et al.*, (2007)].

Nucleobase	LDA	MP2
G	58.86	103.24
A	47.28	90.70
T	47.28	80.08
C	47.28	77.19
U	42.25	71.40

In a later work, Gowtham *et al.,* also studied the adsorption of the same nucleobases on a (5,0) CNT (Gowtham *et al.,* 2008), using the same approach except that the BE calculation was only done with LDA only, and not with MP2. The order of the BE was found to be the same, i.e., G>A>T>C>U with the values being 47.28, 37.63, 32.81, 27.98 and 27.02 kJ/mol, respectively. Their results confirmed that the BEs for CNT were much smaller than those for graphene, that was attributed to the larger curvature of the CNT and resulting smaller area of contact.

Meng *et al.,* (Meng *et al.*, 2007a) first optimized the structures using CHARMM FF which includes an empirical description of dispersion interaction, but this dispersion was neglected again during the re-optimization step using LDA.

Meng *et al*., used a different approach (time-dependent LDA method) to study the binding between DNA nucleosides and a CNT (10,0) (Meng *et al.*, 2007b). From these simulations, the optical absorbance spectrum for DNA nucleosides were obtained, which were used to determine the preferred orientation of the nucleosides on the CNT. Optimized binding structures were also obtained using MM (CHARMM) calculations, and were found in good agreement between the MM results and LDA results. According to MM calculations, the order of the BE for the most stable structures was G>A>T>C with the BE values of 82.01, 78.15, 74.29 and 67.54 kJ/mol, respectively.

The dependence of BE on CNT chirality was studied by Wang and Ceulemans (Wang *et al.*, 2009) using LDA. They considered two connected adenosine-monophosphates with the phosphate groups terminated by H atoms. The resulting molecule was neutral and was taken to interact with different CNTs, including five (m,0) zigzag tubes with m = 7,8,9,10,17 and four (n,n) armchair tubes with n= 4,5,6,7. Periodic boundary condition using supercell approach and the linear combination of numerical atomic orbitals (LCAO) basis set with double-zeta polarizations were used.

In another work, Wang considered all four DNA nucleobases interacting with two types of CNTs: (5,5) and (10,0) (Wang, 2008). Same as his first work (Wang *et al.*, 2007), for each type of CNT, only a small part (C24H12) was made to interact with the nucleobases. Both DFT and MP2 methods were adopted in the simulations. The geometry optimization was carried out at MPWB1K/cc-pVDZ level where carbon and hydrogen atoms were kept frozen in the C24H12 fragments. The optimized structures were then subjected to a single point energy calculation at MP2/6-311++G(d,p) level. The BSSE-corrected BE for the C(5,5) CNT hybrid in vacuum was 46.46 kJ/mol which is quite different from Wang's former study (Wang *et al.*, 2007) in which the BE for the same system was determined to be 32.76 kJ/mol. The order of the BE between nucleobase and

CNT in the gas phase was found to be G>A>T>C for both CNTs. This is in agreement with the DFT studies of Gowtham *et al.,* on the interaction of nucleobases with graphene and (5,0) CNT (Gowtham *et al.*, 2007, 2008), and also with the MM results of Meng *et al.*, for the interaction of nucleosides with a (10,0) CNT.

The simulation works reviewed above are all based on methods that lack correction for dispersion interaction. With the pace of time and advancement in computational chemistry, more accurate dispersion corrected methods have been introduced.

Methods with dispersion-corrected methods

Recent works using dispersion-corrected DFT also gave rise to different results, possibly due to the difference in ways of incorporating dispersion interaction in these methods. The choice of basis sets can affect the BE evaluation, even with the same method (Shukla *et al.*, 2009). In addition, it is also found that BSSE can be large and has to be taken into account (Tournus *et al.*, 2005). Performance of simulation methods and basis set are still being widely evaluated in the computational chemistry community.

Though a large number of dispersion-corrected methods exist in literature however benchmarking has been performed by some of them (Johnson *et al.*, 2004; Dion *et al.*, 2004a; Hohenstein *et al*., 2008; Zhao *et al.*, 2008; Johnson *et al.*, 2009; Rutledge *et al.*, 2010; Zhao *et al.*, 2011; Grimme, 2011; Ehrlich *et al.*, 2013). Among these methods, Minnesota density functional developed by Truhlar's group, e.g., M05, M05-2X, M06, M06-L, M06-2X and M06-HF, are based on meta-GGA approximations (Zhao *et al.*, 2005, 2006; Zhao *et al.*, 2008, 2006 a,b). The exchange-correlation term in all Minnesota functionals depend on kinetic energy.

In the M06 family, M06-2X has shown good performance in several studies where vdW interaction played an important role (Rutledge *et al.*, 2010). Panigrahi *et al.*, employed dispersion-corrected DFT using wB97XD functional to study nucleobase-graphene binding (Panigrahi *et al.*, 2012). Nucleobases in their work were attached to a methyl group, similar to the study by Gowtham *et al.,* (Gowtham *et al.*, 2007). Each nucleobase was placed above a square graphene sheet with eight carbon rings in each direction and H atoms at the edges. The IC (initial configuration) of the base plane was parallel to the graphene surface with a separation distance of 4 Å, which was subjected to a full optimization at wB97XD/6-31G(d,p) level. The separation distance in the optimized structures was found to be around 3.5 Å. BSSE corrected BE was calculated at the same level and found to be 94.16, 85.03, 79.30, 77.04 and 68.41 kJ/mol respectively for G, A, C, T and U, i.e., G>A>C>T>U. Such order is identical to what was observed by Gowtham *et al.*, (Gowtham *et al.*, 2007) on the same system using LDA optimization accompanied by MP2 energy calculation. The BE values are also close to the MP2 results (Gowtham *et al.*, 2007) but almost double to those obtained using LDA alone.

Swathi and Chandra Shekar (with wB97XD functional) examined physisorption of nucleobases on coronene (C24H12) as a model of graphene (Chandra Shekar *et al.*, 2014). Different ICs were considered while the separation distance was considered to 3Å in all ICs. Geometry optimization was carried out at wB97XD/6-31G(d,p) level followed by a single point energy calculation at wB97XD/6-311+G (d,p). The order of the BSSE corrected BEs was determined to be G>T>A>C>U with the values of 75.73, 66.53, 65.27, 64.43 and 56.48 kJ/mol, respectively. BE values in this work were less than the ones obtained by Panigrahi *et al*., (Panigrahi *et al.*, 2012), which may be attributed to the smaller size of graphene in this study compared to that in Panigrahi *et al*. The separation distance in the optimized structures was found to be 3.24, 3.25, 3.30, 3.22 and 3.20 Å, respectively for G, T, A, C and U. These separation distances were also smaller than the ones obtained by Panigrahi *et al.,* (Panigrahi *et al.*, 2012).

Antony and Grimme studied the interaction of nucleobases with graphene in which four different sizes of graphene were considered, with 24 (C24H12), 54 (C54H18), 96 (C96H24) and 150 (C150H30) carbon atoms respectively (Antony *et al.*, 2010). Hybrids were fully optimized at B97-D/TZV(d,p) level. A three dimensional PES scan was also performed for the interaction of nucleobases with the C96H24 fragment, and no other minima was found except the one obtained from optimization. Nucleobases were attached to a methyl group and PBC was applied in their study. Full geometry optimization for the hybrid structures was also performed but no detailed explanations were given for the ICs.

Vovusha *et al.,* studied the interaction of nucleobases with graphene using M05-2X and M06-2X functional. Vovusha *et al.*, 2013 in their study of graphene model included 54 carbons with 18 hydrogen atoms capping the edge carbons. Geometry optimizations were all performed at M05-2X/6-31G(d) level and BEs were evaluated using both M05-2X and M06-2X methods with 6-31+G(d,p) and 6311++G(d,p) basis sets. The separation distance between nucleobases and graphene in the optimized structures was determined to be 3.2-3.5 Å that is close to previously reported results. Results obtained using M06-2X were considerably

larger than the ones obtained using M05-2X method. The order of the BE using M05- 2X was determined to be G>C=T>A>U and G>C>T>A>U respectively with 6-31+G(d,p) and 6-311++G(d,p) basis sets. When M06-2X was used for the BE calculation, the order was changed to G>T>A>C>U and G>T>C>A>U respectively using 6-31+G(d,p) and 6-311++G(d,p) basis sets. This demonstrates the great effect of method and basis set on the value and order of the BE. In most of the previous results on the BE between nucleobases and graphene, BE of A was only second to G, while this was not obtained by Vovusha *et al.*

Studies on semi-empirical and force-field methods

The studies of the binding of nucleobases with graphene or CNT at lower level methods involve classical MM or semi-empirical QM approaches. AM1 (Dewar *et al.*, 1985), PM3 (Stewart, 1989 a,b, 1991) and PM6 (Stewart, 2007) are the widely used semi-empirical methods. Non-bonded interactions including electrostatic and vdW forces that are implemented in classical FFs such as Amber (Cornell *et al.*, 1995) and CHARMM (MacKerel Jr. *et al.*, 1998). It has been shown that Amber FF can even be more accurate than some of the semi-empirical QM methods when evaluating the BE for biological systems (Rutledge *et al.*, 2009; Rutledge *et al.*, 2010).

Optimization process also plays a key role in BE calculation for these weakly bound systems where PES is expected to be near local minima. Direct optimization may lead system to nearby local minima, but not near the global minima. So, optimization is very sensitive to the IC chosen. The different IC result in different BE values and can even change the order of BE for different nucleobases (NB).

Umadevi *et al.*, brought to light the dependence of the curvature by considering the binding of nucleobases with graphene and a series of armchair (n,n) CNTs where n=3, 4 and 5 (Umadevi *et al.*, 2011). The graphene and CNTs were made using the Gaussian software package with H atoms at the edges was used to saturate the dangling bonds at the boundaries. Each system was optimized using ONIOM method at the (M06-2X/6-31G(d):AM1) level. Atoms of the nucleobases and the "reacting atoms" of CNTs were modeled as the high layer using M06-2X/6-31G(d). The atoms in CNT were considered as the low layer using semi-empirical AM1. Single point energy calculations were performed for the optimized structures using the dispersion-corrected B3LYP method (B3LYP-D) with the 6-31G(d) basis set. The BE was found to be graphene>CNT(5,5)> CNT(4,4)> CNT(3,3) for all nucleobases except T, for which the order was graphene>CNT(5,5)> CNT(3,3)>CNT(4,4). The BSSE-corrected BE was 30-51 kJ/mol for CNTs and 50-73 kJ/mol for graphene. The order of the BE with respect to different nucleobases was determined to be G>T>A>C>U for the CNTs and G>A>T>C>U for the graphene. In another work, using the M06-2X/6-311G**, Umadevi *et al*., found the order of binding for nucleobases with graphane in the order G > A > C > T > U (Umadevi *et al.*, 2015).

DISCUSSION AND FUTURE PERSPECTIVES

This paper presents a comprehensive review of past computational work, where three categories of methods have been used: (1) first-principles studies based on methods lacking dispersion correction, (2) first-principles studies based on dispersion corrected methods and (3) studies based on semi-empirical and FF methods. In nearly all studies reviewed above, the nucleobases were found to be parallel to the graphene or CNT with the separation distance being around 3 Å, which confirms the π-π stacking nature of the interaction. On the other hand, drastically different results have been reported for the BE.

Previous QM calculations on BE already illustrates some effects of CNT chirality (Akdim *et al.,* 2012), however it is not yet clear whether such effects are correlated with the electronic structure of the CNT. Finally, it can be noted that BE has been used as the main parameter for comparisons made in this review. Other properties such as charge transfer and density of states have only been reported in some

Table 3. BE (kJ/mol) between nucleobases and graphene [Vovusha *et al.*, (2013)].

	DFT level			
	M05-2X		M06-2X	
Nucleobase	6-31+G(d,p)	6-311++G(d,p)	6-31+G(d,p)	6-311++G(d,p
G	37.62	27.23	65.08	57.46
A	27.01	16.70	52.19	44.23
T	27.98	19.64	52.93	46.23
C	27.98	20.50	51.02	45.10
U	22.19	13.93	46.36	35.00

(<50%) of the cited works and hence are not suitable for systematic comparison. Also, the calculation of charge transfer does not only depend on the QM method but also on the charge distribution scheme (e.g., Mulliken, ESP, RESP, etc.). This makes the comparison among different studies more complicated.

CONCLUSION

In the present work, a thorough review on the theoretical studies, mainly at the QM level, on the binding of nucleobases (and in a few cases, nucleosides or nucleotides) with graphene or CNT has been performed. BE, as an indicator for the stability of the binding, is used to compare different studies. Due to the different simulated systems and procedure considered for the study, a large range of binding energy values were reported, and considerable discrepancies exist among the past investigations. So, the importance of using dispersion-corrected method and proper design of the optimization procedure plays a crucial role in understanding the interaction of the nucleobases with the CNTs or graphene.

ACKNOWLEDGEMENT

AK would like to acknowledge the UGC for the financial support.

REFERENCES

Akdim B, Pachter R, Day PN, Kim SS and Naik RR (2012). On modelling biomolecular-surface non-bonded interactions: application to nucleobase adsorption on single-wall carbon nanotube surfaces. Nanotechnology, 23: 165703(1-6).

Al-Aqtash N and Vasiliev I (2009). Ab Initio Study of Carboxylated Graphene. J. Phys. Chem. C, 113: 1290-12975.

Allen MJ, Tung VC, and Kaner RB (2010). Honeycomb Carbon: A Review of Graphene. Chem. Rev., 110: 132-145.

Al-MashatLaith, Shin K, Kalantar-zadeh K, Plessis JD, Han SH, Kojima RW, KanerRB, Li D, Gou X, Ippolito SJ, and Wlodarski W (2010). Graphene/Polyaniline Nanocomposite for Hydrogen Sensing. J. Phys. Chem. C, 114: 16168-16173.

Bano F, Fruk L, Sanavio B, Glettenberg M, Casalis L, Niemeyer CM, and Scoles G (2009). Toward Multiprotein Nanoarrays Using Nanografting and DNA Directed Immobilization of Proteins. Nano Letters, 9: 2614-2618.

Barone PW, Baik S, Heller DA and Strano MS (2005). Near-Infraed optical sensors based on single-walled carbon nanotubes. Nature Materials, 4: 86-92.

Becke AD (1993). Density functional thermochemistry. III. The role of exact exchange. J. Chem. Phys. 98: 5648-5652.

Chandra SS and Swathi RS (2014). Stability of Nucleobases and Base Pairs Adsorbed on Graphyne and Graphdiyne. J. Phys. Chem. C, 118: 4516-4528.

Chen L, Cooper AC, Pez GP, and Cheng H (2007). Mechanistic Study on Hydrogen Spillover onto Graphitic Carbon Materials. J. Phys. Chem. C, 111: 18995-19000.

Chen RJ, Bangsaruntlp S, Drouvalakls KA, Kam NWS, Shim M, Li Y, Kim W, Utz PJ, Dai H (2003). Noncovalent functionalization of carbon nanotubes for highly specific electronic biosensors. PNAS, 100: 4984-4989.

Chung C, Gautier C, Campidelli S, Filoramo A. (2010) Hierarchical Functionalization of Single-Wall Carbon Nanotubes with DNA through Positively Charged Pyrene. Chem. Commun, 46: 6539-6541.

Cornell WD, Cieplak P, Bayly CI, Gould IR, Merz KM, Ferguson DM, Spellmeyer DC, Fox T, Caldwell JW, and Kollman PA (1995). A Second Generation Force Field for the Simulation of Proteins, Nucleic Acids, and Organic Molecules. J. Am. Chem. Soc., 117: 5179-5197.

Cornell WD, Cieplak P, Bayly CI, Gould IR, Merz KM, Ferguson DM, Spellmeyer DC, Fox T, Caldwell JW, and Kollman PA (1995). A second generation force field for the simulation of proteins, nucleic acids, and organic molecules. Journal of the American Chemical Society, 117(19):5179-5197.

Denis PA (2011).Theoretical investigation of the stacking interactions between curved conjugated systems and their interaction with fullerenes. Chem. Phys. Lett., 516: 82-87.

Denis PA, Iribarne F (2009). On the hydrogen addition to graphene. Journal of Molecular Structure: Theochem, 907: 93-103.

Dewar MJS, Zoebisch EG, Healy EF, and Stewart JJP (1984). AM1: A New General Purpose Quantum Mechanical Molecular Model. J. Am. Chem. Soc., 107: 3902-3909.

Dion M, Rydberg H, Schrçder E, Langreth DC, and Lundqvist BI (2004a). Van derWaals Density Functional for General Geometries. Physical Review Letters, 92: 246401 (1-4).

Dion M, Rydberg H, Schrçder E, Langreth DC, and Lundqvist BI (2004b). Van derWaals Density Functional for General Geometries. Physical Review Letters, 92: 246401(1-4).

Ehrlich S, Moellmann J, and Grimme S (2013). Dispersion-Corrected Density Functional Theory for Aromatic Interactions in Complex Systems. Acc. Chem. Res., 46: 916-926.

Fredlake CP, Hert DG, Mardis ER, Barron AE (2006) What is the future of electrophoresis in large- scale genomic sequencing? Electrophoresis, 27: 3689-3702.

Ghaderi N and Peressi M (2010). First-Principle Study of Hydroxyl Functional Groups on Pristine, Defected Graphene, and Graphene Epoxide. J. Phys. Chem. C, 114: 21625-21630.

Gowtham S, Scheicher RH, Ahuja R, Pandey R and Karna SP (2007). Physisorption of nucleobases on graphene: Density-functional calculations. Physical Review B 76: 033401(1-4).

Gowtham S, Scheicher RH, Pandey R, Karna SP and Ahuja R (2008). First-principles study of physisorption of nucleic acid bases on small-diameter carbon nanotubes. Nanotechnology, 19: 125701 (1-6).

Grimme S (2004). Accurate Description of van der Waals Complexes by Density Functional Theory Including Empirical Corrections. Journal of Computational Chemistry, 25: 1463-1473.

Grimme S (2006). Semi empirical GGA-Type Density Functional Constructed with a Long-Range Dispersion Correction. Journal of Computational Chemistry, 27: 1787-1799.

Grimme S, Antony J, Ehrlich S, and Krieg H (2010). A consistent and accurate ab initio parametrization of density functional dispersion correction DFT-D for the 94 elements H-Pu. The J. Chem. Phys., 132: 154104(1-19).

Grimme S, Ehrlich S, Goerigk L (2010). Effect of the Damping Function in Dispersion Corrected Density Functional Theory. Journal of Computational Chemistry, 32: 1456-1465.

H-G Martin, Pople JA (1988). MP2 Energy Evaluation By Direct Methods. Chemical Physics Letters, 153: 503-506.

Hohenstein EG, Chill ST and Sherrill CD (2008). Assessment of the Performance of the M05-2X and M06-2X Exchange-Correlation Functionals for NoncovalentInteractions in Biomolecules. J. Chem. Theory Comput., 4: 1996-2000.

Hubert V, Gil A, and Frapper G (2010). Trends in the Adsorption of 3d Transition Metal Atoms onto Graphene and Nanotube Surfaces: A DFT Study and Molecular Orbital Analysis. J. Phys. Chem. C, 114: 14141-14153.

Johnson ER, Wolkow RA , DiLabio GA (2004). Application of 25 density functionals to dispersion-bound homomolecular dimmers. Chemical Physics Letters, 394: 334-338.

Johnsona ER, Mackieb ID and DiLabio GA (2009). Dispersion interactions in density-functional theory. J. Phys. Org. Chem., 22: 1127-1135.

Jonkheijm P, Weinrich D, Schrçder H, Niemeyer CM., and Waldmann H (2008). Chemical Strategies for Generating Protein Biochips. Angew. Chem. Int. Ed., 47: 9618-9647.

Kang N, Erbe A and Scheer E (2008). Electrical characterization of DNA in mechanically controlled break-junctions. New Journal of Physics, 10: 023030 (1-9).

Lee C, Yang W, and Parr RG (1988). Development of the Colic-Salvetti correlation-energy formula into a functional of the electron density. Physical Review B, 37: 785-789.

Lee G, Lee B, Kim J, and Cho K (2009). Ozone Adsorption on Graphene: Ab Initio Study and Experimental Validation. J. Phys. Chem. C, 113: 14225-14229.

Li J, Lu Y, Ye Q, Cinke M, Han J and Meyyappan M (2003). Carbon nanotube sensors for gas and organic vapor detection. Nano Lett., 3: 929-933.

Lim SH., Feng L, Kemling. JW, Musto. CJ, and Suslick KS. (2009). An optoelectronic nose for the detection of toxic gases. nature chemistry, 1: 562-567.

Liu Z, Yang K, and Lee ST (2011). Single-walled carbon nanotubes in biomedical imaging. J. Mater. Chem., 21: 586-598.

Lu G., Ocola, L. E. and Chen, J (2009). Gas detection using low-temperature reduced graphene oxide sheets. Appl. Phys. Lett., 94, 083111-083115.

Meijer EJ and Sprik M (1996). A density functional study of the intermolecular interactions of benzene. J. Chem. Phys. 105: 8684-8689.

Meng S, Maragakis P, Papaloukas C, and Kaxiras E (2007a). DNA Nucleoside Interaction and Identification with Carbon Nanotubes. Nano Lett., 7: 45-50.

Meng S, Wang WL, Maragakis P, and Kaxiras E (2007b). Determination of DNA-Base Orientation on Carbon Nanotubes through Directional Optical Absorbance. Nano Letters, 7: 2312-2316.

Meyer JC, Geim AK, Katsnelson MI, Novoselov KS, Booth TJ & Roth S (2007). The structure of suspended graphene sheets. Nature Letters, 446: 60-63.

Min SK, Kim WY, Cho Y and Kim KS. (2011). Fast DNA sequencing with a graphene-based nanochannel device. nature nanotechnology, 6: 162-165.

Moller C and Plesset MS (1934). Note on an Approximation Treatment for Many-Electron Systems. Physical Review, 46: 618-622.

Nelson T, Zhang B, Prezhdo OV (2010). Detection of Nucleic Acids with Graphene Nanopores: Ab Initio Characterization of a Novel Sequencing Device. Nano Letters, 10: 3237-3242.

Panigrahi S, Bhattacharya A, Banerjee S and Bhattacharyya D (2012). Interaction of Nucleobases with Wrinkled Graphene Surface: Dispersion Corrected DFT and AFM Studies. J. Phys. Chem. C, 116: 4374-4379.

Park S, Lee K-S, Bozoklu G, Cai W, Nguyen ST, and Ruoff RS (2008). Graphene Oxide Papers Modified by Divalent Ions-Enhancing Mechanical Properties via Chemical Cross-Linking. Acs Nano, 3: 572-578.

Patolsky F, Zheng G and Lieber CM (2006). Fabrication of silicon nanowire devices for ultrasensitive, label-free, real-time detection of biological and chemical species. Nature protocols, 1: 1711-1724.

Paul A and Bhattacharya B (2010). DNA Functionalized Carbon Nanotubes for Nonbiological Applications. Materials and Manufacturing Processess, 25: 891-908.

Prasongkit J, Grigoriev A, Pathak B, Ahuja R, Scheicher RH (2011). Transverse Conductance of DNA Nucleotides in a Graphene nano gap from first principles. Nano Letters, 11: 1941-1945.

Priyakumar UD and Sastry GN (2003). Cation-pi interactions of curved polycyclic systems: M+ (M = Li and Na) ion

complexation with buckybowls. Tetrahedron Lett. , 44: 6043-6046.

Pumera M, Ambrosi A, Bonanni A, Chng ELK, Poh HL (2010). Graphene for electrochemical sensing and biosensing. Trends in Analytical Chemistry, 29: 954-965.

Quintana Mildred, SpyrouKonstantinos, GrzelczakMarek, Browne Wesley R, Rudolf Petra, and Prato Maurizio (2010). Functionalization of Graphene via 1,3- Dipolar Cycloaddition. Acs Nano, 4: 3527-3533.

Rao CNR, Sood AK, Subrahmanyam KS, and Govindaraj A (2009). Graphene: The New Two-Dimensional Nanomaterial. Angewandte Chemie, 48: 7752-7777.

Ritter KA and Lyding JW (2009). The influence of edge structure on the electronic properties of graphene quantum dots and nanoribbons. Nature materials, 8: 235-242.

Rubes M and Bludsky O (2009). DFT/CCSD(T) Investigation of the Interaction of Molecular Hydrogen with Carbon Nanostructures. ChemPhysChem, 10: 1868-1873.

Rutledge LR and Wetmore SD (2010). The assessment of density functionals for DNA protein stacked and T-shaped complexes. Canadian Journal of Chemistry, 88: 815-830.

Rutledge LR, Durst HF, and Wetmore SD (2009). Evidence for Stabilization of DNA/RNA-Protein Complexes Arising from Nucleobase-Amino Acid Stacking and T-Shaped Interactions. J. Chem. Theory Comput., 5: 1400-1410.

Sanchez-Jimenez G, Childs B and Valle D (2001). Human disease genes. nature analysis, 409: 853-855.

Schedin F, Geim AK, Morozov SV, Hill EW, Blake P, Katsnelson MI and Novoselov KS (2007). Detection of individual gas molecules adsorbed on graphene. Nature Materials Lett., 6: 652-655.

Shapir E, Cohen H, Calzolari A, Cavazzoni C, Ryndyk DA., Cuniberti G, Kotlyar A, Felice RDF and Porath D (2008). Electronic structure of single DNA molecules resolved by transverse scanning tunnelling spectroscopy. Nature Materials, 7: 68-74.

Shtogun YV, Woods LM, Dovbeshko GI (2007). Adsorption of Adenine and Thymine and their Radicals on Single- Walled Carbon Nanotubes. J. Phys. Chem. C, 111:18174-18181.

Shukla MK, Dubey M, Zakar E, Namburu R, Czyznikowsk Z, Leszczynski J (2009). Interaction of nucleic acid bases with single-walled carbon nanotube. Chemical Physics Letters 480: 269-272.

Si Y and Samulski ET (2008). Exfoliated Graphene Separated by Platinum Nanoparticles. Chem. Mater., 20: 6792-6797.

Song B, Elstner M, and Cuniberti G (2008). Anomalous Conductance Response of DNA Wires under Stretching. Nano Letters, 8: 3217-3220.

Stepanian SG ,Karachevtsev MV, Glamazda AY , Karachevtsev VA, Adamowicz L (2008). Stacking interaction of cytosine with carbon nanotubes: MP2, DFT and Raman. Chemical Physics Letters, 459: 153-158.

Stewart JJP (1988). Optimization of Parameters for Semi empirical Methods II. Applications. Journal of Computational Chemistry, 10: 221-264.

Stewart JJP (1989). Optimization of Parameters for Semi empirical Methods I. Method. Journal of Computational Chemistry, 10: 209-220.

Stewart JJP (1990). Optimization of Parameters for Semi empirical Methods III. Extension of PM3 to Be, Mg, Zn, Ga, Ge, As, Se, Cd, In, Sn, Sb, Te, Hg, T1, Pb, and Bi. Journal of Computational Chemistry, 12: 320-341.

Stewart JJP (2007). Optimization of parameters for semi empirical methods V: Modification of NDDO approximations and application to 70 elements. J Mol Model, 13: 1173–1213.

Stoller MD, Park S, Zhu Y, An J, and Ruoff RS (2008). Graphene-Based Ultracapacitors. Nano letters, 8: 3498-3502.

Tachikawa H and Iyama T (2010). Density Functional Theory Method for Study of the Mechanism of C–H Bond Formation on Finite-Sized Graphene Surface. Japanese Journal of Applied Physics, 49: 06GJ12 (1-4).

Tang S and Cao Z (2011). Adsorption of nitrogen oxides on graphene and graphene oxides: Insights from density functional calculations. The journal of chemical physics, 134: 044710(1-4).

Tkatchenko A and Scheffler M (2009). Accurate Molecular Van Der Waals Interactions from Ground-State Electron Density and Free-Atom Reference Data. PRL, 102: 073005(1-4).

Tournus F and Charlier JC (2005). Ab initio study of benzene adsorption on carbon nanotubes. Physical Review B 71:165421 (1-8).

Umadevi D and Sastry GN (2011). Quantum Mechanical Study of Physisorption of Nucleobases on Carbon Materials: Graphene versus Carbon Nanotubes. J. Phys. Chem. Lett., 2:1572-1576.

Umadevi D, Sastry GN (2015). Graphane versus graphene: a computational investigation of the interaction of nucleobases, aminoacids, heterocycles, small molecules (CO2, H2O, NH3, CH4, H2), metal ions and onium ions. Phys. Chem. Chem. Phys., 17: 30260-30269.

Vidic JM, Grosclaude J, Persuy M-A, Aioun J, Salessea R and Pajot-Augy E (2006). Quantitative assessment of olfactory receptors activity in immobilized nanosomes: a novel concept for bioelectronic nose. Lab chip, 6: 1026-1032.

Vovusha H, Sanyal S and Sanyal B (2013). Interaction of Nucleobases and Aromatic Amino Acids with Graphene Oxide and Graphene Flakes. J. Phys. Chem. Lett., 4: 3710-3718.

Wang D, Kou R, Choi D, Yang Z, Nie Z, Li J, Saraf LV, Hu D, Zhang J, Graff GL, Liu J, Pope MA, and Aksay IA. (2010). Ternary Self-Assembly of Ordered Metal Oxide Graphene Nanocomposites for Electrochemical Energy Storage. Acs

Nano, 4: 1587-1595.

Wang H and Ceulemans A (2009). Physisorption of adenine DNA nucleosides on zigzag and armchair single-walled carbon nanotubes: A first-principles study. Physical Review B, 79:195419(1-6).

Wang P, Wu H, Dai Z, Zou X (2011). Simultaneous detection of guanine, adenine, thymine and cytosine at choline monolayer supported multiwalled carbon nanotubes film. Biosensors and Bioelectronics, 26: 3339-3345.

Wang X and Liew KM (2011). Silicon carbide nanotubes serving as a highly sensitive gas chemical sensor for formaldehyde. J. Phys. Chem. C, 115: 10388-10393.

Wang Y (2008). Theoretical Evidence for the Stronger Ability of Thymine to Disperse SWCNT than Cytosine and Adenine: self-stacking of DNA bases vs their cross-stacking with SWCNT. J Phys Chem C Nanomater Interfaces, 112: 14297-14305.

Wang Y, Shao Y, Matson DW, Li J, and Lin Y (2010). Nitrogen-Doped Graphene and Its Application in Electrochemical Biosensing. Acs Nano, 4: 1790-1798.

Wang Yi and Bu Y (2007). Noncovalent Interactions between Cytosine and SWCNT: Curvature Dependence of Complexes via π-π Stacking and Cooperative CH-pi/NH-pi. J. Phys. Chem. B, 111: 6520-6526.

Weizmann Y, Chenoweth DM, and Swager TM (2011). DNA-CNT Nanowire Networks for DNA Detection. J. Am. Chem. Soc., 133: 3238-3241.

Yan Z and Truhlar DG. (2005). Benchmark Databases for Nonbonded Interactions and their use to test Density Functional Theory. J. Chem. Theory Comput., 1: 415-432.

Yarotski DA, Kilina SV, Talin AA, Tretiak S, Prezhdo OV, Balatsky AV, and Taylor AJ (2009). Scanning Tunneling Microscopy of DNA-Wrapped Carbon Nanotubes. Nano Letters, 9: 12-17.

Zhang G, Qi P, Wang X, Lu Y, Li Xiaolin, Tu R, Bangsaruntip S, Mann D, Zhang L, Dai H (2006). Selective Etching of Metallic Carbon Nanotubes by Gas-Phase Reaction. Science, 314: 974-977.

Zhao X (2011). Self-Assembly of DNA Segments on Graphene and Carbon Nanotube Arrays in Aqueous Solution: A Molecular Simulation Study. J. Phys. Chem. C, 115: 6181-6189.

Zhao Y and Truhlar DG (2005). Benchmark Databases for Nonbonded interactions and their use to test Density Functional Theory. J. Chem. Theory Comput., 1: 415-432.

Zhao Y and Truhlar DG (2006a). A new local density functional for main-group thermochemistry, transition metal bonding, thermochemical kinetics, and noncovalent interactions. J. Chem. Phys., 125: 194101 (1-18).

Zhao Y and Truhlar DG (2006b). Density Functional for Spectroscopy: No Long-Range Self-Interaction Error, Good Performance for Rydberg and Charge-Transfer States, and Better Performance on Average than B3LYP for Ground States. J. Phys. Chem. A, 110: 13126-13129.

Zhao Y and Truhlar DG (2008). The M06 suite of density functionals for main group thermochemistry, thermochemical kinetics, noncovalent interactions, excited states, and transition elements: two new functionals and systematic testing of four M06-class functionals and 12 other functional. TheorChem Account, 120: 215-241.

Zhao Y and Truhlar DG. (2008). Density Functionals with Broad Applicability in Chemistry. Acc. Chem. Res, 41: 157-167.

Zhao Y and Truhlar DG. (2011). Applications and validations of the Minnesota density functional. Chemical Physics Letters, 502: 1-13.

Zheng M, Jagota A, Semke ED, Diner BA, Mclean Robert S, Lustig Steve R, Raymond Richardson E. And Tassi Nancy G. (2003). DNA-assisted dispersion and separation of carbon nanotubes. nature materials, 2: 238-242.

Zheng Y, Yang C, Pu W, Zhang J (2009). Carbon Nanotube-based DNA Biosensor for Monitoring Phenolic Pollutants. Microchim. Acta, 166: 21-36.

Zwolak Michael and Ventra M Di (2008). Colloquium: Physical approaches to DNA sequencing and detection. Rev. Mod. Phys., 80: 141-165.

Bull. Mater. Sci.
DOI 10.1007/s12034-017-1478-x

Adsorption of small gas molecules on pure and Al-doped graphene sheet: a quantum mechanical study

DHARMVEER SINGH, ASHEESH KUMAR and DEVESH KUMAR*
Department of Applied Physics, School for Physical Sciences, Babasaheb Bhimrao Ambedkar University, Lucknow 226025, India
*Author for correspondence (dkclcre@yahoo.com)

MS received 26 September 2016; accepted 13 February 2017

Abstract. The interaction of small gas molecules (CCl_4, CH_4, NH_3, CO_2, N_2, CO, NO_2, CCl_2F_2, SO_2, CF_4, H_2) on pure and aluminium-doped graphene were investigated by using the density functional theory to explore their potential applications as sensors. It has been found that all gas molecules show much stronger adsorption on the Al-doped graphene than that of pure graphene (PG). The Al-doped graphene shows the highest adsorption energy with NO_2, NH_3 and CO_2 molecules, whereas the PG binds strongly with NO_2. Therefore, the strong interactions between the adsorbed gas molecules and the Al-doped graphene induce dramatic changes to graphene's electronic properties. These results reveal that the sensitivity of graphene-based gas sensor could be drastically improved by introducing the appropriate dopant or defect. It also carried out the highest occupied molecular orbital–lowest unoccupied molecular orbital energy gap of the complex molecular structure that has been explored by M06/6-31++G** method. These results indicate that the energy gap fine tuning of the pure and Al-doped graphene can be affected through the binding of small gas molecules.

Keywords. DFT; small gas molecules; graphene; aluminium-doping; non-covalent interaction; grapheme-based gas sensors.

1. Introduction

Carbon is the versatile element on the earth's crust and it is found on the earth's surface in different allotropes as graphite, diamonds, charcoal and coke, respectively. The newer allotropes of carbon were discovered such as graphene, carbon nanotubes (CNTs) and fullerenes [1–3]. Graphene is the youngest known allotrope of carbon, which is a two-dimensional and one-atom thick material consisting of sp^2 hybridized carbon atoms arranged in a honeycomb structure. These allotropes of carbon are extensively used in research, that is, from biomedical to environment applications due to their unique physical and chemical properties [4]. The exceptional properties of carbon nano materials, such as electronic, thermal, optical, mechanical and transport properties make them promising candidates for various potential applications [5–7]. From several experimental and theoretical studies it is observed that the transport and electronic properties are extremely sensitive to change in the local chemical environment [8–10]. Carbon nanostructures (CNSs) exhibit non-covalent interaction such as the XH–π, cation–π, anion–π and π–π interaction towards the small gas molecules, metal ions and bio molecules [11–15]. The XH–π weak interactions were extensively studied in recent years [16–20]. These interactions have been considered to be a unique type of hydrogen bonding interaction in which π electron acts as the proton acceptor [14]. Graphene is a sensitive nano material, which detects all the individual events when a gas molecule is adsorbed to or de-adsorbed from its surface [21]. However, it is very difficult to prepare a perfect single layer graphene with zero band gap. Doping is one of the most efficient method to improve the electronic properties of the materials. Wang *et al* have found that the sp^2 hybridization is affected and it changes the electronic properties of the system when B, N and B–N are doped with pure graphene (PG) [22]. Lherbier *et al* showed that the charge mobility and conductivity of graphene changes when B/N impurity atom is added to its surface [23]. Recently, there are several experimental studies on Al, Ga and Pd-doped graphene sheet-based gas sensor [24,25]. Interestingly, the nanoparticles such as Al, Ga and Pd incorporated the significant changes in the sensitivity and selectivity towards the gas molecules. The structure and physical properties of CNSs make them potential candidates as sensors to detect different types of gas molecules. Dai and co-workers were the first to report the gas sensors based on CNTs to detect gas molecules such as NO_2 and NH_3 [26]. Recently, Schedin *et al* experimentally reported that graphene-based gas sensors possess very high sensitivity such that the adsorption of individual gas molecules could be detected [21]. CNSs can absorb a number of species such as gas molecule, metal ions, polymers, organic molecules and biomolecules such as proteins, nucleobases and deoxyribonucleic acid (DNA) on their surface and these adsorption properties provide opportunities for potential industrial applications [27–30].

Published online: 03 October 2017

Roman *et al* studied the adsorption of few amino acids on a single-walled CNT by using the DFT method [31]. CNTs have also been found to be suitable candidates for the negative electrode of the Li-ion batteries, where the Li diffuse between the positive and negative in the ionic state [32,33]. Thus, the fundamental understanding of the interaction of metals with CNTs in the ionic state is important. It is also important to know the role of various factors such as solvent and other chemical environments, which influence such cation–π interaction [34–36]. Umadevi *et al* have found that the charge transfer between graphane and the molecules is an important factor in determining the binding strength of the complex molecular systems [37]. Zhang *et al* studied that doped graphane strongly interacts with CO, NO and NO_2 while NH_3 interacts weakly [38]. Zou *et al* found that the SiG has higher chemical reactions towards the gas molecules due to doping of silicon atom and shows the higher adsorption energy with CO, O_2, NO_2 and H_2O [39]. In the current study, the Al-doped graphene was theoretically investigated to improve its gas sensing efficiency and selectivity towards the various gas molecules. The gas molecule CCl_4, CH_4, NH_3, CO_2, CO, NO_2, CCl_2F_2, SO_2, CF_4 and N_2O, are all of great practical interest for industrial, environmental and medical applications. On the other hand, the effect of doping of the graphene sheet on the binding strength has been estimated. The charge transfer that occurred during the complex formation has also been explored. The change in the highest occupied molecular orbital–lowest unoccupied molecular orbital (HOMO–LUMO) energy gap of PG and Al-doped graphene upon the binding of these gas molecules has also been estimated.

2. Computational methods

The calculations of the interaction between PG, Al-doped graphene and gas molecule is carried out using the density functional theory. The geometrical calculations of all structures have been done by using one method B3LYP/6-31G* [40,41]. Initially, the individual gas molecule is adsorbed on the surface of PG and Al-doped graphene thereafter. Geometry optimization calculations were accomplished using Gaussian09 suite program [42]. It is important to note that complete geometrical configuration was tested but those shown are the lowest energy species feasible for the interaction of the compounds. Single point energy has been done at the M06/6-31++G** level to fine-tune the energy [43–46].

The adsorption energy (E_{ad}) of the small gas molecule (X = CCl_4, CH_4, NH_3, CO_2, N_2, CO, NO_2, CCl_2F_2, SO_2, CF_4, H_2) on the pure and Al-doped graphene is calculated by the following equation (1).

$$E_{ad} = E_{\text{graphene\_X/graphene@Al\_X}} - (E_{\text{graphene/Al@graphene}} + E_X) \quad (1)$$

Here, $E_{\text{graphene\_X/graphene@Al\_X}}$ represents the total energy of a complex molecular system. $E_{\text{graphene/graphene@Al}}$ and E_X represent the total energies of the graphene and gas molecule, respectively. The individual small gas molecule was placed parallel to the surface of graphene and doped graphene at the 3 Å distance. The variation of the charge on gas molecules as well as on pure and doped graphene when the individual gas molecules are kept at the 3 Å distance from its surface was calculated. The charge transfer has been considered as the sum of all atoms in the pure and Al-doped graphene model system. Positive charge transfer values indicate the transfer of charge from graphene to the molecules, while negative charge values indicate the transfer of charge from the molecules to the pure and Al-doped graphene. The HOMO–LUMO energy gap of pure and Al-doped graphene as well as their complexes at M06/6-31++G** level of theory were also calculated. All calculations were carried out using the Gaussian09 program package.

3. Results and discussion

The optimized structure of pure and Al-doped graphene and their complexes with small molecules are shown in figures 1, 2 and 3. The initial configuration of all small gaseous molecules were assigned so that these are oriented exactly parallel to the pure and Al-doped graphene at 3 Å from its surface. In this paper, pure and Al-doped graphene was considered to study the interaction of small gas molecules with X–π non-covalent interaction towards carbon nano materials. Tables 1 and 2 summarize our results on the adsorption energy, equilibrium graphene–molecule distance (d, defined as the distance of nearest atoms between graphene and molecule), the charge transfer (Q, mulliken charge) and HOMO–LUMO energy gap for the most stable configurations of pure and Al-doped graphene adsorbed with various gas molecules in our calculations as shown in figures 2, 3 and tables 1, 2. Subsequently, we look at the binding of the pure and Al-doped graphene with various gas molecules and the trend in the charge transfer. The HOMO–LUMO energy gap of pure and Al-doped graphene with adsorption of various gas molecules were also investigated. When one impurity atom as Al is substituted for one C atom in graphene sheet, the optimized configuration of the graphene sheet is dramatically distorted. The Al atom introduces the deformation of the six-membered ring (6MR) near the doping site to relieve stress, as a result the Al atom protrudes out of the graphene sheet. The optimized carbon–dopant atom distance (Al–C) is 1.751 Å at B3YP/6-31G*, which is in agreement with the previous study [47].

3.1 *Adsorption energy and charge transfer*

The small gas molecules form X–π type complex with the pure and Al-doped graphene that are shown in figures 2 and 3. We observed the adsorption energy of small gas

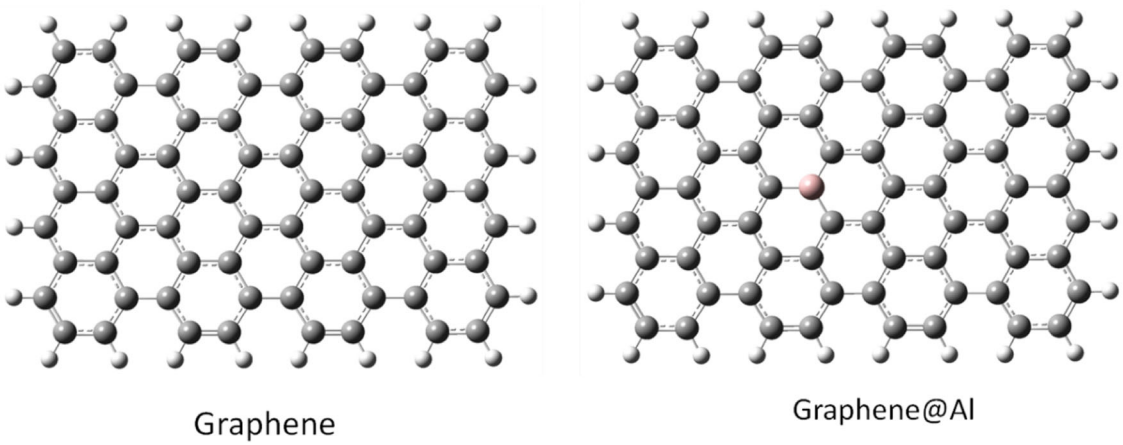

Figure 1. Top view of the optimized structure of pure and Al-doped graphene model system considered in this study.

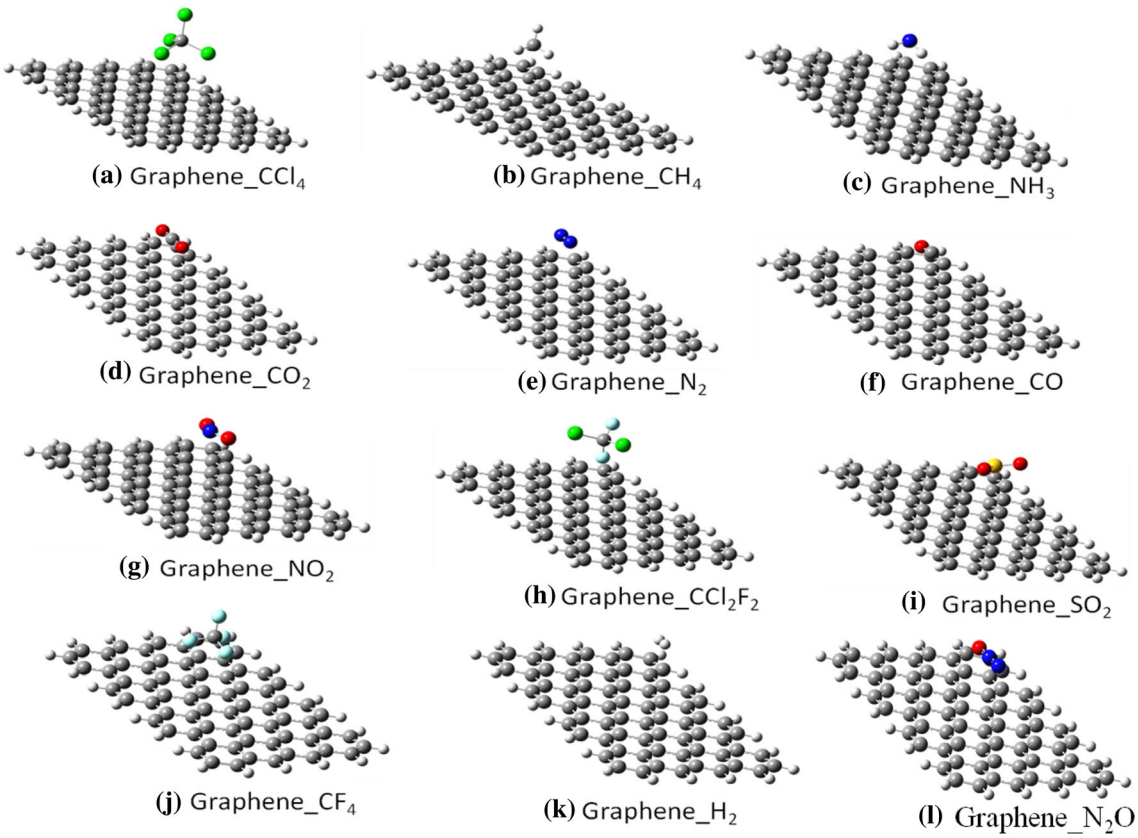

Figure 2. Optimized geometries of pure graphene with small gas molecule adsorbed (**a**) CCl_4, (**b**) CH_4, (**c**) NH_3, (**d**) CO_2, (**e**) N_2, (**f**) CO, (**g**) NO_2, (**h**) CCl_2F_2, (**i**) SO_2, (**j**) CF_4, (**k**) H_2 and (**l**) N_2O by M06/6-31++G** method.

molecule complexes with pure and Al-doped graphene when the gas molecules are kept parallel to the graphene surface at 3 Å distance. Tables 1, 2 and figure 4 display the adsorption energy, charge transfer and molecule sheet distance of the small gas molecule complexes with pure and Al-doped graphene at M06/6-31++g** level of theory.

Interestingly, a different trend in the case of small gas molecule interacting with pure and Al-doped graphene is observed, the adsorption energy of small gas molecules towards the Al-doped graphene is greater than PG. From table 2 and figure 2, the adsorption energy of all gas molecules is higher for the Al-doped graphene than that of PG.

For CCl_4 and CH_4 adsorbed on PG, the most energetically favourable configuration (Graphene_CCl_4) is also identical. The adsorption of CCl_4 and CH_4 on PG is non-covalent interaction with the adsorption energy of -0.394 and

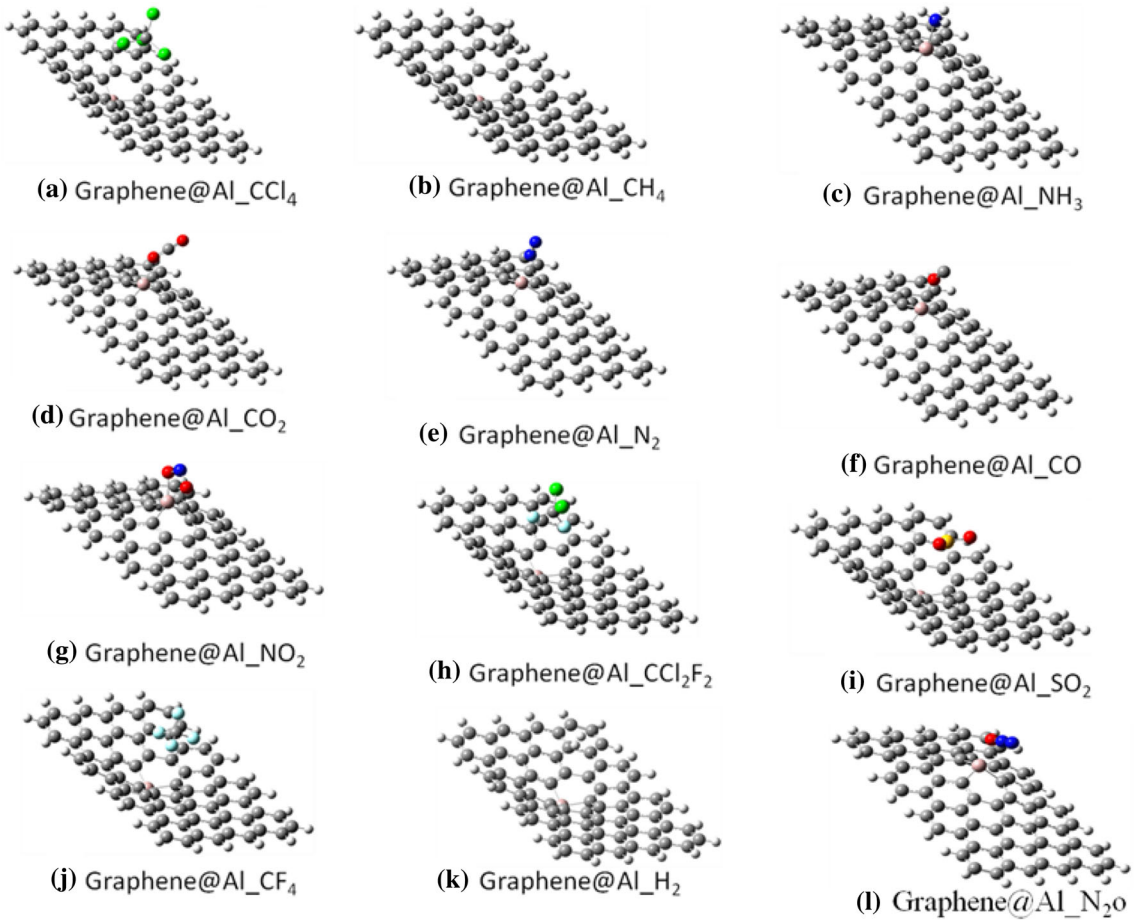

Figure 3. Optimized geometries of aluminium-doped graphene (@Al shown as Al doping in pure graphene) adsorbed with small gas molecules (**a**) CCl_4, (**b**) CH_4, (**c**) NH_3, (**d**) CO_2, (**e**) N_2, (**f**) CO, (**g**) NO_2, (**h**) CCl_2F_2, (**i**) SO_2, (**j**) CF_4, (**k**) H_2 and (**l**) N_2O by M06/6-31++G** method.

Table 1. The adsorption energy (eV), molecule sheet distance (Å), charge transfer (a.u.) and HOMO–LUMO energy gap (eV) at M06/6-31++G** level of theory.

Carbon nanomaterial	Small gas molecule	Adsorption energy (eV)	Molecule sheet distance (Å)	Charge on gas molecule (a.u.)	HOMO–LUMO gap (eV)
Graphene	CCl_4	−0.394	4.498	−0.0196	0.3339
	CH_4	−0.067	3.784	−0.0133	0.3336
	NH_3	−0.145	3.357	0.0334	0.3336
	CO_2	−0.122	3.626	0.0169	0.3336
	N_2	−0.083	3.828	0.014	0.3339
	CO	−0.110	3.732	0.0098	0.3336
	NO_2	−0.996	3.573	0.025	0.8727
	CCl_2F_2	−0.119	3.355	0.0039	0.3336
	SO_2	−0.279	3.578	0.0254	0.3339
	CF4	−0.150	3.404	0.0552	0.3336
	H_2	−0.013	4.946	0.0006	0.3339
	N_2O	−0.123	3.634	0.0180	0.3340

−0.067 eV and the molecule sheet distance of 4.498 and 3.784 Å, respectively. The charge transfer from graphene to CCl_4 and CH_4 molecule is −0.0196 and −0.0133 a.u., which indicates that the PG acts as a donor, and the gas molecule acts as an acceptor. Therefore, PG is less sensitive to the CCl_4 than CH_4 molecule. The most stable configuration of CCl_4

Table 2. The adsorption energy (eV), molecule sheet distance (Å), charge transfer (a.u.) and HOMO–LUMO energy gap (eV) at M06/6-31++G** level of theory.

Carbon nanomaterial	Small gas molecule	Adsorption energy (eV)	Molecule sheet distance (Å)	Charge on gas molecule (a.u.)	HOMO–LUMO gap (eV)
Graphene@Al	CCl_4	−1.354	3.920	−0.007	0.661
	CH_4	−1.242	4.300	0.004	0.616
	NH_3	−2.948	2.053	0.493	1.080
	CO_2	−2.019	2.158	0.423	1.574
	N_2	−1.279	2.210	0.837	0.444
	CO	−1.255	2.344	0.276	0.494
	NO_2	−3.867	1.894	−0.065	0.330
	CCl_2F_2	−1.361	3.956	0.020	0.579
	SO_2	−1.608	3.579	0.045	0.599
	CF_4	−1.354	3.920	0.138	0.662
	H_2	−1.637	6.306	0.001	1.512
	N_2O	−1.409	2.163	0.518	0.453

and CH_4 on graphene@Al is a configuration with the CCl_4 and CH_4 molecule parallel to the graphene sheet and Cl atom of CCl_4 and H atom of CH_4 adsorbed on the top of Al atom, which is shown in figure 3a and b, where the molecular sheet distance is 3.920 and 4.300 Å, respectively. The calculated E_{ad} value is −1.354 and −1.242 eV, which indicates that the graphene@Al has higher adsorption enegy than PG with CCl_4 and CH_4.

The NH_3 molecule shows different adsorption configurations on pure and Al-doped graphene, showing a more complicated adsorption mechanism than the other molecules. On the PG, the configuration with the three hydrogen atoms of NH_3 pointing towards the graphene plane is the favourable one (figure 3c), which gives an adsorption energy and molecule distance of −0.145 eV and 3.357 Å, respectively. This result is consistent with previous reports about NH_3 adsorbed on CNTs (−0.14 eV) and NH_3 adsorbed on graphene (0 ∼ −0.17 eV) [48,49], which indicates a weak interaction between NH_3 and the PG. On the Al-doped graphene, NH_3 is attached to the Al atom with the N atom pointing at the sheet, which gives an adsorption energy of −2.948 eV and an Al–N distance of 2.053 Å (as shown in figure 3c and table 2). The charge transfer from NH_3 to graphene is 0.493 a.u., which indicates that the graphene behaves as charge acceptor and NH_3 molecule as charge donor. The adsorption energy of NH_3 on Al-graphene (−2.948 eV) is much higher than that on the PG, which attributes to the strong interaction between the electron-deficient Al atom and the electron-donating N atom of NH_3. It is also investigated that the Al-doped graphene undergoes an obvious distortion upon NH_3 adsorption (figure 3c), indicating that the B site is transformed from sp^2 to sp^3 hybridization, which matched the previous study [35]. The molecular distance between Al and N is 2.053 Å. This strong interaction is also evident in the electronic total charge density on Al-doped graphene system, which shows large electron density overlap.

The adsorption energy of this complex system is –0.122 eV and molecule–sheet distance is 3.626 Å, which are shown in table 1 and figure 2d. The low adsorption energy and long molecule sheet distance indicate a weak interaction. When the CO_2 molecule is adsorbed on PG, the calculated charge transfer of CO_2 is 0.0169 a.u. In this configuration, the CO_2 molecule acts as a charge donor. When the CO_2 molecule is adsorbed on Al-doped graphene, one oxygen atom of CO_2 shows most stable configuration towards the Al atom of graphene@Al sheet. In this configuration, the adsorption energy and molecule sheet distance (O–Al) is −2.019 eV and 2.158 Å, respectively. This result indicates that the interaction of CO_2 with graphene@Al is much stronger than that of PG due to large transfer of charge. In this configuration, the charge transfer from CO_2 to the graphene@Al is 0.423 a.u., which means that the CO_2 molecule acts as a charge donor and graphene@Al acts as a charge acceptor.

In case of graphene_N_2 configuration, the N–N axis gets aligned parallel to the graphene plane along the axis of two opposite C atoms of the 6MR, which was found to be the most stable configuration. The adsorption energy and the molecule sheet distance of this complex system is –0.083 eV and 3.828 Å, respectively as shown in figure 4a, c and table 1. The charge transfer between N_2 and graphene was calculated from Mulliken population analysis, which is shown in table 1. This result indicates that the interaction is weak in nature due to very small adsorption energy and charge transfer. When adsorbed on Al-doped graphene (graphene@Al), N_2 adopts perpendicular oreintation with Al atom of the graphene sheet. In this configuration, the one N atom of N_2 and Al atom of graphene@Al is very close as shown in figure 3e. The adsorption energy and the molecule sheet distance is −1.279 eV and 2.210 Å, respectively (as shown in figures 4a and c). The charge transfer from N_2 to graphene@Al is 0.837 a.u., which indicates that N_2 acts as a charge donor. In this configuration, the adsorption energy of the complex system is higher than

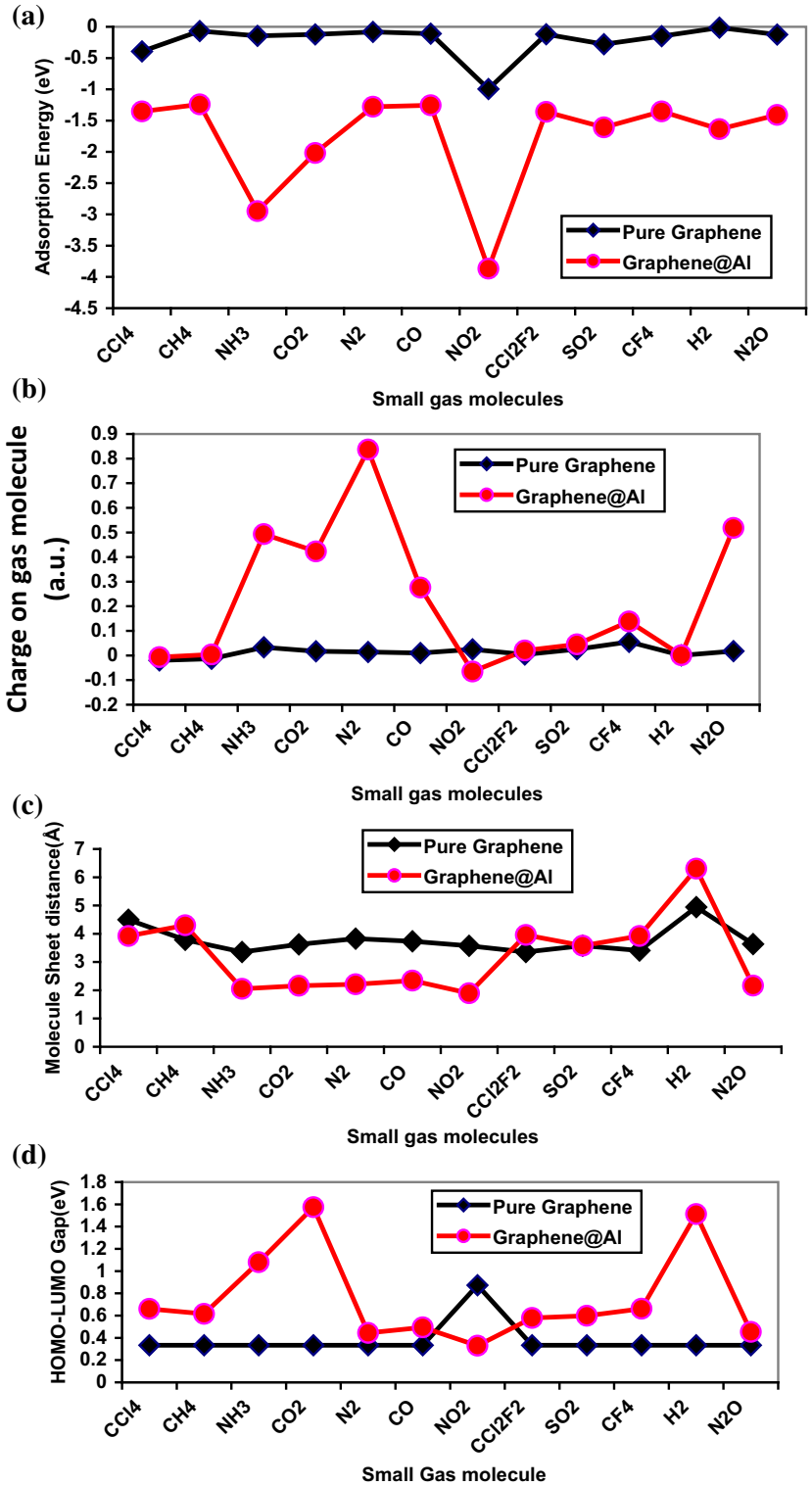

Figure 4. (**a**) The adsorption energy E_{ad}, (**b**) charge transfer, (**c**) molecule sheet distance and (**d**) HOMO–LUMO energy gap of small gas molecules with pure and Al-doped graphene complexes at the M06/-31++G** level of theory. The red line with solid red circles represents the variation for the aluminium-doped graphene whereas the black line with black solid squares represent the variation for pure graphene. The HOMO–LUMO gap for pure graphene is 0.33 eV and for Al-doped graphene is 0.22 eV without any gas molecules.

the graphene_N_2 due to large transfer of charge, which are responsible for strong interaction.

The most stable configuration of CO molecule is similar to the CO_2 and N_2, which are aligned parallel to the PG plane along the axis of two opposite C atoms of the 6MR in the complex molecular structure. The adsorption energy and molecule sheet distance is −0.110 eV and 3.732 Å, respectively (as shown in table 1). When the CO molecule is adsorbed on PG, the charge calculated on the C and O atoms of the CO molecule are 0.100 and −0.090 a.u., respectively, while there is no charge on the carbon atoms of the PG. Therefore, we can say that a very small charge is transferred from CO to the PG. The low adsorption energy and very small charge transfer indicates weak physisorption. When the CO molecule is adsorbed on Al-doped graphene, CO molecule adopts a tilted oreintation with respect to the plane of the Al-containig 6MR, with the O atom close to graphene@Al. In this complex structure, the adsorbed energy and molecule sheet distance are found be −1.255 eV and 2.344 Å, respectively. The charge transfer from CO molecule to graphene@Al is 0.275 a.u. In this configuration, the adsorption energy of graphene@Al_CO is higher than graphene_CO complex (as shown in table 2 and figure 4a).

The adsorption energy and shortest distance from PG to the nearest O atom of NO_2 are −0.996 eV and 3.573 Å, respectively, which indicates a weak interaction between the NO_2 and PG. However, the adsorption energy of NO_2 on PG can remarkably change the electronic properties of PG and the charge transferred from NO_2 to PG is about 0.02504 a.u. It is clear that PG behaves as charge acceptor. In other words, PG is more sensitive to the NO_2 molecule than any other gas molecule. For NO_2 adsorbed on AlG (Al-doped graphene), the most stable configuration (Graphene@Al_NO_2) is similar to that of graphene_NO_2. However, the oxygen atom of NO_2 is bonded to the AlG as shown in figure 2g. The O–Al bond length is 1.894 Å and the adsorption energy for Graphene@Al_NO_2 is −3.867 eV, which indicates that NO_2 is chemisorbed on the graphene@Al. In this configuration, the adsorption energy is greater than graphene_NO_2 due to large charge transferred from graphene@Al to NO_2, about −0.064582 a.u., which is shown in table 2 and figure 4b. It is clear that the graphene@Al behave as charge donor while interacting with the NO_2.

For CCl_2F_2 adsorption on PG, the most energetically favourable configuration is similar to the graphene_CCl_4 and graphene_CH_4. In this configuration, the CCl_2F_2 is adsorbed to PG with one F atom of CCl_2F_2 pointing downwards as shown in figure 2h and table 1. The adsorption of CCl_2F_2 on PG shows interaction with the adsorption energy of −0.119 eV with molecule sheet distance of 3.355 Å, indicating the weak physisorption nature. The calculated charge transfer from CCl_2F_2 is only 0.004 a.u. Therefore, the PG is not senstive to the CCl_2F_2. When the CCl_2F_2 is adsorbed on Al-doped graphene, both florine atoms of CCl_2F_2 get close to the grapehe@Al. In this configuration, the adsorption energy, molecule sheet distance and charge transfer is −1.361 eV, 3.956 Å and 0.02 a.u., respectively, which indicates that interaction is weak in nature due to very small charge transfer (as shown in figure 4b and table 2).

In the graphene_SO_2 complex structure, the S atom of SO_2 is close to the C atom of PG. The adsorption energy E_{ad} and shortest distance from PG to the S atom of SO_2 are −0.279 eV and 3.578 Å, respectively, suggesting a weak interaction between the SO_2 and PG (as shown in figure 4c, d and table 1). However, there is no change in the electronic properties of PG due to the low charge transfer, about 0.025 a.u. from SO_2 to the PG. Therefore, PG is not sensitive to the SO_2 molecule. As shown in figure 3i, the SO_2 is adsorbed on Al-doped graphene, the S atom of SO_2 gets close to the graphene@Al because the Al atom is negatively charged and S atom is positively charged. The charge on Al, S, O(98) and O(99) are −0.283, 0.796, −0.373 and −0.378 a.u., respectively, indicating that Al atom repels both oxygen atoms but attracts the S atom because S atom becomes more positively charged. In this complex structure, the adsorption energy and molecule sheet distance between S and Al is −1.608 eV and 3.579 Å as shown in figure 3i and table 2. However, the charge transfer is very low from SO_2 to grahene@Al, which is about 0.045 a.u.

For CF_4 adsorption on PG, the most energetically favourable configuration is similar to the graphene_CCl4 and graphene_CH4. In this configuration, the CF_4 is adsorbed to PG with one F atom of CF_4 pointing downward as shown in figure 2j and table 1. The adsorption of CF_4 on PG is the non-covalent interaction with the adsorption energy of −0.150 eV and the molecule sheet distance of 3.404 Å, indicating the weak physisorption. The calculated charge transfer from CF_4 is only 0.055 a.u. Therefore, PG is not senstive to CF_4. When CF_4 is adsorbed on Al-doped graphene, one florine atom of CF_4 gets close to graphene@Al. In this configuration, the adsorption energy, molecule sheet distance and charge transfer is −1.354 eV, 3.404 Å and 0.135 a.u., respectively. Therefore, we can say that graphene@Al is more sensitive than PG towards the CF_4 molecule (figure 3j and table 2). In this complex, graphene@Al acts as a charge acceptor.

The H_2 molecule was initially placed parallel to the graphene. After full relaxation, a configuration with the adsorbed H_2 axis gets aligned almost parallel to the graphene surface along the axis of two opposite C atoms of the 6MR and was found to be the most stable one for the PG. The adsorption energy of this system is −0.013 eV and the molecule sheet distance is 3.946 Å as shown in figure 3k and table 1, which are suggesting weak interaction between H_2 and graphene. The charge transfer between H_2 and graphene is 0.0007 a.u. In this configuration, PG is not sensitive towards the H_2 molecule. When adsorbed on graphene@Al, H_2 is oriented perpendicular to the Al-doped graphene plane, with one H(97) atom close to the graphene@Al. In this complex structure, the adsorption energy, molecule sheet distance and charge transfer are −1.637 eV, 6.306 Å and 0.001 a.u., respectively. Interestingly, the graphene@Al has more adsorption energy than PG.

As shown in figure 2l, the most stable configuration of N_2O adsorbed on PG (graphene_N_2O) is similar to graphene_CO_2, where the gas molecule axis is aligned parallel to the graphene plane along the axis of two opposite C atoms of the 6MR. However, the N_2O in graphene_N_2O is located above the centre of the 6MR. The calculated adsorption energy and molecule sheet distance are 0.123 eV and 3.634 Å, respectively. The low adsorption energy and long molecule sheet distance are suggesting weak physisorption. However, it is found that the interaction is significantly improved when a C atom in the PG is replaced by an Al atom. Figure 3l shows the most stable configuration of N_2O adsorbed on graphene@Al, where the oxygen atom of N_2O is close to the Al atom of graphene@Al. The adsorption energy E_{ad} for graphene@Al_N_2O is –1.409 eV, which is clearly higher than that for graphene_N_2O. The interaction distance between the N_2O molecule and the graphene@Al decreases to 2.163 Å, which indicates strong interaction. The charge transfer from N_2O to the graphene is 0.518 a.u. The large transferred charge suggests that the local electronic properties of graphene@Al is remarkably changed due to the adsorption of N_2O on graphene@Al.

The above mentioned results suggest that PG has weak interaction towards all gas molecules. Introducing dopants like Al atom into the graphene significantly increases the molecule–graphene interaction. The order of adsorption energy for small gas molecule complexes is $NO_2 > CCl_4 > SO_2 > CF_4 > NH_3 > N_2O > CO_2 > CCl_2F_2 > CO > N_2 > CH_4 > H_2$ with PG and $NO_2 > NH_3 > CO_2 > H_2 > SO_2 > N_2O > CCl_2F_2 > CF_4 > CCl_4 > N_2 > CO > CH_4$ with Al-doped graphene. Interestingly, our results predicted that Al-doped graphene are more suitable for gas sensing applications, since they have stronger interactions with all small gas molecules than PG. The Al-doped graphene particularly shows the highest sensitivity towards NO_2, NH_3 and CO_2.

3.2 *HOMO–LUMO energy gap*

The primary requisite for a material to perform as a sensor is to undergo a change in its physical property on interacting with an analyte. Such changes can be monitored and recorded to determine the presence of the analyte. The HOMO–LUMO energy gap is defined as the difference between lowest unoccupied molecular orbital and highest occupied molecular orbital. It is the electronic property of any molecular system, which is helpful to design new materials. In order to notice such a depiction in the case of carbon materials, we have calculated the HOMO–LUMO energy gap of the PG and Al-doped graphene in the free state and in the small gas molecule complexes. In general, in the case of X–π complexes, the HOMO–LUMO energy gap of single-walled carbon nanotube (SWCNT) varies with orientation of small gas molecules on the PG and Al-doped graphene. It has been shown that the energy gap of PG is not significant but when the gas molecules is adsorbed on graphene@Al then significant changes in HOMO–LUMO energy gap is observed (as shown in table 2). Therefore, we can say that the variation in HOMO–LUMO energy gap of the graphene upon binding with the various small gas molecules is significant.

4. Conclusion

The adsorption energy of various small gas molecules such as CCl_4, CH_4, NH_3, CO_2, CO, NO_2, CCl_2F_2, SO_2, CF_4 and N_2O with the pure and Al-doped graphene (graphene@Al) has been comprehensively analysed. These calculations reveal that the adsorption energy has preferences of small gas molecules with the doping in graphene as well as molecule sheet distance. It can be seen from the results that the adsorption energy of these gas molecules is higher for the Al-doped graphene than for the PG. PG shows weak sensitivity to all gas molecules. Compared with PG, graphene@Al has a higher chemical reactivity towards all gas molecules due to the doping of Al atom and shows higher adsorption energy with NO_2, NH_3 and CO_2. The strong interactions between graphene@Al and the adsorbed molecules induce dramatic changes in the electronic properties of graphene@Al and make graphene@Al a promising candidate as gas sensing materials for NO_2, NH_3 and CO_2. The Mulliken charge analysis reveals that the gas molecule acts as charge donor and acceptor in different configurations towards the pure and Al-doped graphene and influence the physical properties of carbon materials, which leads to the sensitivity. It has also been found that HOMO–LUMO energy gap of the CNT is always affected by the binding of the small gas molecules. Significant changes occur in the HOMO–LUMO energy gap on PG and graphene@Al on interacting with gas molecules, which provides a handle to tune the electronic and conductivity properties of graphene through gas molecule complexation. These studies can also be applied to develop new carbon-based materials and sensing applications, focusing particularly on the binding mechanism of various gas molecules with graphene. Developing chemical and gas sensors based on carbon materials has become an area of significant research interest since the physical and electronic properties of these materials are vulnerable to external enviroment. It is to hope that our results would be helpful to develop novel carbon material-based gas sensors.

Acknowledgements

Dharmveer Singh and Asheesh Kumar acknowledge their financial support from the University Grants Commission (UGC), New Delhi.

References

[1] Hirsch A 2010 *Nat. Mater.* **9** 868
[2] Rao C N R, Sood A K, Subrahmanyam K S and Govindaraj A 2009 *Angew. Chem. Int. Ed.* **48** 7752

[3] Iijima S 1991 *Nature* **354** 56
[4] Liu J, Cui L and Losic D 2013 *Acta Biomater.* **9** 9243
[5] Dinadayalane T C and Leszcznski J 2010 *Struct. Chem.* **21** 1155
[6] Liang F and Chen B 2010 *Curr. Med. Chem.* **17** 10
[7] Zhu Y, Murali S, Cai W, Li X, Suk J W, Potts J R *et al* 2010 *Adv. Mater.* **22** 3906
[8] Goldoni A, Larciprete R, Petaccia L and Lizzit S 2003 *J. Am. Chem. Soc.* **125** 11329
[9] Guo Z, Feng Y, He S, Qu M, Chen H, Liu H *et al* 2012 *Adv. Mater.* **25** 584
[10] Zhong J, Chiou J, Dong C, Glans P A, Pong W F, Chang C *et al* 2012 *Appl. Phys. Lett.* **100** 201605
[11] Umadevi D, Panigrahi S and Sastry G N 2014 *Acc. Chem. Res.* **47** 2574
[12] Vijay D and Sastry G N 2010 *Chem. Phys. Lett.* **485** 235
[13] Shi G, Ding Y and Fang H 2012 *J. Comput. Chem.* **33** 1328
[14] Grabowski S J and Lipkowski P 2011 *J. Phys. Chem. A* **115** 4765
[15] Mahadevi A S and Sastry G N 2016 *Chem. Rev.* **116** 2775
[16] Charlier J C 2002 *Acc. Chem. Res.* **35** 1063
[17] Huang P, Zhu H, Jing L, Zhao Y and Cao X 2011 ACS *Nano* **5** 7945
[18] Dougherty D A 1996 *Science* **271** 163
[19] Kim S K, Hu S, Tarakeshwar P and Lee J Y 2000 *Chem. Rev.* **100** 4145
[20] Ready A S and Sastry G N 2005 *J. Phys. Chem. A* **109** 8893
[21] Schedin F, Geim A K, Morozov S V, Hill E W, Blake P, Katsnelson M I *et al* 2007 *Nat. Mater.* **6** 652
[22] Wang X, Sun G, Routh P, Kim D H, Huang W and Chen P 2014 *Chem. Soc. Rev.* **43** 7067
[23] Lherbier A, Blase R X, Niquet Y, Triozon F and Roche S 2008 *Phys. Rev. Lett.* **101** 036808
[24] Lv Y-A, G-l Zhuang G-I, Wang J-g, Jia Y-B and Xie Q 2011 *Phys. Chem. Chem. Phys.* **13** 12472
[25] Cho B, Yoon J, Hahm M G, Kim D H, Kim A R, Kahng Y H *et al* 2014 *J. Mater. Chem.* **2** 5280
[26] Kong J, Franklin N, Zhou C, Chapline M, Peng S, Cho K *et al* 2000 *Science* **287** 622
[27] Umadevi D and Sastry G N 2011 *J. Phys. Chem. C* **115** 9656
[28] Umadevi D and Sastry G N 2011 *J. Phys. Chem. Lett.* **2** 1572
[29] Chen W, Duan L and Zhu D 2007 *Environ. Sci. Technol.* **41** 8295
[30] Panigrahi S, Bhattacharya S, Banerjee S and Bhattacharyya D 2012 *J. Phys. Chem. C* **116** 4374
[31] Roman T, Dino W A, Nakanishi H and Kasai H 2006 *Eur. Phys. J. D.* **38** 117
[32] Kumar A, Reddy A L M, Mukherjee A, Dubey M, Zhan X, Singh N *et al* 2011 ACS *Nano* **5** 4345
[33] Reddy A L M, Srivastav A, Gowda S R, Gullapalli H, Dubey M and Ajayan P M 2010 *ACS Nano* **4** 6337
[34] Rao J S, Zipse H and Sastry G N 2009 *J. Phys. Chem. B* **113** 7225
[35] Sharma B, Rao J S and Sastry G N 2011 *J. Phys. Chem. A* **115** 1971
[36] Mahadevi A S and Sastry G N 2011 *J. Phys. Chem. B* **115** 703
[37] Umadevi D and Sastry G N 2015 *Phys. Chem. Chem. Phys.* **17** 30260
[38] Zhang Y H, Chen Y B, Zhou K C, Liu C H, Zeng J, Zhang H L *et al* 2009 *Nanotechnology* **20** 185504
[39] Zou Y, Li F, Zhu Z H, Zhao M W, Xu X G and Su X Y 2011 *Eur. Phys. B* **81** 475
[40] Becke A D 1993 *J. Chem. Phys.* **98** 5648
[41] Ditchfield R, Hehre W J and Pople J A 1971 *J. Chem. Phys.* **54** 724
[42] Frisch M J, Trucks G W, Schlegel H B, Scuseria G E, Robb M A, Cheeseman J R *et al* 2010 Gaussian Inc., Wallingford, CT
[43] Zhao Y and Truhlar D G 2008 *Theor. Chem. Acc.* **120** 215
[44] Petersson G A, Bennett A, Tensfeldt T G, Al-Laham M A, Shirley W A and Mantzaris J 1988 *J. Chem. Phys.* **89** 2193
[45] Petersson G A and Al-Laham M A 1991 *J. Chem. Phys.* **94** 6081
[46] Frisch M J, Pople J A and Binkley J S 1984 *J. Chem. Phys.* **80** 3265
[47] Dai J Y and Yuan J M 2010 *Phys. Rev. B* **81** 165414
[48] Bai L and Zhou Z 2007 *Carbon* **45** 2105
[49] Charles W, Bauschlicher J and Ricca A 2004 *Phys. Rev. B* **70** 115409

RESEARCH ARTICLE

International Journal of Science, Technology and Society
Vol 4, No. 2 (2017) : 00-00

A review on theoretical studies of various types of Drug-DNA Interaction

Ruchi Mishra, Asheesh Kumar, Ramesh Chandra, Devesh Kumar*

Department of Physics, School of Physical and Decision Sciences, Babasaheb Bhimrao Ambedkar University, VidyaVihar, Rae Bareilly Road, Lucknow-226 025, India.

Publication Info

Article history:
Received : 01.07.2017
Accepted : 21.09.2017
DOI:

Key words:
Minor Groove Binders, Intercalators, Major Groove Binders, Molecular Docking, Molecular Dynamics, MMPBSA/ MMGBSA, QM/MM.

Corresponding author:
Devesh Kumar

Email:
*dkclcre@yahoo.com

ABSTRACT

A large number of the currently used chemotherapeutic anticancer agents fall into the category of DNA-binding drugs. Study of interactions of various drugs with DNA plays a key role in pharmacology. Due to the potential application of such drugs to cancer and beyond, further discovery and characterization of such compounds are of considerable interest. The combinations of distinct binding modes will improve the stability of recognition and enhance target specificity with respect to both DNA structure as well as sequence. The current review gives an overview of the recently used computational chemical techniques to understand mechanism of drug-DNA interaction. The discussions will provide a theoretical protocol for complementing experimental techniques, generation of database for structure activity/property relationship in drug-DNA complexes. This will be helpful for the improvement of existing drugs, design of new drugs etc.

INTRODUCTION

Deoxyribonucleic acid (DNA) was first discovered by Friedrich Miescher, when he was working with white blood cells obtained from the pus drained out from surgical bandages and determined that the DNA was rich in phosphorous and acidic in nature. However the role of DNA to store heredity information was not reported before 1940s until Avery and co-workers published that the nucleic acids are the genetic information carriers and not proteins (Avery *et al.*, 1944). In 1950 Chargaff recognized that the composition of DNA is unique for each and every species. Chargaff also found that when DNA is broken into its components, the amount of guanine fluctuated from one organism to another is always equal to the cytosine and the amount of cytosine is equal to the amount of thymine (Chargaff, 1951). Rosalind Frankllin elucidates basic helical structure of DNA on the basis of X-ray crystallography technique. In 1953, Watson and Crick scooped Franklin's and Chargaff's information and cracked the code of DNA structure (Chargaff, 1950; Watson, 1953a; Watson, 1953b). They recognized that the relationship between the nitrogenous bases suggested by Chargaff may be due to the complementary base pairing between adenine-thymine and guanine-cytosine and due to this type of base pairing they discovered the hydrogen bonding between these bases, which is currently known as Watson-Crick hydrogen bonding. With this information they modeled a right-handed double helical structure of DNA in which phosphate backbone lied outside the helix and the bases are held together by hydrogen bonding pointed towards the center of helix.

In 1979, a first crystal structure of left-handed double helical DNA $d(CGCGCG)_2$ at atomic resolution was reported, known as Z-DNA (Wang, 1979). After a year, the single-crystal structure analysis of right-handed B-DNA, with the self-complementary dodecamer sequence $d(CGCGAATTCGCG)_2$ was discovered by Dickerson and co-workers. This dodecamer is one of the most studied DNA fragments (Wing, 1980). These discoveries revealed that how the genetic information passes from one to next generation. The most common conformations of DNA are B-, A-, Z-DNA and B-form DNA is the most common occurring conformation. In this type of DNA, the base pairs are perpendicular to the helix axis and twisted by 36^0 with respect to each other. A single turn in the double helix consists of 10 base pairs (Table 1). The two strands of the

Table 1. Structural properties of A-, B-, Z-form DNA.

Conformation	Helix Sense	Twist/bp (Å)	Rise/bp (Å)	Residues /turn	Sugar pucker	Groove Width (Å)		Groove Depth (Å)	
						Minor	Major	Minor	Major
A-DNA	right	32.7	2.56	11	C3'-endo	11	2.7	2.8	13.5
B-DNA	right	36	3.4	10	C2'-endo	5.7	11.7	7.5	8.8
Z-DNA	left	-9,-51	3.8	12	C3'-endo (Syn)	-	8.8	3.7	3.7

double helix are separated by two different grooves minor groove and major groove. Specific recognition of DNA sequences by small molecules is achieved by the combination of hydrogen bond acceptor/donor sites available on the major groove or minor groove of DNA.

DNA is the pharmacological target of many anticancer drugs which are currently under clinical trials. Transcription and replication are the vital processes essential for the survival of the living system. In transcription, information is fetched from DNA to RNA and has recourse to synthesize protein in the body. In replication, DNA yield self-replication process and reconstruct two identical strands. DNA starts these processes only after receiving the signal which is usually in the form of regulatory protein to a specific region of DNA. If this regulatory protein is mimicked by a drug molecule (mainly heterocyclic aromatic molecule), then the functions of DNA can be artificially modulated, inhibited or activated by this small molecule to cure or control a disease. DNA involved in vital processes such as replication, transcription etc. are of particular interest as target for wide range of anticancer and antibiotic drugs (Chaires, 1998; Chaires, 1997; Chaires, 2008; Hurley, 2002).

Molecular interaction between drugs and DNA is a field of current research and also plays an important role in its biological activity. Many anticancer therapies depend on the interaction of drug molecule with DNA. These interactions may cause damage of DNA in cancerous cells by inhibiting the process of replication or transcription, which inhibits the growth of cancer cells. To design efficient chemotherapeutic agents and better anticancer drugs, it is important to inspect the interaction of drug with DNA. The number of known DNA-based drug targets is very limited in comparison to the protein based drug targets and also the number of available structures of DNA-drug complexes is also small relative to protein-drug complexes deposited in the PDB (Berman *et al.,* 2000).

Different Modes of DNA binding with Drug

There are many binding modes in which drug molecule can interact with DNA such as surface binding to their minor or major grooves, intercalation between adjacent base pairs, covalent attachments to the double helix, or electrostatic binding. Thus both covalent as well as non-covalent interactions were found between drug molecules and DNA. DNA interacting drug molecules are given in Table 1.

Covalent Binding

Many chemotherapeutic drug molecules which are in clinical use bind with DNA not only non-covalently but also by covalent binding. Covalent binding in DNA is irretrievable and regularly points to complete inhibition of DNA processes and subsequent cell death. Drug molecule covalently binds with DNA via inter- and intra-strand cross linking or alkylation. Covalent binders of DNA are the high binding strength (Paul and Bhattacharya, 2012; Liu and Sadler, 2011). The covalent binders are also known as alkylating agents because they can attach an alkyl group to DNA and are also used in the treatment of Cancer. Alkylating agents are the important class of anticancer drugs, they play crucial role in the cure of several types of cancers. Alkylating agents have methyl or other alkyl groups (C_nH_{2n+1}) onto molecules. Chemical structure of some important alkylating agents is shown in Figure 1. Alkylating agents are involved in reaction with the preferential N-7 position of guanine and N-3 of adenine in DNA. Thus the base pairing of the DNA could be inhibited and this leads to miscoding of DNA. Alkylating agents can interact to DNA via three mechanisms. In first mechanism an alkylating agent attaches alkyl group to the nucleic acid bases, this results in the DNA being fragmented by repair enzymes in their attempts to replace the alkylated bases. In second mechanism alkylating agent leads to DNA damage due to formation of cross-links and bonds between atoms in the DNA. In this process, two bases are linked together by alkylating agents that has two DNA-binding sites. Cross-linking prevents DNA from being separated for synthesis or transcription. In third type of mechanism, alkylating agents causes the mispairing of the nucleotides leading to mutations (Silvestri and Brodbelt, 2013; Kondo *et al.,* 2010). The nitrogen

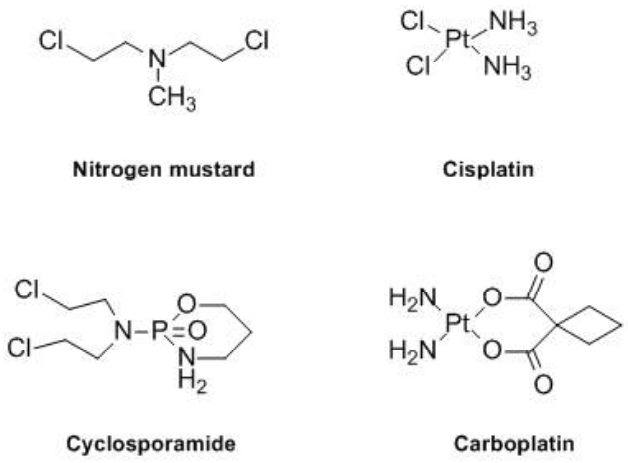

Fig. 1. Chemical structure of some DNA alkylating agents.

mustards were the first alkylating agent used medically, as well as the first modern cancer chemotherapies (Bauer and Povrik, 1997). Cis-platin is one of the anticancer antibiotics, which covalently binds to DNA, which makes an intra/ interstrand cross-link with nitrogens on the DNA bases and is used in the treatment of testicular, ovarian, head and neck cancers. Most alkylating drugs are mono functional methylating agents (e.g. temozolomide[TMZ], N-methyl-N'-nitro-N-nitrosoguanidine [MNNG], and dacarbazine), bifunctional alkylating agents such as nitrogen mustards (e.g. chlorambucil and cyclophosphamide), or chloroethylating agents (e.g. nimustine [ACNU], carmustine [BCNU], lomustine [CCNU], and fotemustine) (Kondo *et al.,* 2010; Rajski and Williams, 1998; Park and Hurley, 1997).

Non-covalent Binding

Non-covalent binding drug may change DNA torsional tension, interrupt protein-DNA interactions, and potentially lead to the breaking of DNA strands. All of these can have substantial effects on gene expression. Non-covalent interactions, in particular hydrogen bonding and stacking interactions, determine the structure of biomolecules (such as nucleic acids and proteins). While it is understood that hydrogen bonding is essential for the specificity of base pairing, ð-ð stacking interactions between planar aromatic rings of nucleobases are equally important contributions to the final stability of nucleic acid structures. Although individually weak, the additive power of these interactions has large cooperative stabilizing effects. Non-covalently binding of drug with DNA is mainly classified into two category viz. groove binders and intercalators. Groove binders are of two types: minor groove binders and major groove binders. Groove binders are highly sequence-specific. The two types of grooves in nucleic acid differ in hydrogen-bonding, electrostatic potential and in degree of hydration. Mainly the large protein molecules binds to the major groove of DNA while small molecules generally bind to the minor groove of DNA which are long elongated structures with a curvature that acquires the shape of the minor groove.

Minor Groove Binders

Minor groove binders usually consist of aromatic rings covalently linked by sigma bonds. Small molecules can form hydrogen bond to the nucleic bases, generally N3 of adenine and O2 of thymine. Minor groove binders generally bind with A-T rich region of the DNA. This preference in addition to the designed propensity for the electro negative pockets of AT sequences is probably due to better vander Waals contacts between the ligand and groove regions and also because of the steric hindrance in the latter, presented by the C2 amino group of the guanine base (Nelson *et al.,* 2007; Khan *et al.,* 2012; Privalov *et. al,* 2007). Sequence specific DNA-binding proteins commonly binds with the major groove because of numerous possibilities for hydrogen bonds with donors and acceptors on the nucleic bases, which provides complex stability and sequence specificity. Proteins and small molecule binding to the minor groove of DNA; depends upon the hydration properties of minor grooves, the latter binding to that AT-rich regions in which water ordering is most prevalent. Thus the minor groove binding is normally driven by the very large entropy of releasing the ordered water, despite an unfavorable enthalpy (Wemmer and Dervan, 1997; Sterkowski and Wilson, 2007; Gilbert and Feigon, 1991). Minor-groove binding usually involves greater binding affinity and higher sequence specificity than that of intercalator binding. Minor-groove has been demonstrated for neutral, mono-charged and multicharged ligands (Baily and Chaires, 1998). Generally, minor-groove binders show AT-rich region selectivity, several factors are responsible for this preference. The electrostatic potential of AT-rich region is greater than that of GC-rich region. On the other hand, the dimensions of the minor groove at AT sites are narrower and deeper than at the GC sites. This difference is due to the differences in the ionic interactions in the two types of base pairs (Hamelberg *et al.,* 2001). The cationic minor-groove binders include the lexitropsins and their conjugates, analogues of Hoechst 33258, DAPI and diarylamidines, Berenil, SN series, and pentamidines (Bhattacharya and Thomas, 2000; Erikson *et al.,* 1993; Brown *et al.* 1979).

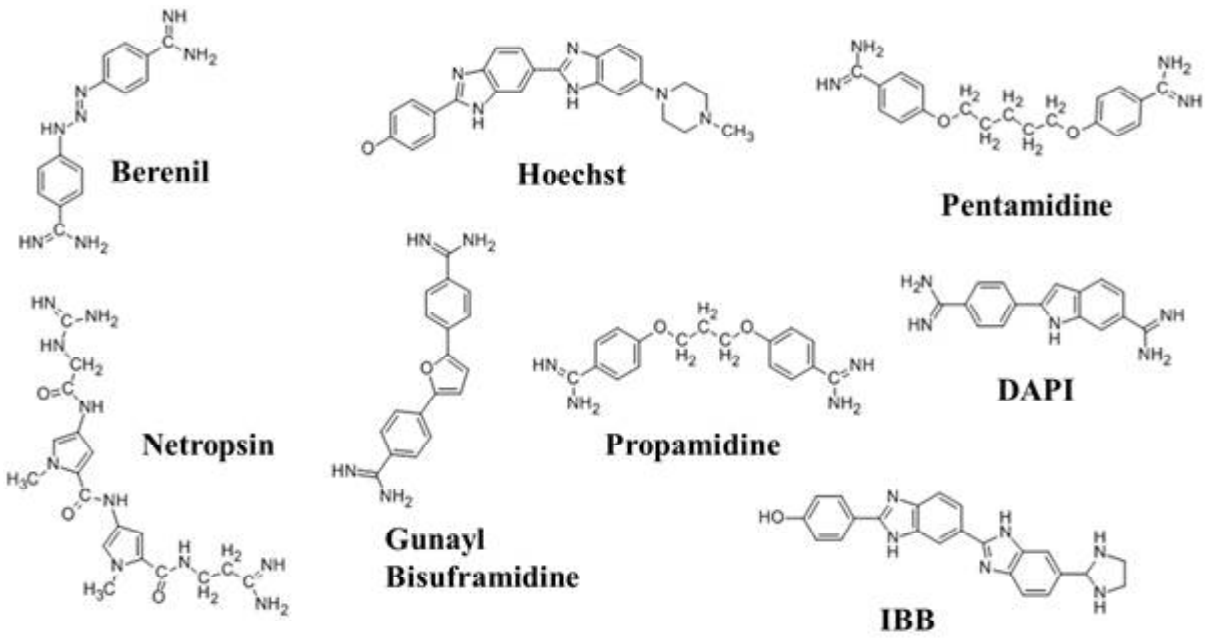

Fig. 2. Chemical Structure of some DNA minor groove binders.

Intercalators

Another type of non-covalently binding drugs is intercalators which are generally planar heterocyclic molecule which stacks between the two adjacent nucleic acid base pairs. The complex remains stabilized because of ð-ð stacking between the drug molecule and DNA bases. Intercalation was first explained by Lerman, in which the drug molecule held rigidly perpendicular to the DNA backbone without breaking up the hydrogen bonding between the nucleic bases (Lerman, 1963). This may be distorting the sugar phosphate backbone and also leads to decrease in the pitch (Williams *et al.,* 1990). The driving forces for the stability of DNA-intercalator complex are vanderWaals, hydrophobic, stacking or charge transfer forces and hydrogen bonding and electrostatic forces also become important for the stabilization of complexes (Wang, 1992). DNA intercalation results in conformational changes in DNA structure, causing lengthening, stiffing and unwinding of DNA helix. Intercalation needs changes in the torsional angles of sugar-phosphate backbone to adjust the incoming aromatic compound, which causes separation between the base pairs with a lengthening of the DNA approximately 3.4Å and decrease in helical twist, unwinding the DNA in the vicinity of the binding site to less than 36° base pair (Neto and Lapis, 2009). Intercalation preferentially occurs at GC-rich sequences because these sequences get unstacked easily. Intercalators generally cause more significant distortion to the conformation of DNA. Echinomycin, noglamycin, triostin A, acridine, cis-Platin, adriamycin, ethidium, propidium, actinomycn D, adriamycin are some examples of the DNA intercalating agents (Pigram *et al.,* 1992).

There are few major binding modes for reversible binding of molecule to the DNA: (i) electrostatic interactions with the anionic sugar phosphate backbone of DNA (ii) interaction with DNA minor groove (iii) interaction with DNA major groove (iv) intercalation between DNA base pairs via DNA minor groove (v) intercalation between DNA base pairs via DNA major groove and (vi) threading intercalation mode. After the intercalation of a structure, the access of another intercalator to binding site next to neighboring intercalation pocket is hindered. This phenomenon is referred as the "neighbor exclusion principle" and could be explained considering that due to intercalation the significant structural changes in DNA with deep alterations in the nucleotide secondary structure (Neto and Lapis, 2009; Yen *et al.,* 1982; Tanious *et al.,* 1991). Intercalating compounds without bulky substituents can intercalate without having significant part of molecule in either minor or major groove, this type of molecules (DACA, proflavin etc.) are called classical intercalators (Pigram *et al.,* 1972). Some of the intercalating molecules have bulky substituents, and these bulky substituents are placed in the major or minor groove along with intercalating moiety. These types

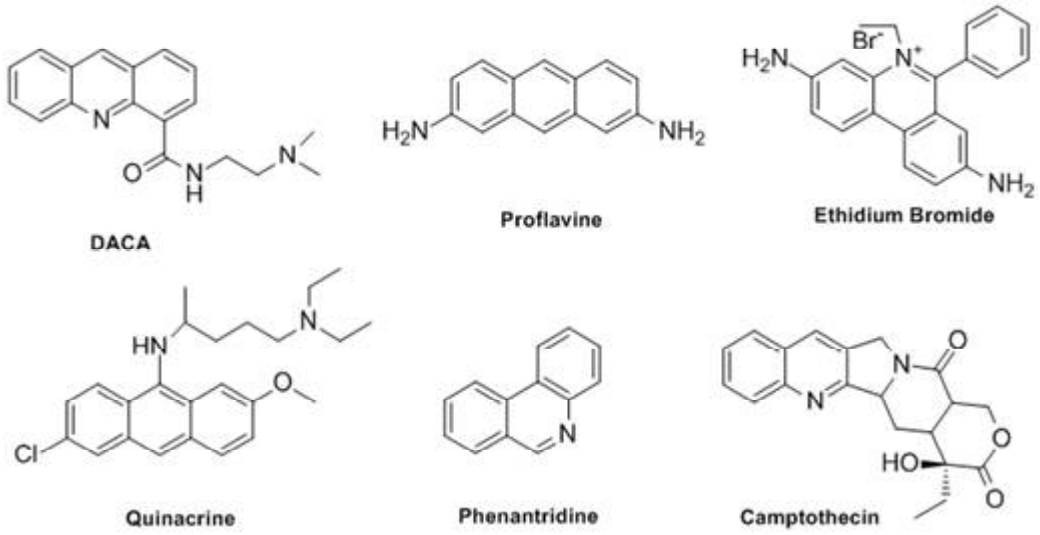

Fig. 3. Chemical Structure of some DNA intercalators.

of intercalators are called threading intercalators (Martinez and Chacon-Garica, 2005). In threading intercalation complexes, an aromatic system inserted between base pairs, while bulky substituent binds strongly with both major and minor groove (Neto and Lapis, 2009; Yen *et al.,* 1982). Other important intercalating drugs are the anthracyclin, daunorubicin, adriamycin, quinacrine and actinomycin have bulky substituents that must be in one groove or the other after the planar aromatic ring of the drugs is bound by intercalation (Tanious *et al.,* 1991; Rao and Kollman, 1987; Bond *et al.,* 1975; Wilson *et al.,* 1998; Martinez and Chacon-Garica, 2005; Denny, 2002; Nakamoto *et al.,* 2008; Wheate *et al.,* 2007; Baraldi *et al.,* 1999; Reddy *et al.,* 1999).

Major Groove Binders

The major groove is wider than the minor groove, the groove width values for B-form of DNA are 11.6 Å and 6.0 Å respectively. Due to this difference in dimension, the major groove is the target for many DNA-interacting proteins. Many biological macromolecules such as proteins interact by the variety of hydrogen bond acceptor and donor supplied in the major groove (Simonsson *et al.,* 1998; Singh and Lambowitz, 2001; Mamoon *et al.,* 2002). It is important for a major groove binding molecule that it could block access to proteins that recognize the same groove. This can be achieved by sequence affinity and sequence selectivity (Scheilf, 1988). DNA duplexes which are made up of polypurine–polypyrimidine sequences can be read by oligomers and bind to the major groove and form hydrogen bond with nucleic bases of the purine strand. These are called triplex-forming oligonucleotides (TFOs) (Thoung and Helene, 1993; Jain and Bhattacharya, 2010). Another form of major-groove recognition could be achieved by peptide nucleic acids (PNAs) (Neilsen, 1999; Ganesh and Kumar, 2005).

DNA interacting organometallic compounds

Many coordination complexes possess an intercalating ligand in their coordination sphere; the study of such complexes reveals the preferential geometry of the metal center, the nature of the intercalating ligand and the number and the position of the substituents over the intercalating ligand in the capacity and selectivity of the coordination complexes to intercalate with DNA. These coordination compounds bind to DNA via two interaction modes: irreversible (covalent or coordination binding) and reversible (intermolecular association). The later binding mode can be further classified into electrostatic interactions, groove binding and intercalation. However, these coordination complexes may exhibit a preference for a particular binding mode or a nucleotide sequence depending upon the size and the shape of the molecule (Han *et al.,* 2004; Hazarika *et al.,* 2012; Juan *et al.,* 2013; Rodrigo 2015).

All mononuclear platinum complexes could form intrastrand and interstrand adducts with DNA. When interstrand lesion is formed, massive distortions of the B-DNA are observed. Similarly, intrastrand lesion, while it forms much more readily than the interstrand lesion, it induces mutational events via the distortion of its nucleic acid target. Binuclear platinum (II) complexes were designed and synthesized and their interactions were studied with calf thymus DNA and a small 49 base pair

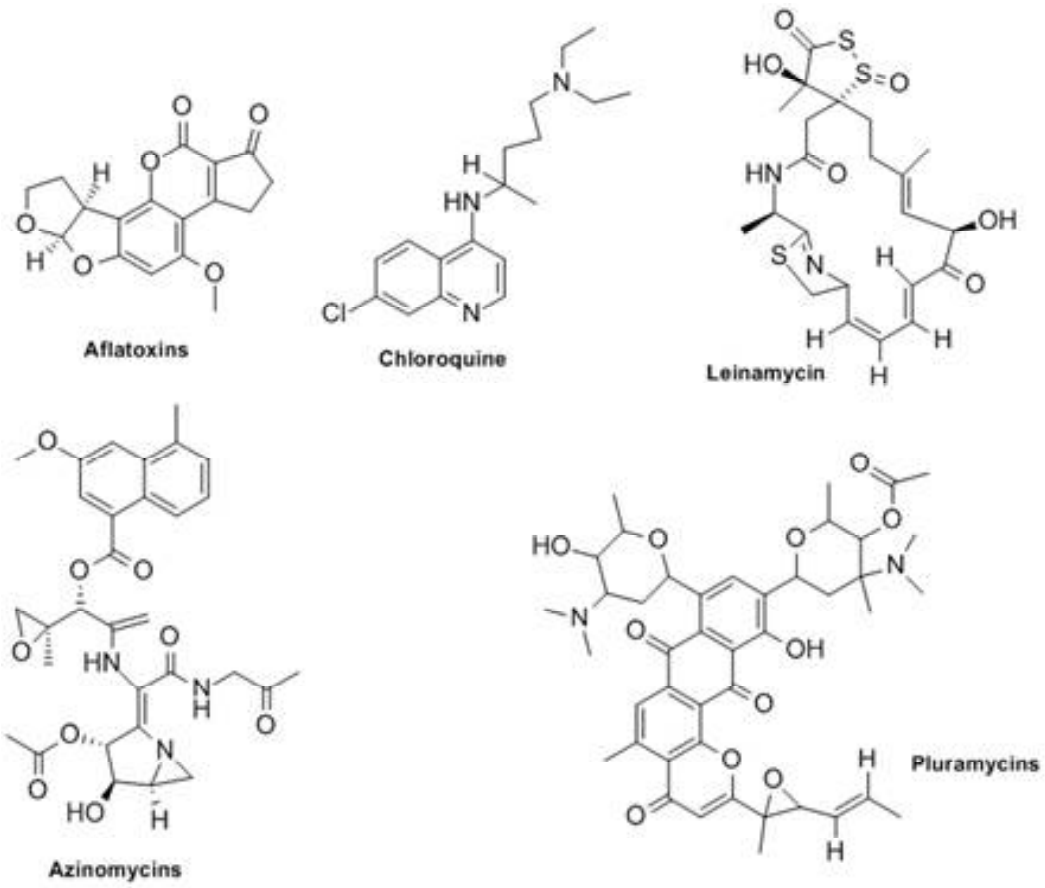

Fig. 4. Chemical Structure of some Major Groove Binders.

oligodeoxyribonucleotide. Owing to the presence of the pyridyl ligands, this compound induces a much higher degree of DNA unwinding than that seen with the either of the ammonia bound complexes, as well as the mononuclear trans-[$PtCl_2$-$(py)_2$]. Similarly, to the mononuclear compound [(Pt(trans)-$(py)_2Cl_2$-µ-(diaminobutane)]$^{2+}$. These alterations likely involve [(Pt(trans)-$(py)_2Cl_2$-µ-(diaminobutane)]$^{2+}$ to undergo ð-stacking interactions upon DNA association which in turn, disfavors the Z-DNA conformations. Importantly, interstrand-cross links formation is very efficient for all three complexes. The directionality is dependent upon the nature of the cross link. Interestingly, this is a unique example of anti-cancer drugs behaving in this manner. Molecules normally reach DNA through one of the grooves and react to either the backbone or the nucleobases. Electrostatic binding occurs due to the interaction between cations with the negatively charged phosphate backbone at the exterior surface of the DNA helix (Konstantinos *et al.,* 2013; Decatris *et al.,* 2004).

The use of transition metal complexes gives a strong tool to the drug chemists to develop and study molecules capable of obtaining specific DNA-drug interactions considering the multiple options of d-block metals from the periodic table. Transition metals are dynamic in geometry, electron affinity and reactivity, making them excellent choices to feed the ongoing field of antineoplastic drug discovery.

The fundamental factors of these interactions still possess greatest gaps in as much as the results provided by experimental designs that do not involve expensive protocols and equipment that are extremely poor to identify the specific interactions due the lower energetic changes involved, making clear the use of methodologies such as computational chemistry to help solve these problems (Ge and Sun, 2007; Wang and Lippard, 2005; Umezawa, 1976; Wong and Giandomenico, 1999; Bonnet, 1995).

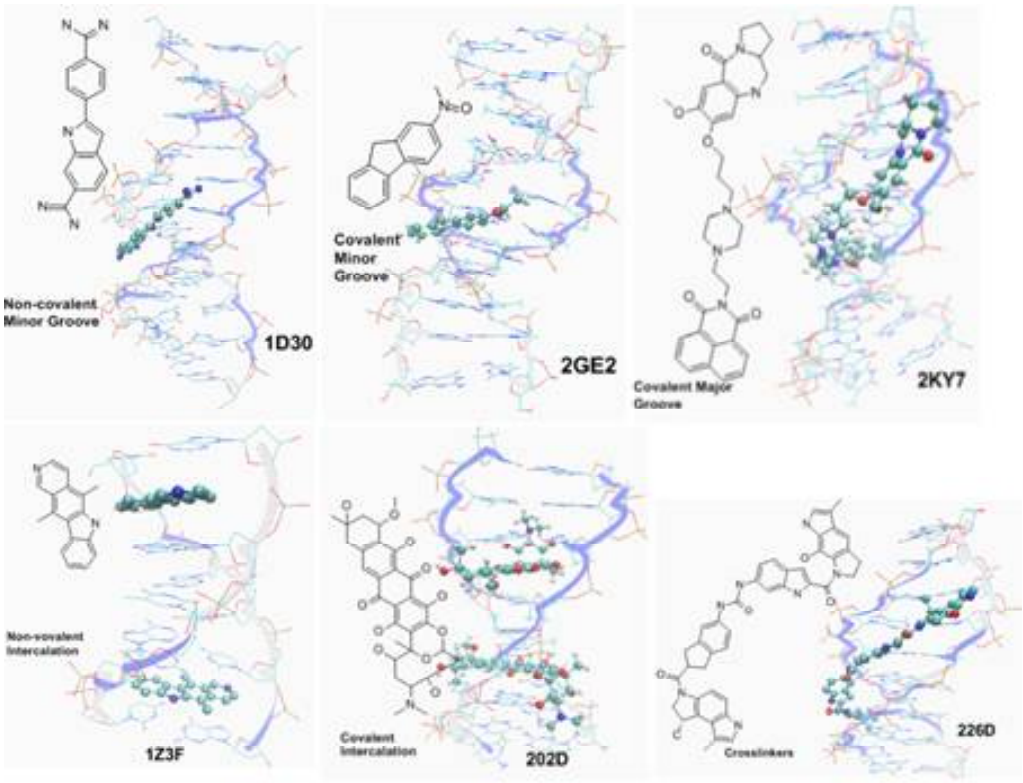

Fig. 5. Different modes of Drug-DNA Binding.

Experimental studies used in drug-DNA interaction

Experimental Studies play crucial role to explore the drug-DNA interaction. Thermodynamic studies provide the necessary information of free energy, enthalpy, entropy, heat capacity and also about the binding constant changes during complex formation. Various experimental techniques which are used to understand the interaction of drug molecule with nucleic acid holds Infrared (IR), Raman, Circular dichorism, UV-visible, Nuclear magnetic resonance (NMR) spectropies, Atomic Force Microscopy (AFM), Electrophoresis, Mass spectrometry, Viscosity measurements, Thermal denutration studies, Cyclic square wave and Differential pulse voltammetry, etc. The above techniques have been used as a primary tool to characterize the behavior of drug-DNA binding and the consequences of such type interaction on the structure of nucleic acid. The commonly used experimental techniques are UV-visible, fluorescence spectroscopies and cyclic voltammetry (Sirajuddin *et al,* 2013). Chaires also provided the change in experimental values of thermodynamic properties during the drug-DNA complex formation (Garbett and Chaires, 2012). This information may be helpful for the theoretical prediction and structural analysis. In the binding of drug molecule with bimolecular system, the solvent water plays important role. In the case of DNA-focused drug approaches there is a need to understand how water take part in the reorganization (CheathamIII *et al.,* 1995; Bellissent-Funel *et al.,* 2016; Yu, 2008; Chalikian and Breslauer, 1998).

Molecular Modelling Studies for drug-DNA interaction

Molecular Docking

Molecular docking method is used to predict the structure (or structures) of the intermolecular complex formed between two or more molecules. The docking program generates large number of possible structures, and so it is required to rank them according to their score to identify those of most interest (Blaney and Dixon, 1995; Abagyan and Totrov, 2001; Kuntz, 1992; Lengauer and Rarey, 1996). The three important components of docking are:

(1) Representation of the system.

(2) Conformational space search via a search algorithm.

(3) Ranking of potential solutions using the scoring function.

Table 2. DNA interacting drug molecules.

Non-covalent Binding drug molecules			Covalent binding drug molecules
Groove Binding		Intercalators	
Minor groove Binders	Major Groove Binders		
Berenil	Chloroquine	Daunomycin	Nitrogen mustard
Netropsin	Netamycine	Nogalamycin	PBDs
Hoechst 33258	Cis-{$Pt(NH_3)_2$(pyridine)}$_2$+	Ethidium bromide	CC1065
Distamycin A	Aminoglycoside (NB33)	Proflavine	Cis-platinum
GunaylBisuframidine	Chlorambucil	Ellipticine	Menogril
SN6999	Nimustein	Diplamine	Clomesone
SN7176	Pluramycins	Chlorpheniramine	Cyclodisone
Pentamidine	Aflatoxins	Bis-napthalimide	
MithramycinPilcamycin	Azinomycins	Doxorubcin	
Chromomycin A3	Leinamycin	Aminoacridines	
Diamidine-2-phenylindole	Ditercalinium	Arylaminoalcohals	
Bisbenzimadoles		Coumarines	
Bleomycin		Cystodytin	
Mitomycin		Diplamine	
FR66979		YO and YOYO-1	
Duocarmycins		QuinolinesQuinoxalines	
CC-1065		Echnomycin	
Yatakemycin		Methapyrilene	
Neocarzinostatin		Tamoxifen	
Calicheamicins		M-AMSA	
Retrorsine		Indoles	
Anthramycins		Aclarubicin	
Saframycins		Idarubicin	
Ecteinascidin 743		Epirubcin	
Isochrysohermidin		Pirarubcin	
		Valrubicin	
		Amrubicin	
		Actinomycin D	
		Camptothecin	
		Topotecan	
		Irinotecan	
		Rebeccamycin	
		Podophyllotoxin	
		Etoposide	
		Teniposide	
		Elsamicin	
		Dynemicin	
		Triostin A	
		Luzopeptins	
		Sandramycin	

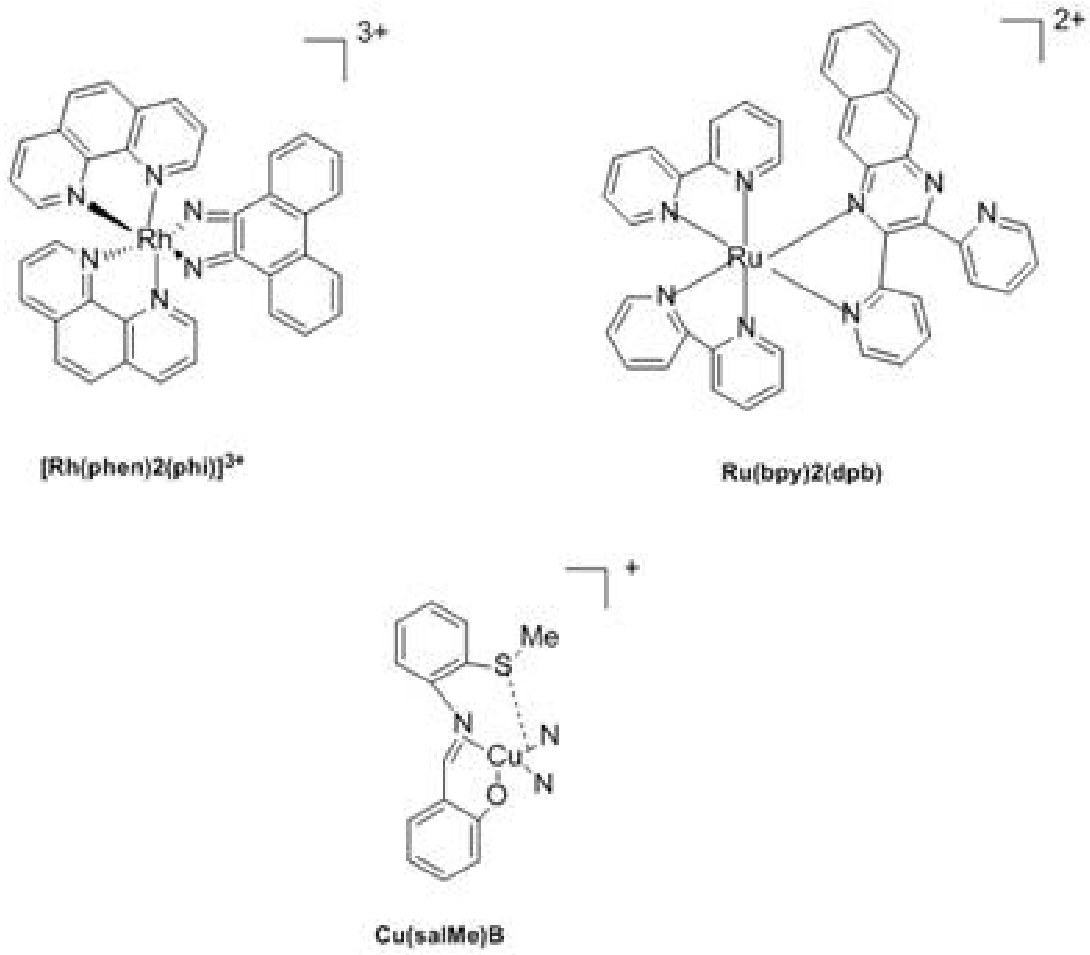

Fig. 6. Chemical Structure of some organometallic compounds.

The aim of docking process is to computationally simulate the molecular identification process and accomplish an optimized conformation so that the free energy of the overall complex is minimized. The docking method involves many degrees of freedom. With six degrees of translational and rotational freedom along with the conformational degrees of freedom of each molecule results large number of possible binding modes between the two molecules. Computationally it would be too expensive to generate all the possible conformations. Various algorithms have been developed to tackle the docking problem. These algorithms can be characterized according to the number of degrees of freedom that they ignore. The search algorithm generates number of conformations for a particular ligand, and scoring functions are then applied in order to identify the energetically most favorable pose (Gane and Dean, 2000; Schneider and Bohm, 2002; Sthal and Rarey, 2001; Koremer, 2003; Gohlke and Klebe, 2002).

Surflex (Surflex, 2007), Autodock (Morris *et al.,* 1998), DOCK (Rarey*et al.,* 1996), GOLD (Jones *et al.,* 1997), Glide, Flex (Rarey *et al.,* 1996), CDOCKER (Wu *et al.,* 2003) are the docking programs which are used for the Molecular Docking of drug and DNA. A study shows that the GOLD and GLIDE docking protocols seem to be very reliable in modelling of nucleic acid ligand complexes (Srivastava *et al.,* 2011). Molecular docking studies show that the intercalators generally bind to the CG –rich region of DNA and minor groove binders to the AT-rich region of DNA (Srivastava *et al.,* 2011; Rashidaa and Ahsen, 2015). ð-ð interaction dominates in case of intercalators. In case of minor groove binders, hydrogen bonds are mainly formed between minor groove binders and the functional groups on the bases are exposed in the grooves via their end groups and also their amide or other linker groups. Other studies shows that if the nature of ligand with DNA is not known, the exact mode of binding of ligand to DNA cannot be predicted on the

basis of molecular docking as a result other molecular modelling techniques such as molecular dynamics simulation and thermodynamics integration will be required to further resolve the problem (Mariya and Ahsen, 2015).

Molecular Dynamics Simulation

Molecular Dynamics (MD) is the most important computational approach for the study of flexible nucleic acids. In MD, the motion of a biomolecular system under the effect of a "force" (i.e a specified force field) is simulated by following its molecular configurations in time, according to Newton's equation of motion (second law). A MD calculation starts with a set of initial co-ordinates and velocities. The force-field calculates the potential energy and the forces acting on the system, and Newton's second law is used to determine the accelerations on each particle. Numerical integration of these accelerations provides a set of new velocities and positions, which are used to build up a trajectory. MD protocols include algorithms to fix the temperature and the pressure, allowing the simulation of nucleic acids under conditions close the physiological ones. MD simulations of nucleic acid are performed using explicit solvent representations including thousands of water molecules and periodic boundary conditions (PBC). Explicit water models used in bio molecular simulations include TIP3P, TIP4P, SPC, extended SPC/E, and F3C models among these TIP3P is the most commonly used model (Jorgensen *et al.,* 1983; Berendsen *et al.,* 1987; Levitt *et al.,* 1997). Ions (generally Na^+ and Cl^-) are introduced to neutralize the system and simulate the given ionic strength. The evolution of trajectories shows the movement from one stable state to a stable one.

In mid 1990s several groups performed successful MD simulations of DNA and RNA with an explicit representation of solvent using the AMBER, CHARMM nucleic acid, or GROMOS force field. Various force fields used in the nucleic acid simulation includes, CHARMM, AMBER, GROMOS, OPLS, ENCAD and BMS26. AMBER (Case *et al.,* 2012), GROMACS (Hess *et al.,* 2008), CHARMM (Brooks *et al.,* 2009) and NAMD (Nelson *et al.,* 1996) are the popular software packages for the simulation of nucleic acid ligand complexes. The three latest force-fields (AMBER-99, CHARMM-27 and BMS) provide accurate representations of standard DNA and RNA structures (York *et al.,* 1995; Cheatham *et al.,* 1995; Weerasinghe *et al.,* 1995; Weiner and Kollman, 1981; Nilsson and Karplus, 1986; Gunsteren and Berendsen, 1986). The root-mean square deviation (RMSD) of the simulated nucleic acids with respect to experimental structures is small, the dihedral distributions are correct, and the average helical parameters are also reasonably close to the accepted experimental values. Among the variety of available force fields, CHARMM and AMBER are the most popular force fields (Cheatham and Young, 2001; Cheatham *et al.,* 1999; Cornell *et al.,* 1995; Foloppe and Mackerell, 2000; Mackerell and Banavali, 2000; Langley, 1998; Modesto *et al.,* 2003). In a number of studies for the minor groove binders and intercalators, computational methods have shown good agreement with the experimental results (Kamal *et al.,* 2007, 2009, 2010a, 2010b).

MMPBSA/MMGBSA Method

The molecular mechanics energies combined with the Poisson-Boltzmann or generalized Born and surface area continuum solvation (MMPBSA/MMGBSA) methods are popular approaches to calculate the free energy difference between two states, generally the bound and unbound state of two solvated molecules, or ultimately to compare free energy of two different solvated conformations of the same molecule (Gohlke and Klebe, 2002; Kolman *et al.,* 2000; Srinivasan *et al.,* 1998; Hou *et al.,* 2011; Homeyer and Gohlke, 2012). Snapshots obtained from MD simulation are used for the calculation, yielding an average of the energies. The free energy of binding is calculated by the equations mentioned below-

$$\Delta G_{bind} = \Delta H - T\Delta S$$

$$\Delta G_{bind} = (\Delta E_{MM} + \Delta G_{SOL}) - T\Delta S$$

Where,

$$\Delta E_{MM} = (E_{MM}{}^{complex} - E_{MM}{}^{receptor} - E_{MM}{}^{ligand})$$

$$\Delta G_{SOL} = (\Delta G_{SOL}{}^{complex} - \Delta G_{SOL}{}^{receptor} - \Delta G_{SOl}{}^{ligand})$$

$$\Delta S = (S^{complex} - S^{receptor} - S^{ligand})$$

where ÄH is the enthalpic contribution to binding energy, $ÄE_{MM}$ is the average difference in molecular mechanics energy, while $ÄG_{SOL}$ term accounts for the solvation free energy(including both polar and non-polar component); T is the temperature and ÄS is a change in entropy.

Thus the net binding free energy of complex system is equal to the sum of an intermolecular energy (calculated using MM force field), a solvation free energy term and an

entropic term. Polar solvation free energies is calculated either solving the linear Poisson Boltzmann (PB) equation or more approximate, or computationally effective Generalized Born (GB) model, whereas the non-polar contribution is estimated from a linear relation to the solvent accessible surface area (SASA). Entropy contributions to the free energy are estimated either by quasi-harmonic analysis or by using normal mode analysis (Schwarzl *et al.,* 2002; Rastelli *et al.,* 2010).

The MMPBSA calculations are based on single minimized structures, rather than on a large number of MD snapshots. This method will save much computational time but ignores dynamical effects. It has been observed that the more time can be saved by performing the minimizations in a GB continuum model. Hou *et al.* reveals that the MMGBSA results varied with the length of simulation, but there is no gain of using simulation longer than 4ns (Hou *et al.,* 2011). H.K. Srivastava *et. al.* proves that the MM-PBSA based interaction energies calculated from the MD Simulations are in good agreement with the experimental values for the DNA-ligand complexes (Srivastava *et al.,* 2011; Spackova *et al.,* 2003). The MMPBSA approach was originally developed for the AMBER software but recently some automatic scripts have also been presented for the freely available GROMACS, NAMD and APBS software. A study reveals that the energies calculated using g_mmpbsa (GROMACS) and the AMBER MM-PBSA package is approximately similar and the difference of 1-3 kcal/mol has been observed due to the difference in $\ddot{A}G_{polar}$ (Kumari *et al.,* 2014). The difference in $\ddot{A}G_{polar}$ is observed because of different algorithms, implemented in APBS and PBSA (Mishra *et al.,* 2015).

Quantum Mechanics/Molecular Mechanics (QM/MM) method

The QM/MM concept was introduced, as early as 1976, by Warshel and Levitt, who presented a semi empirical QM/MM treatment for a chemical reaction in lysozyme (Warshel and Levitt, 1976). Combined QM/MM theory has emerged as the method of choice for modeling local electronic events in large bimolecular systems.The basic idea is to describe the active site (where chemical reactions or electronic excitations occur) by quantum mechanics, as accurately as needed, while capturing the effects of the bimolecular environment by molecular mechanics, i.e., at the classical force field level. The accuracy of QM and speed of MM, combined QM/MM methods enable the modelling of reactive bimolecular systems at reasonable computational cost with the necessary accuracy. Due to the potential uses of this method, this field gained the Nobel Prize in chemistry in 2013. There are two schemes to calculate the total energy of the system the additive and the subtractive scheme (Sherwood *et al.,* 2008, Senn and Theil, 2009, Sherwood *et al.,* 2003). Regarding this boundary schemes, the labeling conventions given in **Figure** that apply to covalent bonds across the QM-MM boundary.

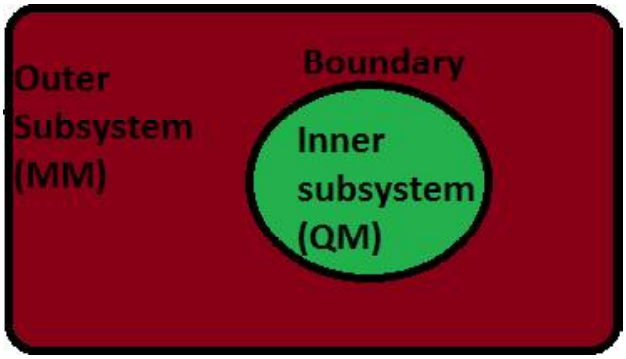

Subtractive schemes:

$$E_{QM/MM}(system) = E_{MM}(system) + E_{QM}(QM) - E_{MM}(QM)$$

Where $E_{QM/MM}$(system) is the total energy, E_{MM}(system) is the MM energy of the entire system, E_{QM}(QM) the QM energy of the QM region and E_{MM}(QM) the energy of the QM region.

The scheme encounters shortcomings due to the treatment of interactions between QM and MM region only at MM level which is inaccurate. This scheme needs the MM parameters for the QM region. Parameters are not usually available for these systems which are present in excited electronic states or contain transition metals.

Additive schemes:

$$E_{QM/MM}(system) = E_{MM}(system) + E_{QM}(QM) - E_{QM-MM}(QM, MM)$$

In this scheme, the total energy of the system $E_{QM/MM}$ (system) comprises of only three components viz., E_{MM} (MM) theMM energy of the MM region only, E_{QM} (QM) the QM energy of the QM region andthe $E_{QM^{\circ}MM}$(QM, MM) a term which interfaces between the QM/MM through the inclusion of bonded and non-bonded interactions. The bonded interactions account for bond stretching, bending and torsion while the non-bonded account for the vander Waals and electrostatic interactions.

The key to such QM/MM methods is the coupling between the electric field from the surrounding and the QM Hamiltonian in the active-site region. This requires careful treatment of the boundary between the QM and MM

regions.

The most important part of QM/MM is partitioning of the system. The basic considerations for QM/MM partitioning are:

(a) The choice of the QM region is usually made by consideration of the chemical problem; chemical arguments normally suggest a minimum-size QM region which can then be enlarged to check the sensitivity of the QM/MM results with regard to such an extension.

(b) If a QM/MM division through covalent bonds cannot be avoided, cut only unconjugated single bonds, preferably without electronically demanding substituent's (e.g., cut unpolar C–C bonds).

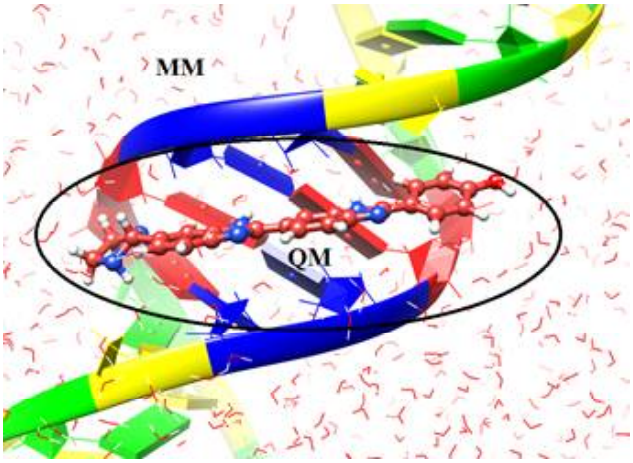

Fig. 7. QM/MM partitioning: *drug* and associated bases (QM region), remaining bases and water molecules and ions (MM region).

A common procedure for QM/MM calculations is to take a crystal structure from protein data bank as a starting point for the calculations and add hydrogen, missing atoms etc. and water molecules (soak the complete system). Thereafter, the system is equilibrated using MM followed by molecular dynamics production run and low-energy snap-shots are studied. These snapshots will eventually be taken for QM/MM calculations.These structures contain the bimolecular system in a droplet of water (20000-30000 atoms) and this setup requires a lot of prior work to avoid errors and wrong choices for the actual QM/MM calculations. Further study of the reaction mechanism is similar to the typical methods for the study of gas-phase reaction (Senn and Theil, 2007, Frieesner and Guallar, 2005).

The computational chemistry techniques, especially the hybrid methods (ONIOM) based on combination of several theoretical approaches, have been developed by Morokuma and co-workers for large biomolecular systems (Svensson *et al.,* 1996, Morokuma *et al.,* 2001, Morokuma, 2003, Kuno *et al.,* 2003). In many studies, the ONIOM method is used for the study of DNA binding drugs (Rebeca *et al.,* 2009, Ahmadia *et al.,* 2011, Robertazzi and Platts, 2006).

CONCLUSION

In this review the different types of small organic molecules which targeted DNA have been discussed. The array of available computational approaches and molecular modelling methods are being used for complementing the experimental efforts to improve the existing drugs and also in designing novel drug candidates which can act as good DNA inhibitor. Advances in computational resources over the last years have made screening of large chemical libraries and application of molecular dynamics and quantum chemical calculations feasible. This review seeks to highlight some recent molecular modelling studies performed at electronic structure level to study the mechanism of drug interaction to DNA which can give an insight in designing inhibitors for the treatment of cancer and AIDS.

ACKNOWLEDGEMENTS

AK like to acknowledge the UGC for financial support. The authors are thankful to Dr G. Narahari Sastry for his support and discussions.

REFERENCES

Abagyan R, Totrov M (2001). High-throughput docking for lead generation. Curr. Opin. Chem. Biol., 5: 375-382.

Ahmadia, F, Jamalia N, Jahangard-Yektaa S, Jafari B, Nourib B, Najafic F, Rahimi-Nasrabadid M (2011). The experimental and theoretical QM/MM study of interaction of chloridazon herbicide with ds-DNA, Spectrochimica Acta Part A, 79: 1004– 1012.

Avery OT, Maclend C, Mc Carty M (1944). Studies on the chemical nature of the substance inducing transformation of pneumococcal types. The Journal of Experimental Medicine, 79: 137-158.

BaillyC ,Chaires JB (1998). Sequence-specific DNA minor groove binders. Design and synthesis of netropsin and Distamycin analogs. Bioconjugate Chem., 9: 513–538.

Baraldi PG, Cacciari B, Guiotto A, Romagnoli R, Zaid AN, Spalluto G (1999). DNA minor-groove binders: results and design of new antitumor agents. IL Farmaco, 54: 15-25.

Bauer GB, Povirk LF (1997). Specificity and kinetics of interstrand and intrastrandbifunctional alkylation by nitrogen mustards

at a G-G-C sequence. Nucleic Acids Research, 25: 1211-1218.

Bellissent-Funel M, Hassanali A, Havenith M, Henchman R, Pohl P, Sterpone F, Spoel D, Xu Y, Garcia AE (2016). Water Determines the Structure and Dynamics of Proteins. Chem. Rev., 116: 7673-7697.

Berendsen HJC, Grigera JR, Straatsma TP (1987). The missing term in effective pair potentials J PhysChem, 91: 6269-6271.

Berman HM, Westbrook J, Feng Z, Gilliland G, Bhatt TN, Weissig H, Shindyalov IN, Bourne PE (2000). The protein Data bank. Nucleic Acid Research, 28: 235-242.

Bhattacharya S, Thomas M (2000). Facile synthesis of oligopeptidedistamycin analogs devoid of hydrogen-bond donors or acceptors at the N-terminus: sequence-specific duplex DNA binding as a function of peptide chain length. Tetrahedron Lett., 41: 5571–5575.

Blaney JM, Dixon JS (1993). A good ligand is hard to find: Automated docking methods Perspectives in Drug Discovery and design, 1: 301-319.

Bond PJ, Langridge R, Jennette KW, Lippard SJ (1975). X-ray fiber diffraction evidence for neighbor exclusiona binding of a platinum metallointercalation reagent to DNA. Proc. Natl. Acad. Sci., 72: 4825-4829.

Bonnett R (1995). Photosensitizers of the porphyrin and phthalocyanine series for photodynamic therapy. Chem. Soc. Rev., 24: 19–33.

Brooks BR, Brooks CL 3rd, Mackerell AD Jr, et al. (2009). CHARMM: the biomolecular simulation program. J Comput Chem., 30: 1545–1614.

Brown DG, Sanderson1 MR, Skelly JV, Terence CJ, Brown2 T, Garman3 E, Stuart3 DI, Neidle1 S (1990). Crystal structure of a berenil–dodecanucleotide complex: the role of water in sequence-specific ligand binding. EMBO J., 9: 1329–1334.

Case DA, Berryman JT, Betz RM, Cerutti DS, Cheatham III TE, Darden TA, Duke RE, Giese TJ, Gohlke H, Goetz AW, Homeyer N, Izadi S, Janowski P, Kaus J, Kovalenko A, Lee TS, LeGrand S, Li P, Luchko T, Luo R, Madej B, Merz KM, Monard G, Needham P, Nguyen H, Nguyen HT, Omelyan I, Onufriev A, Roe DR, Roitberg A, Salomon-Ferrer R, Simmerling CL, Smith W, Swails J, Walker RC, Wang J, Wolf RM, Wu X, York DM, Kollman PA (2015). AMBER 2015, University of California, San Francisco.

Chaires JB (1997). Energetics of drug-DNA interactions. Biopoly., 44: 201-215.

Chaires JB (1998). Drug—DNA interactions. Curr. Opin. Struc. Biol., 8: 314-320.

Chaires JB (2008). Calorimetry and thermodynamics in drug design. Annu. Rev. Biophys., 37:135-151.

Chalikian TV, Breslauer KJ (1998). Thermodynamic analysis of biomolecules: a volumetric approach. Current Opinion in Structural Biology, 8: 657-664.

Chargaff E (1950). Chemical Specificity of Nucleic Acids and Mechanism of their Enzymatic Degradation. Experimentia, 6: 201-209.

Chargaff E (1951). Some recent studies on the composition and structure of nucleic acids. J Cell Physiol. Suppl., 38: 41-59.

Cheatham III TE, Miller JL, Fox T, Darden TA, Kollman, PA(1995). Molecular Dynamics Simulations on Solvated Biomolecular Systems: The Particle Mesh Ewald Method Leads to Stable Trajectories of DNA, RNA, and Proteins. J Am ChemSoc, 117: 4193-4194.

Cheatham TE ,Cieplak P, Kollman PA (1999). A modified version of the Cornell et al. force field with improved sugar pucker phases and helical repeat. J. Biomol. Struct. Dyn., 16: 845-862.

Cheatham TE, Young MA (2001). Molecular Dynamics Simulation of Nucleic Acids: Sucesses, Limitations, and Promise. Biopolymers, 5: 232-256.

Cornell WD, Cieplak P, Bayly CI, Gould IR, Merz KM, Fergurson DM, Spellmeyer DC, Fox T, Caldwell JW, Kollman PA (1995). A Second Generation Force Field for the Simulation of Proteins, Nucleic Acids, and Organic Molecules. J. Am. Chem. Soc., 117: 5179-5197.

Decatris, MP, Sundar S, O'Byrne KJ (2004). Platinum-based chemotherapy in metastatic breast cancer: current status. Cancer Treat. Rev., 30: 53–81.

Denny WA (2002). Acridine Derivatives as Chemotherapeutic Agents. Current Medicinal Chemistry, 9: 1655-1665.

Eriksson S, Kim SK, Kubista M, Norden B (1993). Binding of 42 6-diamino-2-phenylindole (DAPI).to AT regions of DNA: evidence for an allosteric conformational change. Biochemistry, 32: 2987–2998.

Foloppe N, Mackerell AD (2000). All-atom empirical force field for nucleic acids: I. Parameter optimization based on small molecule and condensed phase macromolecular target data. J. Comput. Chem., 21: 86-104.

Friesner RA, Banks JL, Murphy RB, Halgren TA, Klicic JJ, Mainz DT, Repasky MP, Knoll EH, Shelley M, Perry JK, Shaw DE, Francis P, Shenkin PS (2004). Glide: A New approach for rapid, accurate docking and scoring. 1. Method and assessment of docking accuracy. J. Med. Chem. 2004, 47: 1739-1749.

Friesner RA, Guallar V (2005). Ab initio quantum chemical and mixed quantum mechanics/molecular mechanics methods for studying enzymatic catalysis. Annu. Rev. Phys. Chem. 56: 389-427.

Gane PJ, Dean PM (2000). Recent advances in structure-based rational drug design.Curr. Opin. Struct. Biol., 10: 401-404.

Ganesh KN, Kumar VA (2005). Conformationally constrained PNA analogs: Structural evolution towards DNA/RNA binding selectivity. Acc. Chem. Res., 38: 404–412.

Garbett NC, Chaires JB (2012). Thermodynamic studies for drug design and screening. Expert opin. Drug Discov., 7: 299-314.

Gareth J, Peter W, Robert CG, Andrew RL, Robin T (1997). Development and Validation of a Genetic Algorithm for Flexible Docking. J. Mol. Biol., 267: 727-748.

Ge R, Sun H (2007). Bioinorganic chemistry of bismuth and antimony: target sites of metallodrugs. Acc. Chem. Res., 40: 267-274.

Gilbert DE, Feigon J (1991). Structural analysis of drug-DNA interactions. Current Opinion in Structural Biology, 1: 439-445.

Gohlke H, Klebe, G (2002). Approaches to the Description and Prediction of the Binding Affinity of Small-Molecule Ligands to Macromolecular Receptors. Angew. Chem. Int. Ed., 41: 2644-2676.

Gunsteren van, WF, Berendsen HJC (1986). GROMOS 86: Groningen Molecular Simulation Program Package; University of Groningen: Groningen, The Netherlands.

Hamelberg D, Williams LD, Wilson WD (2001). Influence of the dynamic positions of cations on the structure of the DNA minor groove: sequence-dependent effects. J. Am. Chem. Soc., 123: 7745-7755.

Han D, Wang H, Ren N (2004). Molecular modeling of B-DNA site recognition by Ru intercalators: molecular shape selection. J Mol Model, 10: 216-222.

Hazarika P, Bezbaruah B, Deka RP, Deka J, Barman TK, Medhi OK, Medhi C (2012). The DNA binding features of ruthenium complexes compared with cisplatin : docking, force field and QM/MM studies. The Clarion, 1: 24-32.

Hess B, Kutzner C, van der Spoel D, Lindahl E (2008). GROMACS 4: algorithms for highly efficient, load-balanced, and scalable molecular simulation. J Chem Theory Comput., 4: 435-447.

Homeyer N, Gohlke H (2012). Free energy calculations by the molecular mechanics Poisson-Boltzmann surface area method. Mol Inf, 31:114-122.

Hou T, Wang J, Li YY, Wang W (2011). Assessing the performance of the molecular mechanics/Poisson Boltzmann surface area and molecular mechanics/generalized Born surface area methods. II. The accuracy of ranking poses generated from docking. J Comp Chem, 32: 866-877.

Hurley LH (2002). DNA and its associated processes as targets for cancer therapy. Nat. Rev. Cancer, 2: 188-200.

Jain AK, Bhattacharya S (2010). Groove binding ligands for the interaction with parallel-stranded ps-duplex DNA and triplex DNA. Bioconjugate Chem., 21: 1389-1403.

Jones G, Willett P, Glen RC, Leach AR, Taylor R (1997). Development and validation of a genetic algorithm for flexible docking. J. Mol. Biol., 267: 727-748.

Jorgensen WL, Chandrasekhar J, Madura JD, Impey RW, Klein ML (1983). Comparison of simple potential functions for simulating liquid water. J ChemPhys , 79: 926-935.

Juan CG, Rodrigo G, Fernando C, Lena R (2013). Metal-Based Drug-DNA Interactions. J. Mex. Chem. Soc., 57: 245-259.

Kamal A, Rajender, Reddy DR, Reddy MK, Balakishan G, Shaik TB, Chourasia M, Sastry GN, (2009).Remarkable enhancement in the DNA-binding ability of C2-fluoro substituted pyrrolo[2,1-c][1,4]benzodiazepines and their anticancer potential. Bioorg. Med. Chem., 17: 1557-1572.

Kamal A, Khan MNA, Reddy KS, Rohini K, Sastry GN, Sateesh B, Sridhar B (2007). Synthesis, Structure Analysis and Antibacterial Activity of Some Novel 10-Substituted 2-(4-Piperidyl/Phenyl) -5, 5-Dioxo [1,2,4] triazolo [1,5b] [1,2,4] Benzothiadiazine Derivatives. Bioorganic and Medicinal Chemistry Letters, 17: 5400-5405.

Kamal A, Reddy KS, Khan MNA, Shetti RVCRNC, Ramaiah MJ, Pushpavalli SNCVL, Srinivas C, Pal-Bhadra M, Chourasia M, Sastry GN, Juvekar A, Zingde S, Barkume M (2010). Synthesis, Synthesis, DNA-binding ability and anticancer activity of benzothiazole/benzoxazole–pyrrolo[2,1-c][1,4]benzodiazepine conjugates. Bioorg. Med. Chem., 18: 4747-4761.

Kamal A, Shankaraiah N, Reddy C R, Prabhakar S, Markandeya N, Srivastava HK, Sastry GN (2010). Synthesis of bis-1,2,3-triazolo-bridged unsymmetrical pyrrolobenzodiazepinetrimers via 'click' chemistry and their DNA-binding studies. Tetrahedron, 66: 5498-5506.

Khan GS, Shah A, Zia-ur-Rehman, Barker D(2012). Chemistry of DNA minor groove binding agents. Journal of photochemistry and photobiology B: Biology, 115: 105-118.

Kollman PA, Massova I, Reyes C, Kuhn B, Huo S, Lillian C, Matthew L, Taisung L, Yong D, Wei W, Oreola D, Piotr C, Jaysharee S, Case DA, CheathamIII TE (2000). Calculating structures and free energies of complex molecules: combining molecular mechanics and continuum models. AccChem Res, 33: 889-97.

Kondo N, Takahashi A, Ono K, Ohnishi T (2010). DNA Damage Induced by Alkylating Agents and Repair Pathways. Journal of Nucleic Acids, 54351: 1-7.

Konstantinos G, Shaun TM, James AP (2013). QM/MM description of platinum–DNA interactions: comparison of binding and DNA distortion of five drugs. RSC Adv., 3: 4066-4073.

Koremer RT (2003). Molecular modelling probes: docking and scoring. Biochemical Society Transactions, 31: 980-984.

Kumari R, Kumar R, Lynn A (2014). G_mmpbsa - a GROMACS tool for high throughput MM-PBSA calculations. J ChemInf Model, 54: 1951-1962.

Kuntz I (1992). Structure-based strategies for drug design and discovery. Science, 257: 1078-1082.

Langley DR (1998). Molecular dynamic simulations of environment and sequence dependent DNA conformations: the development of the BMS nucleic acid force field and comparison with experimental results. J. Biomol. Struct. Dyn., 16: 487-509.

Lengauer T, Rarey M (1996). Computational methods for biomoleculardocking.Curr. Opin. Struct. Biol., 6: 402-406.

Lerman LS (1963).The structure of the DNA-acridinecomplex. Biochemistry, 49: 95-101.

Levitt M, Hirshberg M, Sharon R, Laidig KE, Daggett V (1997). Calibration and Testing of a Water Model for Simulation of the Molecular Dynamics of Proteins and Nucleic Acids in Solution. J PhysChem B, 101, 5051-5061.

Liu H, Sadler PJ (2011). Metal complexes as DNA intercalators. Accounts of Chemical Research, 44: 349-359.

Kuno M, Hannongbua S, Morokuma K. Theoretical investigation on nevirapine and HIV-1 reverse transcriptase binding site interaction, based on ONIOM method. Chem. Phys. Lett. 380 (2003). 456-463.

MacKerell AD, Jr., Banavali NK (2000). All-atom empirical force field for nucleic acids: 2). Application to solution MD simulations of DNA. J. Comp. Chem. 21: 105–120.

Mamoon NM, Song Y, Wellman SE (2002). Histone h1(0).and its carboxyl-terminal domain bind in the major groove of DNA. Biochemistry, 41: 9222-9228.

Mariya al-Rashidaa, Ahsen, S (2015). In search of a docking protocol to distinguish between DNA intercalators and groove binders: Genetic algorithm Vs shape-complementarity based docking methods. RSC Advances, 1-27.

Martinez R, Chacon-Garcia L (2005). The Search of DNA-Intercalators as Antitumoral Drugs: What it worked and what did not Work. Current Medicinal Chemistry, 12: 127-151.

Mishra R, Gaur AS, Chandra R, Kumar D (2015). Molecular Docking and Molecular Dynamics Study of DNA Minor Groove Binders. International Journal of Pharmaceutical Chemistry and Analysis, 2: 161-169.

Modesto O, Alberto P, Agnes N, Luque FJ (2003). Theoretical methods for the simulation of nucleic acids. Chem. Soc. Rev, 32: 350–336.

Morokuma K (2003). ONIOM and Its Applications to Material Chemistry and Catalysis Korean Chem. Soc. 24: 797-801.

Morokuma K, Musaev DG, Verena T, Basch H, Torrent M, Khoroshun DV (2001). Model studies of the structures, reactivities, and reaction mechanisms of metalloenzymes, IBM J. Res. Dev. 45: 367-375.

Morris GM, Goodsell DS, Halliday RS, Huey R, Hart WE, Belew RK, Olson AJ (1998). Automated docking using a Lamarckian genetic algorithm and an empirical binding free energy function. J. Comp. Chem. 19: 1639-1662.

Nakamoto K, Tsuboi M, Strahan GD (2008). Drug-DNA Interactions: Structures and Spectra. John Wiley & Sons, Inc, 119-208.

Nelson MT, Humphrey W, Gursoy A, Dalke A, Kale LV, Skeel RD, Schulten K (1996). NAMD: a parallel, object oriented molecular dynamics program. Int J SupercomputAppl High Perform Comput. 10 : 251-268.

Nelson SM, Ferguson LR, Denny WA (2007). Non-covalent ligand/DNA interactions: Minor groove binding agents. Mutation Research, 623: 24-40.

Neto BAD, Lapis AAM (2009). Recent Developments in the Chemistry of Deoxyribonucleic Acid (DNA). Intercalators: Principles, Design, Synthesis, Applications and Trends. Molecules, 14: 1725-1746.

Nielsen PE (1999). Peptide nucleic acids as therapeutic agents. Curr. Opin. Struct. Biol., 9: 353–357.

Nilsson L, Karplus M (1986). Empirical energy functions for energy minimization and dynamics of nucleic acids. J Comput Chem, 7: 591-616.

Park HJ, Hurley LH, (1997). Covalent Modification of N3 of Guanine by (+).-CC-1065 Results in Protonation of the Cross-Strand Cytosine. J. Am. Chem. Soc., 119: 629-630.

Paul A, Bhattacharya S (2012). Chemistry and biology of DNA-binding small molecules. Current Science, 102: 212-231.

Pigram WJ, Fuller W, Hamilton LD (1972). Stereochemistry of Intercalation: Interaction of Daunomycin with DNA. Nature New Biology, 235: 17-19.

Privalov PL, Dragon AI, Colyn C, Breslauer KJ, Remeta DP, Minetti CSA (2007). What Drives Proteins into the Major or Minor Grooves of DNA? J. Mol. Biol., 365: 1-9.

Rajski SR, Williams RM (1998). DNA Cross-Linking Agents as Antitumor Drugs.Chem. Rev., 98: 2723-2795.

Rao SNR, Kollman PA (1987). Molecular mechanical simulations on double intercalation of 9-amino acridine into d(CGCGCGC).d(GCGCGCG).: Analysis of the physical basis for the neighbor-exclusion principle. Proc. Natl. Acad. Sci., 84: 5735-5739.

Rarey, M. et al. (1996). A fast flexible docking method using an incremental construction algorithm. J. Mol. Biol. 261, 470–489.

Rastelli G, Del Rio A, Degliesposti G, Sgobba M (2010). Fast and accurate predictions of binding free energies using MM-PBSA and MM-GBSA. J Comput Chem., 31: 797-810.

Rebeca R, Begoña G, Giuseppe R, Arturo S, Giampaolo B, (2009). Computational study of the interaction of proflavine with d(ATATATATAT).2 and d(GCGCGCGCGC).2. Journal of Molecular Structure: THEOCHEM , 915: 86–92.

Reddy BSP, Sondhi SM, Lown JW (1999). Synthetic DNA minor groove-binding drugs. Pharmacology and Therapeutics, 84: 1-111.

Remers WA (1979). The Chemistry of Antitumor Antibiotics, Wiley, New York, 1-290.

Robertazzi A, Platts JA (2006). A QM/MM Study of Cisplatin–DNA Oligonucleotides: From Simple Models to Realistic Systems. Chem. Eur. J. 12: 5747 - 5756.

Schleif R (1988). DNA binding by proteins. Science, 241: 1182-1187.

Schneider G, Bohm H (2002). Virtual screening and fast automated docking methods. Combinational chemistry: reviews, 7: 64-70.

Schwarzl SM, Tschopp TB, Smith JC, Fischer S (2002). Can the calculation of ligand binding free energy be improved with continuum solvent electrostatics and an ideal-gas entropy correction. J ComputChem, 23: 1143-1149.

Senn HM, Thiel W (2009). QM/MM methods for biomolecular systems. AngewChemInt Ed Engl 48:198-229.

Senn, HM, Theil W (2007). QM/MM methods for biological systems in Topics in Current Chemistry. M. Reiher (Ed.)., Springer, Berlin, 268: 173-290.

Sherwood P, Brooks BR, Sansom MS (2008). Multiscale methods for macromolecular simulations.CurrOpinStructBiol 18: 630-640.

Sherwood P, de Vries AH, Guest MF et al (2003). QUASI: a general purpose implementation of the QM/MM approach and its application to problems in catalysis. J Mol StructTheochem, 632:1-28.

Silvestri C, Brodbelt JS (2013). Tandem Mass Spectrometry for Characterization of Covalent Adducts of DNA with Anti-cancer Therapeutics. Mass Specttrom Rev., 32: 247-266.

Simonsson S, Samuelsson T, Elias P (1998). The Herpes Simplex Virus Type 1 Origin Binding Protein specific recognition of phosphates and methyl groups defines the interacting surface for a monomeric dna binding domain in the major groove of DNA. J. Biol. Chem., 273: 24633-24639.

Singh NN, LambowitzAM (2001). Interaction of a group II intron ribonucleoprotein endonuclease with its DNA target site investigated by DNA footprinting and modification interference. J. Mol. Biol., 309: 361-386.

Sirajuddin M, Ali S, Badshah A (2013). Drug-DNA interactions and their study by UV-Visible, fluorescence spectroscopies and cyclic voltammetry. Journal of Photochemistry and Photobiology B: Biology, 124: 1-19.

Spackova N Cheatham TE, Ryjacek F, Lankas F, Meervelt L, Hobza P, Sponer J (2003). Molecular dynamics simulations and thermodynamics analysis of DNA—drug complexes. Minor groove binding between 4',6-diamidino-2-phenylidole and DNA duplexes in solution. J Am Chem Soc., 125: 1759-1769.

Srinivasan J, Cheatham TE, Cieplak P, Kollman PA, Case DA (1998). Continuum solvent studies of the stability of DNA, RNA, and phosphoramidate-DNA helices. J Am ChemSoc, 120: 9401-4409.

Srivastava HK, Chourasia M, Kumar D, Sastry GN (2011). Comparison of Computational Methods to Model DNA Minor Groove Binders. J. Chem. Inf. Model., 51: 558-571.

Stahl M, Rarey M (2001). Detailed Analysis of Scoring Functions for Virtual Screening. J. Med. Chem., 44: 1035-1042.

Sterkowski L, Wilson B (2007). Noncovalent interactions with DNA: An overview. Mutation Research, 623: 3-13.

Surflex, version 2.11; Tripos, Inc.: St. Louis, MO, 2007.

Svensson MJ, Humbel S, Froese RDJ, Matsubara T, Sieber S, Morokuma K (1996). ONIOM: A Multilayered Integrated MO + MM Method for Geometry Optimizations and Single Point Energy Predictions. A Test for Diels-Alder Reactions and Pt (P(t-Bu).3).2 + H2 Oxidative Addition. J. Phys. Chem., 100: 19357-19363.

Tanious FA, Yen S, Wilson WD (1991). Kinetic and Equilibrium Analysis of a Threading Intercalation Mode: DNA Sequence and Ion Effects, Biochemistry, 30: 1813-1819.

Thuong NT, Hélène C (1993). Stereospecific detection and modification of double helix DNA by oligonucleotides. Angew. Chem., Int. Ed. Engl., 32: 666-690.

Umezawa H (1976). Structure and action of bleomycin. Prog. Biochem. Pharmacol., 11: 18-27.

Wang AHJ (1992). Intercalative drug binding to DNA. Current Opinion in Structural Biology, 2: 361-368.

Wang AHJ, Quigley GJ, Kolpak FJ, Crawford JL, Boom JH, Marel G, Rich A (1979). Molecular structure of a left-handed double helical DNA fragment at atomic resolution. Nature, 282: 680-686.

Wang D, Lippard, SJ (2005). Cellular processing of platinum anticancer drugs. Nature Rev. Drug Discov., 4: 307–320.

Wang J, Hou T, Xu X (2006). Recent advances in free energy calculations with a combination of molecular mechanics and continuum models. CurrComput-Aided Drug Design, 2: 95-103.

Warshel A, Levitt M (1976). Theoretical studies of enzymic

reactions: dielectric, electrostatic and steric stabilization of the carbonium ion in the reaction of lysozyme. J. Mol. Biol., 103: 227-249.

Watson JD, Crick FHC (1953a). Molecular Structure of Nucleic Acids. Nature, 171: 737-738.

Watson JD, Crick FHC (1953b). Genetical implications of the structure of De-oxy ribonucleic Acid. Nature, 171: 964-967.

Weerasinghe S, Smith PE, Mohan V, Cheng YK, Pettitt BM (1995). Nanosecond Dynamics and Structure of a Model DNA Triple Helix in Saltwater Solution. J Am ChemSoc, 117: 2147-2158.

Weiner PK, Kollman PA (1981). AMBER: Assisted model building with energy refinement. A general program for modeling molecules and their interactions. J ComputChem , 2: 287-303.

Wemmer DE, Dervan PB (1997). Targeting the minor grove of DNA. Current Opinion in Structural Biology, 7: 355-361.

Wheate NJ, Brodie CR, Collins JG, Kemp S, Janice R, Aldrich-Wright (2007). DNA Intercalators in Cancer Therapy: Organic and Inorganic Drugs and Their Spectroscopic Tools of Analysis. Medicinal Chemistry, 7: 627.

Williams LD, Egli M, Gao Q (1990). Structure of nogalamycine bound to a DNA hexamer. Proc. Natl. Acad. Sci. USA, 87: 2225-2229.

Wilson WD, Tanious FA, Ding D, Kumar A, Boykin DW, Colson P, Houssier C, Bailly C (1998). Nucleic Acid Interactions of Unfused Aromatic Cations: Evaluation of Proposed Minor-Groove, Major-Groove, and Intercalation Binding Modes. J. Am. Chem. Soc., 120: 10310-10321.

Wing R, Drew H, Takano CB, Tanaka S, Itakura K, Dickerson RE (1980). Crystal structure analysis of a complete B-DNA. Nature, 287: 755-758.

Wong E, Giandomenico CM (1999). Current status of platinum based antitumour drugs. Chem. Rev., 99: 2451-2466.

Wu G, Roberston, DH, Brooks CLIII, Vieth M (2003). Detailed analysis of grid-based molecular docking: A case study of CDOCKER A CHARMM-based MD docking algorithm. J. Comput. Chem., 24: 549-562.

Yen S, Gabbay EJ, Wilson WD (1982). Interaction of aromatic Imides with Deoxyribonucleic Acid. Spectrophotometric and Viscometric Studies, Biochemistry, 21: 2070-2076.

York DM, Yang W, Lee H, Darden T, Pedersen LG (1995). Toward the accurate modeling of DNA: the importance of long-range electrostatics. J. Am. Chem. Soc., 117: 5001-5002.

Yu H, Ren J, Chaires JB, Qu X (2008). Hydration of Drug-DNA Complexes: Greater Water Uptake for Adriamycin Compared to Daunomycin. J. Med. Chem., 51: 5909-5911.

Article

Advanced Science, Engineering and Medicine
Vol. 10, 1–5, 2018
www.aspbs.com/asem

Structural Stability and Electronic Properties of $(Ga_nN_n)_m$ Micro Cluster by Using *Ab-Initio* and Tight-Binding Study

Deep Kumar, Asheesh Kumar, Jitendra Kumar, and Devesh Kumar*

Department of Applied Physics, School of Physical Sciences, Babasaheb Bhimrao Ambedkar University, Vidya Vihar, Lucknow, UP, India

First principle calculations were performed to investigate the electronic properties and structural stability of 1-D condensed cluster. The stability of $(Ga_nN_n)_m$ where $n = 1-4$ and $m = 1-6$ micro cluster is calculated. Due to the linear stacking of these stable isomers, the condensed clusters, $(Ga_nN_n)_m$ where $n = 1-4$ and $m = 1-6$ were modeled. The structural stability of clusters and their building blocks were obtained from the electronic density of states, and it infers that *s–p* hybridization plays a key role in microcluster stabilization. The various calculation shows that the $(Ga_3N_3)_m$ clusters are energetically more stable as compared with other sized condensed cluster but such microclusters can be fragmented into two micro clusters by providing external temperature.

Keywords: Micro-Clusters, Density Functional Theory, Gallium Nitrate, Binding Energy, Carbon Nanotube.

1. INTRODUCTION

The one dimension carbon nanotubes (CNT) is studied by several research groups all across the globe. The potential application of CNT was due to their high mechanical strength, ballistic transport and other novel properties[1] explored such as one-dimensional system of inorganic compounds. The carbon nanotubes and nanowires from Mo–S compound have been extensively studied.[2, 3] Synthesis with ultimate structural and electronic properties and the ability to advance tune their properties by adding dopants is also performed.[4] CdS compounds have attracted the attention as a result of which the synthesis of nanowires[5, 6] nanotubes[7] and nanorods[8–10] with controlled dimensions is performed.

In the recent past the low dimensional semiconductor material has become of great interest in the research field of nanoscience.[11–13] The materials of III–V group semiconductor compound due to their paramount technological potential applications such as photoelectronic devices, photonic integrations, ultrahigh frequency microwave and photovoltaic solar cells are studied predominantly. Gallium nitride (GaN) is an important semiconducting material that exhibits a broad range of potential applications for optoelectronics and high power electronic devices. Light emitting diodes have made a boom in the market with its appearance in the recent past year.[14] The high thermal conductivity provides new routes in high-temperature and high–power electronic devices[15, 16] such as metal semiconductor field effect transistor (MESFETs), high electron mobility transistor (HEMTs) and heterojunction bipolar transistor (HBTs).[17, 18] Furthermore high Curie temperature and room temperature ferromagnetic has been predicted in GaN-doped with transition metal (MT) element.[19–21] GaN nanotubes with inner diameters of 30–200 nm and wall thickness of 5–50 nm were also synthesized.[22] Single-walled GaN nanotube was examined computationally by using first-principle methods.[23] Several theoretical studies on Ga_nN_n clusters up to $n = 4-6$ by BelBruno,[24] Kandallam et al.[25–28] and Song et al.[29–31] are also investigated. To predict the lowest energy of $(Ga_nN_n)_x$ clusters, a number of possible structure isomers were considered for the study. These structures were adopted from those previously proposed for the III–V semiconductor compound cluster such as BN,[32–34] AlN and GaAs.

2. COMPUTATIONAL METHOD

Density functional theory has been used for the optimization of GaN condensed nanocluster and to calculate their ground and excited state properties. Geometrical optimizations have been performed without any constraints imposed on the nanocluster structures. Various possible structures for each GaN cluster were drawn using Gauss

*Author to whom correspondence should be addressed.

View 0.5. For geometry optimization, B3LYP method DFT method, Beck's three parameters with correlation function (Lee-Yang-Parr), and relativistic effective core potential with double zeta basis set, LANL2DZ as implemented in Gaussian 09 programme suit were used. For the evaluation of density of states (DOS) spectrum Gauss Sum 3.0 has been used.

The binding energy per atom (BE) of a cluster is calculated using the formula

$$\mathrm{BE} = \frac{nE(\mathrm{Ga}) + nE(\mathrm{N}) - E(\mathrm{Ga}_n\mathrm{N}_n)}{2n}$$

Where $E(\mathrm{Ga})$, $E(\mathrm{N})$, and $E(\mathrm{Ga}_n\mathrm{N}_n)$ are total energy of a single Ga atom, a single N atom, and Ga_nN_n clusters, respectively and n is the number of Ga or N atoms. Similar calculations were performed using the first principle calculations on optimized Ga_nN_n nanowires with $n = 1-4$ in order to perform the comparison.

3. RESULTS AND DISCUSSION

3.1. Atomic Structure of Ga_nN_n Cluster

First principle calculations on the various Ga_nN_n ($n = 1-4$) clusters, were performed to obtain the stable structure which acts as a fundamental building block of condensed cluster or nano assemblies. Optimized structures are shown in Figure 1 with the BE, HOMO–LUMO gap and Ga–N bond distance of stable isomers are reported in Table I(a)–(c). The stable isomers of Ga_nN_n clusters from $n = 4$ to 12 possesses ring and cage (37) geometries respectively, which is quite comparable to earlier reports.

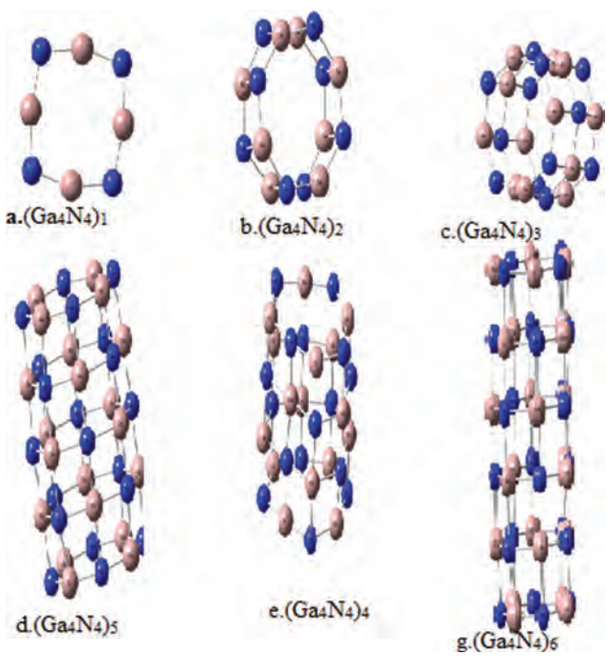

Figure 1. Illustrates the optimized structures of $(Ga_4N_4)_m$ micro cluster.

Table I. The Binding energy, band gap and bond distance $(Ga_2N_2)_n$ where $n = 1-6$.

Atoms	Binding energy/atom (eV)	Band gap (eV)	Bond distance (Å)
	(a)		
$(Ga_2N_2)_1$	10.34	1.49	1.92
$(Ga_2N_2)_2$	10.81	0.84	1.91
$(Ga_2N_2)_3$	11.29	1.30	1.93
$(Ga_2N_2)_4$	11.48	1.33	1.92
$(Ga_2N_2)_5$	11.60	1.54	1.90
$(Ga_2N_2)_6$	11.61	2.43	1.91
	(b)		
$(Ga_3N_3)_1$	10.92	2.11	1.87
$(Ga_3N_3)_2$	11.54	1.60	1.90
$(Ga_3N_3)_3$	11.83	2.12	1.92
$(Ga_3N_3)_4$	11.96	2.32	1.93
$(Ga_3N_3)_5$	12.05	2.39	1.92
$(Ga_3N_3)_6$	12.10	2.49	1.92
	(c)		
$(Ga_4N_4)_1$	11.15	2.65	1.77
$(Ga_4N_4)_2$	11.61	2.35	1.83
$(Ga_4N_4)_3$	11.83	2.52	1.91
$(Ga_4N_4)_4$	11.88	2.43	1.89
$(Ga_4N_4)_5$	12.00	2.69	1.89
$(Ga_4N_4)_6$	11.99	2.42	1.90

3.2. Condensed Clusters

With an understanding of stable isomers of Ga_nN_n with different geometries, condensed cluster of $(Ga_nN_n)_m$ are obtained by linear stacking of m up to 7 units of stable Ga_nN_n isomers ($n = 1-4$). The optimized structure of condensed clusters are shown in Figure 1, the $(Ga_nN_n)_2$ cluster is obtained by condensing one planar Ga_3N_3 isomer at the top while another isomer at the bottom thus increasing the number of Ga–N bonds in the cluster. Similarly, $(Ga_3N_3)_4$ and other condensed clusters, $(Ga_nN_n)_m$ were obtained and optimized structure are shown in Figures 1(b)–(g) further, other–sized $(Ga_nN_n)_2$ cluster are stacked from their basic units of Ga_nN_n.

The Binding Energy and HOMO–LUMO gap of all the condensed (Ga_nN_n) clusters are calculated and the results are shown in Figure 2 along with the cohesive energy per atom and band gap of infinite Ga_nN_n nanowires. As expected, the BE of condensed cluster increases linearly with m and slowly achieves the cohesive energy per atom and band gap of infinite nano wires, as shown in Figure 2(a). In the inset, the BEs, of $(Ga_nN_n)_m$ condensed cluster with respect to the diameter (in terms of n) are shown. Even though the diameter of the $(Ga_3N_3)_m$ condensed clusters is smaller than that of the $(Ga_4N_4)_m$ cluster, beyond $m = 3$. The BE of the cluster is almost equal with that of the latter. The BEs of $(Ga_3N_3)_5$ and $(Ga_4N_4)_5$ are 12.05 and 12.00 eV/atom, respectively. Hence it can be concluded that $(Ga_4N_4)_m$ condensed cluster are more stable as compared to other-sized condensed cluster and preferably this cluster could be extended to

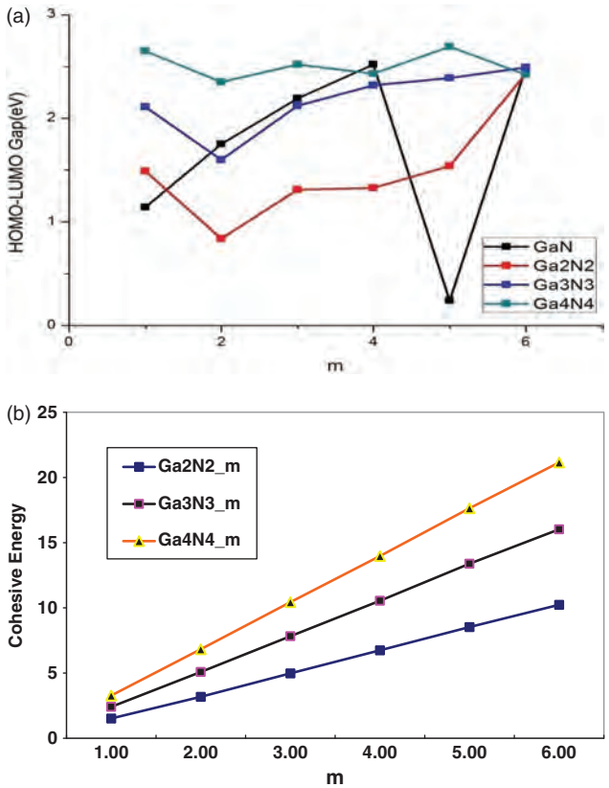

Figure 2. (a) Cohesive energy and (b) HOMO–LUMO gap of $(Ga_nN_n)_m$ are shown. In the inset, BEs of $(Ga_nN_n)_m$ are shown for various n. The band gap shown in figure is less than the bad gap of bulk GaN, which is obtained from the calculation.

nanorod and nanowires. Even our calculations on infinite nanowires support this conclusion as the cohesive energies of $(Ga_3N_3)_3$ and $(Ga_4N_4)_3$ infinite nanowires are almost same (11.83 eV/atom).

Figure 2(b) describes the variation of the HOMO–LUMO gap of the cluster. For $n = 2$, 3 the HOMO–LUMO gap increases as m values increases, and for $n = 4$ its lies between 2.35 to 2.69 eV. The HOMO–LUMO gap for $(Ga_4N_4)_m$ condensed clusters is significantly higher than that of another condensed cluster. This supports our previous statement that $(Ga_4N_4)_m$ condensed clusters are more stable among all the clusters. Further, it may also be noted in Figure 2 that beyond $m = 2$, the HOMO–LUMO gap of $(Ga_1N_1)_m$ atomic wire is less than that of another condensed cluster. It is a consequence of the increase in the number of nonbonding states with the increase in the length of the atomic wire. The HOMO–LUMO gap of all $(Ga_nN_n)_m$ clusters is comparatively less than the band gap of the bulk GaN compound.

3.3. Electronic Structure

To study the structural stability of $(Ga_3N_3)_m$ cluster, total and partial density of states (DOS) of the cluster with $m = 2, 3$ and 4 as shown in Figure 3. The DOS states are

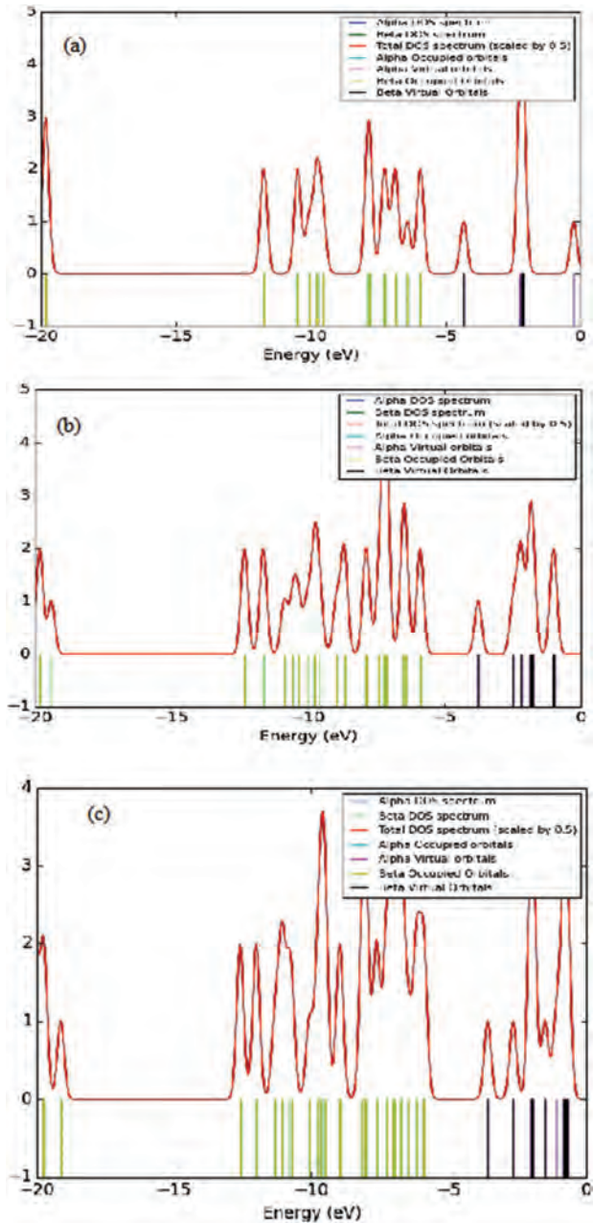

Figure 3. Total and partial DOS of $(Ga_3N_3)_m$ cluster with $m = 2$ (a), $m = 3$ (b), and $m = 4$ (c).

located in the energy range from −13.0 to −0.0 eV. While Ga (S P) states are distributed in the unoccupied region these clusters can be understood on the structural stability of the molecular orbital theory.

3.4. Fragmentation of Condensed Cluster

We also effort the possibility of fragmentation of condensed $(Ga_4N_4)_m$ cluster into smaller units to be aware of their expansion stability for example, that $(Ga_4N_4)_4$ nano wire can fragment into two part of a set of that $(Ga_4N_4)_2$ cluster or that (Ga_4N_4) and that $(Ga_4N_4)_3$

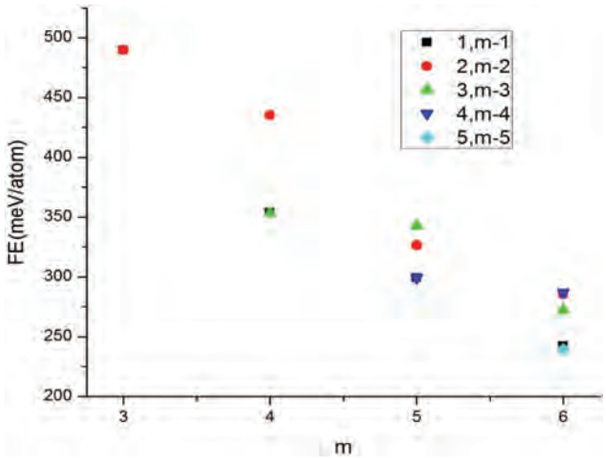

Figure 4. FE versus m of $(Ga_nN_n)_m$ of various possible fragments.

clusters. The fragmentation energy per atom (FE) is calculated from.

$$\mathrm{FE} = \frac{E[(Ga_3N_3)_n] + E[(Ga_3N_3)_{m-n}] - E[(Ga_3N_3)_m]}{6m}$$

Every $(Ga_3N_3)_m$ may be divided into the following two pieces of a possible cluster: $(1, m-1)$, $(2, m-2)$, $(3-m-3)$, $(4, m-4)$. FE is calculated and shown in Figure 4.

Figure 4 shows that when a cluster FE decreases, m values increases. This infers that the condensed clusters under the influence of temperature breaks into smaller units on the order of 450 k. Although the diameter of the condensed cluster as well nanorod-below this temperature can be synthesized.

We condensed the second derivative of the total energy $(\Delta^2 E)$ of the cluster and the cluster understands the structural stability and it is reported in Figure 5. Our calculations conclude that the $\Delta^2 E$ of $(Ga_3N_3)_3$ cluster shows the maximum value and high structural stability of this cluster.

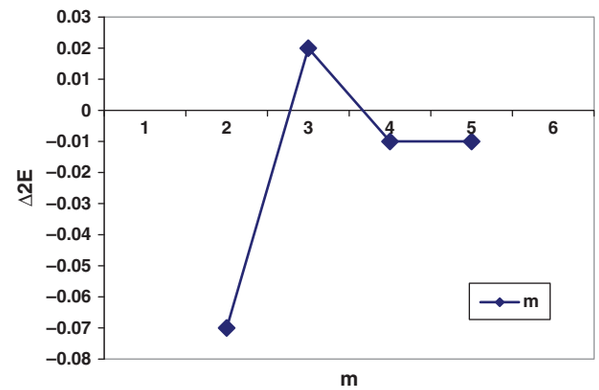

Figure 5. The second derivative of energy of $(Ga_3N_3)_m$ cluster with respect to m. The calculated value by using the formula $\Delta^2 E = E(m+1) + E(m-1) - 2E(m)$.

4. CONCLUSION

The structural stability and electronic properties of $(Ga_nN_n)_m$ $(n = 1-4,\ m = 1-6)$ cluster by implementing first principle calculations is studied in detail. The stability of cluster is explained by the DOS. It is estimated that it creates stability due to *sp*-hybridization along with the different-sized condensed clusters $(Ga_3N_3)_m$ that are found to be more stable. Further, the electronic properties of the cluster are shown to have lower energy gap as compared to the bulk GaN system. It could be used as an interesting photo-catalytic application. Our calculations also revealed that more concentrated clusters have structural stability equivalent to 1-D nanorods obtained from the bulk which are comparable.

Acknowledgments: The author is thankful to the UGC for the financial support and also acknowledges the computing facility provided by the Department of Applied Physics, Babasaheb Bhimrao Ambedkar University, Lucknow without whose support this work would not have been in the present form.

References and Notes

1. G. Dresselhaus, M. S. Dresselhaus, and P. Eklund, Science of Fullerenes and Carbon Nanotubes, Academic Press, San Diego, CA (**1995**).
2. Y. Feldman, E. Wasserman, D. J. Srolovitz, and R. Tenne, *R. Science* 267, 222 (**1995**).
3. V. Nicolosi, P. D Nellist, S. Sanvito, E. C. Cosgriff, S. Krishnamurthy, W. J. Blau, M. L. H. Green, D. Vengust, D. Dvorsek, D. Mihailovic, G. Compagnini, J. Sloan, V. Stolojan, J. D. Carey, S. J. Pennycook, and J. N. Coleman, *Advanced Materials* 19, 543 (**2007**).
4. Iflah Laraib, J. Karthikeyan, and P. Murugan, *Physical Chemistry Chemical Physics* 5471 (**2014**).
5. J. H. Zhan, X. G. Yang, W. X. Zhang, D. W. Wang, Y. Xie, and Y. T. Qian, *Journal of Materials Research* 03, 629 (**2015**).
6. J. Xu, X. Zhuang, P. Guo, Q. Zhang, W. Huang, Q. Wan, W. Hu, X. Wang, X. Zhu, C. Fan, Z. Yang, L. Tong, X. Duan, and A. Pan, *Nano Lett.* 12, 5007 (**2012**).
7. H. Zhang, D. Yang, Y. Ji, X. Ma, J. Xu, and D. Que, *ACS Nano* 4, 98 (**2010**).
8. H. Zhang, X. Y. Ma, J. Xu, and D. R. Yang, *J. Cryst. Growth* 263, 372 (**2004**).
9. A. E. Saunders, A. Ghezelbash, P. Sood, and B. Korgel, *Langmuir* 24, 9043 (**2008**).
10. A. S. Barnard and H. Xu, *J. Phys. Chem. C* 111, 18112 (**2007**).
11. S. Nakamura and G. Fasol, The Blue Laser Diode, Springer, Berlin (**1997**).
12. S. Nakamura, M. Senoh, N. Iwasa, and S. Nagahama, *Appl. Phys. Lett.* 67, 1868 (**1995**).
13. H. Bar-Ilan, S. Zamir, O. Katz, B. Meyler, and J. Salzman, *Materials Science and Engineering A* 14, 30 (**2001**).
14. R. J. Trew, M. W. Shin, and V. Gatto, *Solid-State Electronics* 41, 1561 (**1997**).
15. S. J. Pearton, F. Ren, A. P. Zhang, and K. P. Lee, *Materials Science and Engineering: R. Reports* 3, 55 (**2000**).
16. R. D. Paiva, J. L. A. Alves, R. A. Nogueira, J. R. Leite, and L. M. R. Scolfaro, *Brazilian Journal of Physics* 34, 647 (**2004**).
17. T. Dietl, H. Ohno, F. Matsukura, J. Cibert, and D. Ferrand, *Science* 287, 1019 (**2000**).

18. T. Jungwirth, J. Sinova, J. Masek, J. Kucera, and A. H. Mac-Donald, *Rev. Mod. Phys.* 78, 809 **(2006)**.
19. J. Goldberger, R. He, Y. Zhang, S. Lee, H. Yan, H. J. Choi, and P. Yang, *Nature* 422, 599 **(2003)**.
20. S. M. Lee, Y. H. Lee, Y. G. Hwang, J. Elsner, D. Porezag, and T. Frauenheim, *Phys. Rev. B* 60, 7788 **(1999)**.
21. J. J. BelBruno, *Chem. Rev.* 11, 281 **(2000)**.
22. A. K. Kandalam, R. Pandy, M. A. Blanco, A. Costales, J. M. Recio, and J. M. Newsam, *J. Phys. Chem. B* 104, 4361 **(2000)**.
23. A. K. Kandalam, M. A. Blanco, and R. Pandy, *J. Phys. Chem. B* 105, 6080 **(2001)**.
24. A. K. Kandalam, M. A. Blanco, and R. Pandy, *J. Phys. Chem. B* 106, 1945 **(2002)**.
25. A. K. Kandalam, M. A. Blanco, and R. Pandy, *J. Phys. Chem. B* 107, 4508 **(2003)**.
26. B. Song and P. L. Cao, *Phys. Lett. A* 300, 485 **(2002)**.
27. B. Song, P. L. Cao, and B. X. Li, *Phys. Lett. A* 315, 308 **(2003)**.
28. D. L. Strout, *J. Phys. Chem. A* 104, 3364 **(2000)**.
29. D. L. Strout, *J. Phys. Chem. A* 105, 261 **(2001)**.
30. J. M. Matxain, J. M. Ugalde, M. D. Towler, and R. J. Needs, *J. Phys. Chem. A* 107, 10004 **(2003)**.
31. Ch. Chang, A. B. C. Patzer, E. Sedlmayr, T. Steinke, and D. Sulzle, *Chem. Phys. Lett.* 350, 399 **(2001)**.
32. H. S. Wu, F. Q. Zhang, X. H. Xu, C. J. Zhang, and H. J. Jiao, *J. Phys. Chem. A* 107, 204 **(2003)**.
33. J. Zhao, B. Wang, X. Zhou, and X. Chen, *Chem. Phys. Lett.* 422, 170 **(2006)**.
34. R. Hoffmann, Soli and Surface: A Chemiet's View on Bonding in Extended Structures, VHC Publisher, New York **(1988)**.

Received: 25 July 2017. Accepted: 20 December 2017.

J. Chem. Sci. Vol. 129, No. 5, May 2017, pp. 515–531. © Indian Academy of Sciences.
DOI 10.1007/s12039-017-1268-4

REGULAR ARTICLE

Assessing therapeutic potential of molecules: molecular property diagnostic suite for tuberculosis (MPDS^{TB})

ANAMIKA SINGH GAUR[a], ANSHU BHARDWAJ[b], ARUN SHARMA[b], LIJO JOHN[a], M RAM VIVEK[a], NEHA TRIPATHI[c], PRASAD V BHARATAM[c], RAKESH KUMAR[b], SRIDHARA JANARDHAN[a], ABHAYSINH MORI[c], ANIRBAN BANERJI[a,†], ANDREW M LYNN[e], ANMOL J HEMROM[e], ANURAG PASSI[b], APARNA SINGH[a], ASHEESH KUMAR[g], CHARUVAKA MUVVA[d], CHINMAI MADHURI[f], CHINMAYEE CHOUDHURY[a], D ARUN KUMAR[a], DEEPAK PANDIT[f], DEEPAK R. BHARTI[e], DEVESH KUMAR[g], ER AZHAGIYA SINGAM[d], GAJENDRA PS RAGHAVA[b], HARI SAILAJA[h], HARISH JANGRA[c], KAAMINI RAITHATHA[h], KARUNAKAR TANNEERU[a], KUMARDEEP CHAUDHARY[b], M KARTHIKEYAN[f], M PRASANTHI[a], NANDAN KUMAR[a], N YEDUKONDALU[a], NEERAJ K RAJPUT[b], P SRI SARANYA[a], PANKAJ NARANG[e,†], PRASUN DUTTA[h], R VENKATA KRISHNAN[c], REETU SHARMA[a], R SRINITHI[a], RUCHI MISHRA[g], S HEMASRI[a], SANDEEP SINGH[b], SUBRAMANIAN VENKATESAN[d], SURESH KUMAR[g], UCA JALEEL[h], VIJAY KHEDKAR[f], YOGESH JOSHI[f] and G NARAHARI SASTRY[a,*]

[a]Centre for Molecular Modeling, CSIR-Indian Institute of Chemical Technology, Tarnaka, Hyderabad 500 007, India
[b]Bioinformatics Centre, CSIR-Institute of Microbial Technology, Chandigarh 160 036, India
[c]Department of Medicinal Chemistry, National Institute of Pharmaceutical Education and Research (NIPER), Mohali 160 062, India
[d]Chemical Laboratory, CSIR-Central Leather Research Institute, Chennai 600 020, India
[e]School of Computational and Integrative Sciences, Jawaharlal Nehru University, New Delhi 110 067, India
[f]Chemical Engineering and Process Development, CSIR-National Chemical Laboratory, Pune 411 008, India
[g]Department of Applied Physics, Babasaheb Bhimrao Ambedkar University, Lucknow 226 025, India
[h]Open Source Drug Discovery Consortium, New Delhi, India
E-mail: gnsastry@gmail.com

MS received 5 March 2017; revised 20 March 2017; accepted 22 March 2017

Abstract. Molecular Property Diagnostic Suite (MPDS^{TB}) is a web tool (http://mpds.osdd.net) designed to assist the in silico drug discovery attempts towards Mycobacterium tuberculosis (Mtb). MPDS^{TB} tool has nine modules which are classified into data library (1–3), data processing (4–5) and data analysis (6–9). Module 1 is a repository of literature and related information available on the Mtb. Module 2 deals with the protein target analysis of the chosen disease area. Module 3 is the compound library consisting of 110.31 million unique molecules generated from public domain databases and custom designed search tools. Module 4 contains tools for chemical file format conversions and 2D to 3D coordinate conversions. Module 5 helps in calculating the molecular descriptors. Module 6 specifically handles QSAR model development tools using descriptors generated in the Module 5. Module 7 integrates the AutoDock Vina algorithm for docking, while module 8 provides screening filters. Module 9 provides the necessary visualization tools for both small and large molecules. The workflow-based open source web portal, MPDS^{TB} 1.0.1 can be a potential enabler for scientists engaged in drug discovery in general and in anti-TB research in particular.

Keywords. Tuberculosis; chemoinformatics; open science; neglected diseases; drug discovery portal; web-based technology.

*For correspondence
†Deceased: ANIRBAN BANERJI and PANKAJ NARANG.

1. Introduction

Data and knowledge generated in drug discovery have been escalating exponentially in recent years owing to the demanding nature of pharmaceutical industry to deliver affordable and safer drugs for existing and emerging diseases.[1–10] How to make the knowledge thus generated available to the practicing scientists is an issue of great significance as it reduces the redundancy, enables research activity and focuses on the grand challenges in the healthcare sector.[11–17] Open science and open innovation are extremely important in the drug discovery approaches in general and those directed towards neglected and orphan diseases in particular.[18–27] How the existing knowledge helps medicinal chemists can be addressed by answering the following two questions: a) What is the value or relevance of molecules that were synthesized? and (b) which of those molecules are the most promising? Because currently chemist's ability to synthesize complex molecules has increased tremendously and more often than not, the question is which molecule to synthesize rather than how to synthesize.

Tuberculosis (TB) has become a global threat killing nearly 1.4 million people with 10.4 million new cases in 2015.[28] The disease-causing bacteria Mtb is a rather challenging microorganism that takes over six months of treatment with multiple drugs to curb its infection.[29] The therapeutic interventions further get confounded due to the fact that most of the time Mtb remains in latent phenotype, which is not well understood.[30] The emergence of multi-drug resistant, extensively drug-resistant and totally drug-resistant forms have resulted in long duration therapies with various side effects and toxicity issues with a risk of non-compliance.[31–38] Therefore, the need of new therapy to combat this dreadful disease is inevitable and demands exploration of new chemical space. Computational approaches to obtain and optimize anti-tubercular leads have been extensively employed in this area.[39–44] There are several public databases having diverse chemical classes of the compounds including PubChem, ZINC, KEGG, DrugBank, ASINEX, ChEMBL and NCI.[45–62] The computational tools and databases are required to facilitate rational prioritization and analysis of compounds from the available large chemical space. Further, the development of new algorithms/scripts is required to classify the chemical space for searching or extracting the useful information for each molecule. The tools are needed to predict the physical, chemical and biological properties of small molecules in order to improve search capabilities.

Before synthesizing any molecule, the medicinal chemist should have prior knowledge to optimize various physicochemical properties, structural alerts, in addition to the understanding of protein-ligand interactions that help in improving drug-likeness and avoiding toxicity issues. There are a number of open source scripts and algorithms developed by various developers for solving drug discovery issues.[63,64] Ideally, developing a disease-specific web portal which integrates the publicly available tools could provide a right platform to conduct drug discovery research in TB.

A variety of chemoinformatics analysis tools have been previously implemented in workflow systems. Steinbeck *et al.,* have implemented the chemoinformatics library of Chemistry Development Kit (CDK)[65,66] in the Taverna workflow suite.[67] Steinbeck *et al.*[68] have also implemented CDK in Konstanz information miner (KNIME), which is an open source workflow platform. It contains functions like format conversion, signatures, fingerprints and molecular properties generation. The Galaxy platform[69–71] is another workflow management system that provides easy to use interfaces of tools to the users and allows easy connection of the tools as well. Various instances of Galaxy have already been established.[72] For example, Ballaxy[73] is a Galaxy instance for structural bioinformatics wherein functions like protein preparation, ligand and protein checker, docking and many other tools have been implemented.

The current manuscript presents a web-based MPDS^{TB} Galaxy tool, which provides an open source platform for the chemoinformaticians, bioinformaticians, medicinal chemists, computational biologists, pharmacologists and others scientists to work on the design of anti-tuberculosis (anti-TB) drugs. The Galaxy based web tool is conveniently designed to integrate with any other software or script and can be used by designing user-defined workflows, a feature conveniently exploited by the users of Galaxy in many cases. The MPDS^{TB} tool provides three class of modules: a) Data Library (modules: 1. Literature, 2. Target library, 3. Compound library); b) Data Processing (4. File format conversion, 5. Descriptor calculation); and c) Data Analysis

Principal investigator: G NARAHARI SASTRY
Co-principal investigators: P ANSHU BHARDWAJ, PRASAD V BHARATAM, ANDREW M LYNN, DEVESH KUMAR, GAJENDRA P S RAGHAVA, M KARTHIKEYAN, SUBRAMANIAN VENKATESAN
Core developers: ANAMIKA SINGH GAUR, ANSHU BHARDWAJ, ARUN SHARMA, LIJO JOHN, M RAM VIVEK, NEHA TRIPATHI, PRASAD V BHARATAM, RAKESH KUMAR, SRIDHARA JANARDHAN, G NARAHARI SASTRY
Co-developers: ABHAYSINH MORI, ANIRBAN BANERJI, ANMOL J HEMROM, ANURAG PASSI, APARNA SINGH, ASHEESH KUMAR, CHARUVAKA MUVVA, CHINMAI MADHURI, CHINMAYEE CHOUDHURY, D ARUN KUMAR, DEEPAK PANDIT, DEEPAK R BHARTI, ER AZHAGIYA SINGAM, HARI SAILAJA, HARISH JANGRA, KAAMINI RAITHATHA, KARUNAKAR TANNEERU, KUMARDEEP CHAUDHARY, M PRASANTHI, NANDAN KUMAR, N YEDUKONDALU, NEERAJ K RAJPUT, P SRI SARANYA, PANKAJ NARANG, PRASUN DUTTA, R VENKATA KRISHNAN, REETU SHARMA, R SRINITHI, RUCHI MISHRA, S HEMASRI, SANDEEP SINGH, SURESH KUMAR, UCA JALEEL, VIJAY KHEDKAR, YOGESH JOSHI.

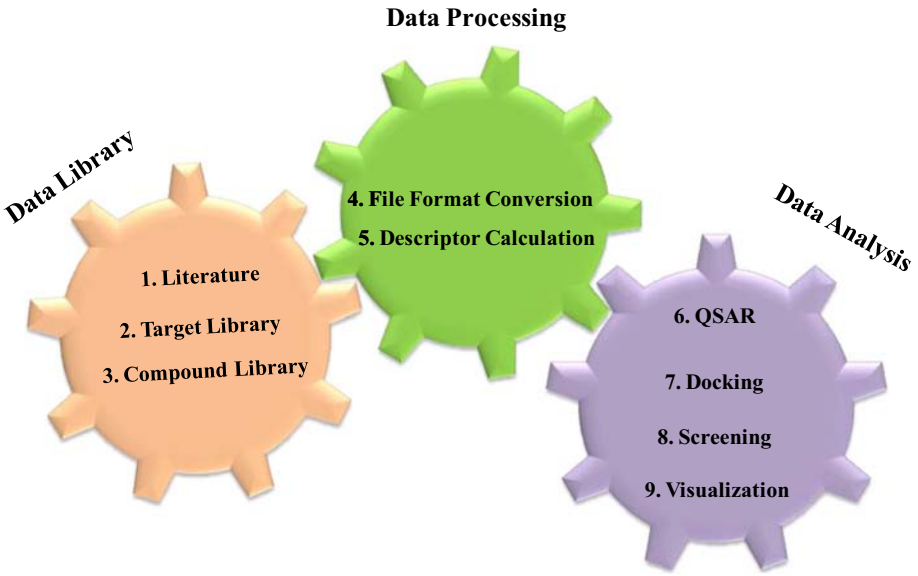

Figure 1. MPDS is structured into data library (literature, target library, compound library), data processing (file format conversion, descriptor calculation) and data analysis (QSAR, docking, screening and visualization).

(6. QSAR, 7. Docking, 8. Screening, 9. Visualization) (Figure 1). While modules 1, 2, 7 and 8 are specific to a particular disease (in this case TB), it is quite possible to make at least three out of the four modules, 2, 7, and 8 as generic. Efforts are underway to achieve this in the near future. However, in MPDS^{TB}1.0.1, only five modules Compound library, QSAR, Docking, Screening, Visualization are generic in nature and can be used 'as is' in drug discovery platforms directed towards other diseases. As the main focus of the current endeavor is to store all the data that is generated for each of the molecules, we decided to generate a unique MPDS ID, which is akin to Aadhar number in India, or social security number in the USA where all the information pertaining to a molecule is stored. A structure-based classification tool has been employed which facilitates the navigation through the chemical space.

The current work has the following major objectives: a) Quantitatively evaluating the multifarious aspects of drug-likeness of a given molecule, in order to diagnose its potential application as a drug; b) Calculate various drug-like physico-chemical properties for prioritization of compounds; c) Provide necessary framework to employ virtual screening of large dataset of compounds; d) Help synthetic medicinal chemists for the design of novel compounds; e) Coordinate the strategic development and integration of chemoinformatics efforts; f) Develop new multi-disciplinary collaborative projects. The current work focuses on the anti-tubercular lead discovery, design and optimization. Expectedly, a suitably altered protocol can be generated for other disease specific Galaxy web MPDS portals by customizing some of the modules. Thus, MPDS in the long run, can emerge as a general purpose open source drug discovery web portal.

2. Methods and modules

Galaxy (http://galaxyproject.org/) is a web-based workflow management system implemented in Python programming language, which is widely used for making data libraries, data integration, data processing and data analysis. In the current work, MPDS^{TB} is developed using Linux (CentOS 6.4) operating system having the python version 2.7. It provides a graphical user interface (GUI) to many computational tools that helps in computational chemistry, drug design, image analysis, climate modeling, linguistics, and biomedical research. Basically, it was developed to analyze the genomic data including gene expression, proteomics, transcriptomics, and gene assembly. Galaxy can be used directly on the web or can be installed in local machines which gives freedom to the users to integrate their own tools. It has flexibility in using diverse biological, chemical data formats and it allows the integration of tools that is written in any programming language or script for which a command line invocation can be constructed. Once the piece of code is written, a tool definition file should be written in XML that describes the working of the tool and its input/output parameters (Table 1).

For each module, the XML code and its complete path should be incorporated into the main configuration file of the Galaxy. The new tool implemented gets displayed in the

Table 1. Description of XML file as implemented in Galaxy MPDS[TB].

Tool ID	Description
<tool id>	Gives a unique name to the tool whose description is mentioned in the XML file.
<name>	It has the name of the tool that will be displayed as hyperlink in Galaxy.
<description>	This is displayed just after the hyperlinked name.
<command>	It describes how the tool (which compiler) will be executed and its input and output parameters.
<inputs>	Defines the input parameters.
<outputs>	Defines the output parameters.
<help>	Describes what the tool does.

tool panel of the Galaxy home page. The Galaxy workspace mainly consists of four areas, the first one is the navigation bar which provide links to Galaxy's major components, analysis workspace, workflows, data libraries, and user repositories (histories, shared data, workflows, pages), the second one is the tool panelist containing the analysis tools and data sources available to the user, the third one is detailed panel display interfaces for tools selected by the user and the fourth one is history panel that shows data and the results of analyses performed by the user, as well as automatically tracked metadata and user-generated annotations.

3. Structure of MPDS[TB]

MPDS[TB] is structured into data library (literature, target library, compound library), data processing (file format conversion, descriptor calculation), and data analysis (QSAR, docking, screening, and visualization) (Table 2). Each of these modules is customized for TB drug discovery and will be described in the following sections.

3.1 *Data library*

3.1a *Module 1: Literature*: Module 1 provides information of druggable protein targets/gene information, FDA-approved drugs, and polypharmacology for Mtb. The genetic information provided includes RvID, gene name, gene product, class of protein, structural details from PDB, active site, function, metabolic pathway, localization, method of validation, drug/inhibitor information, druggability index, and mechanism of action. The literature module provides the list of available FDA approved drugs along with their identification, pharmacology, potential targets and corresponding references. The polypharmacology covers the structure of Mtb cell wall, biosynthetic, metabolic pathways (cell wall, chorismate, amino acids, lipids, carbohydrate, cofactor, nitrogen/sulphur, DNA, protein), bibliography and hyperlinks were given to various servers related to TB.

Table 2. Description of various modules in MPDS[TB] 1.0.1.

Category	Modules	Description
Data Library	Module 1: Literature	Contains Mtb proteins and its genetic information; FDA approved drug information and polypharmacological information.
	Module 2: Target Library	Contains crystal structures and homology models for Mtb proteins.
	Module 3: Compound Library	Contains a single window interface for searching a compound in MPDS compound database.
Data Processing	Module 4: File Format Conversion	Conversions of files from one chemical format to another chemical format, 2D to 3D file conversion using Open Babel.
	Module 5: Descriptor Calculation	Calculation of descriptors and fingerprints using PaDEL and CDK tools.
Data Analysis	Module 6: QSAR	Generation of QSAR models using the data mining tools, McQSAR and SVMlight.
	Module 7: Docking	Ligand Optimization; Conformer Generation and Protein-Ligand docking.
	Module 8: Screening	Prioritization of compounds for drug-like features using DruLiTo tool; Biopharmaceutical Classification System (BCS); Identification of toxicophoric groups in a compound.
	Module 9: Visualization	Visualizing protein-ligand interactions using Jmol and Ligplot.

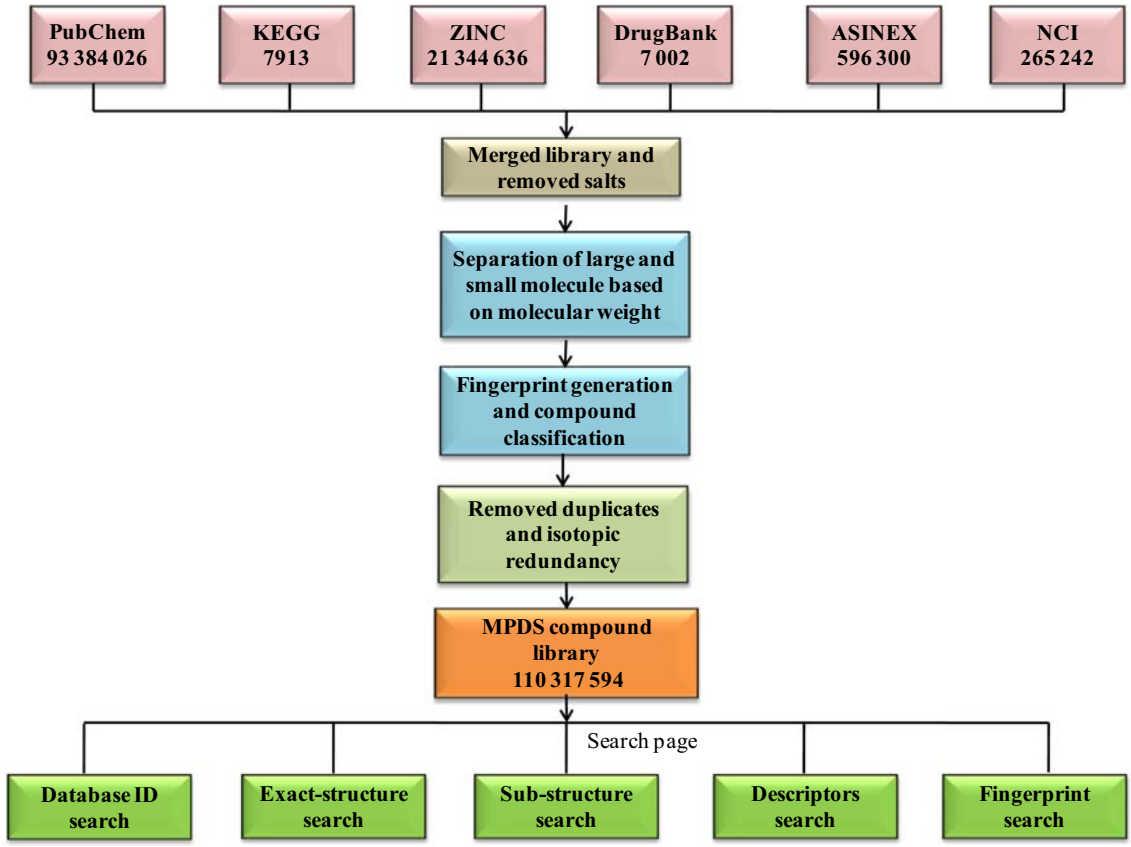

Figure 2. Schema for the generation of MPDS compound library from various data sources and representation of compound search engine.

3.1b *Module 2: Target library*: The target library consists of crystal structures of 140 Mtb proteins which are reported targets and also the ones prioritized through systems level analysis of Mtb interactome. Each protein is also annotated for key residues around the active site. Most of these target structures were collected from protein data bank (PDB) and some of them were homology models. If the structural information is not available, then mutagenesis study results were collected from literature. Multiple sequence alignment of the same family of protein was employed for identification of active site residues for the protein. One of the principal objectives of the target library is to provide a list of prepared proteins in Mtb suitable for molecular docking, and give hyperlink of the data source, if available. The collected PDB structures were prepared by using standard protocols such as assigning bond orders, adding hydrogens, and minimizing protein complexes.

The targets were selected from Mtb H37Rv genome family and they majorly belong to various enzyme classes, such as oxidoreductase, transferase, hydrolase, lyase, isomerase, and ligase. These targets are involved in various biological functions that include signal transduction, peptidoglycan and cell wall synthesis, amino acid synthesis, drug metabolism, DNA precursor synthesis, post-translational modifications and nitrogen metabolism, *etc.* The protein structures in MPDS^{TB} target library can be potentially exploited in structure-based drug design approaches.

3.1c *Module 3: Compound library*: The compound library is generated with the objective of establishing a single window interface to search compounds available across different public domain databases. An efficient small molecule search, implemented using multiple search strategies, facilitates the comprehensive analysis of the available chemical space that may be utilized for identification of novel anti-TB compounds.

Preparation: For the preparation of MPDS^{TB} compound library, existing small molecule databases such as PubChem, Drugbank, KEGG, NCI, ZINC and ASINEX were downloaded. To ensure that globally acceptable standards are followed to store and search this data, each compound in the library is converted into SMILES, InchI and InchIKey using OpenBabel 2.3.2.[74] Indexing of the compound library is done using InchIKey (Figure 2).

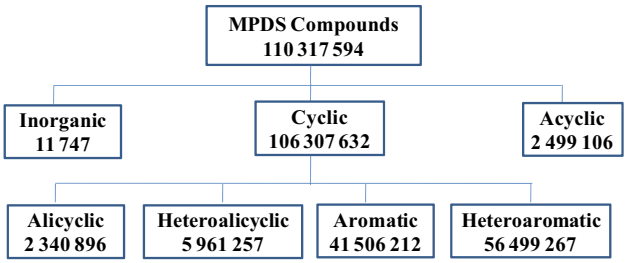

Figure 3. A structure-based chemical classification system of MPDS compound library.

Storage and search: As mentioned above, each compound in the library is stored using InchI standards along with SMILES string and the IDs from where the compound is sourced. Multiple search options are provided through MPDS^{TB} web interface which includes structure-based search, property-based search, and fingerprint-based search (Figure 3). Compound property data is mostly calculated using PaDEL. The pKa values and IUPAC names are calculated using ChemAxon command line tools. The substructure search is implemented using RDkit.[75] A novel fingerprinting algorithm is developed to classify compounds at various levels of structural features. This binary fingerprinting algorithm is developed and employed for the classification and clustering of all the molecules included in the MPDS^{TB} compound library database. Currently, a 30-bit qualitative and partially quantitative fingerprinting scheme is adopted to cluster similar compounds together and reduce the search space. Furthermore, two open source tools, 'molecule cloud' and 'open molecule generator' are also implemented in compound library module to create a molecular cloud of scaffolds and to generate molecule library respectively.[76,77]

3.2 *Data processing*

3.2a *Module 4: File format conversion*: A core requirement of any workflow management system is the connecting links between different analysis tools. Most often these links are based on the file formats that are read by these tools. As there are various molecular file formats to represent chemical structures, an open source file format converter is implemented to facilitate the creation of workflows over the web. Different tools require specific input file formats and will produce output in another specific format. In order to maintain a smooth flow of data between different tools in a workflow, the file format converter module utilizes one of the tools from the Galaxy toolshed to convert one file format to another based on user requirements. As of now, a few input formats like mol2, mol, sdf, SMILES, *etc.,* and output formats, mol2, sdf, mol, pdb are incorporated. This module also contains a tool that generates 3D coordinate from 2D structural file or SMILES which utilizes OpenBabel 2.3.2. The 3D structure generated follows geometrical rules based on hybridization of atoms. Once the structure is generated, the stereochemistry of the structure is taken care of and the lowest free energy conformer is generated by MMFF94 force field using weighted rotor search.

3.2b *Module 5: Descriptor calculation*: In order to computationally assess the properties of the compounds present in MPDS^{TB} compound library or those provided by end users, two descriptor calculation tools, namely, PaDEL and CDK, are incorporated in MPDS^{TB}. These tools may be used to calculate different compound properties. The input format for both of these descriptor tools is sdf and provides the output in CSV format. The descriptor module may read the output from compound library search or user uploaded sdf. The output may be used to build machine-learning models for target specific filters, predicting anti-TB properties, drug-like properties or toxicity of the compounds.

3.3 *Data analysis*

3.3a *Module 6: QSAR*: Two methods of data mining, quantitative structure activity relationships (QSAR) and support vector machine (SVM), are incorporated in MPDS^{TB}. A Multi-conformational Quantitative Structure-Activity Relationship (McQSAR) using Genetic algorithms is implemented for developing QSAR models.[78] The 'Build_QSAR_Model' tool of the QSAR module takes the descriptor file of the compounds with known activity and prompts the user to enter the name of the column whose value needs to be predicted (activity, in this case). In order to remove the redundancy and unwarranted features, the user has been given six options. The feature selection options are as follows: exclude correlated descriptors, exclude identical conformers, exclude inactive compounds, exclude sparse conformers, exclude sparse descriptors and exclude descriptors with zeros. The user also has the flexibility to set the number of times user wants cross-validation step to be repeated. The user can perform four kinds of cross-validation using the percentage of bins 3, 5, 7, 10 folds to divide the compounds. McQSAR can be used to predict the activity of new compounds using the model created by the previously mentioned tool. This accepts two input files: one that contains the descriptors of the compounds whose activity needs to be predicted and the second is a model file created by the 'Build_QSAR_Model' tool (Figure 4).

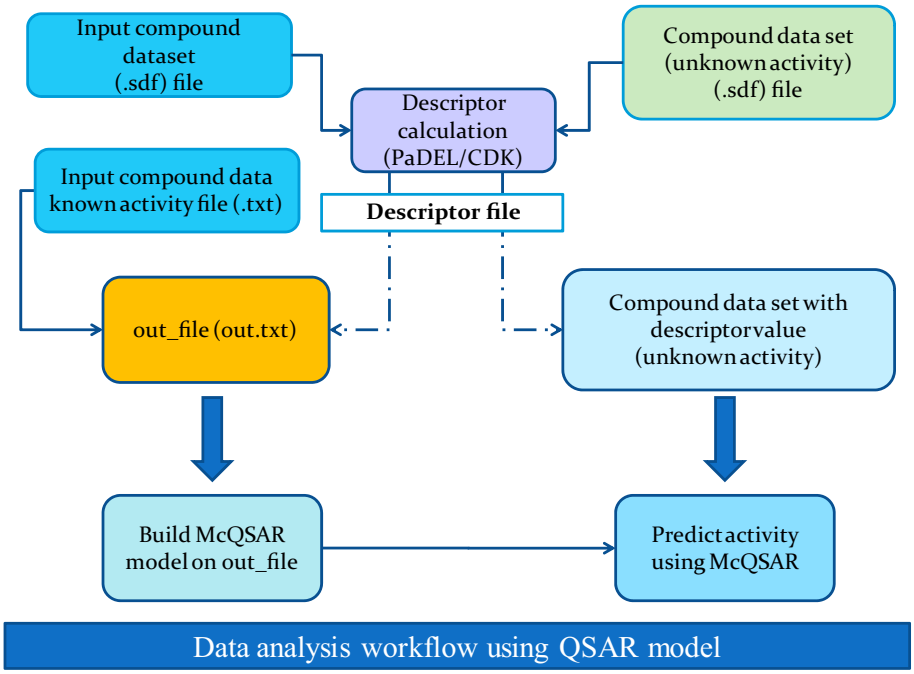

Figure 4. Workflow for QSAR model generation.

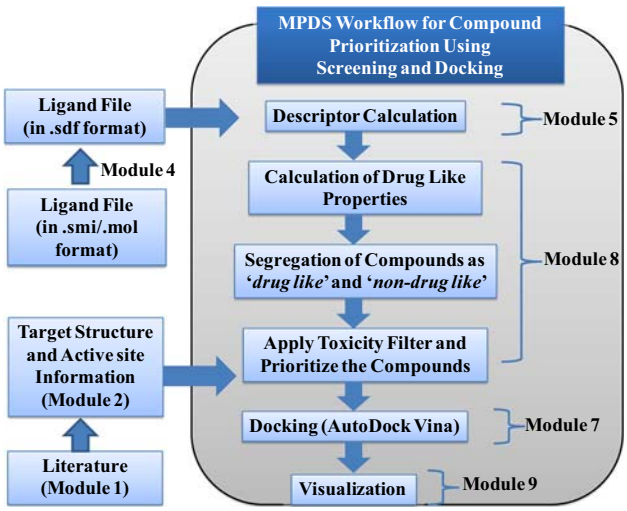

Figure 5. Workflow for compound prioritization using screening and docking modules.

Along with McQSAR, SVMlight[79] has also been incorporated in MPDS[TB] which helps in classifying the compound data into actives and inactives. The 'Build QSAR Model: SVMlight' builds a QSAR model based on descriptor files of active and inactive molecules. Then 'Classify Data: SVMlight' tool takes the model file and the descriptor file of compounds with unknown activity, and classifies them into actives and inactives.

3.3b *Module 7: Docking*: The docking protocol involves multiple steps including energy minimization (chemical structure optimization), conformer generation, docking and its analysis, and visualization. In MPDS[TB], the docking module contains four tools to carry out these steps. The ligand optimization tool incorporates the Phenix electronic Ligand Builder and Optimisation Workbench (eLBOW).[80] The tool uses semi-empirical quantum chemistry based calculations using AM1 (Austin Model 1).[81] Hydrogen atoms are automatically added to the compound by eLBOW. The conformer generation tool utilizes the OpenBabel 2.3.2. genetic algorithm approach to generate diverse conformers based on RMSD. AutoDock Vina[82] has been implemented as the docking software in module 7. Thus, the use of docking module allows the user to carry out efficient and robust docking calculations (Figure 5).

The proteins can be uploaded as a PDB file, or can directly be accessed from target library available in the MPDS[TB] shared library. The ligands can be obtained from the compound library of MPDS[TB] package or a user can upload their choice of ligand in sdf or pdb format with 3D coordinates. The docking calculation can be started using the default parameters and with some user defined parameters. Users can also download the docking results as a zip file containing the complex files in PDB format and the Vina log file containing the ranked binding free energy scores. The docked complexes can be visualized through the visualization module for examining the protein-ligand interactions.

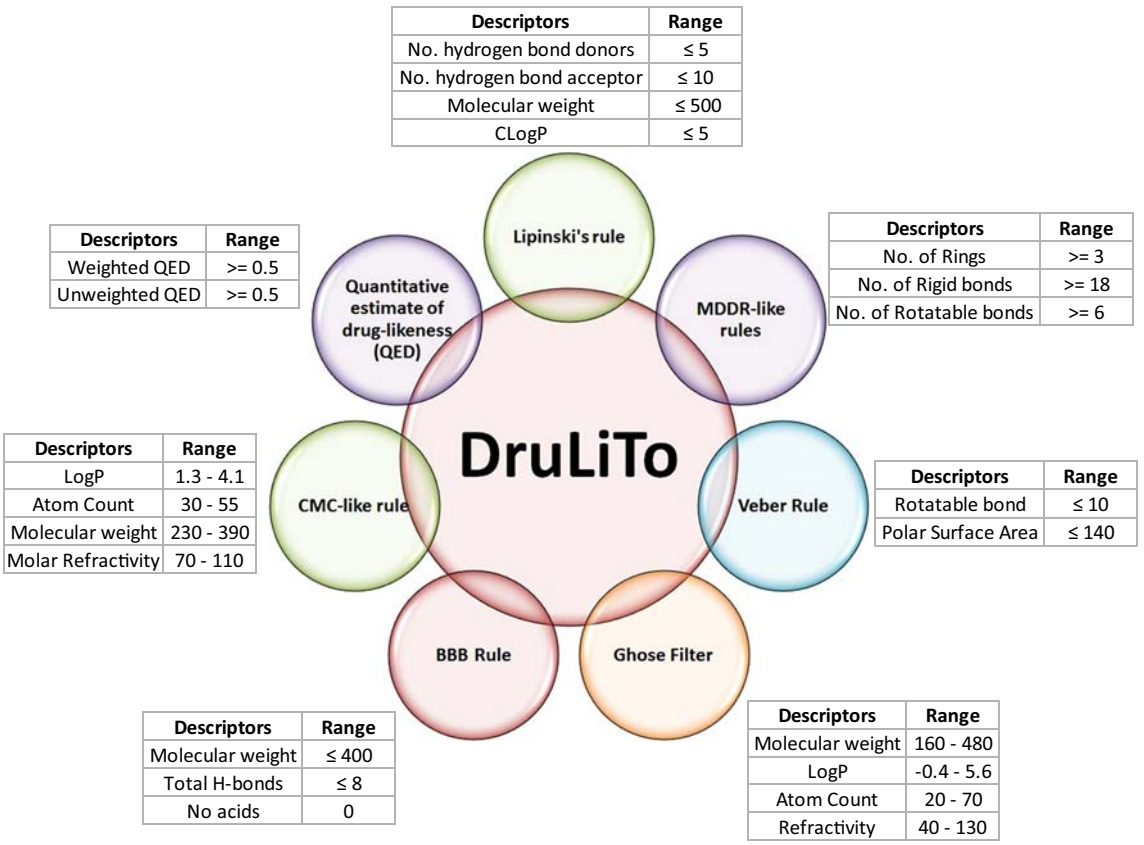

Figure 6. Drug-Likeness prediction tool (DruLiTo) for screening chemical compounds, databases or libraries.

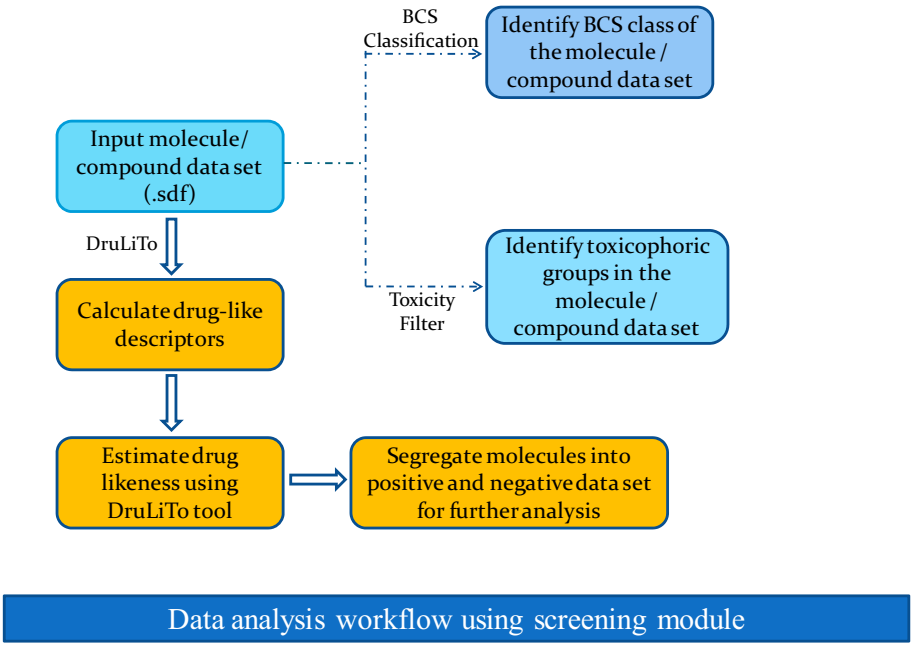

Figure 7. Workflow for compound screening using DruLiTo and filters.

3.3c *Module 8: Screening*: To prioritize compounds for their drug-like features, DruLiTo[83] is integrated into MPDS[TB]. This tool provides the assessment of drug-like features based on eight different published algorithms.[84–88] To calculate drug-likeness of a compound, DruLiTo needs descriptor data, which may be calculated using CDK. DruLiTo uses these descriptors to determine the drug-likeness of the molecule,

based on the different rules as defined by the end user. The user can then segregate the input dataset into passed and failed groups based on one or more rules selected (Figure 6, 7). In addition to this, the biopharmaceutics classification system (BCS) is implemented using in-house scripts to evaluate the solubility and the permeability of compounds. These predictions can subsequently be used to process the positive ligand set or negative ligand set or the original input dataset, all of which are in sdf format, to determine the BCS class (I, II, III, IV) into which the molecules fall based on their predicted permeability and intrinsic solubility values.

Another feature provided in MPDS[TB] is to perform toxicity analysis. A comprehensive list of structural alerts including data from FAF-Drugs2 (204 substructures), OChem and literature are generated. The toxicity filter performs a substructure search on the query molecule and highlights the matched toxicophoric groups from this data and displays it in an image format. It also produces the mol format of the molecules with toxicophoric groups that can be saved. Along with this, a text file listing the molecule ID, the total number of toxicophoric matches found and the SMARTS pattern of the matched groups can also be generated with this module.

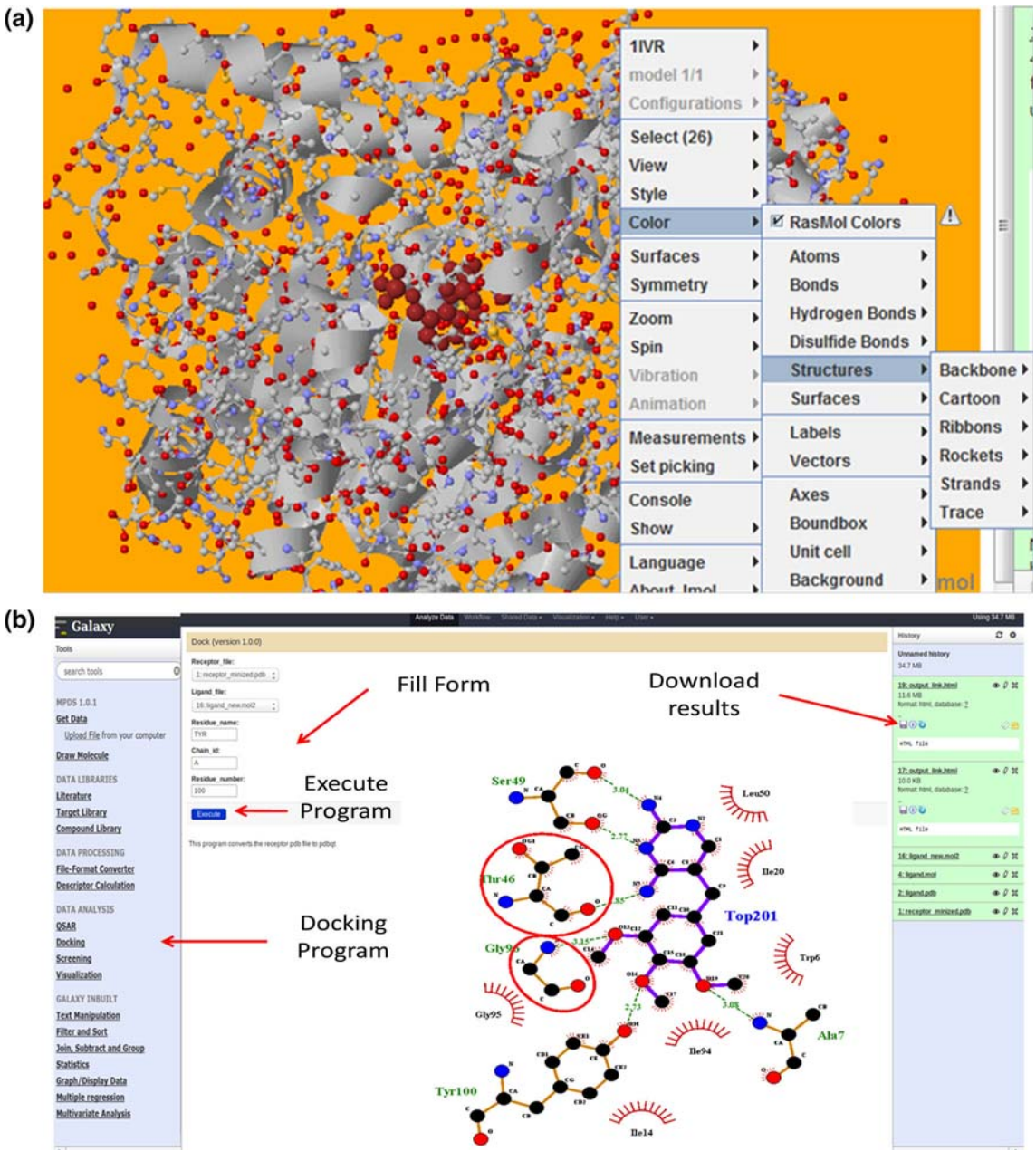

Figure 8. (**a**) Visualization of protein-ligand complex by various structural representations, (**b**) LigPlot for visualizing protein-ligand interactions (hydrogen bonding and hydrophobic contacts).

3.3d *Module 9: Visualization*: Protein-ligand complex can be viewed in LigPlot^{+} tool available in this module in order to examine the protein-ligand interactions. The key interactions of the ligand with active site amino acids are displayed by hydrogen bonding (dashed lines between the atoms) and hydrophobic contacts (an arc with spokes radiating towards the ligand atoms). The protein-ligand complex can be visualized in Jmol by various structural representations (Figure 8).

4. Results and Discussion

4.1 *The compound library and search page*

MPDS^{TB} compound library is a compiled and curated database containing 110.31 million unique compounds (as on 31st December 2016) from various publicly available databases including PubChem, KEGG, ZINC, DrugBank, ASINEX and NCI. Before making unique compounds, salt containing compounds were removed and further, the compounds were separated on the basis of molecular weight taking 750 Da as cut-off. Fingerprints were generated and compounds were classified into classes and clusters. Chemically well-defined classes obtained from fingerprinting algorithm were subjected to redundancy as well as removal of isotopes based on the InchIKey and truncated InChI respectively (Table 3). A class is a chemically well-defined group, whereas cluster is a set of compounds with a size limit of 0.25 million. After classification, the compound library majorly consists of 106.30 million cyclic compounds (2.34 million alicyclic, 5.96 million heteroalicyclic, 41.51 million aromatic and 56.49 million heteroaromatic). For aromatic compounds, class 12 (aromatic compounds contain two rings) has a maximum number of compounds (8.97 million) having 42 clusters, whereas class 20 (aromatic compounds contains more than or equal to four rings) has 0.91 million compounds in clusters. Highest number of compounds is present in the heteroaromatic class 22 (10 million), which are stored in 46 clusters (Figure 9). MPDS^{TB} fingerprinting algorithm and search engine offer a number of advantages over the available fingerprinting algorithms. The various available algorithms match a set of SMARTS patterns against each molecule to calculate each bit of the fingerprint that leads to reduced search time.[89] MPDS-Database uses SMILES notation of the molecules for storage and fingerprinting which makes it faster than the other approaches utilizing SMARTS notation for pattern search and matching. The available fingerprinting algorithms are not suitable for the large data size (110.31 million) as the speed is compromised due to matching a large set of SMARTS patterns against each molecule. The limitation of the current version of MPDS-fingerprinting is that it is not at the stage of being molecule specific. The purpose of designing this fingerprinting algorithm was to reduce the search space to a level where the 2D structural comparison can be performed without compromising the computational power and time utilization. Therefore, more efforts are required to make this fingerprinting robust and molecule specific. Fingerprinting of inorganic molecules is an issue with most of the available fingerprinting algorithms. However, MPDS^{TB} fingerprinting algorithm adopts the structure-based fingerprint classifying the inorganic compounds efficiently. The program for the generation of 30-bit fingerprinting is written in Java (using NetBeans IDE 7.2.1).[90] Further,

Table 3. Distribution of number of compounds in structural classes of MPDS^{TB} compound library.

Chemical Classes	Class‡	No. of clusters$^{£}$	No. of compounds
Acyclic	1	8	1,790,302
	2	4	708,804
Alicyclic	3	7	1,436,757
	4	3	483,877
	5	1	127,301
	6	2	292,961
Heteroalicyclic	7	12	2562,119
	8	11	2,289,075
	9	4	772,643
	10	2	337,420
Aromatic	11	31	6,842,221
	12	42	8,978,649
	13	32	6,898,540
	14	13	2,649,637
	15	31	6,276,919
	16	10	2,071,127
	17	5	1,024,251
	18	15	3,089,744
	19	14	2,771,697
	20	5	903,427
Heteroaromatic	21	16	3,461,762
	22	46	10,086,573
	23	25	5,484,547
	24	32	6,580,855
	25	45	9,268,612
	26	13	2,588,133
	27	12	2,228,509
	28	39	7,829,460
	29	45	8,970,816
Large Molecules	30	7	1,499,109
Inorganic	31	1	11747

‡Class is a chemically well-defined group, $^{£}$Cluster is a set of compounds with a size limit of 0.25 million.

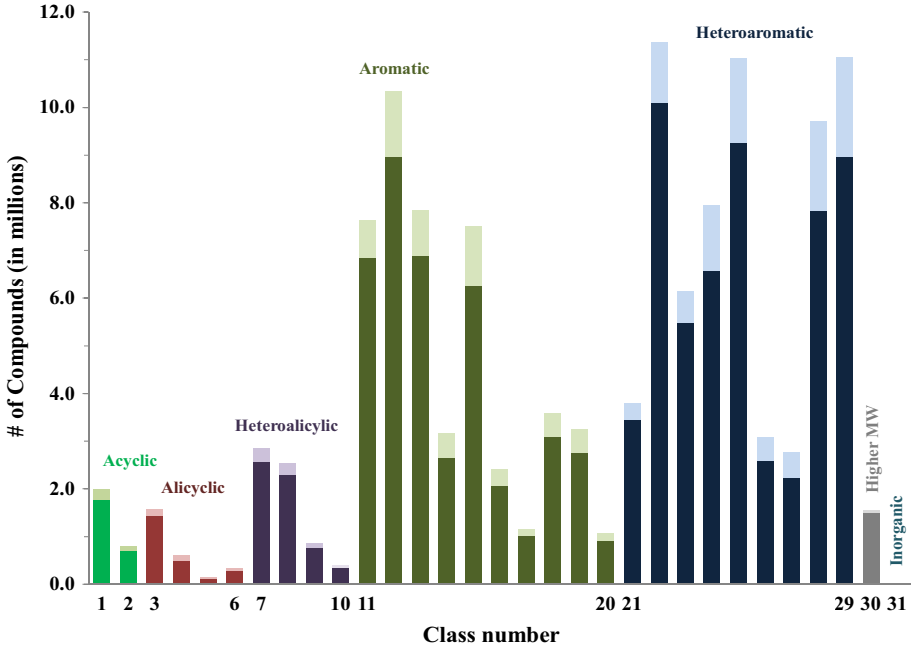

Figure 9. Distribution of unique (dark color) and duplicate (light color) compounds in different chemically well-defined classes.

the choice of SMILES notation for the assignment of fingerprinting and structure search was attributed to the easy and fast handling of the SMILES patterns rather than SMARTS patterns (Table 4).

4.2 *The search page*

MPDS^{TB} provides an interface for searching molecule based on their diverse properties through compound library search tool designed on the Galaxy platform. The user can search the compound library by database ID, exact structure, substructure, descriptor and fingerprint. The result of search page shows a list of molecules fulfilling the criteria, which are further linked to MPDS ID card, displaying the basic information of molecule. The in-house program will calculate molecular fingerprints and searches the query molecules in the database for generating MPDS ID card. For assisting the molecular drawing in MPDS-Galaxy portal, JS draw has been incorporated.

4.3 *Workflow system*

This is one of the most important features of the current platform, which paves the way to generate custom design workflows. The Galaxy workflow system can be used by a graphical drag-and-drop interface in which tools are configured and interconnected between the appropriate input and output points. The user can also extract/download the workflow from the history pane. MPDS^{TB} presents a platform where a data library, data processing and data analysis are configured and interconnected to assist *in silico* drug discovery. The user can utilize the inbuilt workflows or design a new one to carry out chemoinformatics analysis for any given molecule. The MPDS^{TB} workflow system can be interconnected between different modules for a specific task.

4.4 *MPDS ID card*

The output from MPDS^{TB} portal is MPDS ID card (which is akin to Aadhar card in India, or social security number in the USA) that represents a molecular profile report specific to a given molecule. This card reports the vital physico-chemical properties of a molecule essential to estimate the drug-likeness and activity of the molecule in the early stages of the drug discovery and development pipeline. MPDS ID which provides all pertinent information can have several pages. First page is standard and essentially aids in registering the molecule in the database, besides providing vital physico-chemical parameters. However, if more pertinent data are available on the molecule, such as their biological activity, spectroscopic data, toxicity, PK/PD data, *etc*., subsequent pages will be created. The first page of the molecule can be viewed publicly from the portal; second and subsequent pages are stored in the external hard disks at the development site, due to apparent disk storage limitations (Figures 10 and 11).

Table 4. 30-bit fingerprinting scheme and its various levels employed for the classification of molecules in MPDS^{TB} 1.0.1.

Fingerprint Level	Fingerprint bits	Fingerprint bits and Molecular features
Level 1 (Skeleton)	1 2 3 4 5 6	1st bit: Acyclic/Cyclic **Acyclic:** 2nd and 3rd bits: Saturation & Conjugation 4th bit: Straight/Branched 5th bit: Homo/Hetero atomic **Cyclic:** 2nd and 3rd bits: Number of rings 4th and 5th bits: Alicyclic/Aromatic 6th bit: Large/Small
Level 2 (Atom type)	7 8 9 10 11 12	**Acyclic and Cyclic:** 7th bit: Geometrical isomerism 8th bit: Hydrogen Bond Donor 9th bit: Hydrogen Bond Acceptor 10th bit: Halogens 11th bit: Heteroatom in side chain/backbone **Acyclic:** 12th bit: Presence of metal ion **Cyclic:** 12th bit: Presence of fused/unfused rings
Level 3 (Functional group)	13 14 15 16 17 18 19 20	**Acyclic and Cyclic:** 13th bit: Carbonyl group 14th bit: Phosphate containing group 15th bit: Cyanide group 16th bit: Nitro group 17th bit: Sulphur group 18th bit: Amino group 19th bit: Alcohol/Ether group 20th bit: Boron
Level 4 (Size of molecule)	21 22 23 24 25 26	**Acyclic and Cyclic:** 21st, 22nd, 23rd and 24th bits: Number of heavy atoms 25th bit: Chirality 26th bit: Connected/Disconnected structure
Level 5 (Heteroatom type in ring)	27 28 29 30	**Acyclic:** 27th, 28th, 29th and 30th bits: Even/Odd number of carbons **Cyclic:** 27th bit: Nitrogen in ring 28th bit: Oxygen in ring 29th bit: Sulphur in ring 30th bit: Phosphorus in ring
Level 6	–	Number of heteroatom containing rings

5. Conclusions

MPDS^{TB} 1.0.1 is a comprehensive open source Galaxy-based web tool, which provides a platform to integrate the data collection, processing, and analysis customized towards anti-TB drug discovery and design. One of the main features of this program is its ability to assess and estimate the activity of a given molecule using chemoinformatics, bioinformatics tools, and the existing knowledge in the area. The major attainment of MPDS^{TB} is the creation of a unique compound library (110.31 million) by removing duplicates, isotopic redundancy and salts. A structure-based classification program was developed, which classifies the compound library into 31 classes and 533 clusters.

We believe that the web-based chemoinformatics and modeling tools are great enablers to tackle grand challenges in healthcare in general and drug discovery in particular. One of the major bottlenecks for carrying out research in drug discovery in the academia can be

Molecular Property Diagnostic Suite

MPDS ID:27-09-137939

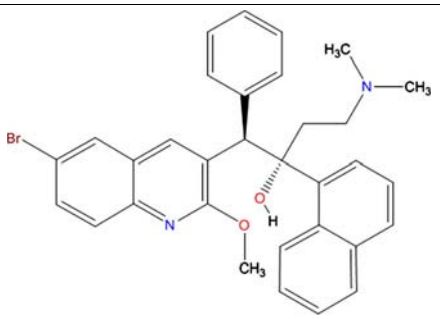

Molecular Formula:

$C_{32}H_{31}BrN_2O_2$

IUPAC Name:

(1R,2S)-1-(6-Bromo-2-methoxy-3-quinolinyl)-4-(dimethylamino)-2-(1-naphthyl)-1-phenyl-2-butanol

Remarks:

Name/Synonyms: Bedaquilina, Bedaquilinum, TMC207, Sirturo, TMC-207, R207910, TMC207, R207910

Molecular Properties:

Mol. Wt	555.5	LogP	6.37
HBD	1	LogS	-6.5
HBA	4	pKa	pKa1: 11.64; pKa2: 13.47; pKa3: 7.67; pKa4: 2.67
Molar refractivity	154.02	Polar surface area	45.59
Heavy atom count	37	Aromatic rings count	5
Rotatable bonds	8	Polarizability	57.29

Figure 10. Molecular Property Diagnostic Suite ID card (MPDS ID Card).

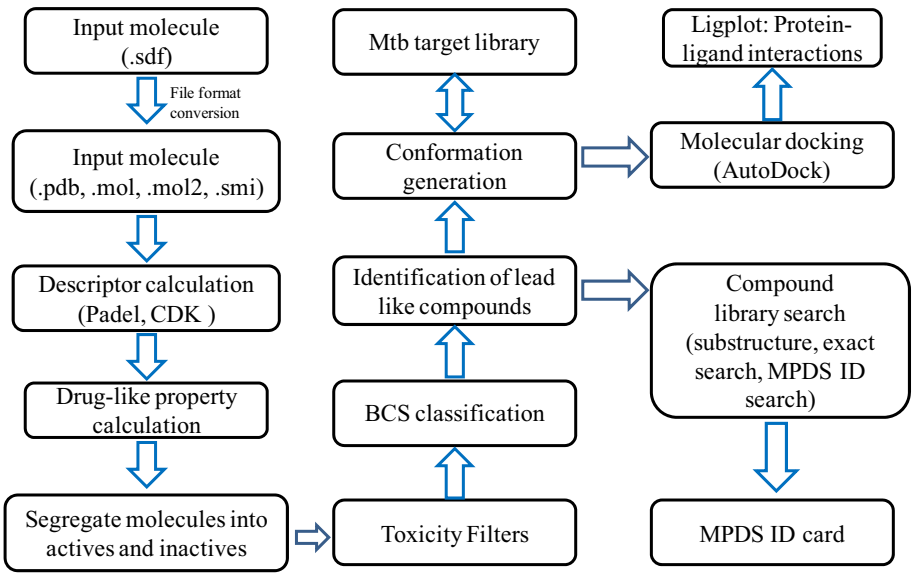

Figure 11. A workflow system for the generation of MPDS ID card by integration of data library, data processing and data analysis modules.

traced to the lack of proper software, access to the comprehensive information on the disease, and also what the contemporary challenges are in developing therapeutics in a given area. Developed countries are not significantly affected by TB and thus the onus of coordinating and conducting frontline research on neglected diseases will be on the developing world. It is very important that India, possessing a tremendous pool of talent and human resource, takes up the leadership role in undertaking research on TB and other neglected diseases. The

current web-based tool, MPDS^{TB} is expected to provide exactly such a platform to drive the research in this area.

Abbreviations

AM1: Austin Model 1; **BCS**: Biopharmaceutics Classification System; **CDK**: Chemistry Development Kit; **CSV**: Comma-Separated Values; **DruLiTo**: Drug Likeness Tool; **eLBOW**: electronic Ligand Builder and Optimisation Workbench; **FAF-Drugs3**: Free ADME-Tox Filtering Tool; **FDA**: Food and Drug Administration; **GUI**: Graphical User Interface; **ID**: Identification number; **InChI**: International Chemical Identifier; **InchIKey**: International Chemical Identifier key; **IUPAC**: International Union of Pure and Applied Chemistry; **KEGG**: Kyoto Enclyclopedia of Genes and Genomes; **KNIME**: Konstanz Information Miner; **McQSAR**: Multi-conformational Quantitative Structure-Activity Relationship; **MMFF94**: Merck Molecular Force Field 94; **MPDS**: Molecular Property Diagnostic Suite; **Mtb**: Mycobacterium tuberculosis; **NCI** National Cancer Institute; **PaDEL**: Pharmaceutical Data Exploration Laboratory; **PDB**: Protein Data Bank; **PK/PD**: PharmacoKinetic/Pharmaco Dynamic; **QSAR**: Quantitative Structure Activity Relationship; **RMSD**: Root Mean Square Deviation; **SDF**: Structure Data File; **SMARTS**: SMiles ARbitrary Target Specification; **SMILES**: Simplified Molecular-Input Line-Entry System; **SVM**: Support Vector Machine; **TB**: Tuberculosis; **XML**: Extensible Markup Language

Acknowledgements

We are thankful to OSDD, CSIR and Sir Dorabji TATA trust for providing TCOF fellowships to some of the authors in the study. CSIR 12th five year program GENESIS (BSC 0121), Department of Science and Technology (New Delhi) and Department of Biotechnology (New Delhi) are also thanked for funding. Code development has taken about 5 years of time starting from 2012 and has witnessed 5 Workshops in IICT, IMTECH, OSDD centre, Bangalore, and NCL. Besides there were several exchange of students between various institutes. We thank CSIR OSDD consortium, NIPER, JNU, and BBAU for providing support. GNS thank J C Bose fellowship of DST. This manuscript is dedicated to the memory of Dr. Anirban Banerji and Dr. Pankaj Narang who have provided a lot of energy and enthusiasm during the kick-start stages of the MPDS teamwork.

References

1. Searls D B 2005 Data integration: Challenges for drug discovery *Nat. Rev. Drug Discovery* **4** 45
2. Nwaka S, Ramirez B, Brun R, Maes L, Douglas F and Ridley R 2009 Advancing drug innovation for neglected diseases-criteria for lead progression *PLoS Negl. Trop. Dis.* **3** e440
3. Sachs J D 2001 A new global commitment to disease control in Africa *Nat. Med.* **7** 521
4. Jagarlapudi S A and Kishan K V 2009 Database systems for knowledge-based discovery *Methods Mol. Biol.* **575** 159
5. Winter M J, Owen S F, Murray-Smith R, Panter G H, Hetheridge M J and Kinter L B 2010 Using data from drug discovery and development to aid the aquatic environmental risk assessment of human pharmaceuticals: Concepts, considerations, and challenges *Integr. Environ. Assess Manage.* **6** 38
6. Lushington G H, Dong Y and Theertham B 2013 Chemical informatics and the drug discovery knowledge pyramid *Comb. Chem. High Throughput Screening* **16** 764
7. Bajorath J 2017 Compound Data Mining for Drug Discovery *Methods Mol. Biol.* **1526** 247
8. Boran A D and Iyengar R 2010 Systems approaches to polypharmacology and drug discovery *Curr. Opin. Drug Discovery Dev.* **13** 297
9. Badrinarayan P and Sastry G N 2011 Virtual high throughput screening in new lead identification *Comb. Chem. High Throughput Screening* **14** 840
10. Reddy A S, Pati S P, Kumar P P, Pradeep H N and Sastry G N 2007 Virtual screening in drug discovery – a computational perspective *Curr. Protein Pept. Sci.* **8** 329
11. Collins P Y, Patel V, Joestl S S, March D, Insel T R, Daar A S; Scientific Advisory Board and the Executive Committee of the Grand Challenges on Global Mental Health, Anderson W, Dhansay M A, Phillips A, Shurin S, Walport M, Ewart W, Savill S J, Bordin I A, Costello E J, Durkin M, Fairburn C, Glass R I, Hall W, Huang Y, Hyman S E, Jamison K, Kaaya S, Kapur S, Kleinman A, Ogunniyi A, Otero-Ojeda A, Poo M M, Ravindranath V, Sahakian B J, Saxena S, Singer P A and Stein D J 2011 Grand challenges in global mental health *Nature* **475** 27
12. Varmus H, Klausner R, Zerhouni E, Acharya T, Daar A S and Singer P A 2003 Public health. Grand Challenges in Global Health *Science* **302** 398
13. Paul S M, Mytelka D S, Dunwiddie C T, Persinger C C, Munos B H, Lindborg S R and Schacht A L 2010 How to improve R&D productivity: The pharmaceutical industry's grand challenge *Nat. Rev. Drug Discov.* **9** 203
14. Dubois D J 2010 Grand Challenges in Pharmacoeconomics and Health Outcomes *Front. Pharmacol.* **1** 7
15. Yildirim O, Gottwald M, Schüler P and Michel MC M 2016 Opportunities and Challenges for Drug Development: Public–Private Partnerships, Adaptive Designs and Big Data *Front. Pharmacol.* **7** 461
16. Gostin L O and Mok E A 2009 Grand challenges in global health governance *Br. Med. Bull.* **90** 78
17. Pai M, Daftary A and Satyanarayana S 2016 TB control: Challenges and opportunities for India *Trans. R. Soc. Trop. Med. Hyg.* **110** 158
18. Wells T N, Willis P, Burrows J N and Hooft V H R 2016 Open data in drug discovery and development: Lessons from malaria *Nat. Rev. Drug Discov.* **15** 661

19. Van Voorhis W C, Adams J H, Adelfio R, Ahyong V, Akabas M H, Alano P, Alday A, Alemán Resto Y, Alsibaee A, Alzualde A, Andrews K T, Avery S V, Avery V M, Ayong L, Baker M, Baker S, Ben Mamoun C, Bhatia S, Bickle Q, Bounaadja L, Bowling T, Bosch J, Boucher L E, Boyom F F, Brea J, Brennan M, Burton A, Caffrey C R, Camarda G, Carrasquilla M, Carter D, Belen Cassera M, Chih-Chien Cheng K, Chindaudomsate W, Chubb A, Colon B L, Colón-López D D, Corbett Y, Crowther G J, Cowan N, D'Alessandro S, Le Dang N, Delves M, DeRisi J L, Du A Y, Duffy S, Abd El-Salam El-Sayed S, Ferdig M T, Fernández Robledo J A, Fidock D A, Florent I, Fokou P V, Galstian A, Gamo F J, Gokool S, Gold B, Golub T, Goldgof G M, Guha R, Guiguemde W A, Gural N, Guy R K, Hansen M A, Hanson K K, Hemphill A, Hooft van Huijsduijnen R, Horii T, Horrocks P, Hughes T B, Huston C, Igarashi I, Ingram-Sieber K, Itoe M A, Jadhav A, Naranuntarat Jensen A, Jensen L T, Jiang R H, Kaiser A, Keiser J, Ketas T, Kicka S, Kim S, Kirk K, Kumar V P, Kyle D E, Lafuente M J, Landfear S, Lee N, Lee S, Lehane A M, Li F, Little D, Liu L, Llinás M, Loza M I, Lubar A, Lucantoni L, Lucet I, Maes L, Mancama D, Mansour N R, March S, McGowan S, Medina Vera I, Meister S, Mercer L, Mestres J, Mfopa A N, Misra R N, Moon S, Moore J P, Morais Rodrigues da Costa F, Müller J, Muriana A, Nakazawa Hewitt S, Nare B, Nathan C, Narraidoo N, Nawaratna S, Ojo K K, Ortiz D, Panic G, Papadatos G, Parapini S, Patra K, Pham N, Prats S, Plouffe D M, Poulsen S A, Pradhan A, Quevedo C, Quinn R J, Rice C A, Abdo Rizk M, Ruecker A, St Onge R, Salgado Ferreira R, Samra J, Robinett N G, Schlecht U, Schmitt M, Silva Villela F, Silvestrini F, Sinden R, Smith D A, Soldati T, Spitzmüller A, Stamm S M, Sullivan D J, Sullivan W, Suresh S, Suzuki B M, Suzuki Y, Swamidass S J, Taramelli D, Tchokouaha L R, Theron A, Thomas D, Tonissen K F, Townson S, Tripathi A K, Trofimov V, Udenze K O, Ullah I, Vallieres C, Vigil E, Vinetz J M, Voong Vinh P, Vu H, Watanabe N A, Weatherby K, White P M, Wilks A F, Winzeler E A, Wojcik E, Wree M, Wu W, Yokoyama N, Zollo P H, Abla N, Blasco B, Burrows J, Laleu B, Leroy D, Spangenberg T, Wells T and Willis P A 2016 Open Source Drug Discovery with the Malaria Box Compound Collection for Neglected Diseases and Beyond *PLoS Pathog.* **28** e1005763
20. Williamson A E, Ylioja P M, Robertson M N, Antonova-Koch Y, Avery V, Baell J B, Batchu H, Batra S, Burrows J N, Bhattacharyya S, Calderon F, Charman S A, Clark J, Crespo B, Dean M, Debbert S L, Delves M, Dennis A S, Deroose F, Duffy S, Fletcher S, Giaever G, Hallyburton I, Gamo F J, Gebbia M, Guy R K, Hungerford Z, Kirk K, Lafuente-Monasterio M J, Lee A, Meister S, Nislow C, Overington J P, Papadatos G, Patiny L, Pham J, Ralph S A, Ruecker A, Ryan E, Southan C, Srivastava K, Swain C, Tarnowski M J, Thomson P, Turner P, Wallace I M, Wells T N, White K, White L, Willis P, Winzeler E A, Wittlin S and Todd M H 2016 Open Source Drug Discovery: Highly Potent Antimalarial Compounds Derived from the Tres Cantos Arylpyrroles *ACS Cent. Sci.* **2** 687
21. Rottmann M, McNamara C, Yeung B K, Lee MC, Zou B, Russell B, Seitz P, Plouffe D M, Dharia N V, Tan J, Cohen S B, Spencer K R, González-Páez GE, Lakshminarayana S B, Goh A, Suwanarusk R, Jegla T, Schmitt E K, Beck H P, Brun R, Nosten F, Renia L, Dartois V, Keller T H, Fidock D A, Winzeler E A and Diagana T T 2010 Spiroindolones, a potent compound class for the treatment of malaria *Science* **329** 1175
22. Meister S, Plouffe D M, Kuhen K L, Bonamy G M, Wu T, Barnes S W, Bopp S E, Borboa R, Bright A T, Che J, Cohen S, Dharia N V, Gagaring K, Gettayacamin M, Gordon P, Groessl T, Kato N, Lee M C, McNamara C W, Fidock D A, Nagle A, Nam T G, Richmond W, Roland J, Rottmann M, Zhou B, Froissard P, Glynne R J, Mazier D, Sattabongkot J, Schultz P G, Tuntland T, Walker J R, Zhou Y, Chatterjee A, Diagana T T and Winzeler E A 2011 Imaging of Plasmodium liver stages to drive next-generation antimalarial drug discovery *Science* **334** 1372
23. Gamo F J, Sanz L M, Vidal J, de Cozar C, Alvarez E, Lavandera J L, Vanderwall D E, Green D V, Kumar V, Hasan S, Brown J R, Peishoff C E, Cardon L R and Garcia-Bustos J F 2010 Thousands of chemical starting points for antimalarial lead identification *Nature* **465** 305
24. Guiguemde W A, Shelat A A, Bouck D, Duffy S, Crowther G J, Davis P H, Smithson D C, Connelly M, Clark J, Zhu F, Jiménez-Díaz M B, Martinez M S, Wilson E B, Tripathi A K, Gut J, Sharlow E R, Bathurst I, El Mazouni F, Fowble J W, Forquer I, McGinley P L, Castro S, Angulo-Barturen I, Ferrer S, Rosenthal P J, Derisi J L, Sullivan D J, Lazo J S, Roos D S, Riscoe M K, Phillips M A, Rathod P K, Van Voorhis W C, Avery V M and Guy R K 2010 Chemical genetics of Plasmodium falciparum *Nature* **465** 311
25. Wells T N 2010 Microbiology. Is the tide turning for new malaria medicines? *Science* **329** 1153
26. Rees S 2015 The promise of open innovation in drug discovery: An industry perspective *Future Med. Chem.* **7** 1835
27. Allarakhia M 2014 The successes and challenges of open-source biopharmaceutical innovation *Expert Opin. Drug Discovery* **9** 459
28. *Global Tuberculosis report*http://apps.who.int/iris/bitstream/10665/250441/1/9789241565394-eng.pdf?ua=1 (accessed on 31st January 2017)
29. *Guidelines for treatment of tuberculosis, fourth edition*http://apps.who.int/iris/bitstream/10665/44165/1/9789241547833_eng.pdf?ua=1&ua=1 (accessed on 31st December 2016)
30. Esmail H, Barry C E, Young D B and Wilkinson R J 2014 The ongoing challenge of latent tuberculosis*Philos. Trans. R. Soc. London, Ser. B* **369** 20130437
31. Davis C E, Carpenter J L, McAllister C K, Matthews J, Bush B A and Ognibene A J 1985 Tuberculosis. Cause of death in antibiotic era *Chest* **88** 726
32. Frieden T R, Sterling T R, Munsiff S S, Watt C J and Dye C 2003 Tuberculosis *Lancet* **362** 887
33. Dye C, Scheele S, Dolin P, Pathania V and Raviglione M C 1999 Consensus statement. Global burden of tuberculosis: estimated incidence, prevalence, and mortality by country. WHO Global Surveillance and Monitoring Project *JAMA* **282** 677
34. Norton B L and Holland D P 2012 Current management options for latent tuberculosis: a review *Infect. Drug Resist.* **5** 163

35. Johnson R, Streicher E M, Louw G E, Warren R M, van Helden P D and Victor T C 2006 Drug resistance in Mycobacterium tuberculosis *Curr. Issues Mol. Biol.* **8** 97
36. Kremer L S and Besra G S 2002 Current status and future development of antitubercular chemotherapy *Expert Opin. Invest. Drugs* **11** 1033
37. Chan E D and Iseman M D 2008 Multidrug-resistant and extensively drug-resistant tuberculosis: a review *Curr. Opin. Infect. Diseases* **21** 587
38. Daley C L and Caminero J A 2013 Management of multidrug resistant tuberculosis *Semin. Respir. Crit. Care Med.* **34** 44
39. Choudhury C, Priyakumar U D and Sastry G N 2014 Molecular dynamics investigation of the active site dynamics of mycobacterial cyclopropane synthase during various stages of the cyclopropanation process *J. Struct. Biol.* **187** 38
40. Choudhury C, Priyakumar U D and Sastry G N 2015 Dynamics based pharmacophore models for screening potential inhibitors of mycobacterial cyclopropane synthase *J. Chem. Inf. Model.* **55** 848
41. Choudhury C, Priyakumar U D and Sastry G N 2016 Dynamic ligand-based pharmacophore modeling and virtual screening to identify mycobacterial cyclopropane synthase inhibitors *J. Chem. Sci.* **128** 719
42. Janardhan S, Ram Vivek M and Sastry G N 2016 Modeling the permeability of drug-like molecules through the cell wall of Mycobacterium tuberculosis: an analogue based approach *Mol. Biosyst.* **12** 3377
43. Reddy A S, Amarnath H S, Bapi R S, Sastry G M and Sastry G N 2008 Protein ligand interaction database (PLID) *Comput. Biol. Chem.* **32** 387
44. Srivastava H K, Choudhury C and Sastry G N 2012 The efficacy of conceptual DFT descriptors and docking scores on the QSAR models of HIV protease inhibitors *Med. Chem.* **8** 811
45. Dobson C M 2004 Chemical space and biology *Nature* **432** 824
46. Lipinski C and Hopkins A 2004 Navigating chemical space for biology and medicine *Nature* **432** 855
47. Barker A, Kettle J G, Nowak T and Pease J E 2013 Expanding medicinal chemistry space *Drug Discovery Today* **18** 298
48. Reymond J L and Awale M 2012 Exploring Chemical Space for Drug Discovery Using the Chemical Universe Database *ACS Chem. Neurosci.* **3** 649
49. Oprea T I and Gottfries J 2001 Chemography: The art of navigating in chemical space *J. Com. Chem.* **3** 157
50. Xu J and Stevenson J 2000 Drug-like index: A new approach to measure drug-like compounds and their diversity *J. Chem. Inf. Comput. Sci.* **40** 1177
51. Irwin J J and Shoichet B K 2005 ZINC-a free database of commercially available compounds for virtual screening *J. Chem. Inf. Model.* **45** 177
52. Bolton E E, Wang Y, Thiessen P A and Bryant S H 2008 PubChem: Integrated platform of small molecules and biological activities *Annu. Rep. Comput. Chem.* **4** 217
53. Wang Y, Xiao J, Suzek T O, Zhang J, Wang J, Zhou Z, Han L, Karapetyan K, Dracheva S and Shoemaker B A 2012 PubChem's BioAssay database *Nucleic Acids Res.* **40** D400
54. Vasilevich N I, Kombarov R V, Genis D V and Kirpichenok M A 2012 Lessons from natural products chemistry can offer novel approaches for synthetic chemistry in drug discovery *J. Med. Chem.* **55** 7003
55. Milne G W and Miller J 1986 The NCI drug information system. 1. System overview *J. Chem. Inf. Comput. Sci.* **26** 154
56. Wishart D S, Knox C, Guo A C, Shrivastava S, Hassanali M, Stothard P, Chang Z and Woolsey J 2006 DrugBank: A comprehensive resource for in silico drug discovery and exploration *Nucleic Acids Res.* **34** D668
57. Kanehisa M, Goto S, Sato Y, Kawashima M, Furumichi M and Tanabe M 2014 Data, information, knowledge and principle: Back to metabolism in KEGG *Nucleic Acids Res.* **42** D199
58. Pence H E and Williams A 2010 ChemSpider: An online chemical information resource *J. Chem. Educ.* **87** 1123
59. Chen C Y 2011 TCM Database@ Taiwan: the world's largest traditional Chinese medicine database for drug screening in silico *PLoS One* **6** e15939
60. Kiss R, Sandor M and Szalai F A 2012 http://Mcule.com: A public web service for drug discovery *J. Cheminf.* **4** P17
61. Olah M, Rad R, Ostopovici L, Bora A, Hadaruga N, Hadaruga D, Moldovan R, Fulias A, Mractc M and Oprea T I 2008 In *Small Molecules to Systems Biology and Drug Design -WOMBAT and WOMBAT-PK: Bioactivity Databases for Lead and Drug Discovery Chemical Biology* S L Schreiber, T M Kapoor and G Wess (Eds.) (Weinheim: Wiley-VCH Verlag GmbH) Vol. **1–3** p. 760
62. Anna G, Louisa J B, Bento A P and Jon C 2012 ChEMBL: A large-scale bioactivity database for drug discovery *Nucleic Acids Res.* **40** D1100
63. Jiang C, Jin X, Dong Y and Chen M 2016 Kekule.js: An Open Source JavaScript Chemoinformatics Toolkit *J. Chem. Inf. Model.* **56** 1132
64. Wojcikowski M, Zielenkiewicz P and Siedlecki P 2015 Open Drug Discovery Toolkit (ODDT): a new open-source player in the drug discovery field *J. Cheminf.* **7** 26
65. Kuhn T, Willighagen E L, Zielesny A and Steinbeck C 2010 CDK-Taverna: An open workflow environment for chemoinformatics *BMCBioinformatics* **11** 159
66. Steinbeck C, Han Y, Kuhn S, Horlacher O, Luttmann E and Willighagen E 2003 The Chemistry Development Kit (CDK): An open-source Java library for Chemo- and Bioinformatics *J. Chem. Inf. Comput. Sci.* **43** 493
67. Wolstencroft K, Haines R, Fellows D, Williams A, Withers D, Owen S, Soiland-Reyes S, Dunlop I, Nenadic A, Fisher P, Bhagat J, Belhajjame K, Bacall F, Hardisty A, Nieva H A, Balcazar V M P, Sufi S and Goble C 2013 The Taverna workflow suite: Designing and executing workflows of Web Services on the desktop, web or in the cloud *Nucleic Acids Res.* **41** W557
68. Beisken S, Meinl T, Wiswedel B, de Figueiredo L F, Berthold M and Steinbeck C 2013 KNIME-CDK: Workflow-driven cheminformatics *BMC Bioinf.* **14** 257
69. Blankenberg D, Von Kuster G, Coraor N, Ananda G, Lazarus R, Mangan M, Nekrutenko A and Taylor J 2010 Galaxy: a web-based genome analysis tool for

experimentalists *Curr. Protoc. Mol. Biol.* Chapter 19 Unit 19.10.1-21
70. Afgan E, Baker D, Beek M V D, Blankenberg D, Bouvier D, Cech M, Chilton J, Clements D, Coraor N, Eberhard C, Gruning B, Guerler A, Jackson J H, Kuster G V, Rasche E, Soranzo N, Turaga N, Taylor J, Nekrutenko A and Goecks J 2016 The Galaxy platform for accessible, reproducible and collaborative biomedical analyses: 2016 update *Nucleic Acids. Res.* **44** W3
71. Blankenberg D, Kuster G V, Bouvier E, Baker D, Afgan E, Stoler N, Galaxy Team, Taylor J and Nekrutenko A 2014 Dissemination of scientific software with Galaxy ToolShed *Genome Biol.* **15** 403
72. *Publicly Accessible Galaxy Servers* https://wiki.galaxyproject.org/PublicGalaxyServers (accessed on 31st December 2016)
73. Hildebrandt A K, Stockel D, Fischer N M, de la Garza L, Kruger J, Nickels S, Rottig M, Scharfe C, Schumann M, Thiel P, Lenhof H P, Kohlbacher O and Hildebrandt A 2015 ballaxy: web services for structural bioinformatics *Bioinformatics* **31** 121
74. O'Boyle N M, Banck M, James C A, Morley C, Vandermeersch T and Hutchison G R 2011 Open Babel: An open chemical toolbox *J. Cheminf.* **3** 33
75. *Landrum G RDKit: Open-Source Cheminformatics* http://www.rdkit.org (accessed on 31st December 2016)
76. Ertl P and Rohde B 2012 The Molecule Cloud - compact visualization of large collections of molecules *J. Cheminf.* **4** 12
77. Peironcely J E, Cherto M R, Fichera D, Reijmers T, Coulier L, Faulon J L and Hankemeier T 2012 OMG: Open Molecule Generator *J. Cheminf.* **4** 21
78. Vainio M J and Johnson M S 2005 McQSAR: a multiconformational quantitative structure-activity relationship engine driven by genetic algorithms *J. Chem. Inf. Model.* **45** 1953
79. Joachims T 1999 *Advances in Kernel Methods- Making Large-Scale SVM Learning Practical* B Scholkopf, C Burges and A Smola (Eds.) (Cambridge: MIT-Press) p. 169
80. Moriarty N W, Grosse-Kunstleve R W and Adams P D 2009 electronic Ligand Builder and Optimization Workbench (eLBOW): a tool for ligand coordinate and restraint generation *Acta Crystallogr., D: Biol. Crystallogr.* **65** 1074
81. Dewar M J S, Zoebisch E G, Healy E F and Stewart J J P 1985 Development and use of quantum mechanical molecular models. 76. AM1: A new general purpose quantum mechanical molecular model *J. Am. Chem. Soc.* **107** 3902
82. Trott O and Olson A J 2010 AutoDock Vina: Improving the speed and accuracy of docking with a new scoring function, efficient optimization and multithreading *J. Comput. Chem.* **31** 455
83. *Drug Likeness Tool (DruLiTo)* http://www.niper.ac.in/pi_dev_tools/DruLiToWeb/DruLiTo_index.html (accessed on 31st December 2016)
84. Lipinski C A, Lombardo F, Dominy B W and Feeney P J 2001 Experimental and computational approaches to estimate solubility and permeability in drug discovery and development settings *Adv. Drug Delivery Rev.* **46** 3
85. Oprea T I 2000 Property distribution of drug-related chemical databases *J. Comput. -Aided. Mol. Des.* **14** 251
86. Ghose A K, Viswanadhan V N and Wendoloski J J 1999 A knowledge-based approach in designing combinatorial or medicinal chemistry libraries for drug discovery. 1. A qualitative and quantitative characterization of known drug databases *J. Comb. Chem.* **1** 55
87. Bickerton G R, Paolini G V, Besnard J, Muresan S and Hopkins A L 2012 Quantifying the chemical beauty of drugs *Nat. Chem.* **4** 90
88. Veber D F, Johnson S R, Cheng H Y, Smith B R, Ward K W and Kopple K D 2002 Molecular properties that influence the oral bioavailability of drug candidates *J. Med. Chem.* **45** 2615
89. Yap C W 2011 PaDEL-descriptor: An open source software to calculate molecular descriptors and fingerprints *J. Comput. Chem.* **32** 1466
90. Jensen C and Scacchi W 2005 *Collaboration, leadership, control, and conflict negotiation and the netbeans.org open source software development community IEEE* 196b